

**SELF-ASSEMBLED RECEPTORS
BASED ON HYDROGEN BONDS**



This research was supported by the Technology Foundation STW, applied science division of NWO and the technology program of the Ministry of Economic Affairs, grant number TST 4624.

Publisher:

Print Partners Ipskamp, Postbus 33, 7500 AH Enschede, the Netherlands,
<http://www.ppi.nl>

© M.G.J. ten Cate, Enschede, 2004

No part of this work may be reproduced by print, photocopy or any other means without the permission in writing of the author.

ISBN 90-365-2053-3

SELF-ASSEMBLED RECEPTORS BASED ON HYDROGEN BONDS

PROEFSCHRIFT

ter verkrijging van
de graad van doctor aan de Universiteit Twente,
op gezag van de rector magnificus,
prof. dr. F.A. van Vught,
volgens besluit van het College van Promoties
in het openbaar te verdedigen
op donderdag 27 mei 2004 om 15.00 uur.

door

Mattijs Gregor Jurriaan ten Cate

geboren op 3 maart 1975
te Hengelo (O)

Dit proefschrift is goedgekeurd door:

Promotor: Prof. dr. ir. D.N. Reinhoudt
Assistent-promotor: Dr. M. Crego Calama

*Je hebt ons zoveel geleerd.
“Nee, andersom,” zei jij.
Maar wie heeft wie geïnspireerd?
Of wie maakt wie nou blij?*

Chris ten Cate - Peeters, 2004

Dit proefschrift is opgedragen ter nagedachtenis aan mijn moeder
Mia ten Cate – van Wakeren †

Voor jou mama!

Contents

Chapter 1

General introduction	1
-----------------------------------	----------

Chapter 2

Hydrogen-bonded assemblies and synthetic receptors.....	5
--	----------

2.1 Biological self-assembly	6
------------------------------------	---

2.2 Hydrogen-bonded molecular recognition motifs.....	7
---	---

2.2.1 <i>Hydrogen bonding patterns</i>	7
--	---

2.2.2 <i>Hydrogen-bonded capsules</i>	9
---	---

2.2.2.1 <i>Macrocycle-based capsules</i>	9
--	---

2.2.2.2 <i>Glycouril-based capsules</i>	14
---	----

2.2.3 <i>G-quartet</i>	15
------------------------------	----

2.2.4 <i>Hydrogen-bonded tubes and helices</i>	16
--	----

2.2.5 <i>Hydrogen-bonded polymers</i>	19
---	----

2.2.6 <i>Rosettes</i>	22
-----------------------------	----

2.2.6.1 <i>The hydrogen bonded motifs based on melamines and isocyanuric or barbituric acids</i>	22
--	----

2.2.6.2 <i>Assemblies with multiple rosette motifs based on melamines and isocyanuric or barbituric acids</i>	24
---	----

2.3 Concluding remarks.....	25
-----------------------------	----

2.4 References	26
----------------------	----

Chapter 3

Towards self-assembled receptors: functionalized double rosette assemblies	35
---	-----------

3.1 Introduction	36
------------------------	----

3.2 Formation of double rosette assemblies	38
--	----

3.3 Characterization of double rosette assemblies	39
---	----

3.4 Results and discussion.....	41
---------------------------------	----

3.4.1	<i>Synthesis and characterization of assemblies with different functionalities</i> ...	42
3.4.2	<i>Thermodynamic stability of assemblies with alkyl, aminoalkyl, ureido and pyridyl functionalities</i>	44
3.4.3	<i>Formation and thermodynamic stability of assemblies with carbohydrate moieties</i>	47
3.4.4	<i>Formation and thermodynamic stability of assemblies with amino acid functionalities</i>	49
3.4.4.1	<i>Thermodynamic stability</i>	49
3.4.4.2	<i>Chiral induction by the lysine group</i>	51
3.4.5	<i>Formation and thermodynamic stability of assemblies with di- and tripeptide functionalities</i>	53
3.5	Conclusions	55
3.6	Experimental.....	57
3.7	References	69

Chapter 4

	Thermodynamic Stability of Hydrogen-Bonded Nanosized Structures: a calorimetric study	71
4.1	Introduction	72
4.2	Results and discussion.....	74
4.2.1	<i>Synthesis</i>	74
4.2.2	<i>Isothermal titration microcalorimetry</i>	75
4.2.3	<i>Self-assembly in apolar solvent</i>	77
4.2.3.1	<i>Single vs. double rosettes</i>	77
4.2.3.2	<i>Barbiturates vs. cyanurates</i>	79
4.2.4	<i>Effect of solvent polarity on double rosette formation</i>	80
4.2.5	<i>Correlation between solvent polarity and ΔG°</i>	82
4.2.6	<i>Double rosette formation in MeOH</i>	84
4.3	Conclusions	86
4.4	Experimental.....	86
4.5	References	88

Chapter 5**Self-organization of guest molecules in self-assembled molecular containers93**

5.1	Introduction	94
5.2	Results and discussion.....	97
5.3	Conclusions	110
5.4	Experimental.....	111
5.5	References	112

Chapter 6**Binding of small guest molecules to multivalent receptors115**

6.1	Introduction	116
6.2	Results and discussion.....	117
6.2.1	<i>Complexation of phenolic guests</i>	118
6.2.1.1	<i>Complexation of p-nitrophenol</i>	118
6.2.1.2	<i>Complexation of Diethylstilbestrol (DES)</i>	121
6.2.1.3	<i>Complexation of Bisphenol A</i>	127
6.2.2	<i>Complexation of aromatic carboxylic acids</i>	128
6.2.3	<i>Binding of n-octylgalactopyranoside</i>	132
6.3	Conclusions	134
6.4	Experimental.....	135
6.5	References	135

Chapter 7**Formation of Hydrogen-Bonded Receptors in Niosomal Membranes: Towards artificial cells.....139**

7.1	Introduction	140
7.2	Results and discussion.....	142
7.2.1	<i>Synthesis</i>	142
7.2.2	<i>Niosome formation</i>	143
7.2.3	<i>Formation of the double rosettes in niosomes</i>	145
7.2.4	<i>Exchange of DEB molecules in double rosettes by BuCYA in niosomes</i>	149

7.3	Conclusions	149
7.4	Experimental.....	150
7.5	References	154
	Summary.....	159
	Samenvatting.....	163
	Dankwoord	167

Chapter 1

General introduction

Supramolecular chemistry has produced a large number of potent receptor molecules, such as crown ethers,¹⁻³ cyclodextrins,⁴ and calixarenes⁵ for a variety of guests. In terms of binding affinity and selectivity, the complexation of structurally simple guests, like cations, anions, and small molecules like urea, have been studied with great success.⁶ However, despite many efforts chemists have not been able to synthesize artificial receptor molecules for structurally more complex molecules like steroids, carbohydrates, and peptides that adequately mimic the function of their natural counterparts.

Complexity is a prerequisite to enable energetically demanding processes in biological systems. However, large covalent synthetic molecules that mimic the natural receptors are difficult to synthesize and structural diversity can be introduced only with large synthetic effort. It seems that the covalent approach has reached the limits of what is synthetically feasible in terms of time requirements and overall yields. A closer look to nature reveals that the complexity in biological systems is often accomplished by self-assembly. Therefore, a noncovalent approach toward receptors seems to be much more efficient. The main advantage is that the assembled structures are generally formed under thermodynamically controlled conditions, often giving rise to quantitative yields of product.⁷ Structural diversity in these systems can be generated in an extremely simple way, i.e. by mixing components carrying different recognition sites. The use of hydrogen bonds as noncovalent interaction in these assemblies is especially attractive due to their directionality. However, due to the ability of water (or other polar solvents) to compete for hydrogen bonding their scope is limited, since water is omnipresent in biological systems. Hence, only the use of motifs with a large number of hydrogen bonds might give assemblies with high thermodynamic stability.

The objective of this thesis is to obtain noncovalent receptor assemblies with different recognition sites which are stable in solvents with significant polarity and that are able to complex (biologically interesting) molecules. The receptor assemblies consist of a hydrogen-bonded platform in which the individual components are functionalized with groups that generate a potential guest-binding region.

In Chapter 2, an overview of hydrogen-bonded assemblies will be given. Different hydrogen bonding patterns are described and the self-assembly of large hydrogen-bonded assemblies, using multiple hydrogen-bonding patterns will be discussed together with their ability to recognize guest molecules.

Chapter 3 describes the formation and stability of hydrogen-bonded double rosette assemblies with alkyl, aminoalkyl, ureido, pyridyl, carbohydrate, amino acid and peptide functionalities. The thermodynamic stability of these hydrogen-bonded assemblies in solvent mixtures of methanol and chloroform was determined by CD spectroscopy.

Chapter 4 describes a detailed calorimetric study of the self-assembly of double rosettes in solvent mixtures of different polarity. The thermodynamics of assembly formation could be correlated with the solvent polarity in order to predict possible assembly formation in polar solvents. The formation of double rosettes in pure methanol was studied experimentally by ^1H NMR and CD spectroscopy.

The ability of double rosettes to complex molecules is described in Chapters 5 and 6. Chapter 5 reports the encapsulation and selectivity exhibited by double rosettes as *endo*-receptors in the recognition of anthraquinone derivatives. The methods used to study the encapsulation are X-ray crystallography, ^1H NMR spectroscopy, ITC and UV spectroscopy.

Chapter 6 describes the binding of multiple phenol derivatives, aromatic carboxylic acids and carbohydrates to the exterior of the hydrogen-bonded receptors (*exo*-receptors). ^1H NMR spectroscopy and ITC were used to determine the complexation of several guests by these receptors.

While Chapters 3 and 4 describe the thermodynamic stability of double rosettes in solution, a novel approach to mimic bio-recognition processes by self-assembled receptors is described in Chapter 7. Because many bio-recognition processes occur at interfaces or at membrane surfaces between two aqueous compartments the formation of

hydrogen-bonded double rosettes in the membranes of non-ionic surfactant based vesicles (niosomes) were studied by CD spectroscopy.

References

1. Staveren, C. J.; Aarts, V. M. L. J.; Grootenhuis, P. D. J.; Droppers, W. J. H.; Van Eerden, J.; Harkema, S.; Reinhoudt, D. N. *J. Am. Chem. Soc.* **1988**, *110*, 8134-8144.
2. Kimura, E. *J. Inclusion Phenom.* **1989**, *7*, 183-191.
3. Sun, D.; Chen, J.; Lu, W.; Zheng, X. *J. Solution Chem.* **1998**, *27*, 1097-1107.
4. *Chem. Rev.*, D'Souza, V. T.; Lipkowitz, K. B., Eds.; **1998**, Vol. 98, 1741-2076.
5. Ikeda, A.; Shinkai, S. *Chem. Rev.* **1997**, *97*, 1713-1734.
6. Houk, K. N.; Leach, A. G.; Kim, S. P.; Zhang, X. *Angew. Chem. Int. Ed.* **2003**, *42*, 4872-4897.
7. Whitesides, G. M.; Mathias, J. P.; Seto, C. *Science* **1991**, *254*, 1312-1319.

Chapter 2

Hydrogen-bonded assemblies and synthetic receptors

The formation of self-assembled aggregates via hydrogen bonds is briefly reviewed. The most representative examples of this type of noncovalent assemblies, such as capsules, tubes, supramolecular polymers and rosettes are described with special attention to the latest developments in supramolecular chemistry. The hydrogen-bonded motifs forming the assemblies and their ability to complex guest molecules are emphasized.

2.1 Biological Self-assembly

Hydrogen bonds and other noncovalent interactions in natural systems are responsible for the transport of signals, selective transport of ions and small molecules across lipid membranes, enzymatic reactions, and formation of larger aggregates.¹ For example, enzymes are highly effective in catalyzing chemical reactions because of their capacity to specifically bind molecules.² The specific binding of the substrate to the enzyme is in part due to the directional character of the hydrogen bonds. The uniqueness and specificity of proteins and nucleic acids are also largely determined by the directive power of the hydrogen bonds.³ The major thermodynamic driving forces in the structure formation of protein complexes are hydrophobic interactions, but the formation of hydrogen bonds define the specific geometry of secondary structures in the proteins, in particular, in an α -helix or in β -sheets.⁴ Double helix formation in nucleic acids is driven by base pair stacking, and the large number of hydrogen bonds leads to a cumulative effect on the stability.⁵ In the DNA hydrogen bonding allows for only complementary strands to come together since the hydrogen bond formation depends on the specific patterns of hydrogen bond donors and acceptors.

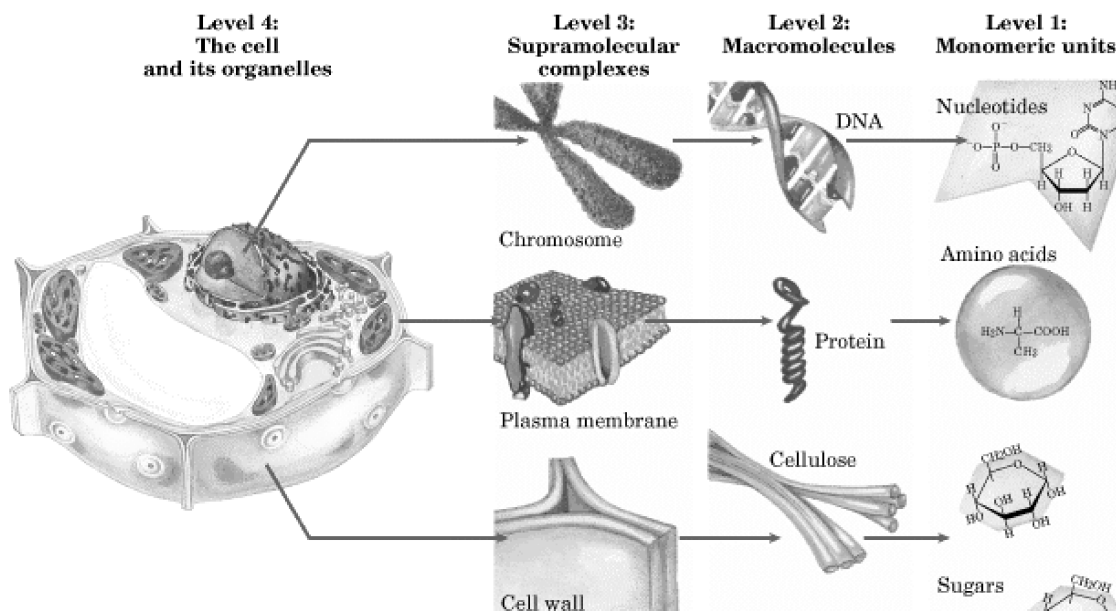


Figure 2.1 Self-assembly hierarchy of biological material.

In general, self-assembly seems to be nature's favorite, most economic, and reliable way to generate the level of complexity in biological systems required to promote energetically demanding processes (Figure 2.1).⁶ Due to the high efficiency of nature using noncovalent interactions to assemble complex aggregates, self-assembly is nowadays considered as one of the most promising ways for building synthetic functional nanostructures.⁷ There are synthetic systems that mimic, to some extent, complex natural systems using self-assembly as a source of inspiration. For example, the mimicry of light harvesting systems in bacteria by self-assembled porphyrin arrays^{8,9} and photoinduced electron transfer through donor-acceptor interfaces based on Watson-Crick base pairing¹⁰ or salt bridges¹¹. Another nice example reported by Nolte *et al.*¹² is a self-assembled catalyst that features all the important components present in the natural cytochrome P450. The group of Rebek¹³ has reported enzyme mimics where self-assembled molecular capsules accelerate Diels-Alder reactions. More examples of capsules and other synthetic self-assembled systems that mimic features of natural systems, such as entrapment, release and transport are described in the next sections.

2.2 Hydrogen-bonded molecular recognition motifs

Molecular self-assembly concerns molecules and supramolecular entities that complementarily assemble into nanoscale aggregates by weak noncovalent forces such as hydrogen bonding, metal coordination, ionic interactions, and van der Waals interactions. This dynamic noncovalent approach has a number of advantages compared to the covalent approach. The main advantages are that the target assembly is the thermodynamically most stable aggregate, is defect free, and displays self-healing.¹⁴ There are many self-assembled molecular systems¹⁵⁻¹⁹ but this chapter focuses on hydrogen bonding as the noncovalent recognition motif. The ability of these systems to complex guest molecules is emphasized.

2.2.1 Hydrogen bonding patterns

A large variety of organic functionalities self-assemble to form homodimers (*e.g.* phenols, amines, *trans*-amides, sulfonamides and phosphoamides) or heterodimers (*e.g.* pyridines and carboxylates) via the formation of a single hydrogen bond in apolar

solvents. However, the low stability of the single hydrogen bond limits their applicability. Other functionalities dimerize via the formation of two AD•DA or AA•DD (A = acceptor, D = donor) hydrogen bonds (*e.g.* homodimers based on carboxylic acids,²⁰ imides,²¹ ureas^{20,22} and heterodimers based on carboxylic acids and either amides,²³ 2-amido-or aminopyridines,²⁴ or 2-aminopyrimidones²⁵) to form stronger complexes. Common AD•DA complexes, with two repulsive secondary interactions have low formation constants ($K_f \sim 60 \text{ M}^{-1}$).²⁶ On the other hand, AA•DD with two attractive secondary interactions form complexes which are much more stable ($K_f \sim 10^2\text{-}10^3 \text{ M}^{-1}$).^{26,27}

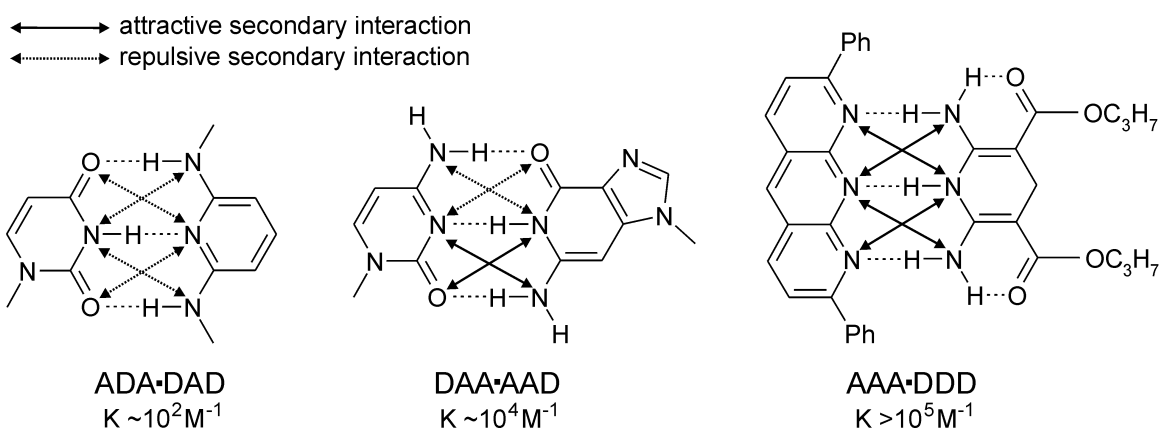


Figure 2.2 Molecular structures of several hydrogen-bonded dimers showing the differences in thermodynamic stability due to attractive and repulsive secondary interactions.

Assembly motifs with three hydrogen bonds exhibit significantly higher stability than the corresponding motifs based on two hydrogen bonds.^{28,29} Zimmerman found for a series of dimeric complexes with ADA•DAD, DAA•AAD and AAA•DDD motifs (having 0, 2, and 4 favorable secondary interactions, respectively), formation constants of 10^2 , $10^3\text{-}10^4$ and $>10^5 \text{ M}^{-1}$, respectively (Figure 2.2).^{30,31} Meijer *et al.* have described the formation of a series of 2-ureido-pyrimidone derivatives through the formation of four hydrogen bonds.³² Dimerization constants of 10^5 and $>10^6 \text{ M}^{-1}$ in chloroform were reported for DADA•ADAD and AADD•DDAA complexes, respectively.

Many large natural and synthetic hydrogen-bonded assemblies use multiple hydrogen-bonding patterns to assemble. A well-known example from nature is the assembly of DNA and RNA where multiple DA•AD patterns are formed by the hydrogen-bonded

base pairs adenine·thymine and adenine·uracil and DDA•AAD patterns by guanine·cytosine (Watson-Crick).³³⁻³⁵

2.2.2 Hydrogen-bonded capsules

Self-assembled capsules are supramolecular structures with enclosed cavities that are formed when multiple molecules assemble by reversible noncovalent interactions. In general, capsules are designed to act as *endo*-receptors where guest molecules are encapsulated in their cavities. Different types of hydrogen-bonded capsules have been described.³⁶ Most molecular capsules are based on macrocycles (Figure 2.3a,b) and glycouril derivatives (Figure 2.3 c,d).

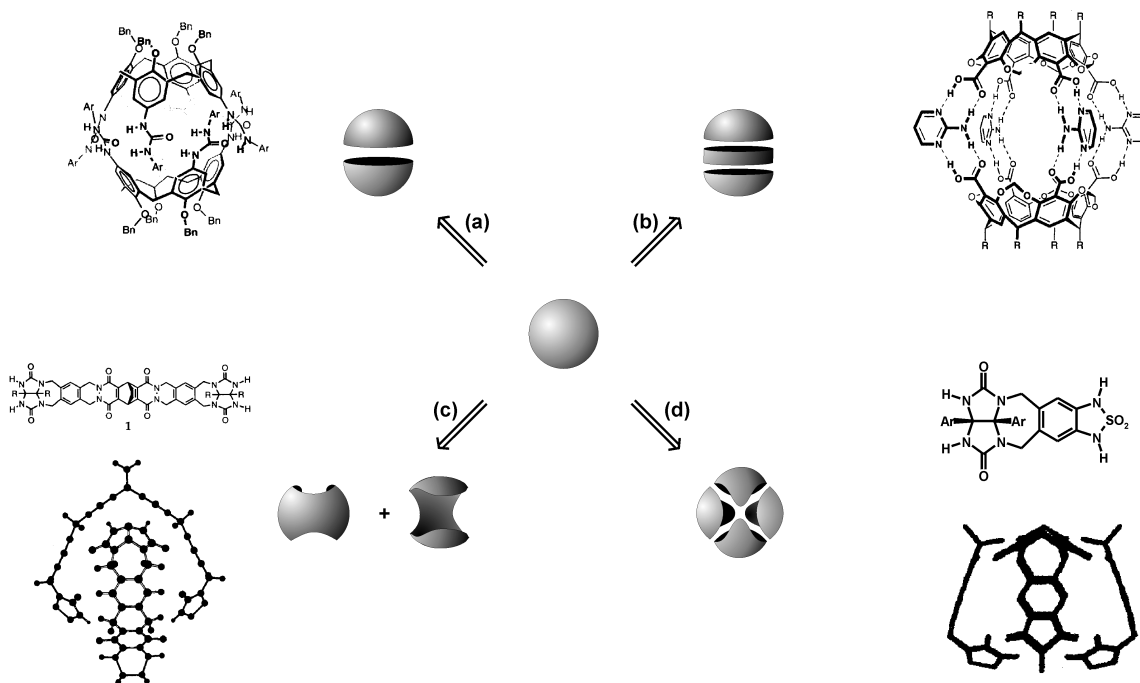


Figure 2.3 Strategies for the synthesis of hydrogen-bonded capsules.

2.2.2.1 Macrocycle-based capsules

The easiest way to generate macrocycle-based capsules is the self-assembly of two complementary building blocks (Figure 2.3a), either by bisecting a sphere along the equator or by cutting it twice along the 'tropic of Capricorn and Cancer' (Figure 2.3b). The rigidity and curvature of macrocycles like calixarenes, resorcinarenes and cavitands are ideal for their self-assembly into discrete hydrogen-bonded capsules.

Calixarenes

The assembly of upper rim substituted tetracarboxylic acid calix[4]arenes with lower rim substituted tetra(3-pyridyl) or tetra(4-pyridyl) calix[4]arenes gives heteromeric capsules through the formation of four hydrogen bonds, with association constant of 10^3 - 10^4 M⁻¹ in chloroform (Figure 2.4a).³⁷ A similar capsule, reported by Shinkai *et al.*, featured tetracarboxylic and tetrapyridyl calix[4]arenes both functionalized at the upper rim (Figure 2.4b).³⁸

Dimerization of 1,3-bis(ureido) calix[4]arenes was reported by our group.³⁹ The capsules were formed through the formation of four hydrogen bonds between the ureido moieties situated at the upper rim of the calix[4]arenes.

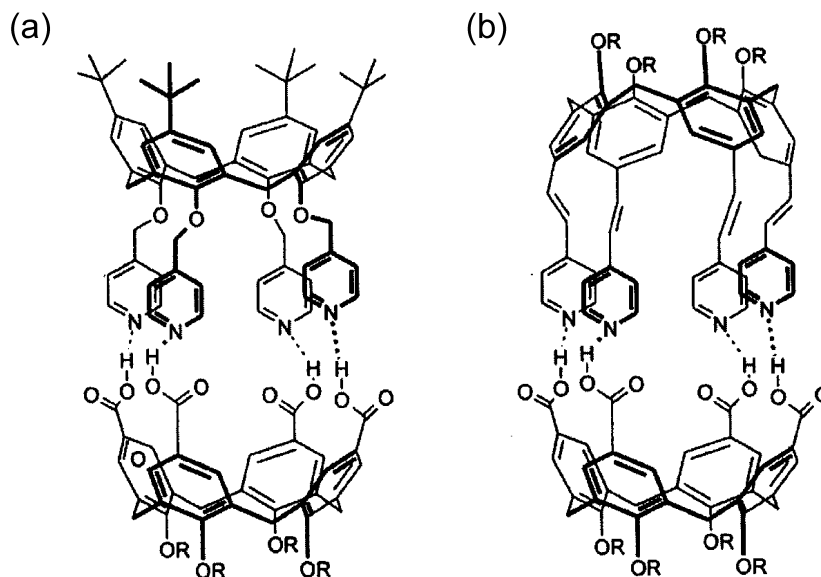


Figure 2.4 Hydrogen-bonded capsules formed through four hydrogen bonds between tetracarboxylic acid groups at the upper rim of the calix[4]arenes and tetrapyridyl groups at the lower rim (a) or upper rim (b) of the other calix[4]arene.

Rebek *et al.*^{40,41} showed that self-complementary tetraureido calix[4]arenes form capsules by dimerization through the formation of 16 hydrogen bonds (Figure 2.3a). X-ray crystallography showed that the eight ureido groups interdigitate in a head to tail array of hydrogen bonds.⁴² The resulting cavities were capable to encapsulate molecules such as benzene, toluene, pyrazine and chloroform and bicyclic aliphatic and tetra-alkylammonium cations.⁴³ The association of the capsule is affected when urea derivatives or small percentages polar solvents are added which compete for hydrogen

bonding.⁴⁴ Nevertheless, when bulky residues are attached to the ureido functionalities kinetically stable capsules could be formed in competitive solvents for hydrogen bonding such as DMSO.⁴⁵

For tetraureido calix[4]arenes functionalized with aryl and sulfonyl moieties at the distal urea nitrogen, the monomeric units self-assemble exclusively into heteromeric chiral capsules, where the chirality arises from the directionality of the hydrogen-bonded belt.^{46,47} The preference for the heterodimerization is rationalized by the increased acidity of the sulfonyl urea that complements the relative basicity of the aryl urea. Recently, Böhmer reported supramolecular chirality of tetraureido calix[4]arene capsules by the spatial rearrangement of two calix[4]arenes composed of two different phenolic ureido units.⁴⁸

Elongated tetraureido calix[4]arenes were introduced to produce expanded cavities for guest encapsulation.⁴⁹ Though these capsules failed to encapsulate neutral molecules of appropriate size and shape, positively charged alkyl pyridinium derivatives were strongly complexed inside these capsules.

Recently, the dimerization of calix[4]arene derivatives with four alanine moieties at the upper rim in polar, protic solvents was reported.⁵⁰ In MeOH:H₂O (24:1) an association constant of 10^4 M^{-1} for the dimerization was reported. These capsules self-assemble through the formation of hydrogen bonds between the alanine functionalities of the monomeric units. Depicted in Figure 2.5 are the two modes of interaction suggested for the dimer formation (Figure 2.5).

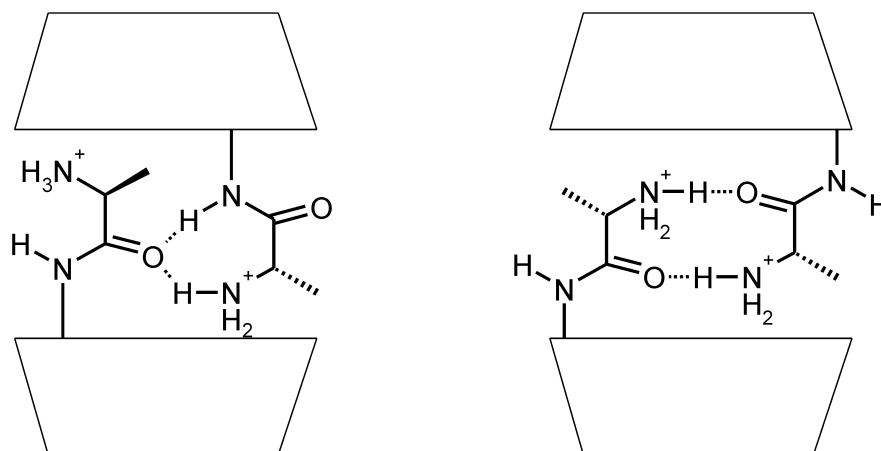


Figure 2.5 Proposed interactions in the tetraalanine calix[4]arene dimer.

Resorcinarenes

Atwood⁵¹ and Aoki⁵² reported the formation of similar dimeric hydrogen-bonded capsules from resorcinarenes in the solid state that are linked through 16 intermolecular hydrogen bonds involving eight molecules of 2-propanol or water, respectively.

Böhmer and coworkers prepared a resorcinarene dimer held together by eight hydrogen bonds between phenolic hydroxyl groups and ester carbonyl groups in solution.⁵³ ¹H NMR and X-ray crystallography showed that these capsules are able to entrap tropylium cations.

The assembly of a heterotopic resorcinarene capsule via four pyridyl-carboxylic acid interactions in chloroform has been described by Reinhoudt *et al.*⁵⁴ The capsule was stable in the presence of four equivalents of pyridine. Recently, Yamaguchi *et al.* reported also heterodimeric resorcinarene capsules via four pyridyl-carboxylic acid interactions in solution and in the solid state.⁵⁵ These capsules encapsulate different 1,4-substituted benzenes.

Resorcinarenes provide also scaffolds for larger hexameric capsules (six half spheres). MacGillivray and Atwood⁵⁶ have studied the formation of a large hexameric capsule based on resorcinarenes in the solid state (Figure 2.6). The capsule is held together by 60 hydrogen bonds and consisting of six units of resorcinarenes and eight water molecules. In addition, Shivanyuk and Rebek demonstrated that the same hexameric capsule can be obtained in chloroform saturated with water.^{57,58}

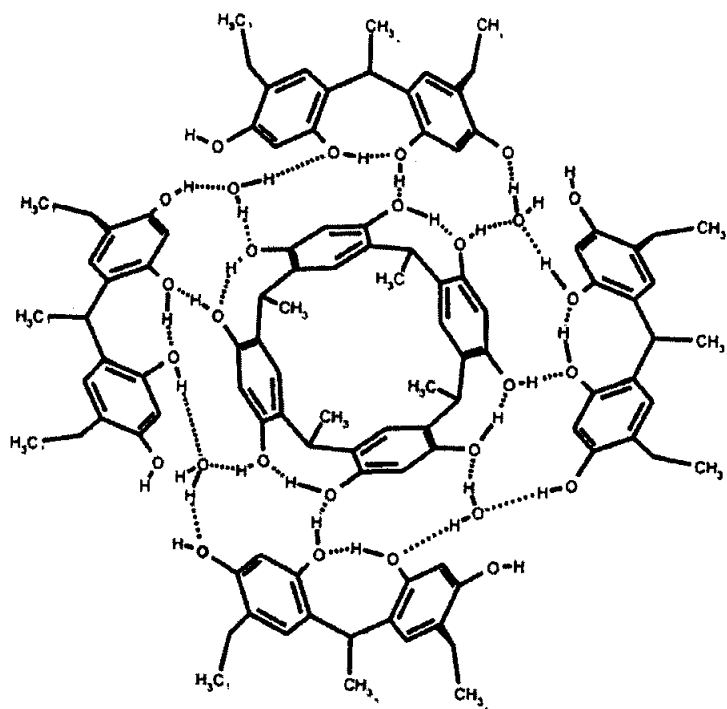


Figure 2.6 Hexameric capsule of self-complementary resorcinarenes.

Cavitands

Sherman *et al.* reported capsule formation in which two cavitands are held together by four charged hydrogen bonds between hydroxyl groups.⁵⁹⁻⁶¹ The capsules complex selectively pyrazine molecules.

Rebek and coworkers have elongated resorcinarenes with pyrazine-2,3-dicarboxylic acid imides to obtain cavitands which dimerized into neutral cylindrical capsules (Figure 2.7).^{62,63} These capsules exhibit affinity for anions,⁶⁴ and in combination with a calixarene based capsule with known affinity for cations,⁴³ these authors were able to arrange a capsule-separated ion pair. The cylindrical dimeric container also selectively encapsulates pairwise one benzene and one larger aromatic molecule such as *p*-xylene, *p*-chlorotoluene or *p*-methylbenzylalcohol. The overall length of the pairs matched the dimensions of the cavity and prevented encapsulation of two identical molecules. Furthermore, these elongated capsules are able to encapsulate larger molecules like dicyclohexyl carbodiimide and *trans*-stilbene methanol in a 1:1 host:guest ratio.

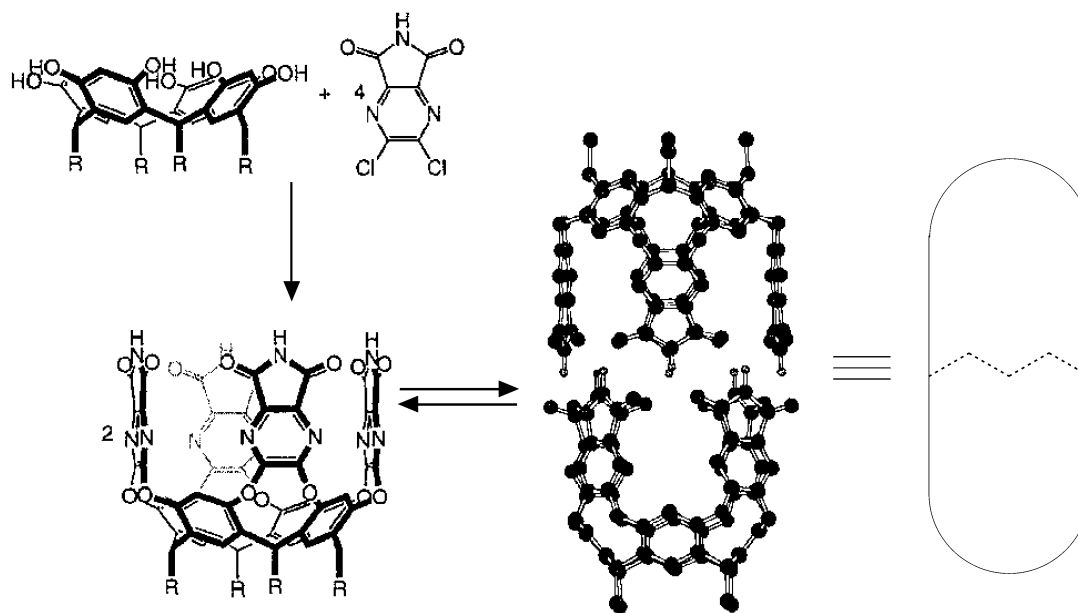


Figure 2.7 Elongated cylindrical capsules reported by Rebek and coworkers.

Another elongated cavitand-based capsule, reported in solution and in the solid state by Furukawa and coworkers,⁶⁵ involves two tetracarboxylic acid cavitands that are connected via four 2-aminopyrimidine molecules through the formation of 16 hydrogen bonds (Figure 2.3b). Two molecules of nitrobenzene are encapsulated in this noncovalent capsule.⁶⁵

2.2.2.2 Glycouril-based capsules

Glycouril based capsules are assembled from two identical halves like a tennis ball (Figure 2.3c). The assembly of two curved bis(glycouril) units into 'molecular tennis balls' held together by eight hydrogen bonds was first reported in 1993.⁶⁶ The cavity of the 'tennis ball' has inner dimensions of 50-55 Å³ making it possible to encapsulate small guest molecules such as methane.⁶⁷ Further expansion of the spacer between the glycouril units led to larger capsules referred to as 'softball'⁶⁸ with calculated cavity volumes of 290 Å³.⁶⁹ The larger 'softball' was able to encapsulate adamantane or ferrocene derivatives.⁶⁹ Furthermore, building blocks with three glycouril moieties were synthesized and resulted upon dimerization in flattened spheres or 'jelly doughnuts'.⁷⁰ A 'tennis ball like' capsule

composed of four self-complementary components is formed by hydrogen bonding between sulfamides and glycouril moieties (Figure 2.3d).⁷¹

2.2.3 G-quartet

The G-quartet is a noncovalent assembly in which four guanosines (G) assemble by hydrogen bonding between the Hoogsteen and Watson-Crick faces of adjacent guanosines (Figure 2.8).⁷² In a cation-templated process guanosine derivatives self-assemble in water to give G-quartets.⁷³ Davis *et al* have shown the formation of isoG-quartets by assembly of lipophilic nucleosides in the presence of metal ions in nonpolar solvents.⁷⁴ With K^+ picrates the formation of octamers was observed by sandwiching of a K^+ cation by two G-quartets^{75,76} or two isoG-quartets.^{77,78} With another guanosine derivative and metal picrate, D_4 -symmetric hexadecamers were formed, in which two M^{2+} metal ions are complexed between two G-quartets and four picrate anions are hydrogen bonded to NH amino protons of the two central G-quartets (Figure 2.8).⁷⁹⁻⁸¹ Cation templated G-duplexes of hydrogen-bonded isoG-pentamers were also reported (Figure 2.8).^{82,83} Normally, templating alkali metal cations are needed to prevent formation of ribbon-like structures. Sessler and coworkers have recently shown that a sterically demanding group attached to the C8 position of guanosine derivatives enables the molecules to self-assemble into G-quartets in absence of templating cations, both in solid state and in solution.⁸⁴

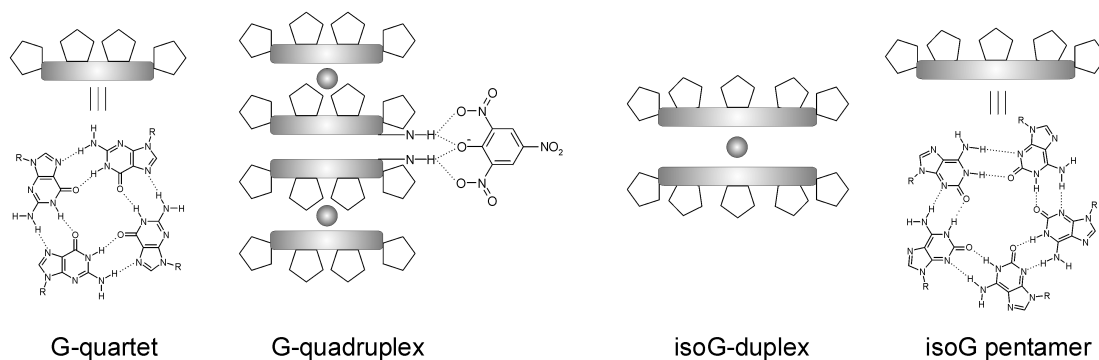


Figure 2.8 Different hydrogen bonded assemblies of Guanosine (G) and isoGuanosine (isoG).

2.2.4 Hydrogen-bonded tubes and helices

Hollow tubular structures perform diverse biological functions in nature, including chemical transport through membrane channels.⁸⁵ There are several possible ways to design open-ended tubular structures.¹⁵ Macrocycles can be stacked to form continuous tubes, rod like molecules can be assembled in lamellar fashion to form molecular bundles, helical molecules can be coiled to form hollow folded structures and wedge-shaped molecules can assemble into discs that subsequently stack to form continuous cylinders.

Tubes

Peptides comprised of an even number of alternating *D*- and *L*-amino acids, displaying conformational equivalent β -type dihedral angles, can form closed rings capable to stack through backbone-backbone hydrogen bonding.⁸⁶ Ghadiri and coworkers exploited this motif to construct peptide nanotubes.¹⁵ The first reported nanotubes consisted of cyclic octapeptide rings (Figure 2.9) with the sequence *cyclo*[(*L*-Gln-*D*-Ala-*L*-Glu-*D*-Ala)₂].⁸⁷ Stacking of the ring-shaped subunits through antiparallel β -sheet hydrogen bonding formed hollow tubes with internal diameters of 7-8 Å. An advantage of cyclic *D,L*-peptide nanotubes is that the internal diameter can be controlled by adjusting the internal diameter of the cyclic peptide subunit. To demonstrate the flexibility of this design, a cyclic dodecamer peptide, *cyclo*[(*L*-Gln-*D*-Ala-*L*-Glu-*D*-Ala)₃], was synthesized. The peptide nanotubes formed from these dodecamers have a van der Waals diameter of 13 Å.⁸⁸ In lipid bilayers, peptide nanotubes act as excellent transport channels for Na⁺ and K⁺ ions,⁸⁹ glucose⁹⁰ and glutamic acid.⁹¹

Seebach *et al.* reported that cyclic β -tetrapeptides form hollow tubular structures analogously to those formed by alternating *D*- and *L*- α -amino acids.⁹² Ghadiri's group further investigated these self-assembled cyclic β^3 -peptide nanotubes as ion channels.⁹³

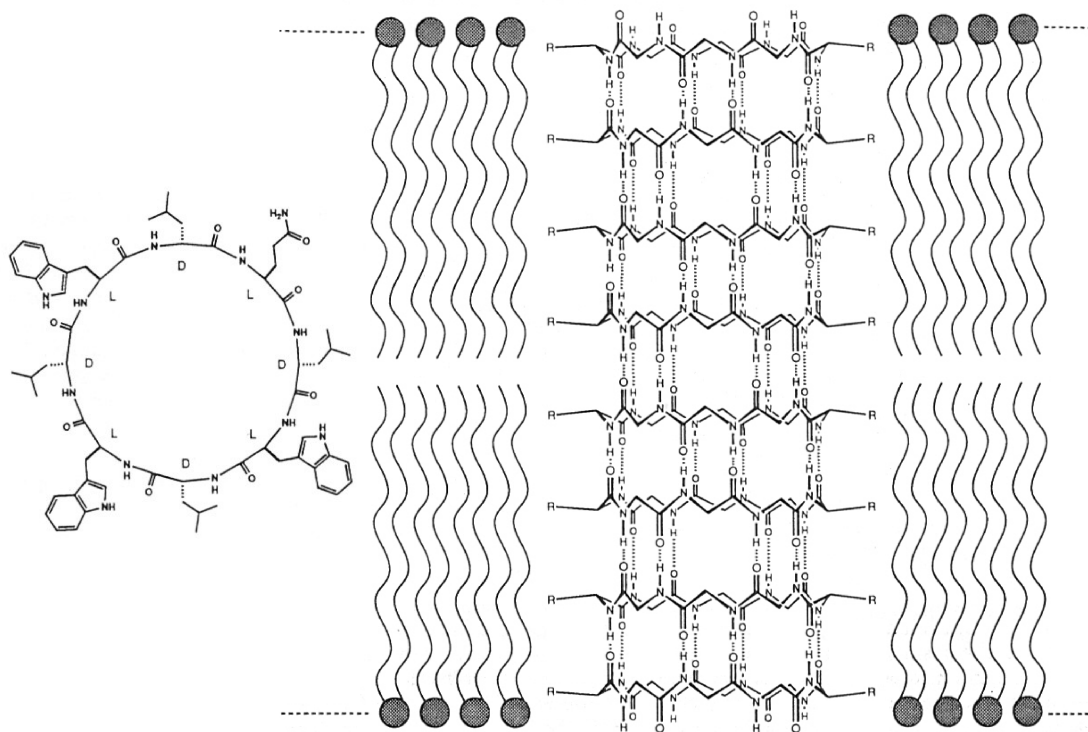


Figure 2.9 Chemical structure of the cyclic octapeptide (left) and peptide subunits in a self-assembled tubular configuration embedded in a lipid bilayer membrane (right).

Matile *et al.* have reported the self-assembly of rigid rod-shaped polyols functionalized with amino acids into rigid-rod β -barrels (Figure 2.10).⁹⁴⁻⁹⁶ These lamellar nanotubes self-assemble by forming antiparallel β -sheets with interdigitating peptide chains. The size of the pores could be controlled by the size of the interdigitating peptide chains.⁹⁷

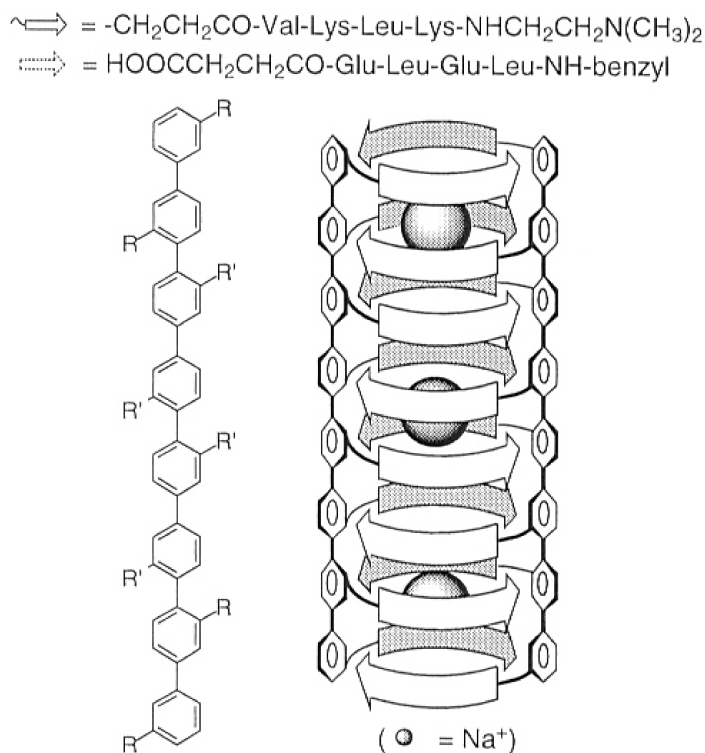


Figure 2.10 Structure of rigid-rod polyol (left) and self-assembled rigid-rod β -barrel (right)

Helical tubes

Kunitake and coworkers prepared amphiphilic supramolecular architectures in organic media by mixing dialkylated melamines with naphthalenebis(dicarboximide).⁹⁸ These authors suggested that either stacking of cyclic heterododecamers or helically grown tapes are responsible for the observed tubular structures. Fenniri and coworkers have used a rosette motif that assembles into helical nanotubes in water.⁹⁹ The rosette structure was based on the hierarchical self-assembly of six *L*-modules **1a** after which stacking of rosettes **1a**₆ gave helical nanotubes (Figure 2.11). Self-assembly of six modules **1b**, bearing crown ether moieties, and subsequent stacking resulted into racemic mixtures of left- and right-handed helical nanotubes.^{100,101} Recognition of chiral amino acids in their zwitterionic form by **1b** induced one helical form of the nanotube.

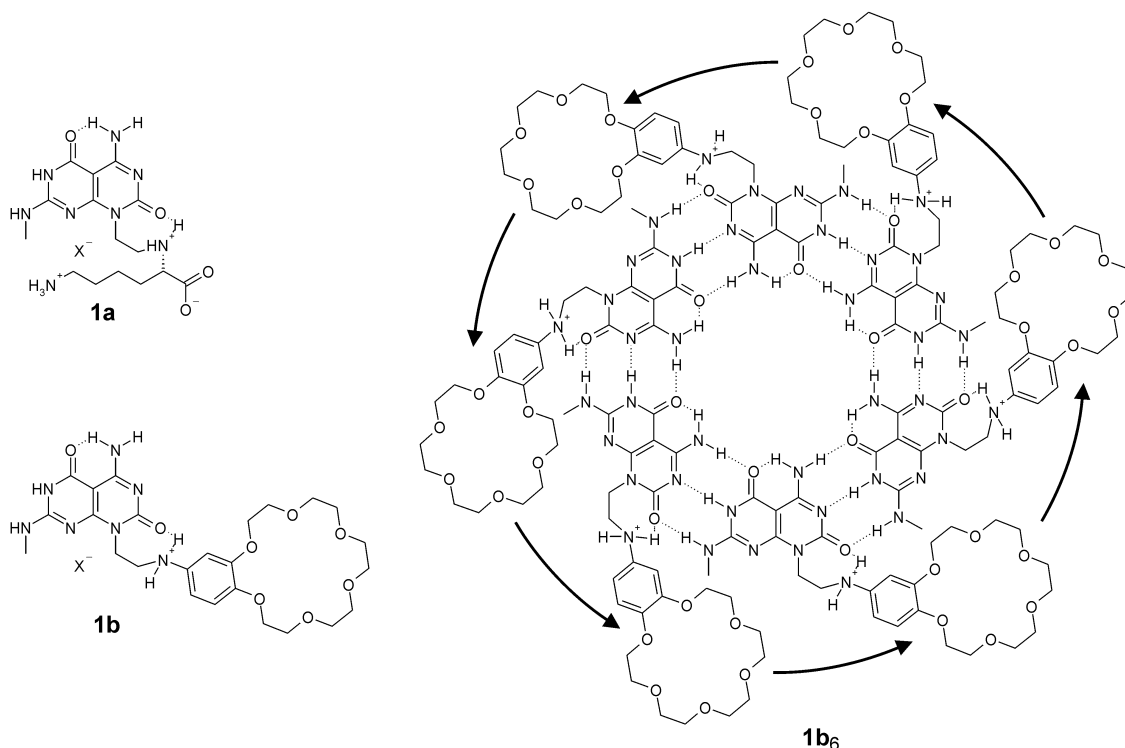


Figure 2.11 Structures of **1a** and **1b** and self-assembled rosette **1b₆**.

2.2.5 Hydrogen-bonded polymers

The term hydrogen-bonded polymers is a broad concept and can be defined as the self-assembly of monomeric units in linear aggregates through hydrogen bonding. Although by this definition many self-assembled structures in biological system can be regarded as supramolecular polymers, work on synthetic supramolecular polymers is relatively new.¹⁰² A reason for this can be that the noncovalent interactions in supramolecular polymers should be strong enough to allow significant degrees of polymerization and at the same time reversible.¹⁰³ Furthermore, cyclization is an inevitable side reaction that can occur in any step of the polymerization process. In general, the amount of cyclic species increases upon dilution since at low concentrations intramolecular cyclization is favored over intermolecular extension. For hydrogen-bonded polymers dimer formation due to association of self-complementary units is possible.

The arrangement of multiple hydrogen bonds in a recognition unit by Lehn *et al.* led to the first hydrogen-bonded polymers.^{104,105} Uracil (**2**) and diacylaminopyridine (**3**) derivatives assemble in a polymeric fashion through formation of three hydrogen bonds

between the recognition units (Figure 2.12).^{104,105} The linkers between the recognition units are based on tartaric acid. As a consequence, species based on *L*-tartaric acid give right-handed helices, and those based on *D*-tartaric acid left-handed helices.¹⁰⁴ Despite the relatively low association constant of the triple hydrogen bonds ($\sim 10^3 \text{ M}^{-1}$) these polymers have high degrees of polymerization in the bulk, because the molecules induce a mesophase in which the molecules line up and bind to each other.^{103,106} A way in which high degrees of polymerization can be obtained is the use of rigid linker units. Lehn and coworkers demonstrated this by synthesizing monomeric units comprising the same uracil and diacylamino pyridine recognition units grafted onto an anthracene moiety (Figure 2.13a).^{107,108} The hydrogen-bonded polymers obtained from these units are formed with high degrees of polymerization in lyotropic solutions.

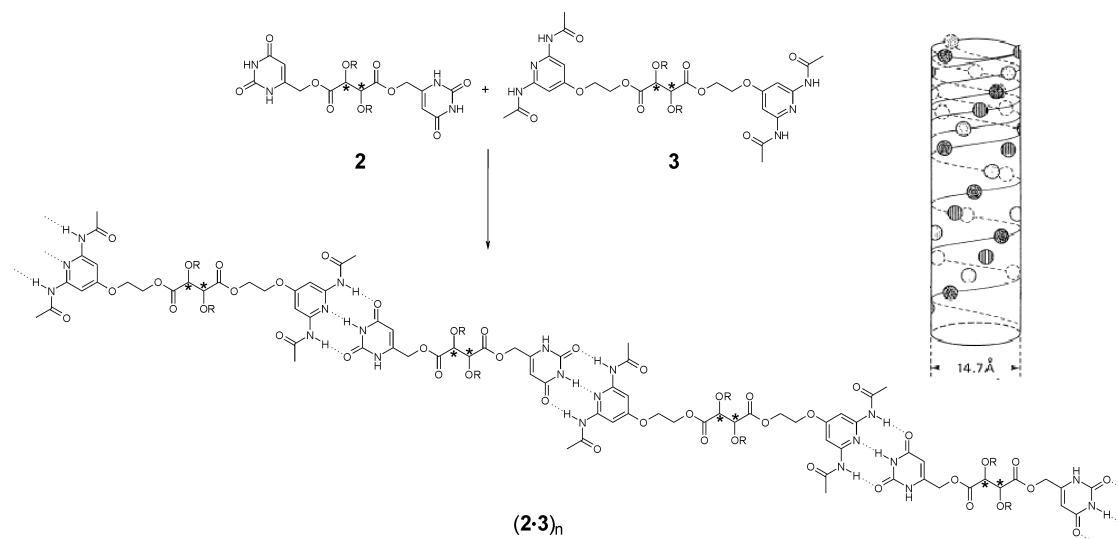


Figure 2.12 Hydrogen-bonded assembly of supramolecular helical fibers $(2\cdot 3)_n$ from 2 and 3.

Griffin *et al.* have described the formation of supramolecular polymers based on a single hydrogen bond between heterocomplementary diacids and dipyridines.^{109,110} These polymers exhibited thermotropic liquid-crystalline behavior. Another supramolecular polymeric system described by Boileau *et al.* is based on the association of self-complementary polysiloxane dicarboxylic acids through the formation of two hydrogen bonds between carboxylic acid moieties.¹¹¹

The most obvious approach to increase the interactions strength between the monomeric units, and thereby the degree of polymerization, is to increase the number of

hydrogen bonds per recognition unit. Rebek *et al.* connected two calix[4]arenes, functionalized at the upper rim with four ureido functionalities that self-assemble into polymeric capsules (Figure 2.13b).¹¹²

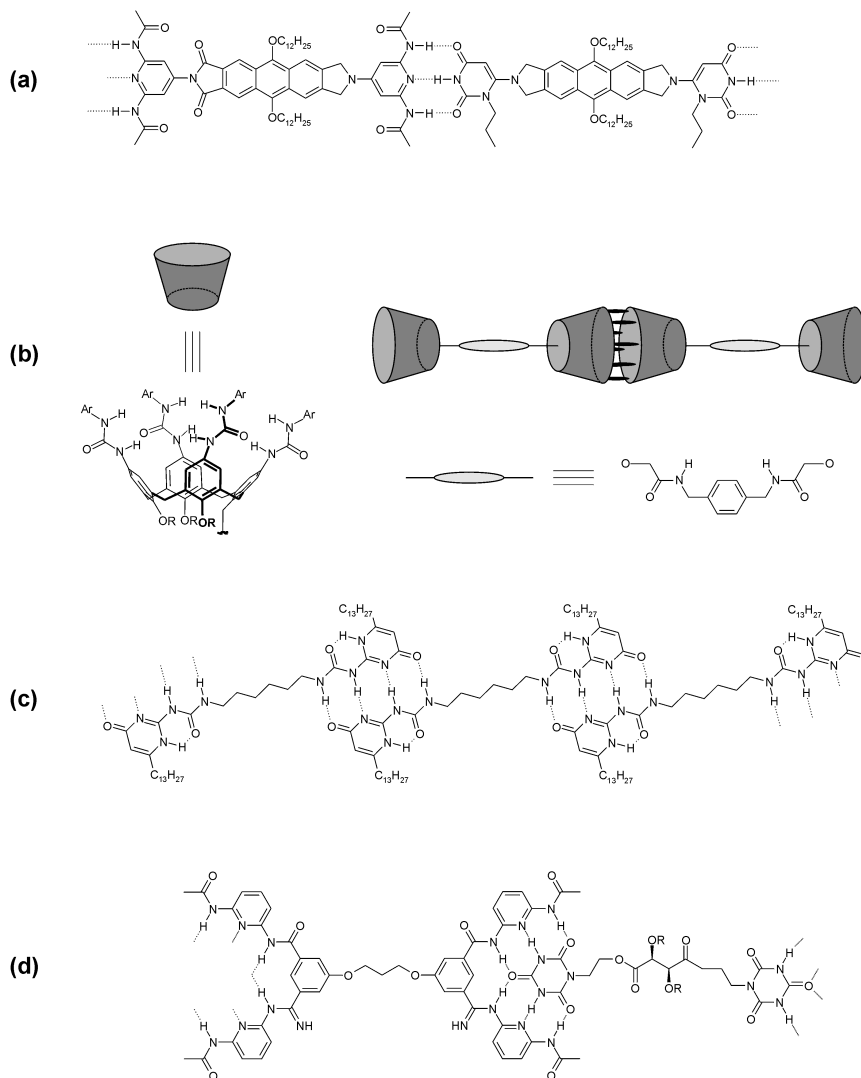


Figure 2.13 Hydrogen-bonded polymers based on multiple hydrogen bonding recognition sites.

The group of Meijer used quadruple hydrogen bonding (DDAA•AADD)^{32,113} for the formation of supramolecular polymers from self-complementary monomers (Figure 2.13c).¹¹⁴ The spontaneous polyassociation of these ditopic self-complementary monomeric units generate polymers with significant length in dilute isotropic solutions. The polymers display a concentration and temperature dependent viscosity, attributed to

changes in polymer length. Addition of monotopic end-capping units lowered the viscosities, allowing control over the polymerization process.

Lehn and coworkers have designed a hydrogen-bonded heteropolymer based on the assembly of a Janus type cyanuric wedge (ADA-ADA array) with a corresponding diaminopyridine-substituted isophthalimide (DAD-DAD array; see figure 2.13d).¹¹⁵

The assembly of helical fibers by hydrogen bonding between chiral 1,2-diaminohexanes and 1,2-dihydroxyhexanes in benzene has been reported by Hanessian *et al.*¹¹⁶ These assemblies possess a tertiary structure in which the cyclohexane rings wrap around the core of a triple-stranded helicate.

Hanabusa *et al.* described the formation of right- and left-handed helical fibers from the (R,R) and (S,S) enantiomers of long alkyl amide functionalized *trans*-1,2-cyclohexanes, respectively.¹¹⁷

Lehn and coworkers have published that 2'-pyridyl-2-pyridinecarboxamide oligomers form single and double strand helices in solution due to the bent conformation induced by intramolecular hydrogen bonding.¹¹⁸ Recently, Gottarelli *et al.* have reported the formation of supramolecular helices of 8-oxyguanosine through hydrogen bonding between the lactams.¹¹⁹ The absence of metal templates excluded formation of columnar G-quartet aggregates.

Achiral *meta*-substituted phenylene dioxamic acid diethyl ester monomers form one-dimensional hydrogen-bonded polymers that assemble into meso-helical structures in the solid state.¹²⁰

2.2.6 Rosettes

2.2.6.1 Hydrogen bonded motifs based on melamines and isocyanuric or barbituric acids

The three orthogonal ADA hydrogen-bonding arrays of isocyanuric acid (CA) are complementary with the three DAD arrays of melamine (M). Infinite 2D lattices of alternating CA and M molecules through hydrogen bonding are formed when both compounds are mixed in 1:1 ratio (Figure 2.14).¹²¹ Three submotifs can be discerned in this 2D lattice, the infinite *linear* and *crinkled* tapes and the cyclic *rosette* motif. Whitesides and Lehn showed that blocking of one of the hydrogen bonding arrays of both

cyanuric acid and melamine unit gives either one of the isolated submotifs.¹²²⁻¹²⁴ Reinhoudt *et al.* reported the assembly of well-defined tape-like structures that are stable in solution.¹²⁵ However, the cyclic rosette motif is more attractive for noncovalent synthesis because this motif has a defined shape and size.

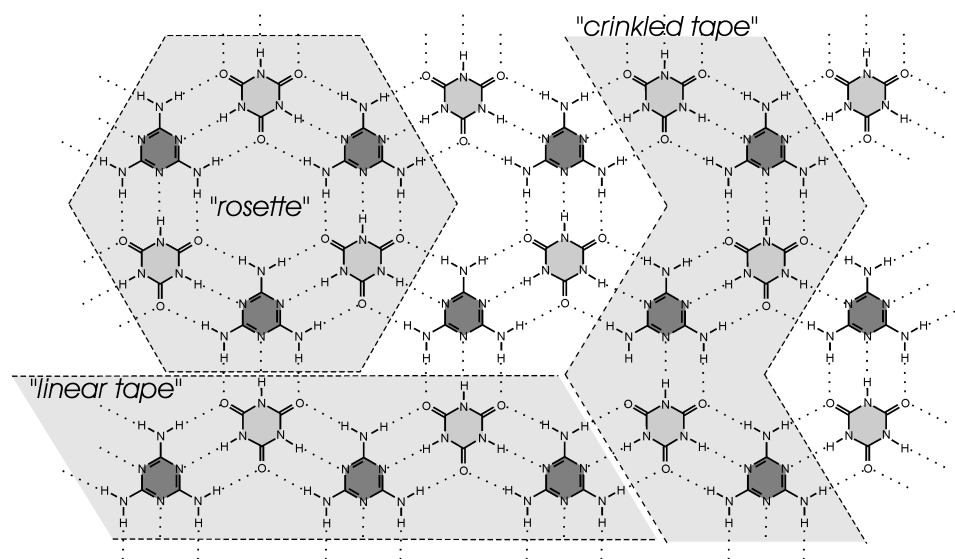


Figure 2.14 2D lattice of alternating isocyanuric acid (light grey) and melamine (dark grey) molecules held together through ADA•DAD hydrogen bond arrays. The three possible motifs, *i.e.* linear tape, crinkled tape and rosette, are highlighted.

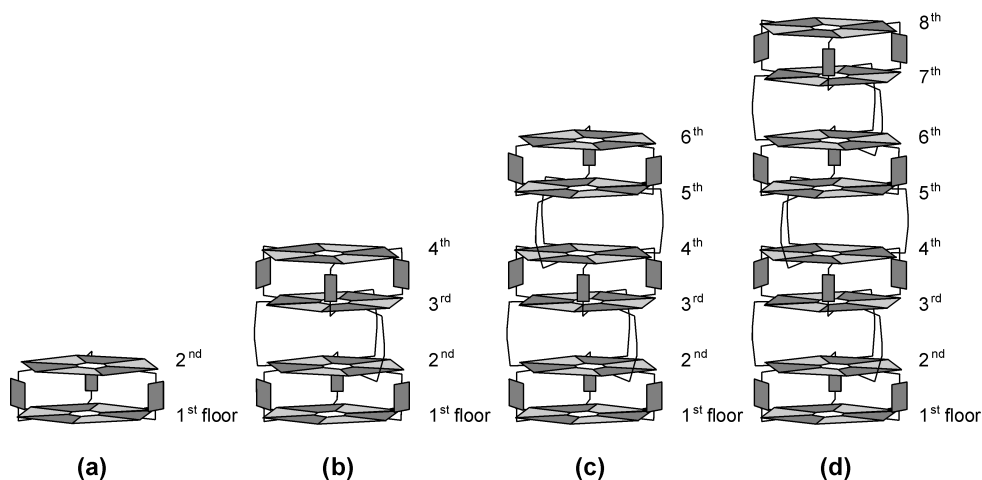
Whitesides *et al.* showed two different methods to promote selective formation of rosettes, *i.e.* *covalent preorganization* and *peripheral crowding*. The rosette structure was formed selectively when three melamine units were covalently connected through a C_3 -symmetrical central hub.¹²² This *covalent preorganization* of the melamines minimized the unfavorable entropy of rosette formation. The concept of *peripheral crowding* originates from a series of melamines functionalized with different *para* substituted phenyl moieties. Melamines with small substituents, like halogens or methyl, formed preferentially linear or crinkled tapes, while large substituents, such as *tert*-butyl gave exclusively cyclic rosette structures.¹²⁶ This indicated that molecular steric interactions around the periphery of the rosette might be used to form cyclic aggregates. The evidence for this concept came from crystallographic data and it was assumed that the solid state data reflect the thermodynamic equilibrium in solution, and that the solubility of the tapes

is much lower than that of the rosettes in apolar solvents. These assumptions are contradicting since the first is only valid when both solubilities are comparable. Our group showed that the ratio tape:rosette is largely determined by the association constants between the components and the cyclization of a linear hexamer.¹²⁷

While rosette assemblies exhibit a high thermodynamic stability, they are kinetically labile. The continuous exchange of individual components between assemblies allows for self-healing and defect-free assemblies. The exchange rate of components in these hydrogen-bonded assemblies depends strongly on the number of hydrogen bonds that have to be broken.

2.2.6.2 Assemblies with multiple rosette motifs based on melamines and isocyanuric or barbituric acids

Our group has used the rosette motif to form larger and well-defined hydrogen-bonded assemblies. Calix[4]arenes diametrically substituted with two melamine units at the upper rim form double rosette assemblies (Figure 2.15a) in the presence of two equivalents 5,5'-diethylbarbituric acid (DEB) (see also Chapter 3, sections 3.2 and 3.3).¹²⁸ Extended tetra-, hexa- and octarosettes (Figure 2.15b-d) are obtained when calix[4]arene dimelamine units are covalently attached.¹²⁹⁻¹³¹ Each rosette motif is formed through 18 hydrogen bonds. The rapid increase of number of hydrogen bonds (double rosette = 36, tetra-rosette = 72, hexa-rosette = 108 and octa-rosette = 142) in these extended assemblies renders a high thermodynamic stability. The size and degree of complexity of the rosette assemblies reaches that of small proteins. The octarosette has a size of 3.0 nm x 3.3 nm x 5.5 nm and a molecular weight of ~20kD, which is larger than small proteins like cytochrome *c* (~12kD) and myoglobin (~16 kD).



components	9	15	21	27
hydrogen bonds	36	72	108	144
height	~ 1.2 nm	~ 3.0 nm	~ 4.8 nm	~ 5.5 nm

Figure 2.15 Schematic representation of (a) double rosette, (b) tetrarosette, (c) hexarosette and (d) octarosette. Each floor represents one rosette motif.

The ability of double- and tetrarosettes to complex guest molecules with different binding modes makes them useful as receptors, as it is also shown in Chapters 5 and 6 of this thesis. For example, sacharides are stereoselectively encapsulated between the second and third floor (*endo*-receptor) of the tetrarosettes (Figure 2.15),¹³² while double rosette assemblies that are functionalized with ureido functionalities at the top and at the bottom bind *p*-substituted phenol derivatives at the surface of the assemblies (*exo*-receptor).¹³³ Also, double rosettes bind chiral carboxylic acids at the receptor surface when aminoalkyl or pyridyl functionalities are present.^{134,135} The double rosette assemblies are, so far, the only well-defined synthetic hydrogen-bonded receptors with *exo*-recognition.

2.3 Concluding remarks

In the past decade, self-assembly has been converted into a powerful tool to mimic complex biological systems, while the directive power of the hydrogen bond renders the assemblies unique. The development of molecules with arrays of several hydrogen bonds has increased the stability of the assemblies in such a way that large stable and complex self-assembled aggregates are obtained. The use of some of these hydrogen-bonded

complexes as *endo*- or *exo*-receptors allows the complexation of ions and small molecules, while tubular assemblies are able to transport ions and small molecules through membranes. Furthermore, in the last fifteen years the synthesis of supramolecular polymers assembled through hydrogen bonding has been achieved with high degree of polymerization.

The examples presented in this chapter show the enormous potential of hydrogen-bonded assemblies for the development of mimics of biological systems. In the work described in this thesis, hydrogen-bonded assemblies are further exploited to generate stable self-assembled receptors with the final aim to mimic natural antibodies. The stability of the hydrogen-bonded assemblies after the introduction of structural diversity is described, and stable assemblies are used as receptors to complex one or more guest molecules. Finally, these hydrogen-bonded receptors are incorporated in synthetic bilayer membranes mimicking the natural receptors in cell membranes.

2.4 References

1. Stryer, L. *Biochemistry*; 4th ed. Freeman and Company: New York, 1995.
2. Kirby, A. J. *Angew. Chem. Int. Ed.* **1996**, *35*, 707-724.
3. Schuster, P.; Wolschann, P. *Monatshefte Für Chemie* **1999**, *130*, 947-960.
4. Jeffrey, G. A.; Saenger, W. *Hydrogen Bonding in Biological Structures.*; Springer Verlag: Berlin, 1991.
5. Pörschke, D. *Chemical Relaxation in Molecular Biology.*; Pecht, I.; Rigler, R., Spriner-Verlag: Berlin, 1977.
6. Fiamengo, R.; Crego-Calama, M.; Reinhoudt, D. N. *Curr. Opin. Chem. Biol.* **2001**, *5*, 660-673.
7. Special Issue "Supramolecular Chemistry and Self-Assembly" *Science* **2002**, *295*, 2400-2421.
8. Haycock, R. A.; Yartsev, A.; Michelsen, U.; Sundström, V.; Hunter, C. A. *Angew. Chem. Int. Ed.* **2000**, *39*, 3616-3619.
9. Haycock, R. A.; Hunter, C. A.; James, D. A.; Michelsen, U.; Sutton, L. R. *Org. Lett.* **2000**, *2*, 2435-2438.
10. Sessler, J. L.; Sathiosatham, M.; Brown, C. T.; Rhodes, T. A.; Wiederrecht, G. J.

- Am. Chem. Soc.* **2001**, *123*, 3655-3660.
11. Kirby, J. P.; Roberts, J. A.; Nocera, D. G. *J. Am. Chem. Soc.* **1997**, *119*, 9230-9236.
 12. Schenning, A. P. H. J.; Spelberg, L. J. H.; Hubert, D. H. W.; Feiters, M. C.; Nolte, R. J. M. *Chem. Eur. J.* **1998**, *4*, 871-880.
 13. Kang, J.; Rebek, J. Jr. *Nature* **1997**, *385*, 50-52.
 14. Whitesides, G. M.; Mathias, J. P.; Seto, C. *Science* **1991**, *254*, 1312-1319.
 15. Bong, D. T.; Clark, T. D.; Granja, J. R.; Ghadiri, M. R. *Angew. Chem. Int. Ed.* **2001**, *40*, 988-1011.
 16. Swiegers, G. F.; Malefetse, T. J. *Chem. Rev.* **2000**, *100*, 3483-3537.
 17. Conn, M. M.; Rebek, J. Jr. *Chem. Rev.* **1997**, *97*, 1647-1668.
 18. Prins, L. J.; Reinhoudt, D. N.; Timmerman, P. *Angew. Chem. Int. Ed.* **2001**, *40*, 2382-2426.
 19. MacDonald, J. C.; Whitesides, G. M. *Chem. Rev.* **1994**, *94*, 2383-2420.
 20. Zhao, X.; Xhang, Y.-L.; Fowler, F.; Lauher, J. W. *J. Am. Chem. Soc.* **1990**, *112*, 6627-6634.
 21. Hine, J.; Hahn, S.; Hwang, J. *J. Org. Chem.* **1988**, *53*, 884-887.
 22. Etter, M. C.; Urbańczyk-Lipkowska, Z.; Zia-Ebrahimi, M.; Panunto, T. W. *J. Am. Chem. Soc.* **1990**, *112*, 8415-8426.
 23. Wash, P. L.; Maverick, E.; Chiefari, J.; Lightner, D. A. *J. Am. Chem. Soc.* **1997**, *119*, 3802-3806.
 24. Garcia-Tellado, F.; Geib, S. J.; Goswami, S.; Hamilton, A. D. *J. Am. Chem. Soc.* **1991**, *113*, 9265-9269.
 25. Liao, R.-F.; Lauher, J. W.; Fowler, F. W. *Tetrahedron* **1996**, *52*, 3153-3162.
 26. Zimmerman, S. C.; Murray, T. J. *Tetrahedron Lett.* **1994**, *35*, 4077-4080.
 27. Sartorius, J.; Schneider, H. J. *Chem. Eur. J.* **1996**, *2*, 1446-1452.
 28. Hamilton, A. D.; Little, D. *Chem. Commun.* **1990**, 297-300.
 29. Park, T. K.; Schroeder, J.; Rebek Jr., J. *J. Am. Chem. Soc.* **1991**, *113*, 5125-5127.
 30. Murray, T. J.; Zimmerman, S. C. *J. Am. Chem. Soc.* **1992**, *114*, 4010-4011.

31. Fenlon, E. E.; Murray, T. J.; Balloga, M. H.; Zimmerman, S. C. *J. Org. Chem.* **1993**, *58*, 6625-6628.
32. Beijer, F. H.; Kooijman, H.; Spek, A. L.; Sijbesma, R. P.; Meijer, E. W. *Angew. Chem. Int. Ed.* **1998**, *37*, 75-78.
33. Williams, L. D.; Chawla, B.; Shaw, B. S. *Biopolymers* **1987**, *26*, 591-603.
34. Williams, L. D.; Williams, N. G.; Shaw, B. S. *J. Am. Chem. Soc.* **1990**, *112*, 829-833.
35. Roberts, C.; Bandaru, R.; Switzer, C. *J. Am. Chem. Soc.* **1997**, *119*, 4640-4649.
36. A review about self-assembled capsules: Conn, M. M.; Rebek J., Jr. *Chem. Rev.* **1997**, *97*, 1647-1668.
37. Vreekamp, R. H.; Verboom, W.; Reinhoudt, D. N. *J. Org. Chem.* **1996**, *61*, 4282-4288.
38. Koh, K.; Araki, K.; Shinkai, S. *Tetrahedron Lett.* **1994**, *35*, 8255-8258.
39. Scheerder, J.; Vreekamp, R.; Engbersen, J. F. J.; Verboom, W.; Duynhoven, J. P. M.; Reinhoudt, D. N. *J. Org. Chem.* **1996**, *61*, 3476-3481.
40. Shimizu, K. D.; Rebek Jr, J. *Proc. Natl. Acad. Sci. USA* **1995**, *92*, 12403-12407.
41. Brody, M. S.; Schalley, C. A.; Rudkevich, D. M.; Rebek, J. Jr. *Angew. Chem. Int. Ed.* **1996**, *38*, 1640-1644.
42. Mogck, O.; Böhmer, V.; Vogt, W. *Tetrahedron* **1996**, *52*, 8489-8496.
43. Schally, C. A.; Castellano, R. K.; Brody, M. S.; Rudkevich, D. M.; Siuzdak, G.; Rebek Jr, J. *J. Am. Chem. Soc.* **1999**, *121*, 4568-4579.
44. Hamann, B. C.; Shimizu, K. D.; Rebek, J. Jr. *Angew. Chem. Int. Ed.* **1996**, *35*, 1326-1329.
45. Vysotsky, M. O.; Thondorf, I.; Böhmer, V. *Chem. Commun.* **2001**, 1890-1891.
46. Castellano, R. K.; Rebek, J. Jr. *J. Am. Chem. Soc.* **1998**, *120*, 3657-3663.
47. Castellano, R. K.; Kim, B. H.; Rebek, J. Jr. *J. Am. Chem. Soc.* **1997**, *119*, 12671-12672.
48. Pop, A.; Vysotsky, M. O.; Saadioui, M.; Böhmer, V. *Chem. Commun.* **2003**, 1124-1125.
49. Cho, Y. L.; Rudkevich, D. M.; Rebek Jr, J. *J. Am. Chem. Soc.* **2000**, *122*, 9868-9869.

50. Brewster, R. E.; Shuker, S. B. *J. Am. Chem. Soc.* **2002**, *124*, 7902-7903.
51. Rose, K. N.; Barbour, L. J.; Orr, G. W.; Atwood, J. L. *Chem. Commun.* **1998**, 407-408.
52. Murayama, K.; Aoki, K. *Chem. Commun.* **1998**, 607-608.
53. Shivanyuk, A.; Paulus, E. F.; Böhmer, V. *Angew. Chem. Int. Ed.* **1999**, *38*, 2906-2909.
54. Higler, I.; Grave, L.; Breuning, E.; Verboom, W.; De Jong, F.; Fyles, T.; Reinhoudt, D. N. *Eur. J. Org. Chem.* **2000**, 1727-1734.
55. Kobayashi, K.; Ishii, K.; Sakamoto, S.; Shirasaka, T.; Yamaguchi, K. *J. Am. Chem. Soc.* **2003**, *125*, 10615-10624.
56. MacGillivray, L. R.; Atwood, J. L. *Nature* **1997**, *389*, 469-472.
57. Shivanyuk, A.; Rebek Jr., J. *Proc. Natl. Acad. Sci. USA* **2001**, *98*, 7662-7665.
58. Shivanyuk, A.; Rebek Jr., J. *Chem. Commun.* **2001**, 2424-2425.
59. Chapman, R. G.; Sherman, J. C. *J. Am. Chem. Soc.* **1995**, *117*, 9081-9082.
60. Chapman, R. G.; Olovsson, G.; Trotter, J.; Sherman, J. C. *J. Am. Chem. Soc.* **1998**, *120*, 6252-6260.
61. Chapman, R. G.; Sherman, J. C. *J. Am. Chem. Soc.* **1998**, *120*, 9818-9826.
62. Heinz, T.; Rudkevich, D. M.; Rebek Jr., J. *Nature* **1998**, *394*, 764-766.
63. Körner, S. K.; Tucci, F. C.; Rudkevich, D. D.; Heinz, T.; Rebek Jr., J. *Chem. Eur. J.* **2000**, *6*, 187-195.
64. Hayashida, O.; Shivanyuk, A.; Rebek Jr., J. *Angew. Chem. Int. Ed.* **2002**, *41*, 3423-3426.
65. Kobayashi, K.; Shirasaka, T.; Yamaguchi, K.; Sakamoto, S.; Horn, E.; Furukawa, N. *Chem. Commun.* **2000**, 41-42.
66. Wyler, R.; De Mendoza, J.; Rebek Jr., J. *Angew. Chem. Int. Ed.* **1993**, *32*, 1699-1701.
67. Branda, N.; Wyler, R.; Rebek Jr., J. *Science* **1994**, *263*, 1267-1268.
68. Meissner, R. S.; Rebek Jr., J.; De Mendoza, J. *Science* **1995**, *270*, 1485-1488.
69. Meissner, R.; Garcias, X.; Mecozzi, S.; Rebek Jr., J. *J. Am. Chem. Soc.* **1997**, *119*, 77-85.

70. Grotzfeld, R. M.; Branda, N.; Rebek Jr., J. *Science* **1996**, *271*, 487-489.
71. Martín, T.; Obst, U.; Rebek Jr., J. *Science* **1998**, *281*, 1842-1845.
72. Huizenga, D. E.; Szostak, J. W. *Biochemistry* **1995**, *34*, 656-665.
73. Guschlbauer, W.; Chantot, J. F.; Thiele, D. *J. Biomol. Struct. Dynam.* **1990**, *8*, 491-511.
74. Davis, J. T.; Tirumala, S.; Jenssen, J. R.; Radler, E.; Fabris, D. *J. Org. Chem.* **1995**, *60*, 4167-4176.
75. Marlow, A. L.; Mezzina, E.; Spada, G. P.; Masiero, S.; Davis, J. T.; Gottarelli, G. *J. Org. Chem.* **1999**, *64*, 5116-5123.
76. Forman, S. L.; Fettinger, J. C.; Pieraccini, S.; Gottarelli, G.; Davis, J. T. *J. Am. Chem. Soc.* **2000**, *122*, 4060-4067.
77. Davis, J. T.; Tirumala, S. K.; Marlow, A. L. *J. Am. Chem. Soc.* **1997**, *119*, 5271-5272.
78. Tirumala, S. T.; Davis, J. T. *J. Am. Chem. Soc.* **1997**, *119*, 2669-2776.
79. Shi, X.; Fettinger, J. C.; Davis, J. T. *J. Am. Chem. Soc.* **2001**, *123*, 6738-6739.
80. Kotch, F. W.; Fettinger, J. C.; Davis, J. T. *Org. Lett.* **2000**, *2*, 3277-3280.
81. Shi, X.; Fettinger, J. C.; Davis, J. T. *Angew. Chem. Int. Ed.* **2001**, *40*, 2827-2831.
82. Cai, M.; Marlow, A. L.; Fettinger, J. C.; Fabris, D.; Haverlock, T. J.; Moyer, B. A.; Davis, J. T. *Angew. Chem. Int. Ed.* **2000**, *39*, 1283-1285.
83. Marlow, A. L.; Davis, J. T. *Tetrahedron Lett.* **1999**, *40*, 3539-3542.
84. Sessler, J. L.; Sathiosatham, M.; Doerr, K.; Lynch, V.; Abboud, K. A. *Angew. Chem. Int. Ed.* **2000**, *39*, 1300-1303.
85. Eisenberg, B. *Acc. Chem. Res.* **1998**, *31*, 117-123.
86. DeSantis, P.; Morosetti, S.; Rizzo, R. *Macromolecules* **1974**, *7*, 52-58.
87. Ghadiri, M. R.; Granja, J. R.; Milligan, R. A.; McRee D.E.; Khazanovich, N. *Nature* **1993**, *366*, 324-327.
88. Khazanovich, N.; Granja, J. R.; McRee, D. E.; Milligan, R. A.; Ghadiri, M. R. *J. Am. Chem. Soc.* **1994**, *116*, 6011-6012.
89. Ghadiri, M. R.; Granja, J. R.; Buehler, L. K. *Nature* **1994**, *369*, 301-304.

90. Granja, J. R.; Ghadiri, M. R. *J. Am. Chem. Soc.* **1994**, *116*, 10785-10786.
91. Sánchez-Quesada, J.; Kim, H. S.; Ghadiri, M. R. *Angew. Chem. Int. Ed.* **2001**, *40*, 2503-2506.
92. Seebach, D.; Matthews, J. L.; Meden, A.; Wessels, T.; Baerlocher, C.; McCusker, L. B. *Helv. Chim. Acta.* **1997**, *80*, 173-182.
93. Clark, T. D.; Buehler, L. K.; Ghadiri, M. R. *J. Am. Chem. Soc.* **1998**, *120*, 651-656.
94. Weiss, L. A.; Sakai, N.; Ghebremariam, B.; Ni, C.; Matile, S. *J. Am. Chem. Soc.* **1997**, *119*, 12142-12149.
95. Baumeister, B.; Matile, S. *Chem. Eur. J.* **2000**, *6*, 1739-1749.
96. Sakai, N.; Majumdar, N.; Matile, S. *J. Am. Chem. Soc.* **1999**, *121*, 4294-4295.
97. Baumeister, B.; Sakai, N.; Matile, S. *Angew. Chem. Int. Ed.* **2000**, *39*, 1955-1958.
98. Kimizuka, N.; Kawasaki, T.; Hirata, K.; Kunitake, T. *J. Am. Chem. Soc.* **1995**, *117*, 6360-6361.
99. Fenniri, H.; Mathivanan, P.; Vidale, K. L.; Sherman, D. M.; Hallenga, K.; Wood, K. V.; Stowell, J. G. *J. Am. Chem. Soc.* **2001**, *123*, 3854-3855.
100. Fenniri, H.; Deng, B.-L.; Ribbe, A. E. *J. Am. Chem. Soc.* **2002**, *124*, 11064-11072.
101. Fenniri, H.; Deng, B. L.; Ribbe, A. E.; Hallenga, K.; Jacob, J.; Thiyagarajan, P. *Proc. Natl. Acad. Sci. USA* **2002**, *99*, 6487-6492.
102. Osawa, F.; Asakura, S. *Thermodynamics of the Polymerization of Protein.*; Academic Press: New York, 1975.
103. Ten Cate, A. T.; Sijbesma, R. P. *Macromol. Rapid. Commun.* **2002**, *23*, 1094-1112.
104. Gulik-Krzywicki, T.; Fouquey, C.; Lehn, J.-M. *Proc. Natl. Acad. Sci. USA* **1993**, *90*, 163-167.
105. Fouquey, C.; Lehn, J.-M.; Levelut, A.-M. *Adv. Mater.* **1990**, *2*, 254-257.
106. Ciferri, A. *Liq. Cryst.* **1999**, *26*, 489-494.
107. Kotera, M.; Lehn, J.-M.; Vigneron, J.-P. *Chem. Commun.* **1994**, 197-200.
108. Kotera, M.; Lehn, J.-M.; Vigneron, J.-P. *Tetrahedron* **1995**, *51*, 1953-1972.
109. Bladon, P.; Griffin, A. C. *Macromolecules* **1993**, *26*, 6604-6610.
110. Alexander, C.; Jariwala, C. P.; Lee, C. M.; Griffin, A. C. *Macromol. Symp.* **1994**,

- 77, 283-294.
111. Abed, S.; Boileau, S.; Bouteiller, L.; Lacoudre, N. *Polymer Bull.* **1997**, *39*, 317-324.
112. Castellano, R. K.; Rudkevich, D. M.; Rebek Jr., J. *Proc. Natl. Acad. Sci. USA* **1997**, *94*, 7132-7137.
113. Beijer, F. H.; Sijbesma, R. P.; Kooijman, H.; Spek, A. L.; Meijer, E. W. *J. Am. Chem. Soc.* **1998**, *120*, 6761-6769.
114. Sijbesma, R. P.; Beijer, F. H.; Brunsveld, L.; Folmer, B. J. B.; Hirschberg, J. H. K.; Lange, R. F. M.; Lowe, J. K. L.; Meijer, E. W. *Nature* **1997**, *278*, 1601-1604.
115. Berl, V.; Schmutz, M.; Krische, M. J.; Khoury, R. G.; Lehn, J.-M. *Chem. Eur. J.* **2002**, *8*, 1227-1244.
116. Hanessian, S.; Gomtsyan, A.; Simard, M.; Roelens, S. *J. Am. Chem. Soc.* **1994**, *116*, 4495-4496.
117. Hanabusa, K.; Yamada, M.; Kimura, M.; Shirai, H. *Angew. Chem. Int. Ed.* **1996**, *35*, 1949-1951.
118. Berl, V.; Huc, I.; Khoury, R. G.; Krische, M. -J.; Lehn, J.-M. *Nature* **2000**, *407*, 720-723.
119. Giorgi, T.; Lena, S.; Mariani, P.; Cremonini, M. A.; Masiero, S.; Pieraccini, S.; Rabe, J. P.; Samori, P.; Spada, G. P.; Gottarelli, G. *J. Am. Chem. Soc.* **2003**, *125*, 14741-14749.
120. Blay, G.; Fernández, I.; Pedro, J. R.; Ruiz-García, R.; Muñoz, M. C.; Carrasco, R. *Eur. J. Org. Chem.* **2003**, 1627-1630.
121. Ranganatham, A.; Pedireddi, V. R.; Rao, C. N. R. *J. Am. Chem. Soc.* **1999**, *121*, 1752-1753.
122. Seto, C. T.; Whitesides G. M. *J. Am. Chem. Soc.* **1990**, *112*, 6409-6411.
123. Zerkowski, J. A.; Seto, C. T.; Wierda, D. A.; Whitesides, G. M. *J. Am. Chem. Soc.* **1990**, *112*, 9025-9026.
124. Lehn, J.-M.; Mascal, M.; DeCian, A.; Fischer, J. *Chem. Commun.* **1990**, 479-481.
125. Lipkowski, P.; Bielejewska, A.; Kooijman, H.; Spek, A. L.; Timmerman, P.; Reinhoudt, D. N. *Chem. Commun.* **1999**, 1311-1312.
126. Mathias, J. P.; Simanek, E. E.; Zerkowski, J. A.; Seto, C. T.; Whitesides, G. W. *J. Am. Chem. Soc.* **1994**, *116*, 4316-4325.
127. Bielejewska, A. G.; Marjo, C. E.; Prins, L. J.; Timmerman, P.; De Jong, F.;

- Reinhoudt, D. N. *J. Am. Chem. Soc.* **2001**, *123*, 7518-7533.
128. Vreekamp, R. H.; van Duynhoven, J. P. M.; Reinhoudt, D. N. *Angew. Chem. Int. Ed.* **1996**, *35*, 1215-1218.
129. Jolliffe, K. A.; Timmerman, P.; Reinhoudt, D. N. *Angew. Chem. Int. Ed.* **1999**, *38*, 933-937.
130. Paraschiv, V.; Crego-Calama, M.; Timmerman, P.; Reinhoudt, D. N. *J. Org. Chem.* **2001**, *66*, 8297-8301.
131. Prins, L. J.; Neuteboom, E. E.; Paraschiv, V.; Crego-Calama, M.; Timmerman, P.; Reinhoudt, D. N. *J. Org. Chem.* **2002**, *67*, 4808-4820.
132. Ishi-I, T.; Mateos-Timoneda, M. A.; Timmerman, P.; Crego-Calama, M.; Reinhoudt, D. N.; Shinkai, S. *Angew. Chem. Int. Ed.* **2003**, *42*, 2300-2305.
133. Kerckhoffs, J. M. C. A.; Ishi-I, T.; Paraschiv, V.; Timmerman, P.; Crego-Calama, M.; Shinkai, S.; Reinhoudt, D. N. *Org. Biomol. Chem.* **2003**, *1*, 2596-2603.
134. Ishi-I, T.; Crego-Calama, M.; Timmerman, P.; Reinhoudt, D. N.; Shinkai, S. *Angew. Chem. Int. Ed.* **2002**, *41*, 1924-1929.
135. Ishi-I, T.; Crego-Calama, M.; Timmerman, P.; Reinhoudt, D. N.; Shinkai, S. *J. Am. Chem. Soc.* **2002**, *124*, 14631-14641.

Chapter 3

Towards self-assembled receptors: functionalized double rosette assemblies

In this chapter, calix[4]arene dimelamines are described that are functionalized with alkyl, aminoalkyl, ureido, pyridyl, carbohydrate, amino acid and peptide functionalities, and assembled with barbituric acid or cyanuric acid derivatives into well-defined hydrogen-bonded assemblies. The thermodynamic stability of these hydrogen-bonded assemblies was studied by CD spectroscopy in mixtures of CHCl₃ and MeOH. The stability depends on steric factors and the polarity of the functional groups connected to the assembly components.

3.1 Introduction

Natural receptors exhibit extraordinary high binding affinity and selectivity for a particular substrate. The binding affinity and selectivity arises from the cooperative action of many main and side chain functionalities oriented in a *three-dimensional* fashion around the target molecule.

In general, a rational-based design of synthetic molecules is used to mimic the binding properties of natural antibodies. However, large covalent systems are difficult to synthesize and structural diversity can only be introduced into the scaffolds at the expense of challenging and time consuming synthesis. Therefore, self-assembly of nanostructures using multiple weak *noncovalent* interactions is considered to be a powerful tool for the understanding, modeling, and mimicking of biological systems.¹ A major advantage is that self-assembled structures are generally formed under thermodynamically controlled conditions, often giving rise to quantitative yields of product.²

Natural antibodies provide a perfect example of self-assembled receptors, since they consist of four different peptide chains, two heavy (H) and two light (L) chains (Figure 3.1a), which are held together mainly by noncovalent interactions, reinforced by covalent disulfide bonds.³ Natural antibodies have a hyper variable region (Fab) and a constant region (Fc). Because differences between antibodies arise from differences in the Fab fragments it is not surprising that specific antigen recognition sites are located in this part of the antibody. Such self-assembled systems provide nature with a powerful tool to generate many different antibodies.

For the design of synthetic receptors in our group a strategy was developed that is similar to the assembly of antibodies.⁴ This approach consists of the formation of a synthetic self-assembling platform in which a double rosette motif is formed based on multiple hydrogen-bonds^{5,6} (see Section 3.2). Functionalization of the individual components with small functional groups (X or Y) generates noncovalent assemblies with functional fragments that generate a potential guest-binding region (variable region). Structural diversity in the guest-binding region can be generated both at a covalent level (variation in functional groups) and at a supramolecular level (statistical combination of fixed number of molecular components, Figure 3.1b).

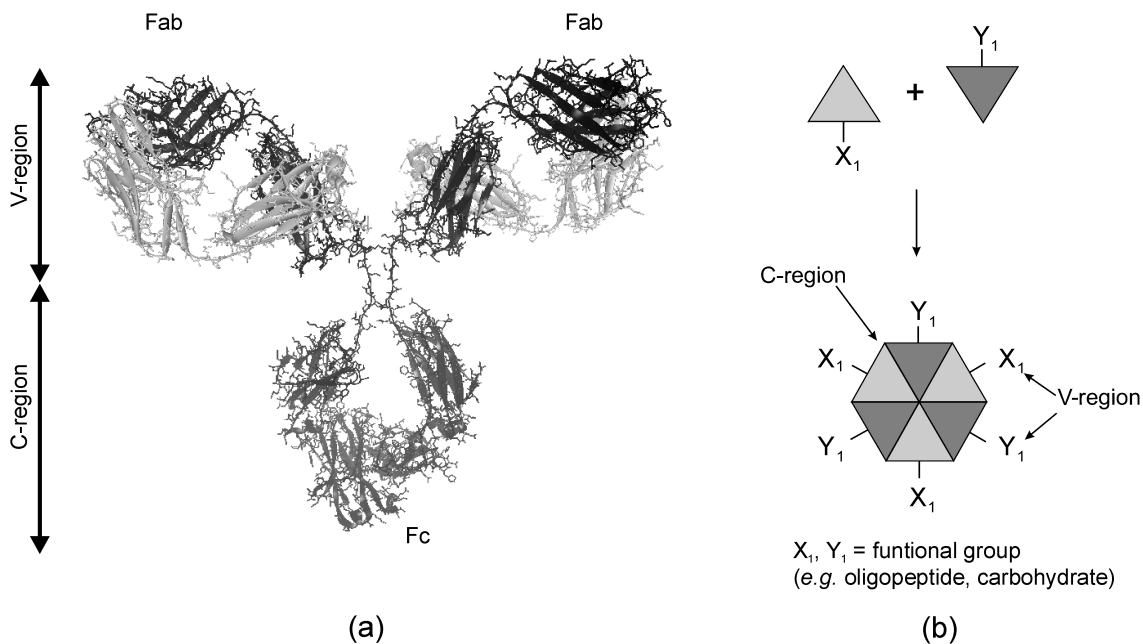


Figure 3.1 (a) Structure of a natural antibody (Human IgG1); heavy peptide chains and light peptide chains are depicted in black and gray, respectively, (b) Self-assembly of small functional groups via synthetic self-assembled platforms (rosettes).

In general, a major drawback in the use of hydrogen-bonded supramolecular systems is their low stability in polar solvents, because these solvents compete with the hydrogen bonding motif that holds the system together. On the other hand, natural host-guest recognition events take place in aqueous environment or at cell membranes. Therefore, the study of the formation and the stability of self-assembled hydrogen bonded systems in polar solvents is very important.

This chapter focuses on the formation and stability of differently functionalized hydrogen-bonded assemblies in competitive solvent mixtures of different polarity. Both, steric hindrance induced by linear or branched alkyl chains and the effect of simple polar functionalities, such as amino alkyl, ureido, and pyridyl moieties on the stability of double rosettes were investigated. Subsequently, the stability of more complex assemblies bearing sugars, amino acids or small peptide fragments was examined. Before discussing the results of these studies, the formation and characterization of the double rosettes involved are described.

3.2 Formation of double rosette assemblies

Using the rosette motif introduced by Whitesides,^{7,8} our group has reported the noncovalent synthesis of double rosette assemblies $1_3 \cdot (\text{DEB}/\text{CYA})_6$ that are held together by a total of 36 hydrogen bonds. The assemblies are formed spontaneously by mixing of calix[4]arenes diametrically substituted at the upper rim with two melamine units (**1**) with 2 equivalents of either barbituric acid (BAR) or cyanuric acid (CYA) derivatives (Figure 3.2). The assemblies consist of two flat rosette motifs connected via three calix[4]arene molecules. The assemblies are stable in apolar solvents like chloroform, benzene and toluene even at 10^{-4} M.^{5,9}

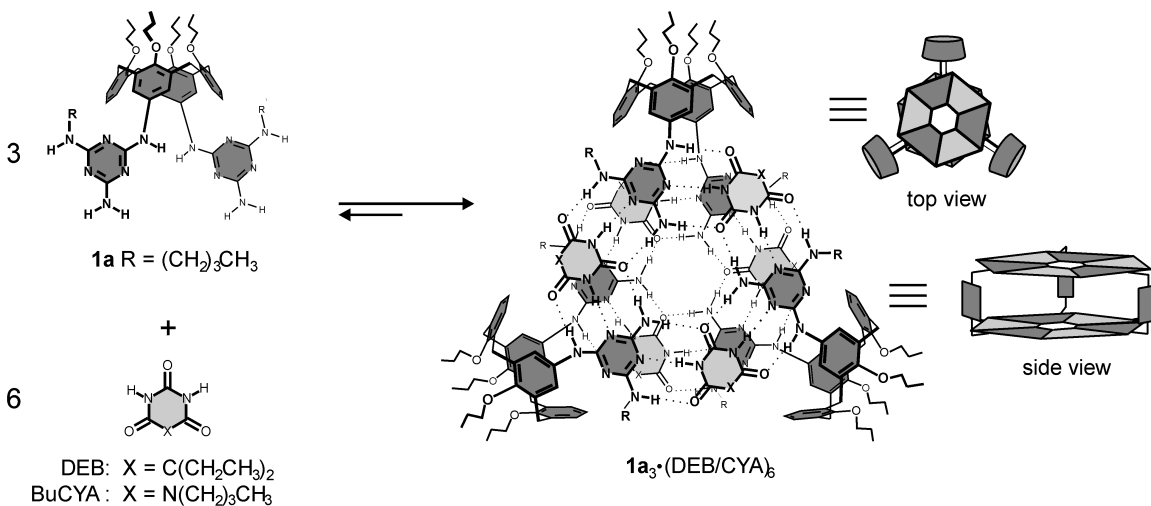


Figure 3.2 Formation of the double rosette assemblies $1_3 \cdot (\text{DEB}/\text{BuCYA})_6$ from three calix[4]arene dimelamines **1a** and six 5,5-diethylbarbiturate (DEB) or *n*-butyl cyanurate (BuCYA) molecules.

Three conformational isomers of double rosette assemblies can be formed, i.e. one staggered (D_3) isomer and two eclipsed (symmetrical (C_{3h}) and unsymmetrical (C_s)) isomers (Figure 3.3). In the *staggered* isomer the two melamines on each calix[4]arene are in an anti-parallel orientation with respect to each other, while in the *eclipsed* isomers the melamines on each calix[4]arene unit are parallel.

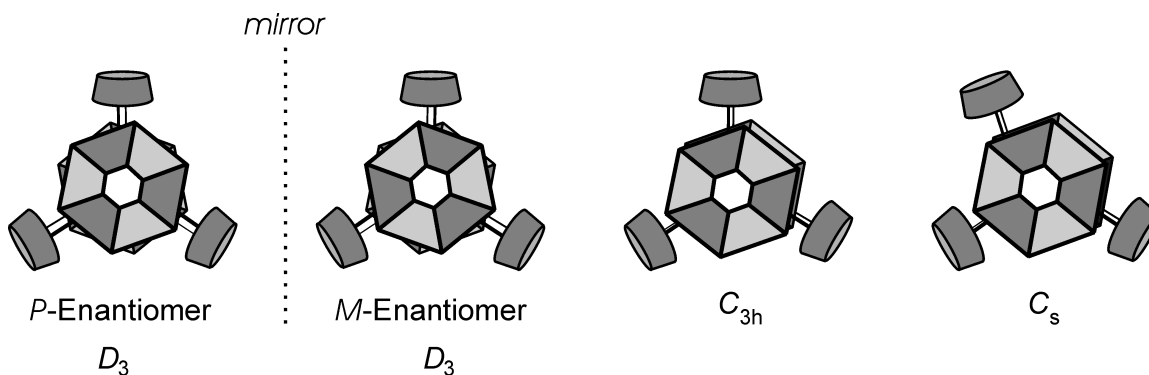


Figure 3.3 Schematic representations of the three isomeric forms for double rosette assemblies: staggered (D_3), symmetrical eclipsed (C_{3h}), and unsymmetrical eclipsed (C_s).

3.3 Characterization of double rosette assemblies

Double rosette assemblies can be characterized by ^1H NMR spectroscopy in solution.^{10,11} In the region between 13 and 16 ppm, diagnostic signals for the BAR/CYA hydrogen-bonded imide NH protons are present. The number of signals that is observed depends on the symmetry of the assembly. For the D_3 and the C_{3h} symmetry only two different hydrogen-bonded imide NH protons can be distinguished and therefore two different signals are observed. For the C_s isomer six hydrogen-bonded imide NH protons are different and thus six signals are observed. With some CYA derivatives all possible isomers are formed,¹² while with BAR derivatives preferentially D_3 isomers are obtained.

Assemblies $\mathbf{1}_3\cdot(\text{DEB}/\text{BuCYA})_6$ are formed as an equal mixture of (*M*)- and (*P*)-enantiomers when the building blocks do not contain chiral centers (Figure 3.3).^{5,9,13,14} When one of the assembly components (**1** or BAR/CYA) is chiral, complete induction of supramolecular chirality is observed. For example, when *R,R* dimelamines assemble with BAR or CYA only the (*M*)-diastereomer is formed, while the assembly of *S,S* dimelamines with BAR or CYA gives only the (*P*)-diastereomer. This property makes it possible to study double rosette formation using circular dichroism (CD) spectroscopy.¹⁵ Double rosette assemblies exhibit a very strong induced CD signal ($|\Delta\epsilon_{\text{max}}| \sim 100 \text{ l}\cdot\text{mol}^{-1}\cdot\text{cm}^{-1}$), while the individual chiral components are hardly CD active ($|\Delta\epsilon_{\text{max}}| < 8.1 \text{ l}\cdot\text{mol}^{-1}\cdot\text{cm}^{-1}$). The observed CD is a direct result of assembly formation. The CD curves of these (*M*)- and (*P*)-assemblies are perfect mirror images, reflecting their enantiomeric

relationship. Therefore, the sign of the CD curve is a good probe for the supramolecular chirality of double rosettes (Figure 3.4).

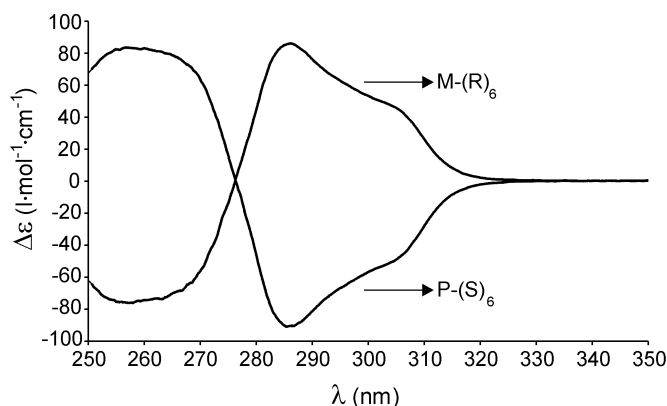


Figure 3.4 Example of CD spectra obtained for (*M*)- and (*P*)-double rosettes after chiral induction by *R,R*-dimelamines and *S,S*-dimelamines, respectively.

MALDI-TOF mass spectrometry using the Ag^+ -labeling technique^{6,16} gives also evidence for double rosette formation. This technique is extremely mild and provides a non-destructive method to generate positively charged assemblies by coordination of Ag^+ to a cyano group or by complexation of Ag^+ between two phenyl rings.

The X-ray crystal structure of assembly **1a**₃•(DEB)₆ provides unequivocal evidence that the assembly exists as the *D*₃-isomer (Figure 3.5). Furthermore, it shows that the calix[4]arene units are fixed in a *pinched cone* conformation, which is the only conformation that allows simultaneous participation of the calix[4]arene units in both the upper and the lower rosette motif. The two rosette motifs are stacked on top of each other with an interatomic separation of 3.5 Å at the edges to 3.2 Å in the centre of the rosette.⁹ The assemblies have a height of 1.2 nm and a width of ~3.0 nm.

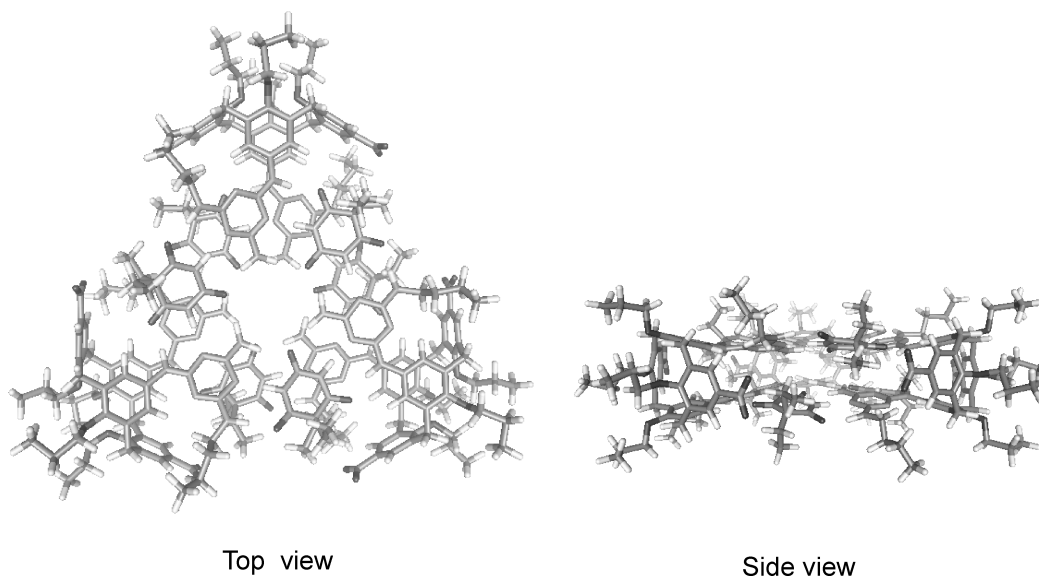


Figure 3.5 X-ray crystal structure of assembly $1a_3 \cdot (DEB)_6$.

3.4 Results and discussion

The concave 3D-positioning of different functionalities around a central cavity provides the basis for natural receptors to bind substrates and catalyze biochemical transformations with exquisite regio- and stereoselectivity. To mimic natural antibodies structural diversity has to be introduced to the double rosette assemblies.

The thermodynamic stability of double rosette assemblies might be affected when different functionalities are introduced in the double rosette platform. For example, hydrogen bond donating or accepting groups can possibly interfere with the rosette platform formation, while bulky groups can cause steric strain in the assembly and decrease their thermodynamic stability.

Previously it was shown, that double rosette assemblies with DEB and dimelamines functionalized with amide or ureido functionalities are stable in chloroform.¹⁷ A double rosette assembled from dimelamines functionalized with glycine and DEB has the same stability, while increase of the bulky side chains of the amino acids using valine or leucine decreases the stability.

With the aim to generate stable and structural diverse double rosettes, calix[4]arene dimelamines bearing alkyl (**1a-c**), aminoalkyl (**2a-g**), ureido (**3**), pyridyl (**4a-c**), sugar (**5a-e**), amino acid (**6a-f**), dipeptide (**7a-e**), and tripeptide (**8a-b**) functionalities were synthesized (Chart 3.1). Subsequently, the thermodynamic stability of the corresponding

rosette with these dimelamines after self-assembly with DEB, BuCYA, BzCYA, (*R*)-PhEtCYA or (*S*)-PhEtCYA in a mixture of chloroform and an increasing percentage of a competitive solvent for hydrogen bonding, was determined.

3.4.1 Synthesis and characterization of assemblies with different functionalities

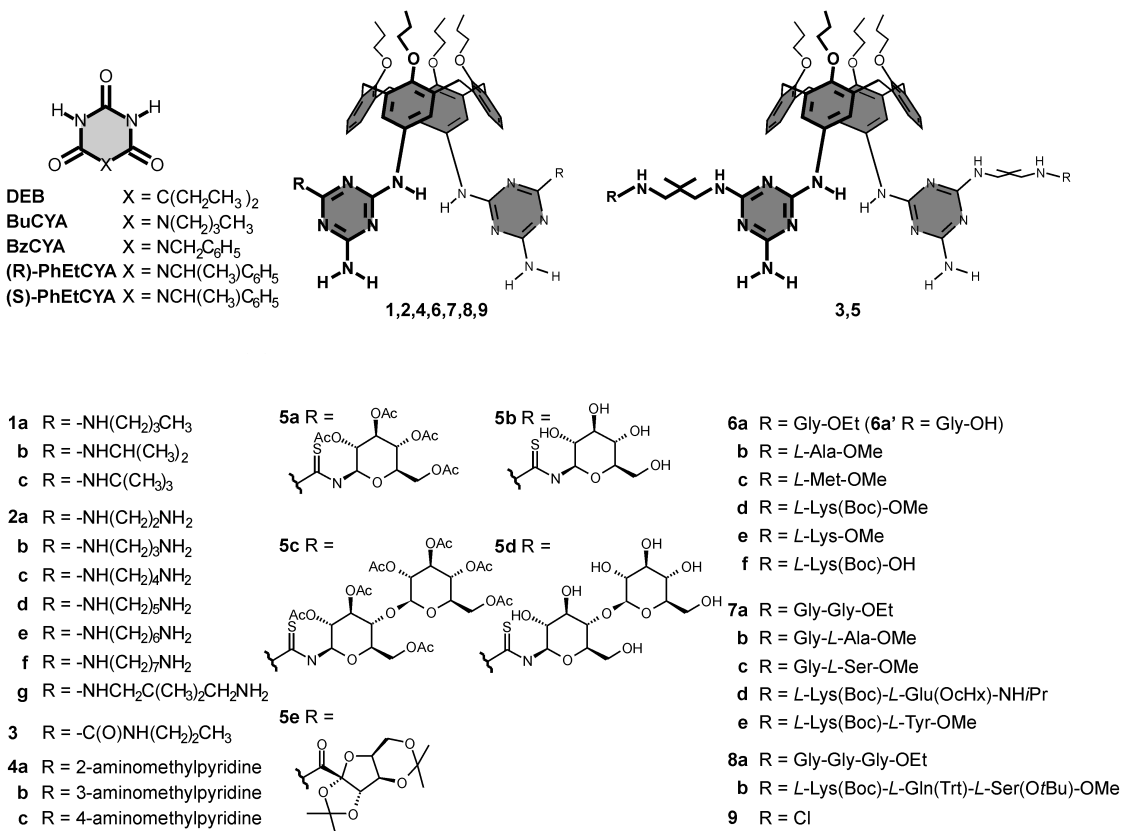


Chart 3.1 Molecular structures of dimelamines 1-9 and BAR/CYA derivatives.

Compounds **1-8** were synthesized starting from calix[4]arene bis(chlorotriazine) **9**.⁹ Dimelamines **1** were synthesized according to literature procedures.⁹ Dimelamines **2** were synthesized by reaction of **9** with an excess of the corresponding diaminoalkane at 90°C (**2a-g**, 53-92%). Reaction of **2g** with excess of propyl isocyanate in THF at room temperature afforded dimelamine **3** (78%).¹⁷ Syntheses of dimelamines **4** are described elsewhere.¹⁸

Reaction of **2g** with tetra-O-acetyl-β-D-glucopyranosylisothiocyanate and hepta-O-acetyl-β-D-cellobiosylisothiocyanate¹⁹⁻²¹ in THF gave dimelamines **5a** (36%) and **5c** (88%), respectively. Successive deacetylation of **5a** and **5c** with a catalytic amount of a

sodium methoxide solution afforded dimelamines **5b** and **5d**, respectively. Compound **5e** was obtained in 41% yield by coupling of **2g** and gulonic acid with HBTU in the presence of HOBT and DIPEA in CH₂Cl₂ at room temperature.

Dimelamines **6a-d** were obtained by reaction of **9** with excess of Glycine ethyl ester (**6a**, 74%), *L*-Alanine methyl ester (**6b**, 74%), *L*-Methionone methyl ester (**6c**, 69%), or *L*-Lysine(Boc) methyl ester (**6d**, 84%) in presence of DIPEA in THF. Deprotection of the ϵ -amino group of dimelamine **6d** with TFA/CH₂Cl₂ (1:1) afforded compound **6e** in 24% yield. Hydrolysis of compound **6d** with sodium hydroxide in THF/MeOH (1:1) gave **6f** (83%).

Dimelamine **7a** (85%) was synthesized by reaction of **9** with excess of Gly-Gly ethyl ester in presence of DIPEA in THF. Hydrolysis of **6a** with sodium hydroxide in THF/MeOH (1:1) and coupling of *L*-Alanine methyl ester, *L*-Serine methyl ester or Gly-Gly ethyl ester using standard peptide coupling conditions (HATU, DIPEA in CH₂Cl₂) afforded **7b** (50%), **7c** (23%) and **8a** (68%), respectively.

Coupling of Boc-*L*-glu(OcHx)-OH with *isopropyl* amine using peptide coupling conditions (EDC, HOBT, DIPEA in CHCl₃) gave Boc-*L*-glu(OcHx)-NH*i*Pr (88%), which after deprotection with TFA/CH₂Cl₂ (1:1) was coupled with **6f** using standard peptide coupling conditions (EDC, HOBT, DIPEA in CH₂Cl₂) giving **7d** (48%). Dimelamine **7e** (66%) was obtained similarly to **7d** but using *L*-tyrosine methyl ester.

Fmoc-*L*-Gln(Trt)-*L*-Ser(*O**t*Bu)-OMe was prepared by coupling of Fmoc-*L*-Gln(Trt)-OH and *L*-Ser(*O**t*Bu)-OMe with HBTU and DIPEA in acetonitrile. Successive Fmoc cleavage with diethylamine gave *L*-Gln(Trt)-*L*-Ser(*O**t*Bu)-OMe (90%). Coupling of **6f** with *L*-Gln(Trt)-*L*-Ser(*O**t*Bu)-OMe using standard peptide coupling conditions (EDC, HOBT, DIPEA in CH₂Cl₂) afforded **8b** (45%).

The double rosette formation with dimelamines **1-8** and various BAR/CYA was confirmed by ¹H NMR spectroscopy. The ¹H NMR spectra of assemblies **1-8**₃•(BAR)₆ exhibit diagnostic signals between $\delta = 14.5$ -14.0 ppm (s, NH_a), 13.5-13.0 ppm (s, NH_b), 8.5-8.0 ppm (s, ArNH_c), 7.4-7.2 ppm (s, NH_d), 7.0-6.5 ppm (2s, NH_{e,f}), and ~6.0 ppm (s, ArH_h) (Figure 3.6a). ¹H NMR spectra of assemblies **1-8**₃•(CYA)₆ exhibit diagnostic signals between $\delta = 15.0$ -14.0 ppm (s, NH_a), 14.0-13.0 ppm (s, NH_b), 8.8-8.3 ppm (s, ArNH_c), 7.7-7.3 ppm (s, NH_d), 7.2-6.6 ppm (NH_{e,f}), and ~6.0 ppm (ArH_h) (Figure 3.6b).

Formation of assemblies $\mathbf{1-8}_3 \cdot (\text{BAR}/\text{CYA})_6$ was quantified by integration of the appropriate ^1H NMR signals²² and confirmed by MALDI-TOF mass spectrometry using the Ag^+ -labeling technique (see Section 3.3).

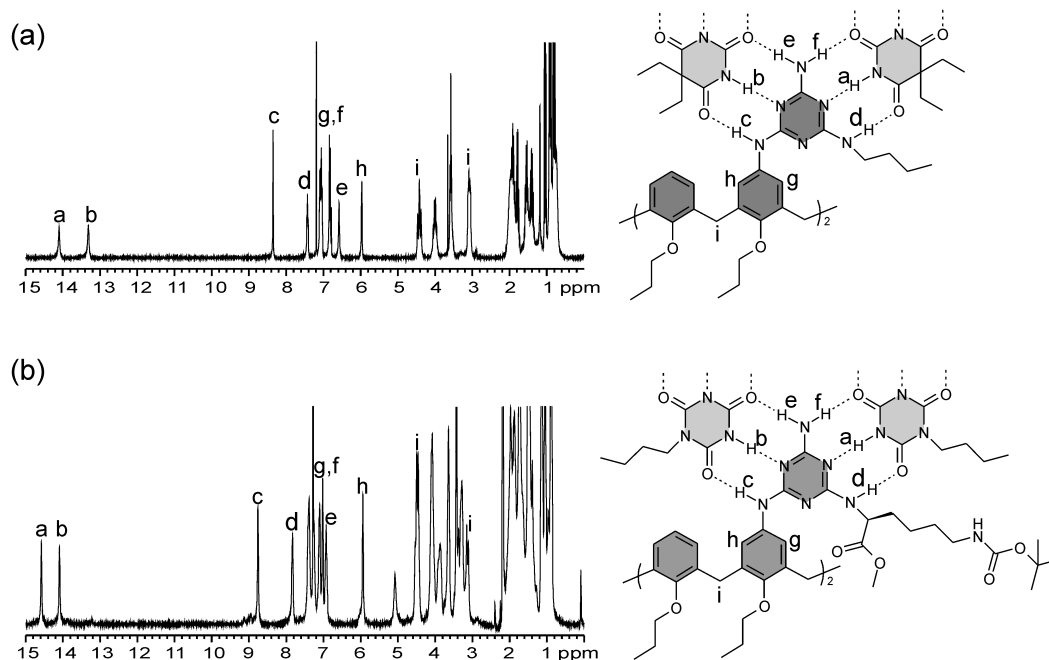


Figure 3.6 ^1H NMR spectra of assembly (a) $\mathbf{1a}_3 \cdot (\text{DEB})_6$ and (b) $\mathbf{6d}_3 \cdot (\text{BuCYA})_6$. Spectra were recorded at 300 MHz in CDCl_3 at 298 K.

3.4.2 Thermodynamic stability of assemblies with alkyl, aminoalkyl, ureido and pyridyl functionalities

The spontaneous assembly of double rosettes in apolar solvents is an enthalpy driven process that involves the cooperative formation of 36 hydrogen bonds. The change in entropy is unfavorable, because upon assembly formation the translational and rotational degrees of freedom of 9 molecular components are reduced.²³

The effect of linear (**1a**) and branched (**1b,c**) alkyl functionalities on the thermodynamic stability of the corresponding double rosettes was investigated by CD spectroscopy. The formation of hydrogen bonds favors the assembly of the double rosettes enthalpically. Hydrogen-bonding solvents lower this enthalpy causing double rosettes eventually to dissociate. The amount of polar solvent required for dissociation can be taken as a measure for the stability of the double rosettes.²⁴ Double rosettes with chiral building blocks display very intense and characteristic CD spectra (see Section 3.3)

that are not observed for the individual components. The CD signal is therefore a direct measure of assembly formation. Since calix[4]arene dimelamines **1a-c** are not chiral, (*R*)-PhEtCYA was used as chiral building block. For the CD titration experiments the percentage of methanol in chloroform was increased while the total concentration of dimelamine and of (*R*)-PhEtCYA was kept constant at 3 mM and 6 mM, respectively. Under these conditions the maximum concentration of double rosette assemblies is 1 mM. Unless mentioned otherwise, CD titrations were started with rosette solutions in neat CHCl₃, and subsequently the amount of MeOH was increased up to MeOH/CHCl₃ (1:1). The parameter $\chi_{\text{polar solvent}}$ was used to quantify the thermodynamic stability of double rosette assemblies. $\chi_{\text{polar solvent}}$ is defined as the percentage of polar solvent in chloroform at which 50% of the assembly is still intact.

Figure 3.7 shows the results of CD titration experiments with assemblies **1a-c** \cdot ((*R*)-PhEtCYA)₆. At MeOH/CHCl₃ (1:1) the double rosette **1a** \cdot ((*R*)-PhEtCYA)₆ is still present for 58%. Though χ_{MeOH} lies beyond the range of the titration experiment a χ_{MeOH} of 60% was estimated (see Figure 3.7). The branched *isopropyl* functionalities in **1b** \cdot ((*R*)-PhEtCYA)₆ resulted in less stable double rosettes ($\chi_{\text{MeOH}} = 17\%$). Further branching by *tert*butyl moieties in **1c** \cdot ((*R*)-PhEtCYA)₆ gave a further decrease of stability ($\chi_{\text{MeOH}} = 7\%$). The decrease in thermodynamic stability is obviously due to a larger steric strain of the rosette platforms induced by the more voluminous branched alkyl functionalities.

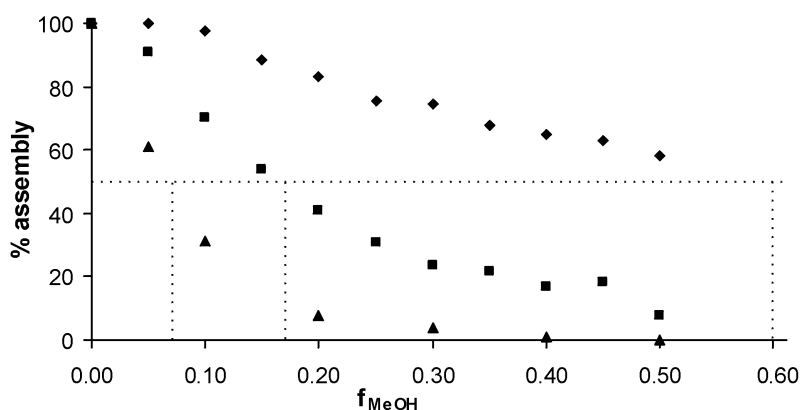


Figure 3.7 CD titrations of \blacklozenge : **1a** \cdot ((*R*)-PhEtCYA)₆, \blacksquare : **1b** \cdot ((*R*)-PhEtCYA)₆, and \blacktriangle : **1c** \cdot ((*R*)-PhEtCYA)₆. Spectra were recorded in MeOH/CHCl₃ mixtures (f_{MeOH}) at 298 K. [*dimelamine*] = 3 mM, [(*R*)-PhEtCYA₆] = 6 mM.

For the series of amino alkyl functionalized double rosette assemblies **2a-f**₃•((*R*)-PhEtCYA)₆ no significant change in thermodynamic stability was observed when the length of the amino alkyl chain was increased from aminoethyl to aminoheptyl (Figure 3.8). The χ_{MeOH} values are in the range of 39 to 48%. The amino group present in assemblies **2a-f**₃•((*R*)-PhEtCYA)₆ enhances the solubility in more polar solvents (mixtures) compared to double rosettes **1a-c**₃•((*R*)-PhEtCYA)₆, but this terminal group does not enhance the stability. When a CD titration with assembly **2e**₃•((*R*)-PhEtCYA)₆ was performed in MeOH/CHCl₃ mixtures ranging from neat chloroform to neat methanol (Figure 3.8) a linear decrease of intact assemblies with increasing amount of methanol was found between ratios 1:9 and 8:2 (MeOH/CHCl₃). Above a ratio of 8:2 complete dissociation of double rosette **2e**₃•((*R*)-PhEtCYA)₆ was observed.

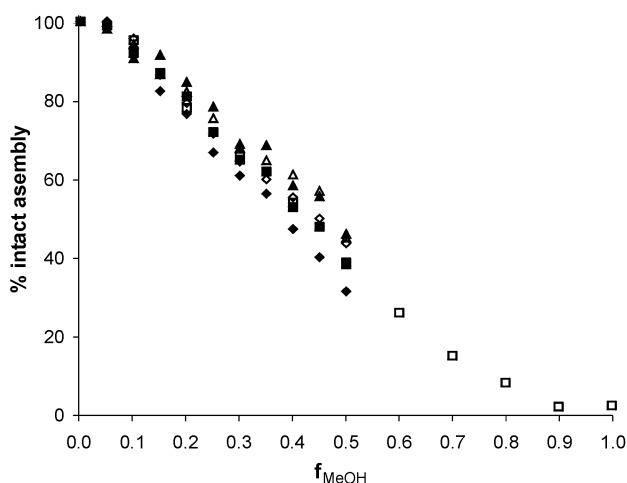


Figure 3.8 CD titrations of ♦: **2a**₃•((*R*)-PhEtCYA)₆, ■: **2b**₃•((*R*)-PhEtCYA)₆, ▲: **2c**₃•((*R*)-PhEtCYA)₆, ◈: **2d**₃•((*R*)-PhEtCYA)₆, □: **2e**₃•((*R*)-PhEtCYA)₆, and Δ: **2f**₃•((*R*)-PhEtCYA)₆. Spectra were recorded in MeOH/CHCl₃ mixtures (f_{MeOH}) at 298 K. [dimelamine] = 3 mM, [(*R*)-PhEtCYA₆] = 6 mM.

CD titrations with ureido functionalized double rosette **3**₃•((*R*)-PhEtCYA)₆ performed in MeOH/CHCl₃ mixtures ranging from neat methanol to chloroform gave a χ_{MeOH} of 82%. Thus, the ureido functionalities in **3**₃•((*R*)-PhEtCYA)₆ increase considerably the stability compared to assembly **1a**₃•((*R*)-PhEtCYA)₆ bearing butyl moieties. This increase is probably the result of a very rigid conformation adopted by the 2,2-dimethylpropyl side

chain allowing the ureido moiety to fold back over the calix[4]arene aromatic rings and to form an extra hydrogen bond with one of the nitrogen atoms of the triazine ring.¹⁷

For pyridyl functionalized assemblies **4a-c**₃•((*R*)-PhEtCYA)₆ a χ_{MeOH} of 53% was found, comparable to the stability of aminoalkyl functionalized assemblies **2a-f**₃•((*R*)-PhEtCYA)₆

3.4.3 Formation and thermodynamic stability of assemblies with carbohydrate moieties

Carbohydrates are involved in a large variety of biological molecular recognition processes.^{25,26} Therefore, the introduction of carbohydrate oligomers in double rosette assemblies is very interesting for the mimicking of natural recognition events. However, before studying the properties of these assemblies as receptors it is important to assess their thermodynamic stability.

Double rosette assemblies **5a**₃•(BuCYA)₆ and **5c**₃•(BuCYA)₆, bearing *protected* glucosyl and cellobiosyl moieties, respectively, are formed for 80% in CDCl₃ as estimated by ¹H NMR spectroscopy.²² Furthermore, only one set of singlets was observed within the region from 13 to 15 ppm for both assemblies, indicating the presence of only one diastereomer in solution. CD spectroscopy revealed that both **5a**₃•(BuCYA)₆ and **5c**₃•(BuCYA)₆ exhibit *P*-helicity.

CD titration experiments with **5a**₃•(BuCYA)₆ in MeOH/CHCl₃ gave a χ_{MeOH} value of 18% (Table 3.1). Assembly **5c**₃•(BuCYA)₆ is formed in pure chloroform, but addition of methanol results in rapid dissociation. Free dimelamine **5c** exhibits a significant CD intensity induced by its 16 chiral centers that coincide with double rosette **5c**₃•(BuCYA)₆ but the CD spectrum differs in shape. The observed CD signals are the sum of the CD intensities attributed to free dimelamine **5c** and to assembly **5c**₃•(BuCYA)₆. CD titrations showed that above MeOH/CHCl₃ (2:8) the observed CD spectrum matches the spectrum of **5c**, indicating that assembly **5c**₃•(BuCYA)₆ is completely dissociated. CD titrations indicated that χ_{MeOH} is <5% for **5c**₃•(BuCYA)₆.

Table 3.1. Thermodynamic stability for the self-assembly of double rosettes **5a-e**₃•(BuCYA)₆ in MeOH/CHCl₃ mixtures determined by CD titration experiments (298K). Maximum possible concentration of intact assembly over the whole titration is 1.0 mM.

R	assembly	χ_{MeOH} (solv. range)
Glucopyranosyl(OAc) ₄	5a ₃ •(BuCYA) ₆	18% (0-50% MeOH)
Glucopyranosyl(OH) ₄	5b ₃ •(BuCYA) ₆	n.d.*
Cellobiosyl(OAc) ₇	5c ₃ •(BuCYA) ₆	<5% (0-50% MeOH)
Cellobiosyl(OH) ₇	5d ₃ •(BuCYA) ₆	<20% (20-100% MeOH)
Gulonyl	5e ₃ •(BuCYA) ₆	10% (0-50% MeOH)

* Not determined

¹H NMR spectroscopy in chloroform indicated that assemblies **5b**₃•(BuCYA)₆ and **5d**₃•(BuCYA)₆, bearing *unprotected* glucosyl and cellobiosyl moieties, are formed for >95 % and 76%, respectively. CD titrations with **5d**₃•(BuCYA)₆ were performed in a range from MeOH/CHCl₃ (2:8) (where 34% assembly is formed) to neat MeOH (χ_{MeOH} is <20%). As observed for CD titrations with **5c**₃•(BuCYA)₆, also free **5d** contributes significant to the observed CD signal. Because the shape of the CD spectra varies between free **5d** and **5d**₃•(BuCYA)₆ it is possible to quantify the double rosette formation. CD intensities at 260 nm were used because the assembly exhibit strong CD intensity at this wavelength, while the CD intensity for free **5d** is minimal. From these data $\Delta\epsilon_{260}$ values of 147.1 l·mol⁻¹·cm⁻¹ and 0.4 l·mol⁻¹·cm⁻¹ were calculated for **5d**₃•(BuCYA)₆ and free **5d**, respectively. In addition, **5d**₃•(BuCYA)₆ was formed for 25% and 7% in mixtures of MeOH and CHCl₃ in 3:7 and 4:6 ratio, respectively. At higher MeOH/CHCl₃ ratios assembly **5d**₃•(BuCYA)₆ is not formed.

¹H NMR spectroscopy indicated that assembly **5e**₃•(BuCYA)₆, bearing *L*-gulose moieties, was formed for 65% in CDCl₃. This assembly forms the *M*-diastereomer. CD titration measurements in MeOH/CHCl₃ gave a χ_{MeOH} of 10% (Table 3.1).

3.4.4 Formation and thermodynamic stability of assemblies with amino acid functionalities

3.4.4.1 Thermodynamic stability

For assembly (*P*)-**6a**₃•((*R*)-PhEtCYA)₆ a χ_{MeOH} value of 43% was obtained (Table 3.2). Dimelamine **6a** has the achiral amino acid Gly, thus (*R*)-PhEtCYA was used for the CD titration experiments to induce the formation of only one diastereomer.

Table 3.2. Thermodynamic stability for the self-assembly of double rosettes **6**₃•(BAR/CYA)₆ in MeOH/CHCl₃ mixtures determined by CD titration experiments (298K). Maximum possible concentration of intact assembly over the whole titration is 1.0 mM.

Entry	R	assembly	χ_{MeOH} (solv. range)
1	Gly-OEt	6a ₃ •((<i>R</i>)-PhEtCYA) ₆	43% (0-50% MeOH)
2	Ala-OMe	6b ₃ •(BuCYA) ₆ 6b ₃ •((<i>R</i>)-PhEtCYA) ₆	Quantitative (0-50% MeOH)* 39% (0-50% MeOH)
3	Met-OMe	6c ₃ •(BzCYA) ₆	Quantitative (0-50% MeOH)*
4	Lys(Boc)-OMe	6d ₃ •(DEB) ₆ 6d ₃ •(BuCYA) ₆ 6d ₃ •(BzCYA) ₆	3.2% (0-50% MeOH) Quantitative (0-50% MeOH)* Quantitative (0-50% MeOH)*
5	Lys-OMe	6e ₃ •(BuCYA) ₆	49% (0-100% MeOH)
6	Lys(Boc)-OH (<i>M</i> -isomeer!)	6f ₃ •(DEB) ₆ 6f ₃ •(BuCYA) ₆ 6f ₃ •((<i>R</i>)-PhEtCYA) ₆ 6f ₃ •((<i>S</i>)-PhEtCYA) ₆	No rosette 40% (0-100% MeOH) No rosette Rosette formation <15% in CDCl ₃

* Assembly formation is quantitative over the whole solvent range

Assembly **6b**₃•(BuCYA)₆, bearing alanine methyl ester moieties, is stable upon addition of 50% of MeOH (Figure 3.9 and Table 3.2, entry 2). Further increase of MeOH concentration was not possible due to solubility limitations. CD titrations with assembly **6b**₃•((*R*)-PhEtCY)₆ gave a χ_{MeOH} of 39%, a value comparable with that for **6a**₃•((*R*)-PhEtCYA)₆. These results indicate that the methyl side chain moiety of alanine does not interfere with the stability of assembly **6b**₃•(BuCYA)₆. Furthermore, assembly **6b**₃•(BuCYA)₆ is more stable than assembly **6a**₃•((*R*)-PhEtCYA)₆. It is possible that branching of the cyanurate side chain in (*R*)-PhEtCYA close to the double rosette core causes more steric hindrance than BuCYA. CD titrations showed that assemblies **6c**₃•(BzCYA)₆, and **6d**₃•(BzCYA)₆, bearing *L*-methionine methyl ester and *L*-Lysine(Boc) methyl ester moieties, are stable up to 50% of methanol (Table 3.2, entries 3

and 4). Also here, further increase of methanol concentration was not possible due to solubility limitations. These results indicate that branching of the cyanurate side chain, as in (*R*)-PhEtCYA is indeed unfavorable. Furthermore, these results show that the methylsulfonyl and *tert*-butoxycarbonyl aminobutyl side chain functionalities of **6c** and **6d**, respectively, do not affect the stability of assemblies **6c**•(BzCYA)₆, and **6d**•(BzCYA)₆. CD titrations with **6d**•(BuCYA)₆ showed that this assembly is also stable in 50% of MeOH (Table 3.2, entry 4). Figure 3.9 clearly indicates that small differences in cyanurate side chain functionalities can decrease the stability of double rosette assemblies, while the effect of amino acid side chain functionalities at the calix[4]arene dimelamine units is almost negligible.

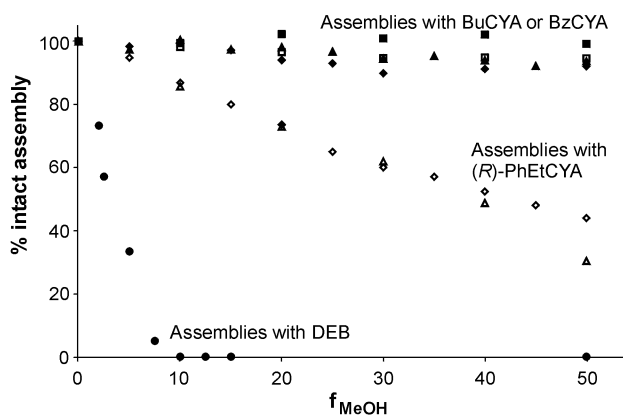


Figure 3.9 CD titrations of assemblies **6a**₃•(*R*)-PhEtCYA)₆ (◇), **6b**₃•(*R*)-PhEtCYA)₆ (Δ), **6b**₃•(BuCYA)₆ (□), **6c**₃•(BzCYA)₆ (■), **6d**₃•(DEB)₆ (●), **6d**₃•(BuCYA)₆ (◆), and **6d**₃•(BzCYA)₆ (▲). Spectra were recorded in MeOH/CHCl₃ (*f*_{MeOH}) mixtures at 298 K where the maximum assembly concentration was kept constant (1.0 mM).

Previously, our group has reported²⁷ that the assembly of one melamine to one cyanurate (CYA) gives a complex that is much stronger than the complex between one melamine and one barbiturate (BAR) due to the higher acidity of the CYA. Association constants of 10² and 10⁴ M⁻¹ were reported for melamine•BAR and melamine•CYA, respectively. In agreement with this, we found a very low stability ($\chi_{\text{MeOH}} = 3.2\%$; Table 3.2 entry 4) for assembly **6d**₃•(DEB)₆, formed with diethyl barbiturate instead of cyanurate derivatives.

For **6e**₃•(BuCYA)₆, bearing unprotected (side chain) *L*-lysine methyl ester moieties the χ_{MeOH} is 49% (Table 3.2 entry 5). This indicates that the free ϵ -amino group of the lysine in **6e** gives a less stable double rosette assembly **6e**₃•(BuCYA)₆ compared to **6d**₃•(BuCYA)₆ (formed quantitatively in 0-50% MeOH in CHCl₃ at 1 mM), in which the ϵ -amino group of the lysine is Boc-protected. For assembly **6f**₃•(BuCYA)₆, with free carboxylic acid groups the χ_{MeOH} is 40%. Assembly **6f**₃•(BuCYA)₆ is less stable than its methyl ester analogue **6d**₃•(BuCYA)₆. Assembly **6f**₃•(DEB)₆ was not formed at any ratio MeOH/CHCl₃ at 1.0 mM concentration, emphasizing the weaker association between melamine•BAR compared to melamine•CYA. Previous results indicate that the stability of double rosettes was mainly affected by the molecular structure of the cyanurates and not by the side chain functionality of the amino acid esters. Because dimelamine **6d** is bulkier than dimelamines **6e** and **6f**, charge or electronic influences of the ϵ -amino or carboxylic acid groups in **6e**₃•(BuCYA)₆ and **6f**₃•(BuCYA)₆, respectively, rather than steric hindrance seem to decrease their stability.

3.4.4.2 Chiral induction by the lysine group

Dimelamines **6b**, **6c**, **6d** and **6e**, having *L*-alanine methyl ester, *L*-methionine methyl ester, ϵ N-Boc-*L*-lysine methyl ester or *L*-lysine methyl ester moieties, respectively, all induce (*P*)-helicity. However, the CD spectrum observed for **6f**₃•(BuCYA)₆, bearing the *L*-lysine amino acid with free carboxylic acid group, is inverted compared to the double rosettes **6b**-**6e**₃•(DEB/CYA)₆ with the amino acid ester functionalities. This indicates that dimelamine **6f** induces (*M*)-helicity for the double rosette **6f**₃•(BuCYA)₆ (Figure 3.10), even though the chirality of dimelamine **6f** (*L*-lys) is the same as of the other lysine functionalized dimelamine derivatives **6d** and **6e**.

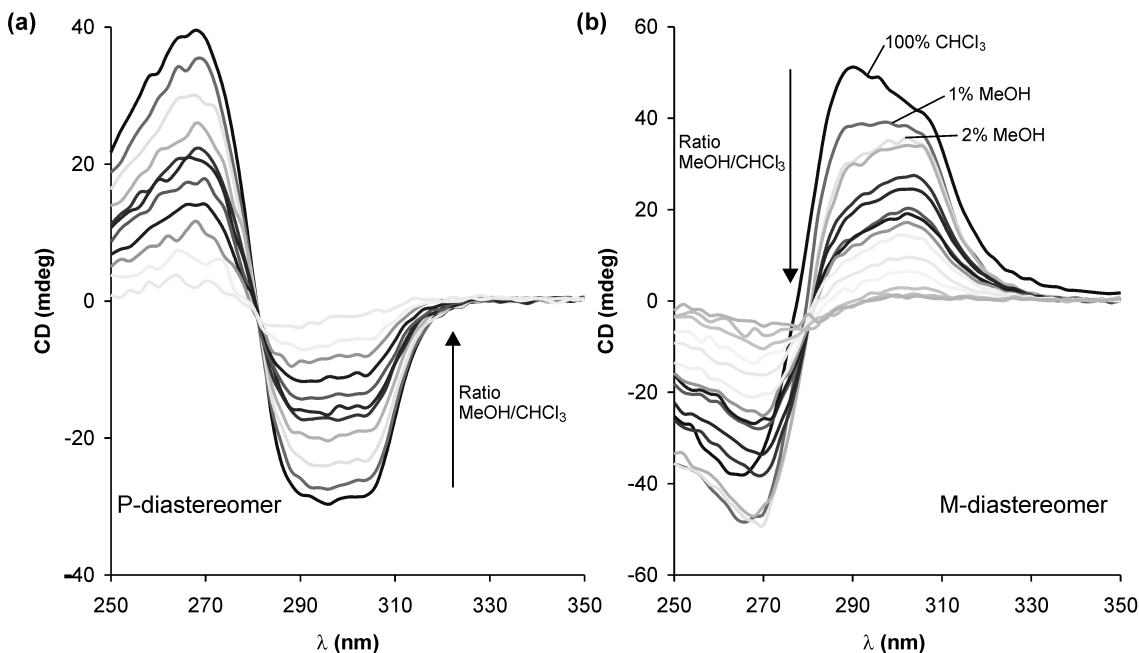


Figure 3.10 CD titrations of assemblies (a) $6e_3 \cdot (BuCYA)_6$ and (b) $6f_3 \cdot (BuCYA)_6$. Spectra were recorded in MeOH/CHCl₃ mixtures at 298 K where the maximum assembly concentration was kept constant (1.0 mM).

The formation of assemblies $6f_3 \cdot ((R)\text{-PhEtCYA})_6$ and $6f_3 \cdot ((S)\text{-PhEtCYA})_6$ was studied to confirm that in all cases *L*-**6f** induces the *M*-helicity. Generally, when chiral dimelamines and chiral cyanurate derivatives have an opposite preference for induction of (*M*)- or (*P*)-helicity, the formation of double rosettes is not observed.^{28,29} Assembly $6b_3 \cdot ((R)\text{-PhEtCYA})_6$ is only formed in the (*P*)-helical form, thus (*R*)-PhEtCYA induces only the (*P*)-helicity. ¹H NMR and CD spectroscopy studies indicate the formation of the assembly $6f_3 \cdot ((S)\text{-PhEtCYA})_6$ with the (*M*)-helicity but assembly $6f_3 \cdot ((R)\text{-PhEtCYA})_6$ is not formed. Thus, *L*-**6f** induces only the (*M*)-helicity.

It is known that the induction of helicity by amino acid residues could depend on the solvent polarity and on the pH.³⁰ Though it is difficult to explain this change in helicity it is likely that differences in polarity between the different lysine moieties of **6d**, **6e** and **6f** are playing a role. The complete inversion of helicity as observed for $6f_3 \cdot (BuCYA)_6$, compared to other amino acid functionalized assemblies, indicates that small structural changes within assembly components could largely affect the structure of the assembly.

3.4.5 Formation and thermodynamic stability of assemblies with di- and tripeptide functionalities

¹H NMR spectroscopy showed that assemblies **7a₃**•((R)-PhEtCYA)₆, **7b₃**•(BuCYA)₆ and **7c₃**•(BuCYA)₆, bearing Gly-Gly-OEt, Gly-L-Ala-OMe and Gly-L-Ser-OMe functionalities, respectively, were formed quantitatively in CDCl₃, while **7d₃**•(BuCYA)₆ and **7e₃**•(BuCYA)₆, bearing L-Lys(Boc)-L-Glu(OcHx)-NH*i*Pr and L-Lys(Boc)-L-Tyr-OMe functionalities were formed only for 84% and 65%, respectively.

Table 3.3 Thermodynamic stability for the self-assembly of double rosettes **7a-e₃**•((R)-PhEtCYA/BuCYA)₆ and **8a-b₃**•((R)-PhEtCYA/ BuCYA)₆ in MeOH/CHCl₃ mixtures determined by CD titration experiments (298K). Maximum possible concentration of intact assembly over the whole titration is 1.0 mM.

R	assembly	χ_{MeOH} (solv. range)
Gly-Gly-OEt	7a₃ •((R)-PhEtCYA) ₆	25% (0-100% MeOH)*
Gly-L-Ala-OMe	7b₃ •(BuCYA) ₆	50% (0-100% MeOH)*
Gly-L-Ser-OMe	7c₃ •(BuCYA) ₆	n.d.**
L-Lys(Boc)-L-Glu(OcHx)-NH <i>i</i> Pr	7d₃ •(BuCYA) ₆	7% (0-100% MeOH)*
L-Lys(Boc)-L-Tyr-OMe	7e₃ •(BuCYA) ₆	8% (20-100% MeOH)*
Gly-Gly-Gly-OEt	8a₃ •((R)-PhEtCYA) ₆	23% (0-100% MeOH)*
L-Lys(Boc)-L-Gln(Trt)-Ser(O <i>t</i> Bu)-OMe	8b₃ •(BuCYA) ₆	Rosette formation ~40% in CDCl ₃

* CD titrations were performed from neat CHCl₃ to neat MeOH due to the increased solubility of dimelamines **7** and **8** in methanol.

** Not determined.

CD titration experiments were performed with **7a₃**•((R)-PhEtCYA)₆, **7b₃**•(BuCYA)₆, **7d₃**•(BuCYA)₆ and **7e₃**•(BuCYA)₆ in MeOH/CHCl₃ (Table 3.3). Because dipeptide functionalized dimelamines **7a-e** are soluble in methanol, titrations could be performed from neat chloroform to neat methanol. For these dipeptide functionalized double rosettes, it was found that an increase of the ratio MeOH/CHCl₃ leads to the dissociation of the double rosettes. Assembly **7a₃**•((R)-PhEtCYA)₆ ($\chi_{\text{MeOH}} = 25\%$) is less stable than the corresponding (mono) Gly derivative **6a₃**•((R)-PhEtCYA)₆ ($\chi_{\text{MeOH}} = 43\%$; Table 3.2).

These results indicate that the presence of a dipeptide instead of a single amino acid decreases severely the stability of the assembly.

Assembly **7b₃**•(BuCYA)₆ with Gly-*L*-Ala functionalities ($\chi_{\text{MeOH}} = 50\%$) was formed for 50% in MeOH/CHCl₃ (1:1), while **6b₃**•(BuCYA)₆, bearing only *L*-Ala, was formed quantitatively (Table 3.2). Furthermore, the double rosettes **7d₃**•(BuCYA)₆ and **7e₃**•(BuCYA)₆, with bulkier dipeptides are less stable (χ_{MeOH} values of 7% and 8%, respectively) than **7b₃**•(BuCYA)₆. Because the lysine at the first position did not affect the formation of **6d₃**•(BuCYA)₆ (formed quantitatively in MeOH/CHCl₃ (1:1); Table 3.2), these results indicate that bulkier amino acids in the second position decrease the stability in MeOH/CHCl₃ solvent mixtures. However, above MeOH/CHCl₃ (2:8) no further dissociation of **7d₃**•(BuCYA)₆ and **7e₃**•(BuCYA)₆ was observed as it can be seen by CD titrations. The percentage intact assemblies for **7d₃**•(BuCYA)₆ and **7e₃**•(BuCYA)₆ remained around 20% (Figure 3.11), even in pure methanol!

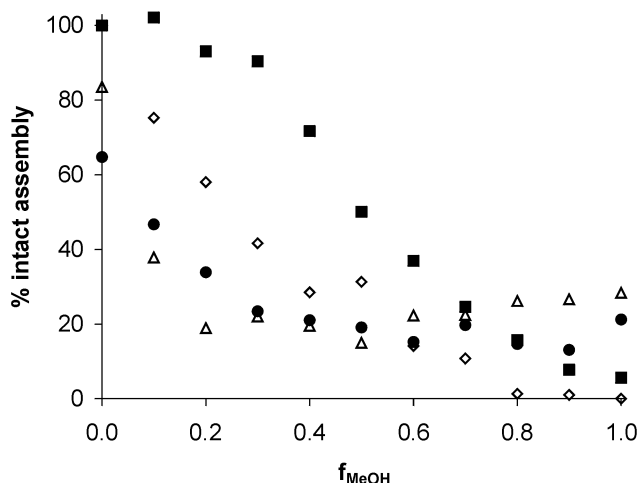


Figure 3.11 CD titrations of assemblies **7a₃**•((*R*)-PhEtCYA)₆ (■), **7b₃**•(BuCYA)₆ (◇), **7d₃**•(BuCYA)₆ (△) and **7e₃**•(BuCYA)₆ (●). Spectra were recorded in MeOH/CHCl₃ (f_{MeOH}) mixtures at 298 K where the maximum assembly concentration was kept constant (1.0 mM).

For tripeptide functionalized double rosettes, ¹H NMR spectroscopy indicated that the double rosette assembly **8a₃**•((*R*)-PhEtCYA)₆, bearing Gly-Gly-Gly-OEt moieties, was formed quantitatively in chloroform. CD titrations gave $\chi_{\text{MeOH}} = 23\%$ which is similar to **7a₃**•((*R*)-PhEtCYA)₆ bearing the corresponding dipeptide Gly-Gly-OEt. This indicates

that the introduction of the third amino acid does not decrease further the stability. The ^1H NMR spectrum of the assembly $\mathbf{8b}_3\cdot(\text{BuCYA})_6$, bearing *L*-Lys(Boc)-*L*-Gln(Trt)-*L*-Ser(*O**t*Bu)-OMe moieties showed the diagnostic signals for double rosette formation in chloroform. However, it was not possible to quantify the rosette formation due to peak broadening in the ^1H NMR spectrum. To estimate the double rosette formation, the CD signal (at 300 nm) obtained for $\mathbf{8b}_3\cdot(\text{BuCYA})_6$ in chloroform was compared with the intensity of the CD signal of $\mathbf{6d}_3\cdot(\text{BuCYA})_6$ in the same solvent. This resulted in an estimated formation of $\mathbf{8b}_3\cdot(\text{BuCYA})_6$ of 40% in chloroform. CD titrations showed that increased polarity led also here to dissociation. Assembly $\mathbf{8b}_3\cdot(\text{BuCYA})_6$ was formed about 15-20% in neat MeOH (Table 3.3) which is comparable with assemblies $\mathbf{7d}_3\cdot(\text{BuCYA})_6$ and $\mathbf{7e}_3\cdot(\text{BuCYA})_6$ (20% of rosette formation also in neat MeOH). It seems that bulky and polar amino acids at the second and possibly at the third position increase the stability of double rosettes in *neat* MeOH, contrary to what is observed for MeOH/ CHCl_3 mixtures with high content of CDCl_3 . These could suggest that with larger and bulky peptide functionalities at the assemblies other stabilizing effects, *e.g.* hydrophobic effects, might start to play a role in the self-assembly process.

In summary, amino acids at the first position of the peptide functionalities do not affect the formation of double rosettes at 1 mM concentration in MeOH/ CHCl_3 solvent mixtures, while amino acids at the second position in di- and tripeptide functionalities decrease the stability of double rosette assemblies in the same solvent mixtures. This decrease in stability becomes larger when more bulky amino acids are used in the second position. Interestingly, it seems that the introduction of the third amino acid hardly affects the stability of double rosettes when compared with the dipeptides. Surprisingly, in neat MeOH assembly formation (~20%) is only observed when bulky and polar amino acids are present at the second (and third) position.

3.5 Conclusions

The results shown in this chapter demonstrate that noncovalent hydrogen-bonded double rosettes with different functionalities in the building blocks can be formed in MeOH/ CHCl_3 solvent mixtures. In general, increase of the solvent polarity leads to less stable assemblies.

Furthermore, the functionalities strongly influence the stability of the double rosettes. Steric hindrance close to the rosette platform exerted by the functional groups of the building blocks decreases the stability. Aminoalkyl groups decrease the stability compared to *n*-alkyl functionalities. For linear aminoalkyl groups, it was observed that the chain length does not affect the stability. The stability of the double rosettes bearing pyridyl groups is comparable to the stabilities of assemblies with aminoalkyl groups. The ureido functionalized double rosette is the most stable.

Double rosettes with protected glucosyl and cellobiosyl moieties are also formed quantitative in neat chloroform, while assemblies with unprotected glucosyl and cellobiosyl moieties are formed for only 80%. Carbohydrate moieties lead to a dramatic decrease in stability of double rosettes in polar solvents when compared to double rosettes having alkyl, aminoalkyl, pyridyl or ureido moieties.

Double rosettes with amino acid or peptide functionalities are more stable than double rosettes with carbohydrate moieties in polar solvents. The stability of double rosettes with different amino acid functionalities in polar solvents strongly depends on the barbiturate or cyanurate derivative. In all cases, assemblies with DEB are less stable than those with cyanurates. Assemblies of amino acid ester functionalized dimelamines **6a-d** with BuCYA or BzCYA are stable up to at least 50% of methanol in chloroform, while double rosettes with the more bulky branched (*R*)-PhEtCYA have χ_{MeOH} values of 40%. Assemblies with different lysine derivatives showed that free amino groups or free carboxylic acid groups within the assembly decrease the stability, probably due to ionic or electronic influences.

In apolar solvents, di- and tripeptide peptide functionalized assemblies are less stable compared to single amino acid functionalized assemblies. Amino acids at the first position of the peptide functionalities do not seem to affect the stability of double rosettes (at 1 mM), while amino acids at the second position decrease the stability of double rosette assemblies. This decrease in stability becomes larger when bulkier amino acids are present in the second position. The introduction of a third amino acid hardly influences the stability of the double rosettes.

Assembly formation in neat MeOH is observed only when bulky amino acids are present at the second (and third) position. This would indicate that the introduction of

larger and/or bulkier peptides might stabilize double rosettes in polar solvents. This behavior is important for host-guest recognition in aqueous solvents.

Overall, the large range of functionalities that can be introduced on the rosette platform allows a large molecular diversity. This is useful to generate hydrogen-bonded receptor assemblies that resemble the natural antibodies. Introduction of large diverse peptides to the double rosettes seems therefore especially attractive because they might mimic the binding sites of these natural receptors.

3.6 Experimental

General Methods:

¹H NMR spectra were recorded on a Varian Unity 300 (¹H NMR 300MHz) spectrometer in chloroform-*d*₁, methanol-*d*₄ or dimethylsulphoxide-*d*₆. Residual solvent protons were used as internal reference, and chemical shifts are given relatively to trimethylsilane (TMS). FAB spectra were measured on a Finningan MAT 90 spectrometer with *m*-nitrobenzyl alcohol (NBA) matrix. MALDI-TOF mass spectra were recorded on a PerSpective Biosystems Voyager-De-RP spectrometer. A 337 nm UV nitrogen laser producing 3 ns pulses was used in the linear and reflectron modes. Elemental analyses were performed using a Carlo Erba EA1106. CD spectra were measured on a JASCO J-715 spectropolarimeter using a cell width of 0.01 cm. THF was distilled from Na/benzophenone and CH₂Cl₂ from K₂CO₃. All commercially available reagents were reagent grade and used without further purification. Flash chromatography was performed on silica gel (SiO₂, E. Merck 0.040 – 0.063 mm, 230 – 240 mesh). Bis(chlorotriazine)calix[4]arene **9**,⁹ alkyl derivatives **1**,⁹ aminoalkyl derivative **2g**,¹⁷ ureido derivative **3**,¹⁷ pyridyl derivatives **4**,¹⁸ and tetra-O-acetyl-β-D-glucopyranosylisothiocyanate and hepta-O-acetyl-β-D-cellobiosyl-isothiocyanate²¹ were synthesized according to literature procedures.

General procedure for the preparation of calix[4]arene dimelamines 2a-f: A solution of the calix[4]arene bis(chlorotriazine) **9** and the appropriate diamino compound (excess) was stirred at 90°C overnight. After cooling down the solution to room temperature the product was precipitated in ice water. The white precipitate was filtered off and washed

with water and/or methanol. Resulting in calix[4]arene dimelamines **2a-f** as a white powder. (In some cases, THF was added prior to precipitation in water for better removal of excess diamino compound.)

5,17-*N,N*-Bis[4-amino-6-(2-aminoethylamino)-1,3,5-triazin-2-yl]diamino-25,26,27,28-tetra propoxycalix[4]arene (2a) was prepared from bis(chlorotriazine) **9** (250 mg, 0.28 mmol) and 1,2-ethanediamine (8 ml). Pure dimelamine **2a** was obtained as white solid in 63% yield (165 mg, 0.18 mmol). ^1H NMR (CDCl_3): $\delta=7.2\text{--}6.8$ (br m, 6H, ArH), $6.5\text{--}6.1$ (br m, 4H, *o*-NHAr), $5.3\text{--}5.0$ (br m, 6H, NH/NH₂), 4.38 and 3.05 (ABq, 8H, $^2J_{\text{HH}}=13.4$ Hz, Ar-CH₂-Ar), 4.0-3.9 (m, 4H, OCH₂), 3.6-3.5 (m, 4H, OCH₂), 3.4-3.2 (br m, 4H, NHCH₂), 2.6 (br m, 4H, CH₂NH₂), 2.0-1.8 (m, 8H, OCH₂CH₂), 1.1 and 0.95 (t, 12H, $^3J_{\text{HH}}=7.4$ Hz, OCH₂CH₂CH₃). MS (FAB): $m/z = 927.3$ ([M+H⁺], calcd 927.5). Anal. Calcd for C₅₀H₆₆N₁₄O₄•4MeOH: C 61.46, H 7.83, N 18.58; found C 61.29, H 6.98, N 17.82.

5,17-*N,N*-Bis[4-amino-6-(3-aminopropylamino)-1,3,5-triazin-2-yl]diamino-25,26,27,28-tetra propoxycalix[4]arene (2b) was prepared from bis(chlorotriazine) **9** (2.00 g, 2.1 mmol) and 1,3-propanediamine (25 ml). Pure dimelamine **2b** was obtained as white solid in 58% yield (1.26 g, 1.32 mmol). ^1H -NMR ($\text{DMSO-}d_6$): $\delta=8.6\text{--}8.4$ (br m, 2H, NH), $\delta=7.55\text{--}7.35$ (br m, 4H, NH₂), $7.5\text{--}7.3$ (br m, 2H, ArH), $\delta=6.4\text{--}6.0$ (br m, 4H, ArH), 4.32 and 3.05 (ABq, 8H, $^2J_{\text{HH}}=13.4$ Hz, Ar-CH₂-Ar), 3.9-3.8 (m, 4H, OCH₂), 3.6-3.5 (m, 4H, OCH₂), 2.6 (br m, 4H, CH₂NH₂), 2.0-1.8 (m, 8H, OCH₂CH₂), 1.6 (m, CH₂, 4H), 1.1 and 0.95 (t, 12H, $^3J_{\text{HH}}=7.4$ Hz, OCH₂CH₂CH₃). MS (FAB): $m/z = 955.3$ ([M+H⁺], calcd 955.6). Anal. Calcd for C₅₂H₇₀N₁₄O₄•H₂O: C 64.18, H 7.46, N 20.15; found C 64.29, H 7.35, N 19.87.

5,17-*N,N*-Bis[4-amino-6-(4-aminobutylamino)-1,3,5-triazin-2-yl]diamino-25,26,27,28-tetra propoxycalix[4]arene (2c) was prepared from bis(chlorotriazine) **9** (250 mg, 0.28 mmol) and 1,4-butyldiamine (5 g). THF (8 ml) was added prior to precipitation in water (50 ml). Pure dimelamine **2c** was obtained as white solid in 89% (248 mg, 0.25 mmol). ^1H NMR (CDCl_3): $\delta=7.0\text{--}6.7$ (br m, 6H, ArH), $6.4\text{--}6.0$ (br m, 4H, *o*-NHAr), $5.0\text{--}4.7$ (br

m, 6H, NH/NH₂), 4.36 and 3.05 (ABq, 8H, ²J_{HH}=13.7 Hz, Ar-CH₂-Ar), 3.9 (t, 4H, ³J_{HH}=8.0 Hz, OCH₂), 3.65-3.55 (m, 4H, OCH₂), 3.3-3.2 (m, 4H, NHCH₂), 2.7-2.6 (m, 4H, CH₂NH₂), 1.9-1.7 (br m, 8H, -OCH₂CH₂-), 1.6-1.4 (br m, 8H, CH₂), 1.0 and 0.85 (t, 12H, ³J_{HH}=7.4 Hz, OCH₂CH₂CH₃). MS (FAB): *m/z* = 983.6 ([M+H⁺], calcd 983.6). Anal. Calcd for C₅₄H₇₄N₁₄O₄: C 65.96, H 7.59, N 19.94; found C 65.90, H 7.61, N 19.82.

5,17-*N,N*-Bis[4-amino-6-(5-aminopentylamino)-1,3,5-triazin-2-yl]diamino-25,26,27,28-tetra propoxycalix[4]arene (2d) was prepared from bis(chlorotriazine) **9** (250 mg, 0.28 mmol) and 1,5-pentylidiamine (5 g). Pure dimelamine **2d** was obtained as white solid in 91% (260 mg, 0.26 mmol). ¹H-NMR (CDCl₃): δ=7.0–6.7 (br m, 6H, ArH), 6.4–6.0 (br m, 4H, *o*-NHAr), 4.9–4.6 (br m, 6H, NH/NH₂), 4.36 and 3.05 (ABq, 8H, ²J_{HH}=13.4 Hz, Ar-CH₂-Ar), 3.9 (m, 4H, OCH₂), 3.65-3.55 (m, 4H, OCH₂), 3.3-3.2 (m, 4H, NHCH₂), 2.7-2.6 (m, 4H, CH₂NH₂), 1.9-1.7 (br m, 8H, -OCH₂CH₂-), 1.6-1.2 (br m, 12H, CH₂), 1.0 and 0.85 (t, 12H, ³J_{HH}=7.5 Hz, OCH₂CH₂CH₃). MS (FAB): *m/z* = 1011.7 ([M+H⁺], calcd 1011.6). Anal. Calcd for C₅₆H₇₈N₁₄O₄•1.5H₂O: C 64.78, H 7.86, N 18.88; found C 64.71, H 7.87, N 18.87.

5,17-*N,N*-Bis[4-amino-6-(6-aminohexylamino)-1,3,5-triazin-2-yl]diamino-25,26,27,28-tetra propoxycalix[4]arene (2e) was prepared from bis(chlorotriazine) **9** (250 mg, 0.28 mmol) and 1,6-hexylidiamine (2 g). THF (4 ml) was added prior to precipitation in water (25 ml). Pure dimelamine **2e** was obtained as white solid in 92% (271 mg, 0.26 mmol). ¹H-NMR (CDCl₃): δ=7.0–6.7 (br m, 6H, ArH), 6.4–6.0 (br m, 4H, *o*-NHAr), 4.9–4.6 (br m, 6H, NH/NH₂), 4.36 and 3.05 (ABq, 8H, ²J_{HH}=13.4 Hz, Ar-CH₂-Ar), 3.9 (m, 4H, OCH₂), 3.68-3.58 (m, 4H, OCH₂), 3.24 (q, 4H, ³J_{HH}=6.6 Hz, NHCH₂), 2.7-2.55 (m, 4H, CH₂NH₂), 1.9-1.7 (br m, 8H, -OCH₂CH₂-), 1.6-1.2 (br m, 16H, CH₂), 1.0 and 0.85 (t, ³J_{HH}=7.5 Hz, OCH₂CH₂CH₃). MS (FAB): *m/z* = 1039.7 ([M+H⁺], calcd 1039.7). Anal. Calcd for C₅₈H₈₂N₁₄O₄: C 67.02, H 7.95, N 18.87; found C 66.74, H 7.97, N 18.27.

5,17-*N,N*-Bis[4-amino-6-(7-aminoheptylamino)-1,3,5-triazin-2-yl]diamino-25,26,27,28-tetra propoxycalix[4]arene (2f) was prepared from bis(chlorotriazine) **9** (250 mg, 0.28 mmol) and 1,7-pentylidiamine (1 g). Pure dimelamine **2f** was obtained as white solid

in 53% (271 mg, 0.26 mmol). $^1\text{H-NMR}$ (CDCl_3): $\delta=7.0\text{--}6.7$ (br m, 6H, ArH), 6.4–6.0 (br m, 4H, *o*-NHAr), 4.9–4.6 (br m, 6H, NH/NH₂), 4.36 and 3.05 (ABq, 8H, $^2J_{\text{HH}}=13.4$ Hz, Ar-CH₂-Ar), 3.95-3.85 (m 4H, OCH₂), 3.68-3.58 (m, 4H, OCH₂), 3.23 (q, 4H, $^3J_{\text{HH}}=6.3$ Hz, NHCH₂), 2.7-6 (t, 4H, $^3J_{\text{HH}}=6.8$ Hz, CH₂NH₂), 1.9-1.7 (br m, 8H, -OCH₂CH₂-), 1.6-1.2 (br m, 20H, CH₂), 1.0 and 0.85 (t, $^3J_{\text{HH}}=7.4$ Hz, OCH₂CH₂CH₃). MS (FAB): $m/z = 1067.7$ ($[\text{M}+\text{H}^+]$, calcd 1067.7). Anal. Calcd for C₆₀H₈₆N₁₄O₄: C 67.51, H 8.12, N 18.37; found C 66.97, H 8.05, N 18.18.

Calix[4]arene bis(tetra-O-acetyl- β -D-glucopyranosyl)dimelamine (5a). Dimelamine **2g** (424 mg, 0.42 mmol) was dissolved in freshly distilled THF (20 ml). Tetra-O-acetyl- β -D-glucopyranosylisothiocyanate (408 mg, 1.05 mmol) was added and the solution was stirred at room temperature for 4 hours. The solution was concentrated *in vacuo* and the product was purified by column chromatography (CH₂Cl₂:MeOH:NH₄OH = 95:4.5:0.5) to give pure **5a** as a white solid in 36% yield. $^1\text{H-NMR}$ (CDCl_3): $\delta = 7.2\text{--}6.8$ (br m, 10H, ArH), 6.34 (s, 2H, gluc), 5.40-5.22 (m, 2H, gluc), 5.1-4.9 (m, 4H, CH₂ gluc),), 4.38 and 3.05 (ABq, 8H, $^2J_{\text{HH}}=13.4$ Hz, Ar-CH₂-Ar), 4.25 (m, 2H, gluc), 4.06-3.90 (br m, 8H, OCH₂ + CH₂), 3.85-3.75 (m, 4H, OCH₂), 2.65-2.45 (m, 2H, CH₂), 2.2-1.8 (br m, 32H OAc + CH₂), 1.0 and 0.85 (m, 12H, CH₃ + OCH₂CH₂CH₃). MALDI-TOF-MS: $m/z = 1790.7$ ($[\text{M}+\text{H}^+]$, calcd 1789.8).

Calix[4]arene bis(β -D-glucopyranosyl)dimelamine (5b). 1 ml of a freshly prepared sodium methoxide solution (23 mM) was added to a solution of dimelamine **5a** (100 mg, 0.06 mmol) in MeOH (4 ml). The solution was stirred for 3 hours at room temperature. Amberlite IR 120 (H⁺) washed with MeOH was added to the solution for exchange of Na⁺ for H⁺. The Amberlite resin was filtered off and the product concentrated *in vacuo* to give pure **5b** as a white solid in 85% yield. $^1\text{H-NMR}$ (DMSO-*d*₆): $\delta = 9.0\text{--}8.0$ (m, NH + NH₂), 7.6-7.3 (m, 4H, ArH), 6.27 (m, 6H, ArH), 5.4-4.8 (m, 6H, CH₂ gluc + CH gluc), 4.43 (m, 2H, CH gluc), 4.33 (d, 4H, $^2J_{\text{HH}}=12.0$ Hz, Ar-CH₂-Ar), 3.89 (m, 4H, OCH₂), 3.7-2.9 (br m, CH gluc, OH, OCH₂, Ar-CH₂-Ar, solvent), 1.90-1.74 (m, 8H, CH₂), 1.06 (t, 6H, $^3J_{\text{HH}}=7.4$ Hz, CH₃), 0.94-0.76 (m, 18H, CH₃). MALDI-TOF-MS: $m/z = 1457.9$ ($[\text{M}+\text{H}^+]$, calcd 1454.8).

Calix[4]arene bis(hepta-O-acetyl- β -D-cellobiosyl)dimelamine (5c). Dimelamine **2g** (424 mg, 0.42 mmol) was dissolved in freshly distilled THF (20 ml). Hepta-O-acetyl- β -D-cellobiosyl-isothiocyanate (711 mg, 1.05 mmol) was added and the solution was stirred at room temperature for 12 hours. The solution was concentrated *in vacuo* and the product was purified by column chromatography (CH₂Cl₂:MeOH:NH₄OH = 95:4.5:0.5) to give **5c** as a white solid in 88% yield. ¹H-NMR (CD₃OD): δ = 7.0-6.2 (m, 10H, ArH), 5.78 (d, 4H, thiourea), 5.20 (t, 4H, ³J_{HH}=8.8 Hz, CH gluc), 5.09 (t, 4H, ³J_{HH}=9.4 Hz, CH gluc), 4.96 (t, 4H, ³J_{HH}=9.8 Hz, CH gluc), 4.81 (t, 4H, ³J_{HH}=8.6 Hz, CH gluc), 4.53 and 3.05 (ABq, 8H, ²J_{HH}=13.4 Hz, Ar-CH₂-Ar), 4.11 (d, 4H, ²J_{HH}=7.6 Hz, CH₂), 3.99 (d, 4H, ²J_{HH}=7.6 Hz, CH₂), 3.93 (m, 4H, OCH₂), 3.74-3.68 (m, OCH₂ + CH₂ + solvent), 2.1-1.8 (m, 50H, OAc + CH₂), 1.0 and 0.85 (m, 12H, CH₃). ¹³C-NMR (DMSO-*d*₆): δ = 184.6, 170.7, 170.5, 170.0, 169.8, 169.6, 169.5, 167.2, 164.7, 155.4, 152.2, 135.8, 134.7, 133.5, 127.8, 122.1, 120.9, 120.799.8, 82.0, 77.0, 76.8, 76.5, 73.9, 73.3, 72.8, 71.6, 71.4, 70.9, 68.3, 62.8, 62.0, 47.2, 37.3, 31.8, 31.0, 29.5, 29.2, 23.7, 23.5, 23.0, 22.6, 21.1, 20.9, 20.8, 20.7, 14.4, 11.1, 10.4 ppm. MS (FAB): *m/z* = 2368.1 ([M+H⁺], calcd 2365.0).

Calix[4]arene bis(β -D-cellobiosyl)dimelamine (5d). 1 ml of a freshly prepared sodium methoxide solution (23 mM) was added to a solution of dimelamine **5c** (100 mg, 0.06 mmol) in MeOH (4 ml). The solution was stirred for 3 hours at room temperature. Amberlite IR 120 (H⁺) washed with MeOH was added to the solution for exchange of Na⁺ for H⁺. The Amberlite resin was filtered off and the product concentrated *in vacuo* to give pure **5d** as white solid in 85% yield. ¹H-NMR (DMSO-*d*₆): δ = 9.0-8.0 (m, NH + NH₂), 7.7-7.3 (m, 4H, ArH), 6.27 (m, 6H, ArH), 5.38-08 (brm, 8H, CH₂ celb + CH celb), 5.00 (m, 4H, CH₂ celb), 4.75 (m, 2H, CH celb), 4.59 (m, 6H, CHcelb), 4.4-4.2 (br m, 8H Ar-CH₂-Ar + CH celb), 3.88 (m, 4H, OCH₂), 3.8-2.8 (br m, CH celb + OH + OCH₂ + CH₂, solvent), 1.92-1.76 (m, 8H, CH₂), 1.06 (t, 6H, ³J_{HH}=7.2 Hz, CH₃), 0.94-0.78 (m, 18H, CH₃). ¹³C-NMR (DMSO-*d*₆): δ = 155.4, 152.6, 136.0, 134.0, 133.3, 129.4, 128.7, 127.7, 122.1, 121.2, 103.6, 84.1, 80.7, 77.8, 77.1, 76.9, 76.5, 73.8, 72.8, 70.5, 61.5, 60.6, 51.4, 47.3, 37.1, 31.0, 23.8, 23.5, 23.0, 11.1, 10.4 ppm. MALDI-TOF-MS: *m/z* = 1780.6 ([M+H⁺], calcd 1776.8).

Calix[4]arene bis(*L*-gulosyl)dimelamine (5e). A mixture of **2g** (295 mg, 0.29 mmol), (-)-2,3,4,6-di-*O*-isopropylidene-2-keto-*L*-gulonic acid (340 mg, 1.1 mmol), HBTU (443 mg, 1.1 mmol), HOBT (157 mg, 1.1 mmol) and DIPEA (0.4 ml, 2.3 mmol) in CH₂Cl₂ (15 ml) was stirred at room temperature for 3 days. CH₂Cl₂ was added and the organic layer was washed with 1M HCl, 10% Na₂CO₃ and brine, and dried over Na₂SO₄. The product was concentrated *in vacuo* to give dimelamine **5e** as a solid in 41% yield. ¹H-NMR (CDCl₃): δ = 8.01 (d, 4H, ²J_{HH}=8.1 Hz, CH₂ gul), 7.4-6.8 (m, ArH + solvent), 5.39 (s, 2H, CH), 5.18 (s, 2H, CH), 4.77 (s, 2H, CH),), 4.37 and 3.12 (ABq, 8H, ²J_{HH}=9.0 Hz, Ar-CH₂-Ar), 3.78-3.69 (m, 4H, OCH₂), 3.66-3.59 (m, 4H, OCH₂), 1.84-1.59 (m, 8H, CH₂), 1.47 (s, 12H, CH₃ gul), 1.19 (s, 12H, CH₃ gul), 1.06-1.00 (m, 6H, CH₃), 0.82-0.72 (m, 18H, CH₃). MALDI-TOF-MS: *m/z* = 1525 ([M+H⁺], 1523.8).

5,17-*N,N*-Bis[4-amino-6-(2-(ethanoic acid ethyl ester)amino)-1,3,5-triazin-2-yl] diamino-25,26,27,28-tetra propoxycalix[4]arene (6a) A solution of calix[4]arene bis(chlorotriazine) **9** (250 mg, 0.28 mmol), glycine ethyl ester hydrochloride (400 mg, 2.8 mmol) and DIPEA (0.4 ml, 2.3 mmol) in freshly distilled THF (20 ml) was stirred at 90°C for 1 week. The product was precipitated in water, and recrystallized from methanol. Pure dimelamine **6a** was obtained as a white solid in 74% yield (213 mg, 0.21 mmol). ¹H-NMR (DMSO-*d*₆): δ = 7.5-7.2 (br m, 6H, ArH), 6.4-6.0 (br m, 4H, *o*-NHAr), 4.32 and 3.11 (ABq, 8H, ²J_{HH}=12.9 Hz, Ar-CH₂-Ar), 4.1-4.0 (m, 8H, NHCH₂C(O)O + C(O)OCH₂), 3.95-3.85 (m, 4H, OCH₂), 3.65-3.55 (m, 4H, OCH₂), 1.95-1.75 (br m, 8H, OCH₂CH₂), 1.25-1.05 (br m, 6H, CH₃), 1.05 and 0.89 (t, 6H, ³J_{HH}=7.3 Hz, OCH₂CH₂CH₃). MS (FAB): *m/z* = 1013.3 ([M+H⁺], calcd 1013.5). Anal. Calcd for C₅₄H₆₈N₁₂O₈: C 64.01, H 6.76, N 16.59; found C64.43, H 6.94, N 16.62.

5,17-*N,N*-Bis[4-amino-6-(2-(ethanoic acid)amino)-1,3,5-triazin-2-yl] diamino-25,26,27,28-tetra propoxycalix[4]arene (6a'). To a solution of dimelamine **6a** (800 mg, 0.79 mmol) in THF/MeOH (20 ml; 1:1 v/v) a solution of 1 N NaOH (5 ml, 5 mmol) in water was added. The mixture was stirred at room temperature for 4 hours (TLC CH₂Cl₂:MeOH:AcOH = 90:9.5:0.5). The solution was quenched with aqueous citric acid

solution (0.5 M). Then, the compound was extracted with CH₂Cl₂ and the organic layer was separated and washed with brine. The organic layer was dried over Na₂SO₄ and the product was concentrated *in vacuo*. Compound **6a'** was obtained as a solid in 85% yield (642 mg, 0.67 mmol). ¹H-NMR (DMSO-*d*₆): δ = 12.4 (br s, COOH), 7.43 (s, 4H, ArH), 6.24 (m, 6H, ArH), 4.30 and 3.08 (ABq, 8H, ²J_{HH}=12.6 Hz, Ar-CH₂-Ar), 3.91 (m, 8H, OCH₂+CH₂), 3.61 (m, 4H, OCH₂), 2.0-1.8 (m, 8H, CH₂), 1.06 and 0.89 (t, 12H, CH₃). MS (FAB): *m/z* = 957.4 ([M+H⁺], calcd 956.5).

5,17-*N,N*-Bis[4-amino-6-(2-(propanoic acid methyl ester)amino)-1,3,5-triazin-2-yl]diamino-25,26,27,28-tetra propoxycalix[4]arene (6b) A solution of calix[4]arene bis(chlorotriazine) **9** (250 mg, 0.28 mmol), *L*-alanine methyl ester hydrochloride (198 mg, 1.4 mmol) and DIPEA (1.0 ml, 5.7 mmol) in freshly distilled THF (10 ml) was stirred at 90°C for 1 week. The solution was concentrated *in vacuo* and the crude was redissolved in CH₂Cl₂ and the organic layer was washed successively with 0.5 M HCl, 0.1 M NaHCO₃ and brine. In addition, the organic layer was dried over MgSO₄ and concentrated *in vacuo*, resulting in a light brown powder. Dimelamine **6b** was obtained in 74% yield (213 mg, 0.21 mmol). ¹H-NMR (DMSO-*d*₆): δ = 6,35-6,05 (br m, 10H, ArH), 4.66-4.45 (br m, 2H, chiral CH), 4.3 and 3.1 (ABq, 8H, ²J_{HH}=12.9 Hz, Ar-CH₂-Ar), 3.9 (t, 4H, ³J_{HH}=7.8 Hz, OCH₂), 3.68-3.49 (br m, 10H, OCH₂ + C(O)OCH₃), 2.0-1.7 (br m, 8H, OCH₂CH₂), 1.35 (d, 6H, ²J_{HH}=7.2 Hz, CH₃), 1.07 and 0.88 (t, 12H, ³J_{HH}=7.4 Hz, OCH₂CH₂CH₃). MS (FAB): *m/z* = 1013.6 ([M+H⁺], calcd 1013.5). Anal. Calcd for C₅₄H₆₈N₁₂O₈•2H₂O : C 61.82, H 6.92, N 16.02; found C62.02, H 6.86, N 16.10.

5,17-*N,N*-Bis[4-amino-6-(2-(4-(methylthio)butanoic acid methyl ester)amino)-1,3,5-triazin-2-yl]diamino-25,26,27,28-tetra propoxycalix[4]arene (6c) A solution of calix[4]arene bis(chlorotriazine) **9** (250 mg, 0.28 mmol), *L*-methionine methyl ester hydrochloride (560 mg, 2.8 mmol) and DIPEA (0.4 ml, 2.3 mmol) in freshly distilled THF (10 ml) was stirred at 90°C for 1 week. After completion of the reaction the solution was concentrated *in vacuo*, the crude was redissolved in CH₂Cl₂ and the organic layer was washed successively with 0.5 M HCl, 0.1 M NaHCO₃ and brine. In addition, the organic layer was dried over MgSO₄ and concentrated *in vacuo*, resulting in a white

powder. Pure dimelamine **6c** was obtained in 69% yield (221 mg, 0.19 mmol). $^1\text{H-NMR}$ (DMSO- d_6): $\delta = 6,43-6,04$ (br m, 10H, ArH), 4.82-4.55 (br m, 2H, chiral CH), 4.3 and 3.1 (ABq, 8H, $^2J_{\text{HH}}=12.8$ Hz, Ar-CH₂-Ar), 3.9 (t, 4H, $^3J_{\text{HH}}=8.1$ Hz, OCH₂), 3.7-3.5 (br m, 10H, OCH₂ + C(O)OCH₃), 2.65-2.4 (br m, 4H, CHCH₂CH₂S), 2.16-1.65 (br m, 18H, OCH₂CH₂ + CHCH₂ + CHCH₂CH₂SCH₃), 1.64 and 0.87 (t, 12H, $^3J_{\text{HH}}=7.4$ Hz, OCH₂CH₂CH₃). MS (FAB): $m/z = 1133.5$ ([M+H⁺], calcd 1133.5).

5,17-N,N-Bis[4-amino-6-(2-(6-N-Boc-aminohexanoic acid methyl ester)amino)-1,3,5-triazin-2-yl]diamino-25,26,27,28-tetra propoxycalix[4]arene (6d) A solution of calix[4]arene bis(chlorotriazine) **9** (1.0 g, 1.14 mmol), N_ε-BOC-*L*-lysine methyl ester hydrochloride (3.0 g, 10.2 mmol) and DIPEA (2.0 ml, 11.4 mmol) in freshly distilled THF (20 ml) was stirred at 90°C for 1 week. The solution was cooled down to room temperature. Then the product was precipitated in water, and recrystallized from methanol. Pure dimelamine **6d** was obtained as white powder in 85% yield (1.28 g, 0.96 mmol). $^1\text{H-NMR}$ (DMSO- d_6): $\delta = 6,3-6,05$ (br m, 10H, ArH), 4.58-4.40 (br m, 2H, chiral CH), 4.3 and 3.1 (ABq, 8H, $^2J_{\text{HH}}=12.6$ Hz, Ar-CH₂-Ar), 3.9 (t, 4H, $^3J_{\text{HH}}=8.0$ Hz, OCH₂), 3.7-3.5 (br m, 10H, OCH₂ + C(O)OCH₃), 2.96-2.78 (m, 4H, CH₂NHC(O)O), 2.0-1.8 (br m, 8H, OCH₂CH₂), 1.75-1.65 (m, 4H, CHCH₂), 1.45-1.2 (br m, 26H, Boc + CHCH₂CH₂CH₂), 1.07 and 0.87 (t, 12H, $^3J_{\text{HH}}=7.4$ Hz, OCH₂CH₂CH₃). MS (FAB): $m/z = 1327.9$ ([M+H⁺], calcd 1327.7). Anal. Calcd for C₇₀H₉₈N₁₄O₁₂: C 61.66, H 7.54, N 14.38; found C 61.89, H 7.50, N 14.42.

5,17-N,N-Bis[4-amino-6-(2-(6-aminohexanoic acid methyl ester)amino)-1,3,5-triazin-2-yl]diamino-25, 26,27,28-tetra propoxycalix[4]arene (6e). Dimelamine **6d** (500 mg, 0.38 mmol) was dissolved in CH₂Cl₂ (8 ml) and trifluoroacetic acid (8 ml). The solution was stirred for 2 hours at room temperature. The product was concentrated *in vacuo*. Toluene was used for azeotropic removal of residual trifluoroacetic acid. The product was dissolved in CH₂Cl₂ and washed twice with 1 N NaOH. The organic layer was dried over Na₂SO₄ and the product was concentrated *in vacuo*. Pure dimelamine **6e** was obtained as a white solid in 24% yield. $^1\text{H NMR}$ (CDCl₃): $\delta = 7.1-6.1$ (br m, 10H, ArH), 4.64-4.58 (br m, 2H, chiral CH), 4.3 and 3.1 (ABq, 8H, $^2J_{\text{HH}}=12.6$ Hz, Ar-CH₂-Ar), 3.9 (br m, 4H,

OCH₂), 3.7-3.5 (br m, 10H, OCH₂ + C(O)OCH₃), 2.64-2.49 (m, 4H, CH₂NH₂), 2.0-1.6 (br m, 12H, OCH₂CH₂ + CHCH₂), 1.45-1.2 (br m, 8H, CHCH₂CH₂CH₂), 1.07 and 0.87 (t, 12H, ³J_{HH}=7.4 Hz, OCH₂CH₂CH₃). MALDI-TOF-MS: *m/z* = 1149.8 ([M+Na⁺], calcd 1149.6). Anal. Calcd for C₆₀H₈₂N₁₄O₈: C 63.92, H 7.33, N 17.39; found C 60.18, H 7.23, N 15.61.

5,17-*N,N*-Bis[4-amino-6-(2-(6-*N*-Boc-aminohexanoic acid)amino)-1,3,5-triazin-2-yl]diamino-25, 26,27,28-tetra propoxycalix[4]arene (6f). To a solution of dimelamine **6d** (500 mg, 0.38 mmol) in THF/MeOH (10 ml; 1/1 v/v) was added 1 N NaOH (1.5 ml, 1.5 mmol) in water. The mixture was stirred at room temperature for 14 hours (TLC CH₂Cl₂/MeOH/AcOH = 90:9.5:0.5). The solution was quenched with aqueous citric acid solution (0.5 M). Then CH₂Cl₂ was added and the organic layer was separated. The organic layer was washed once more with aqueous citric acid solution (0.5 M), followed by 5% aqueous NaHCO₃ solution, and brine. The organic layer was dried over Na₂SO₄ and the product was concentrated *in vacuo*. Dimelamine **6f** was obtained in 83% yield (0.41 g, 0.32 mmol). ¹H NMR (DMSO-*d*₆): δ = 8.07 (s, 2H, NH), 6.8-6.0 (br m, 10H, ArH), 4.31 and 3.08 (ABq, 8H, ²J_{HH}=12.6 Hz, Ar-CH₂-Ar), 4.15 (m, 2H, chiral CH), 3.86 (m, 4H, OCH₂), 3.78 (m, 4H, CH₂), 3.63 (m, 4H, OCH₂), 2.86 (m, 10H, CH₂+OCH₃), 2.0-1.6 (br m, 16H, CH₂), 1.4 (br s, 18H, BOC), 1.05 and 0.90 (m, 12H, CH₃). MS (FAB): *m/z* = 1321.7 ([M+Na⁺], calcd 1321.7).

Calix[4]arene bis(Gly-Gly-OEt)dimelamine (7a). A solution of calix[4]arene bis(chlorotriazine) **9** (100 mg, 0.11 mmol), glycineglycine ethyl ester hydrochloride (201 mg, 1.02 mmol) and DIPEA (0.4 ml, 2.3 mmol) in freshly distilled THF (10 ml) was stirred at 90°C for 1 week. The solution was cooled down and the product was precipitated in water, filtered off and washed with water. Pure **7a** was obtained as a white solid in 85% yield. ¹H NMR (DMSO-*d*₆): δ = 7.45 (s, 4H, ArH), 6.25 (m, 6H, ArH), 4.29 and 3.07 (ABq, 8H, ²J_{HH}=12.6 Hz, Ar-CH₂-Ar), 4.03 (m, 4H, CH₂), 3.90-3.75 (m, 16H, OCH₂+CH₂), 3.60 (m, 4H, CH₂), 2.0-1.75 (m, 8H, CH₂), 1.2-1.0 (m, 12H, CH₃), 0.87 (t, 6H, CH₃). MS (FAB): *m/z* = 1127.5 ([M+H⁺], calcd 1127.6).

Calix[4]arene bis(Gly-*L*-Ala-OMe)dimelamine (7b). A mixture of **6a'** (120 mg, 0.13 mmol), *L*-alanine methyl ester hydrochloride (35 mg, 0.25 mmol), HATU (106 mg, 0.28 mmol) and DIPEA (0.11ml) in CHCl₃ (10 ml) was stirred for 14 hours at room temperature. Then CHCl₃ was added and the organic layer was washed successively with 5% citric acid, 5% NaHCO₃, brine and dried over MgSO₄. The product was purified by column chromatography (CH₂Cl₂:MeOH:NH₄OH = 90/9.5/0.5) to give pure **7b** as a white solid in 50% yield. ¹H-NMR (CD₃OD): δ = 6.9-6.4 (br m, 10H, ArH), 4.48 (s, 2H, CH), 4.36 and 3.05 (ABq, 8H, ²J_{HH}=12.6 Hz, Ar-CH₂-Ar), 3.91 (s, 4H, CH₂), 3.85 (t, 4H, OCH₂), 3.67 (t, 4H, OCH₂), 3.57 (s, 6H, OCH₃), 1.9-1.8 (m, 8H, CH₂), 1.19 (s, 6H, CH₃), 0.98 and 0.89 (t, 12H, CH₃). MS (FAB): *m/z* = 1127.5 ([M+H⁺], calcd. 1127.6).

Calix[4]arene bis(Gly-*L*-Ser-OMe)dimelamine (7c). A mixture of **6a'** (150 mg, 0.16 mmol), *L*-serine methyl ester hydrochloride (50 mg, 0.32 mmol), HATU (135 mg, 0.35 mmol) and DIPEA (0.14ml) in CHCl₃ (10 ml) was stirred for 14 hours at room temperature. Then, CHCl₃ was added and the solution was washed successively with 5% citric acid, 5% NaHCO₃, brine and dried over MgSO₄. The product was purified by column chromatography (CH₂Cl₂:MeOH:NH₄OH = 90/9.5/0.5) to give **7c** as a white solid in 23% yield. ¹H-NMR (CD₃OD): δ = 6.8-6.4 (br m, 10H, ArH), 4.38 and 3.05 (ABq, 8H, ²J_{HH}=12.6 Hz, Ar-CH₂-Ar), 4.49 (m, 4H, CH₂), 3.87 (t, 4H, OCH₂), 3.67 (m, 10H, OCH₂+OCH₃), 1.9-1.8 (m, 8H, CH₂), 0.98 and 0.89 (t, 12H, CH₃). MS (FAB): *m/z* = 1159.6 ([M+H⁺], calcd. 1159).

Calix[4]arene bis(*L*-Lys(Boc)-Glu(OcHx)-NH*i*Pr)dimelamine (7d). Dimelamine **9** (225 mg, 0.17 mmol), HOBT (70 mg, 0.52 mmol) and DIPEA (0.15 ml, 0.87 mmol) were dissolved in CH₂Cl₂ (10 ml) and the solution was cooled in an ice bath. EDC·HCl (100 mg, 0.52 mmol) was added to this solution and after stirring the solution for 10 minutes, *L*-Lys(Boc)-Glu(OcHx)-NH*i*Pr (142 mg, 0.52 mmol) in CH₂Cl₂ (10 ml) was added. The mixture was stirred for 4 hours at room temperature, then concentrated *in vacuo* and the residue redissolved in ethylacetate (150 ml). The organic layer was washed successively with 0.5 M citric acid, 5% NaHCO₃, brine and dried over Na₂SO₄. The product was purified by column chromatography (CH₂Cl₂:MeOH:NH₄OH = 90/9.5/0.5). Pure **7d** was

obtained as a white solid in 48% yield. $^1\text{H-NMR}$ (CDCl_3): $\delta = 7.2\text{-}6.7$ (br m, 10H, ArH), 4.8-4.6 (br m, 2H, CH), 4.38 (m, 4H, Ar-CH₂-Ar), 4.0-3.8 (br m, 8H, OCH₂ + CH₂), 3.7-3.5 (br m, 4H, OCH₂), 3.11 (m, 8H, Ar-CH₂-Ar + CH₂), 2.35 (m, 2H, CH), 2.1-1.0 (br m, 64H, CH₂+ OcHx + CH₃+ Boc), 0.85 (t, 6H, CH₃). MALDI-TOF-MS: $m/z = 1802.9$ ($[\text{M}+\text{H}^+]$, calcd 1803.1).

Calix[4]arene bis(L-Lys(Boc)-Tyr-OMe)dimelamine (7e). A solution of **6f** (130 mg, 0.10 mmol), HOBT (54 mg, 0.40 mmol) and DIPEA (0.17 ml, 1.0 mmol) in freshly distilled THF (10 ml) was cooled in an ice bath. EDC·HCl (77 mg, 0.4 mmol) was added. After stirring for 10 minutes, *L*-tyrosine methyl ester (78 mg, 0.4 mmol) was added. The mixture was stirred for 8 hours at room temperature, then the solution was concentrated *in vacuo* and the residue redissolved in CH₂Cl₂ (75 ml) The organic layer was washed successively with 0.5 M citric acid, 5% NaHCO₃ and brine, and dried over Na₂SO₄. The product was purified using column chromatography (CH₂Cl₂:MeOH:NH₄OH = 95/4.5/0.5) to give pure **7e** as a solid in 66% yield. $^1\text{H-NMR}$ (CDCl_3): $\delta = 7.2\text{-}6.4$ (br m, 18H, ArH + TyrH), 4.85-4.7 (m, 6H, CH₂ + CH), 4.37 (d, 4H, Ar-CH₂-Ar), 4.20 (m, 2H, CH), 3.96 (m, 4H, OCH₂), 3.76-3.52 (m, 10H, OCH₂ + OCH₃), 3.2-2.7 (m, 12H, Ar-CH₂-Ar + CH₂), 2.0-1.2 (m, 34H, CH₂ + Boc), 1.03 and 0.81 (t, 12H, CH₃). MALDI-MS: $m/z = 1654.0$ ($[\text{M}+\text{H}^+]$, calcd 1653.9).

Calix[4]arene bis(Gly-Gly-Gly-OEt)dimelamine (8a). A mixture of **6a'** (290mg, 0.30 mmol), Gly-Gly-OEt·HCL (150mg, 0.75 mmol), HATU (342 mg, 0.90 mmol) and DIPEA (0.26 ml, 1.5 mmol) in CHCl₃ (20 ml) was stirred at room temperature for 14 hours. The mixture was washed successively with 0.5 M HCl, NaHCO₃ (5%), brine and dried over Na₂SO₄. The crude product was purified by column chromatography (CH₂Cl₂:MeOH:NH₄OH = 90/9.5/0.5) to give pure **8a** as a white solid in 68% yield. $^1\text{H-NMR}$ (CDCl_3): $\delta = 6.9\text{-}6.3$ (br m, 10H, ArH), 4.36 and 3.04 (ABq, 8H, $^2J_{\text{HH}}=12.5$ Hz, Ar-CH₂-Ar), 3.90 (t, 4H, $^3J_{\text{HH}}=8.0$, OCH₂), 3.62 (t, 4H, $^3J_{\text{HH}}=6.6$, OCH₂), 3.90 (q, 4H, $^3J_{\text{HH}}=6.6$, OCH₂), 2.73 (s, 18H, CH₂ + CH₃), 1.94-1.72 (m, 8H, CH₂), 0.99 and 0.85 (t, 12H, CH₃). MS (FAB): $m/z = 957.4$ ($[\text{M}+\text{H}^+]$, calcd 1240.6). Anal. Calcd for C₆₂H₈₀N₁₆O₁₂·2H₂O: C=58.29, H=6.63, N=17.54; found C=58.36, H=6.50, N=17.25.

***L*-Gln(Trt)-*L*-Ser(O*t*Bu)-OMe.** *L*-Fmoc-Gln(Trt)-OH (750 mg, 1.23 mmol), *L*-Ser(O*t*Bu)-OMe (275 mg, 10.30 mmol) and DIPEA (0.4 ml, 2.46 mmol) were dissolved in acetonitrile (10 ml). HBTU (493 mg, 1.30 mmol) was added and the reaction mixture was stirred at room temperature for 1 hours. The solvent was evaporated under reduced pressure and the crude product was purified by column chromatography (CH₂Cl₂:MeOH:NH₄OH = 95/4.5/0.5) to give pure Fmoc-*L*-Gln(Trt)-*L*-Ser(O*t*Bu)-OMe as a white solid in 90% yield. ¹H-NMR (CDCl₃): δ = 7.82 (d, 2H Fmoc), 7.64 (d, 2H, Fmoc), 7.52 (t, 2H, Fmoc), 7.29 (m, 17H, Trt + Fmoc), 7.10 (d, 1H, NH), 5.83 (d, 1H, NH), 4.65 (m, 1H, Fmoc), 4.44 (d, 2H, Fmoc), 4.18 (q, 2H, CH), 3.82-3.78 (dd, 1H, CH₂), 3.69 (s, 3H, OCH₃), 3.48-3.44 (dd, 1H, CH₂), 2.42 (t, 2H, CH₂), 2.18-2.12 (br m, 2H, CH₂), 1.08 (s, 9H, *t*Bu). MS (FAB): *m/z* = 768.3 ([M+H⁺], calcd 768.4).

Subsequently, Fmoc-*L*-Gln(Trt)-*L*-Ser(O*t*Bu)-OMe (850 mg, 1.12 mmol) was dissolved in acetonitrile (10 ml) and diethylamine (5 ml) was added and the solution mixture was stirred for 1.5 hours at room temperature. The solvents were evaporated and the residue was triturated with diethylether. The obtained white solid was filtered off and washed twice with diethylether. The obtained product was used without further purification.

Calix[4]arene bis(Lys(Boc)-Gln(Trt)-Ser(O*t*Bu)-OMe)dimelamine (8b). A solution of **6f** (182 mg, 0.14 mmol), HOBT (39 mg, 0.29 mmol) and DIPEA (0.1 ml, 0.5 mmol) in CH₂Cl₂ (10 ml) was cooled to 0°C. EDC·HCl (59 mg, 0.31 mmol) in CH₂Cl₂ (4 ml) was added. After 10 minutes of stirring *L*-Gln(Trt)-*L*-Ser(O*t*Bu)-OMe (158 mg, 0.29 mmol) and DIPEA (0.1 ml, 0.05 mmol) in CH₂Cl₂ (8 ml) was added. The solution was stirred for 24 hours at room temperature after which the solvents were removed under reduced pressure. The residue was taken up in CH₂Cl₂ and washed successively with 0.5 M citric acid, 1 N Na₂CO₃, 5% NaHCO₃, and brine. The organic layer was dried over Na₂SO₄, concentrated and the product was purified by column chromatography (CH₂Cl₂:MeOH:NH₄OH = 95/4.5/0.5) to give pure **8b** as a white solid in 45% yield. ¹H-NMR (DMSO-*d*₆): δ = 7.4-6.8 (br m, 25H, ArH + Trt), 4.5 (m, 2H, CH), 4.32 (d, 4H, Ar-CH₂-Ar), 4.2 (m, 4H, CH), 3.88 (t, -OCH₂), 3.7-3.5 (m, 10H, OCH₂ + OCH₃), 3.2-2.7 (m,

20H, Ar-CH₂-Ar, CH₂), 2.4-1.8 (m, 8H, CH₂), 1.4-1.0 (m, 48H, CH₂ + Boc + tBu), 0.95-0.75 (m, 12H, CH₃). MALDI-MS: $m/z = 2356.4$ ($[M+Ag^+]$, calcd 2354.3).

3.7 References

1. Fiammengo, R.; Crego-Calama, M.; Reinhoudt, D. N. *Curr. Opin. Chem. Biol.* **2001**, *5*, 660-673.
2. Whitesides, G. M.; Simanek, E. E.; Mathias, J. P.; Seto, C. T.; Shin, D. N.; Mammen, M.; Gordon, D. M. *Acc. Chem. Res.* **1995**, *28*, 37-44.
3. Benjamini, E.; Sunshine, G.; Leskowitz, S. *Immunology, A Short Course*; 3rd ed., Wiley: New York, 1996.
4. Stryer, L. *Biochemistry*; 4th ed. Freeman and Company: New York, 1995.
5. Vreekamp, R. H.; Van Duynhoven, R. H.; Hubert, M.; Verboom, W.; Reinhoudt, D. N. *Angew. Chem. Int. Ed.* **1996**, *35*, 1215-1218.
6. Timmerman, P.; Jolliffe, K. A.; Crego-Calama M.; Weidmann, J. L.; Prins, L. J.; Cardullo, F.; Snellink-Ruel, B. H. M.; Fokkens, R. H.; Nibbering, N. M. M.; Shinkai, S.; Reinhoudt, D. N. *Chem. Eur. J.* **2000**, *6*, 4104-4115.
7. Seto, C. T.; Whitesides, G. M. *J. Am. Chem. Soc.* **1990**, *112*, 6409-6411.
8. Zerkowski, J. A.; Seto, C. T.; Wierdo, D. A.; Whitesides, G. M. **1990**, *112*, 9025-9026.
9. Timmerman, P.; Vreekamp, R. H.; Hulst, R.; Verboom, W.; Reinhoudt, D. N.; Risannen, K.; Udachin, K. A.; Ripmeester, J. *Chem. Eur. J.* **1997**, *3*, 1823-1832.
10. Timmerman, P.; Prins, L. J. *Eur. J. Org. Chem.* **2001**, *17*, 3191-3205.
11. Reinhoudt, D. N.; Timmerman, P.; Cardullo, F.; Crego-Calama, M. *NATO*; Ungaro, R.; Dalcanale, E., Kluwer Academic Publishers: Dordrecht, 1999; pp181-195.
12. Prins, L. J.; Jolliffe, K. A.; Hulst, R.; Timmerman, P.; Reinhoudt, D. N. *J. Am. Chem. Soc.* **2000**, *122*, 3617-3627.
13. Prins, L. J.; Huskens, J.; De Jong, F.; Timmerman, P.; Reinhoudt, D. N. *Nature* **1999**, *398*, 498-502.
14. Prins, L. J.; De Jong, F.; Timmerman, P.; Reinhoudt, D. N. *Nature* **2000**, *408*, 181-184.
15. Eliel, E. L.; Wilen S.H. *Stereochemistry of Organic Compounds*; John Wiley &

- Sons, Inc.: New York, 1994.
16. Jolliffe, K. A.; Crego-Calama, M.; Fokkens, R.; Nibbering, N. M. M.; Timmerman, P.; Reinhoudt, D. N. *Angew. Chem. Int. Ed.* **1998**, *37*, 1247-1251.
 17. Kerckhoffs, J. M. C. A.; Crego-Calama, M.; Luyten, I.; Timmerman, P.; Reinhoudt, D. N. *Org. Lett.* **2000**, *2*, 4121-4124.
 18. Ishi-i, T.; Crego-Calama, M.; Timmerman, P.; Reinhoudt, D. N.; Shinkai, S. *J. Am. Chem. Soc.* **2002**, *124*, 14631-14641.
 19. Yamamoto, I.; Fukui, K.; Yamamoto, S.; Ohta, K.; Matsuzaki, K. *Synthesis* **1985**, 686-688.
 20. Ogura, H.; Takahashi, H. *Heterocycles* **1982**, 87-90.
 21. Oshovsky, G. V.; Verboom, W.; Fokkens, R. H.; Reinhoudt, D. N. Accepted for publication in *Chem. Eur. J.* **2004**.
 22. The percentage of assembly was determined by comparison of the H_a+H_b intensity with the ArCH₂Ar of the calix[4]arene part. Assembly **1a**₃•(DEB)₆ is used as standard, for which this ratio was arbitrarily set to 100%.
 23. Detailed analyses of energetic parameters are described in Chapter 4.
 24. Mammen, M.; Simanek, E. E.; Whitesides, G. M. *J. Am. Chem. Soc.* **1996**, *118*, 12614-12623.
 25. Dwek, R.A. *Chem. Rev.* **1996**, *96*, 683-720.
 26. Mammen, M.; Choi, S.-K.; Whitesides, G.M. *Angew. Chem. Int. Ed.*, **1998**, *37*, 2754-2794.
 27. Bielejewska, A. G.; Marjo, C. E.; Prins, L. J.; Timmerman, P.; De Jong, F.; Reinhoudt, D. N. *J. Am. Chem. Soc.* **2001**, *123*, 7518-7533.
 28. Prins, L. J. *Thesis: Non-Covalent Synthesis of Chiral Hydrogen-Bonded Assemblies*, University of Twente, Enschede the Netherlands, ISBN 90-365-1627-7, 2001.
 29. Occasionally double rosette formation could be observed with ¹H NMR spectroscopy, but these assemblies are hardly CD active because either the opposite chirality inducing components strongly affect the orientation of the chromophores responsible for the CD activity or coincidentally cause opposite CD activity of identical intensity.
 30. Cheuk, K. K. L.; Lam, J. W. Y.; Lai, L. M.; Dong, Y.; Tang, B. Z. *Macromolecules* **2003**, *36*, 9752-9762.

Thermodynamic Stability of Hydrogen-Bonded Nanosized Structures: a calorimetric study*

In this chapter a calorimetric study of the self-assembly of hydrogen-bonded aggregates (rosettes) in solvent mixtures of different polarity is described. The C_{50} parameter, defined as the concentration when 50% of the components are incorporated in the assembly, is used to compare assemblies with different stoichiometry. ΔG° , ΔH° and $T\Delta S^\circ$ values indicate that the thermodynamics of double rosettes reflect the independent assembly of two individual single rosette structures or two rosettes reinforced by additional stabilizing interactions. In more polar solvents the stability of double rosettes decreased. From the correlation of ΔG° with solvent polarities it can be predicted that it should be possible to assemble double rosettes in pure methanol or water. In methanol this was proven by ^1H NMR and CD spectroscopy.

* Part of this work has been accepted for publication: Ten Cate, M.G.J.; Huskens, J.; Crego-Calama, M.; Reinhoudt, D.N., *Chem. Eur J.* **2004** (in press).

4.1 Introduction

Because hydrogen bonds are weak ($2\text{-}10\text{ kcal}\cdot\text{mol}^{-1}$),¹ self-assembly in polar solvents has received little attention. Most of the self-assembly studies in polar solvents are carried out using metal coordination²⁻¹⁴ or a combination of hydrogen bonding with other weak noncovalent interactions such as cation- π and π - π stacking which has led to molecular capsules stable in polar organic solvents.¹⁵⁻¹⁷ Furthermore, the use of multiple ionic interactions has been used to obtain stable supramolecular complexes in polar solvents.¹⁸⁻²³ Polar solvents such as methanol and water have the ability to act as hydrogen bond donor and acceptor, thereby competing for hydrogen bonding during assembly formation. This results in a decrease in stability of the hydrogen-bonded assemblies.

Whitesides *et al.* described qualitatively the stabilities of multiparticle hydrogen-bonded aggregates based in the number of hydrogen bonds and the number of particles.²⁴ Three indices I_{Tm} , I_G and $I_G/(n-1)$ were introduced to estimate relative stabilities of hydrogen-bonded aggregates based on a rosette motif. The I_{Tm} index is directly related to the number of hydrogen bonds and the number of particles and has shown to be the most valuable. The I_G index corresponds to a free energy of assembly and assumes an average net enthalpy of formation of each hydrogen bond in the solvent of interest²⁵ and an average translational and rotational energy. The $I_G/(n-1)$ index corresponds to a free energy of association per particle (n is the number of particles). These indices are useful to estimate qualitatively the relative stability among different aggregates with similar hydrogen bonding patterns. However, these indices do not distinguish differences in hydrogen bond strength within comparable assemblies. Neither do they distinguish between differences in stability due to steric strain or electronic influences induced by substituents that are present in the assembly.

This chapter describes quantitatively the thermodynamics of the self-assembly of hydrogen-bonded single and double rosettes in solvent mixtures of different polarity. The energetic parameters for the formation of single rosette assemblies as reported by Whitesides *et al.* in apolar solvent were analyzed,²⁶ and compared with the data of larger double rosette.

The single rosette $\mathbf{1}_3 \cdot (\text{BuCYA})_3$ (Figure 4.1), assembled from three *N,N*-di(4-*tert*-butylphenyl) melamine (**1**) molecules and three *n*-butyl cyanuric acid (BuCYA) molecules, has six DAD•ADA interactions with a formation of eighteen hydrogen bonds in total.

The double rosette motif involves calix[4]arenes diametrically substituted at the upper rim with two functionalized melamine units. Here, the calix[4]arene dimelamines bear a butyl or *L*-lysine(Boc) methyl ester moiety, which form well-defined assemblies $\mathbf{2}_3 \cdot (\text{DEB}/\text{BuCYA})_6$ with two equivalents of 5,5'-diethyl barbituric acid (DEB) or *n*-butyl cyanuric acid (BuCYA). Thus, the double rosette assemblies consist of three calix[4]arene dimelamines and six DEB (or BuCYA) with twelve DAD•ADA interactions. Each dimelamine is forming twelve hydrogen bonds (4 x DAD) and each DEB (or BuCYA) six hydrogen bonds (2 x ADA), giving a total of 36 hydrogen bonds within the assembly.²⁷⁻²⁹ Double rosettes, as studied by ¹H NMR and MALDI-TOF-MS,^{30,31} are stable in aprotic organic solvents such as dichloromethane, chloroform, benzene, and toluene even at 10⁻⁴ M. The high stability of this multiple DAD•ADA system makes it very useful to study the influence of more polar solvents on hydrogen-bonding. Previously our group reported association constants of 10² and 10⁴ M⁻¹ for melamine•barbiturate and melamine•cyanurate, respectively.³² In addition, experiments where chiral barbiturates in double rosettes were exchanged by achiral cyanurates³³ demonstrate that double rosettes with cyanurates are more stable than double rosettes with barbiturates. It is therefore expected that quantification of the thermodynamics for self-assembly of double rosettes will give a higher stability for double rosettes $\mathbf{2}_3 \cdot (\text{BuCYA})_6$ than for double rosettes $\mathbf{2}_3 \cdot (\text{DEB})_6$.

Isothermal titration microcalorimetry (ITC) was used to determine thermodynamic parameters of these self-assembly processes. ITC is the only technique able to measure directly the change in binding enthalpy (ΔH°) for reversible interactions. A more indirect method to determine thermodynamic parameters is the van't Hoff analysis.³⁴ This method requires variable temperature UV or NMR spectroscopy, assuming a zero heat capacity for the reaction that is an approximation. Besides measurement of ΔH° , well-designed ITC experiments allow the calculation of formation constants (K_f) and therefore, appropriate analyses of ITC data can give a very detailed thermodynamic analysis. ITC

has found widespread application within supramolecular chemistry, especially within host-guest recognition,³⁵⁻³⁸ but to the best of our knowledge, there are no examples of ITC studies for the assembly of complex noncovalent systems from multiple molecular components.

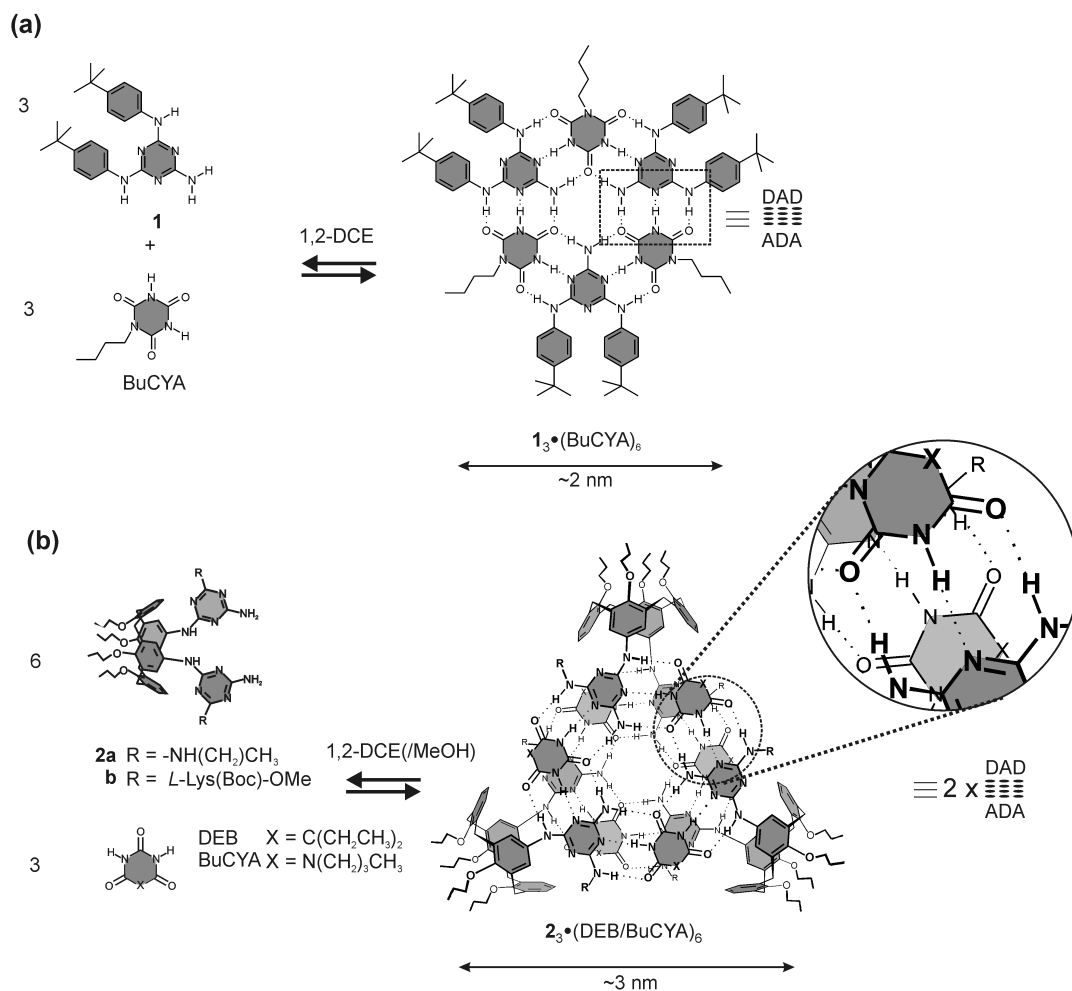


Figure 4.1 Structures of melamine **1**, **2a,b**, DEB, and BuCYA and self-assembly of a) single rosette $1_3 \bullet (\text{BuCYA})_3$, b) double rosettes $2_{a,b} \bullet (\text{DEB/BuCYA})_6$. The magnification shows the DAD•ADA binding motif present in the assemblies.

4.2 Results and discussion

4.2.1 Synthesis

Melamine **1** and **2a** were synthesized following literature procedures.^{28,32} The synthesis of compound **2b** is described in Chapter 3.

Characterization of the corresponding double rosette using ^1H NMR spectroscopy,^{30,33} confirmed the formation of the hydrogen-bonded assemblies $1_3\cdot(\text{DEB})_3$, $2_3\cdot(\text{BuCYA}/\text{DEB})_6$.

4.2.2 Isothermal titration microcalorimetry

As a typical example, Figure 4.2 shows the results of an ITC measurement for the formation of $2a_3\cdot(\text{BuCYA})_6$ using 0.050, 0.075, and 0.10 mM solutions of BuCYA in 1,2-DCE inside the ITC cell and 0.25, 0.375, and 0.50 mM of **2a** in 1,2-DCE as titrant, respectively.³⁹

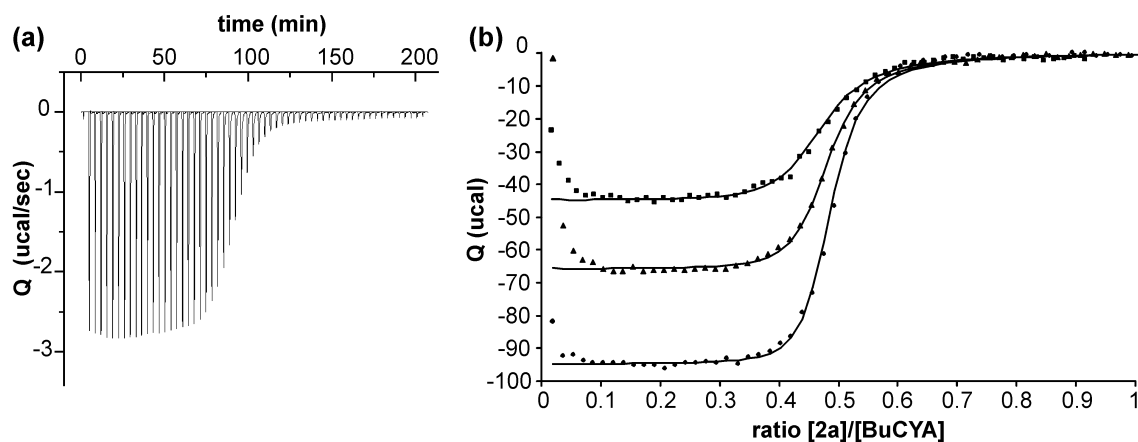


Figure 4.2 (a) ITC measurement (1,2-DCE, 298K) for the formation of $2a_3\cdot(\text{BuCYA})_6$; cell: 0.075 mM BuCYA, burette: 0.375 mM **2a**, (b) ITC titration curves obtained for formation of $2a_3\cdot(\text{BuCYA})_6$ (■, cell: 0.050 mM BuCYA, burette: 0.25 mM **2a**, ▲, cell: 0.075 mM BuCYA, burette: 0.375 mM **2a**, ●, cell: 0.010 mM BuCYA, burette: 0.50 mM **2a**).

The strong heat effects measured when dimelamine **2a** was added to BuCYA clearly indicate that the self-assembly process is strongly enthalpy driven. In addition, at all concentrations the ITC measurements indicate for **2a**:BuCYA complex formation a 1:2 ratio. This is consistent with the formation of a double rosette, where three molecules **2** and six molecules BuCYA self-assemble. Furthermore, the concentration dependence of the ITC titration curves in these experiments is typical for high-order self-assembly processes.

To determine ΔG° , ΔH° and $T\Delta S^\circ$ from the observed heat effects the ITC data have to be fitted to an appropriate binding model. The process of rosette formation can be divided in two parts. First, the formation of linear aggregates between melamines and barbiturates (or cyanurates) and second the cyclization towards rosette assemblies. Cyclization of linear aggregates is concentration dependent and driven by entropy. For self-assembly processes the complex or aggregate with the lowest stoichiometry, in which the hydrogen bonds are used the most efficiently, is preferred. Furthermore, preorganization of the building blocks can stimulate the rosette assemblies to cyclize, because during the formation of the linear aggregates only minor conformational changes have to be made for cyclization towards rosette assemblies, and therefore the entropy change within the cyclization step is minimal. On the other hand, favorable enthalpy changes due to hydrogen bonding will occur. Because of this, cyclization is strongly favored. For the self-assembly of single and double rosettes no other species than free melamine, free barbiturate (or cyanurate) and rosette assemblies in solution are observed with ^1H NMR spectroscopy and MALDI-TOF mass spectrometry.^{30,33}

For the equation shown in Figure 4.1, which means that single rosette assemblies are directly formed from three melamines and three barbiturates; follows that the formation constant (K_f) can be written as (K_f is expressed in M^{-5}):

$$K_f = \frac{[\mathbf{1}_3 \cdot \text{BuCYA}_3]}{[\mathbf{1}]^3 [\text{BuCYA}]^3} \quad (\text{Eq. 4.1})$$

Analogously, double rosette assemblies are directly formed from three calix[4]arene dimelamines and six barbiturates (or cyanurates), and the formation constant (K_f) can be written as (K_f is expressed in M^{-8}):

$$K_f = \frac{[\mathbf{2}_3 \cdot \text{BuCYA}_6]}{[\mathbf{2}]^3 [\text{BuCYA}]^6} \quad (\text{Eq. 4.2})$$

To analyse the obtained ITC data a nonlinear least-squares minimization protocol was used in a 3:3 and 3:6 complexation model for single and double rosette assemblies,

respectively. The heat effects, measured at three different concentrations, observed in the example shown in Figure 4.2 could be fitted to a 3:6 complexation model using $K_f = 2.7 \times 10^{43} \text{ M}^{-8}$ and $\Delta H^\circ = -123 \text{ kcal}\cdot\text{mol}^{-1}$ ($\Delta G^\circ = -59 \text{ kcal}\cdot\text{mol}^{-1}$ and $T\Delta S^\circ = -64 \text{ kcal}\cdot\text{mol}^{-1}$). Consistency in the results of the calorimetric titrations at all three concentrations clearly indicates that the applied model is valid.

4.2.3 Self-assembly in apolar solvent

4.2.3.1 Single vs. double rosettes

The results obtained after fitting the ITC data to the earlier described models are shown in table 4.1. Because it is not possible to compare directly the K_f (M^{-5}) of single rosettes with the K_f (M^{-8}) of double rosettes,⁴⁰ the concentration of the assembly that is present when 50% of the components are incorporated in the complex (C_{50}) were calculated (see table 1).⁴¹ Single rosette $\mathbf{1}_3\cdot(\text{BuCYA})_3$ with a C_{50} of 25 μM is less stable than double rosette $\mathbf{2b}_3\cdot(\text{BuCYA})_6$ ($C_{50} = 7.1 \mu\text{M}$). Thus, indicating that double rosette assemblies are stable at lower concentrations. Furthermore, the ΔH° for $\mathbf{2b}_3\cdot(\text{BuCYA})_6$ of $-96 \text{ kcal}\cdot\text{mol}^{-1}$ is about twice the value of ΔH° for $\mathbf{1}_3\cdot(\text{BuCYA})_3$ ($\Delta H^\circ = -50 \text{ kcal}\cdot\text{mol}^{-1}$). This implies that, in this case, the enthalpy change of double rosette assemblies is a summation of the enthalpy change of two single rosettes (formation of 36 (2 x 18) hydrogen bonds). In addition, for the double rosette $\mathbf{2a}_3\cdot(\text{BuCYA})_6$ the enthalpy change ($\Delta H^\circ = -123 \text{ kcal}\cdot\text{mol}^{-1}$) is about 2.5 times higher compared to the single rosette $\mathbf{1}_3\cdot(\text{BuCYA})_3$. In this case, the enthalpy change of the double rosette assembly is larger than the summation of the enthalpy of two single rosettes, which could indicate additional stabilizing interactions.

Table 4.1 *Thermodynamic parameters determined by ITC (298 K) for the self-assembly of single and double rosette assemblies in 1,2-DCE.*

Assembly	K_f	ΔH° (kcal·mol ⁻¹)	C_{50}^* (μ M)	ΔG° (kcal·mol ⁻¹)	$T\Delta S^\circ$ (kcal·mol ⁻¹)
1₃•(BuCYA)₃	$(1.4 \pm 0.3) \times 10^{20} \text{ M}^{-5}$	-50 ± 5	25 ± 1	-27.5 ± 0.2	-23 ± 5
2a₃•(DEB)₆	$(1.5 \pm 0.6) \times 10^{31} \text{ M}^{-8}$	-110 ± 2	23 ± 4	-42.3 ± 0.8	-68 ± 3
2a₃•(BuCYA)₆	$(2.7 \pm 2.0) \times 10^{43} \text{ M}^{-8}$	-123 ± 11	0.7 ± 0.1	-59.1 ± 0.5	-64 ± 11
2b₃•(DEB)₆	$(3.8 \pm 1.0) \times 10^{29} \text{ M}^{-8}$	-68 ± 5	35 ± 1	-40.3 ± 0.2	-28 ± 6
2b₃•(BuCYA)₆	$(1.4 \pm 0.8) \times 10^{34} \text{ M}^{-8}$	-96 ± 1	7.1 ± 0.6	-47.9 ± 0.4	-49 ± 1

* See ref. 40 & 41

For assembly **1₃•(BuCYA)₃** the $T\Delta S^\circ$ is $-22.5 \text{ kcal}\cdot\text{mol}^{-1}$, whereas for assemblies **2a₃•(BuCYA)₆** and **2b₃•(BuCYA)₆** $T\Delta S^\circ$ values of -64.0 and $-48.5 \text{ kcal}\cdot\text{mol}^{-1}$ were calculated, respectively. Single and double rosettes are built by assembling six and nine building blocks, respectively, leading to six and twelve enthalpic contributions for the six and twelve hydrogen bonding arrays (DAD•ADA) being formed, while entropically, the translational energies of only five or eight building blocks are restricted relative to the starting building block. Obviously, the lower number of entropic contributions is a direct consequence of the cyclization occurring in the assembly formation. When it is assumed that $T\Delta S^\circ$ is determined merely by gathering of building blocks, the entropy factor for the association of one particle to another has to be the same for single and double rosettes because each association consists of the same hydrogen-bonding arrays. For assemblies **1₃•(BuCYA)₃**, **2a₃•(BuCYA)₆** and **2b₃•(BuCYA)₆** values of $T\Delta S^\circ = -4.6$, -8.0 and $-6.1 \text{ kcal}\cdot\text{mol}^{-1}$ per additional building block are calculated, respectively. These data reinforce the hypothesis that assembly **2b₃•(BuCYA)₆** is basically a summation of two single rosette assemblies, where the stability is merely determined by hydrogen-bond formation and the gathering of building blocks. The somewhat larger unfavorable entropic contribution for **2b₃•(BuCYA)₆**, compared to **1₃•(BuCYA)₃**, can most likely be attributed to larger restriction of rotational mobility of the calixarene building blocks linking the

two rosette planes compared to the single rosette. Comparing $1_3 \bullet (\text{BuCYA})_3$ and $2a_3 \bullet (\text{BuCYA})_6$, with identical hydrogen bonding arrays, different values of entropic contribution per building block are obtained. The somewhat larger enthalpy value observed for $2a_3 \bullet (\text{BuCYA})_6$ (as mentioned above) is partially counterbalanced by larger unfavorable entropic contributions, which is a commonly observed enthalpy-entropy compensation effect (see below).

A possible explanation of the fact that assembly $2a_3 \bullet (\text{BuCYA})_6$ is more stable than $2b_3 \bullet (\text{BuCYA})_6$ ($C_{50} = 0.7 \mu\text{M}$ and $7.1 \mu\text{M}$, respectively) and it displays a larger enthalpy change (Table 1), can be found by molecular modeling. Gas-phase molecular modeling (Quanta 97, CHARMM 24.0) shows for $2a_3 \bullet (\text{BuCYA})_6$ that the two rosette motifs in $2a_3 \bullet (\text{BuCYA})_6$ are stacked on top of each other with an interatomic separation of 3.2 \AA at the edges and 2.8 \AA in the centre of the rosette, while for $2b_3 \bullet (\text{BuCYA})_6$ the interatomic separation is 3.4 \AA at the edges and 3.2 \AA in the centre of the rosette (Figure 4.3). Consequently, the surface arrangement in $2a_3 \bullet (\text{BuCYA})_6$ can lead to better stacking and/or to hydrogen-bonding interactions between the two rosette layers. In addition, $T\Delta S^\circ$ will be larger for $2a_3 \bullet (\text{BuCYA})_6$ than for $2b_3 \bullet (\text{BuCYA})_6$ because of restrictions in mobility due to formation of the additional interactions. The exact role of the different functionalities remains unclear, though steric or electronic influences by the bulkier lysine functionality are conceivable.

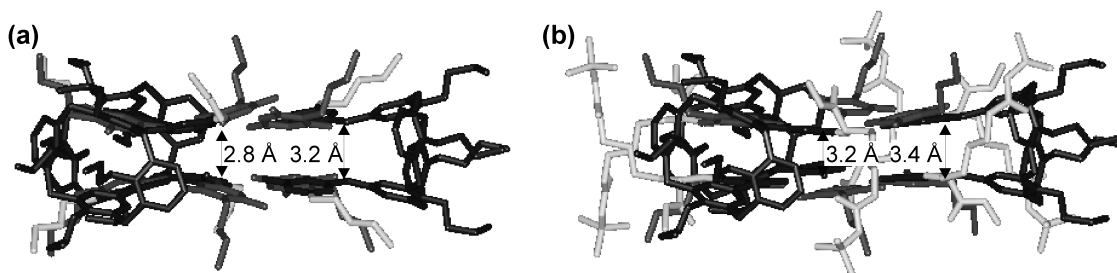


Figure 4.3 Gas-phase minimized structures of (a) $2a_3 \bullet (\text{BuCYA})_6$ and (b) $2b_3 \bullet (\text{BuCYA})_6$

4.2.3.2 Barbiturates vs. cyanurates

Previously, our group³² has reported that the self-assembly of a melamine to a cyanurate (CYA) gives a stronger complex than between melamine and barbiturate (BAR), due to the higher acidity of the CYA. Association constants of 10^2 and 10^4 M^{-1} were reported for melamine•BAR and melamine•CYA, respectively. Double rosette

assemblies contain twelve of these binding motifs. Therefore, assemblies $2_3 \bullet (\text{BuCYA})_6$ are expected to be more stable than the corresponding assemblies $2_3 \bullet (\text{DEB})_6$.

Effectively, as can be seen in table 4.1, assemblies $2a_3 \bullet (\text{DEB})_6$ and $2b_3 \bullet (\text{DEB})_6$ exhibit lower K_f values compared to its BuCYA analogues. The difference in ΔH° between $2b_3 \bullet (\text{DEB})_6$ and $2b_3 \bullet (\text{BuCYA})_6$ ($\Delta H^\circ = -68.2$ and -96.4 kcal·mol⁻¹, respectively) is mainly due to stronger hydrogen bonding provided by BuCYA. Differences between enthalpy as well as entropy change are less pronounced between assemblies $2a_3 \bullet (\text{DEB})_6$ and $2a_3 \bullet (\text{BuCYA})_6$ ($\Delta H^\circ = -110.2$ and -123.1 kcal·mol⁻¹, $T\Delta S^\circ = -67.9$ and -64.0 kcal·mol⁻¹, respectively), supporting the hypothesis that the stability of double rosettes with **2a** are not determined only by the formation of twelve DAD•ADA binding motifs but that additional stabilising interactions may contribute.

4.2.4 Effect of solvent polarity on double rosette formation

ITC measurements with single rosette $1_3 \bullet (\text{BuCYA})_3$ and double rosettes $2a_3 \bullet (\text{DEB})_6$ and $2b_3 \bullet (\text{DEB})_6$ in MeOH/1,2-DCE mixtures were not possible. The low stability of these noncovalent complexes requires concentrations exceeding the solubility of the components. However, the high stability of double rosette assemblies $2a_3 \bullet (\text{BuCYA})_6$ and $2b_3 \bullet (\text{BuCYA})_6$, containing the cyanurate derivative, make them perfect candidates for stability studies by ITC. The thermodynamic parameters associated with formation of double rosette assemblies $2a_3 \bullet (\text{BuCYA})_6$ and $2b_3 \bullet (\text{BuCYA})_6$ in different MeOH/1,2-DCE solvent mixtures are shown in table 4.2.

Table 4. 2 Thermodynamic parameters determined by ITC (298 K) for the self-assembly of double rosette assemblies in different mixtures of 1,2-DCE and MeOH.

Assembly	MeOH in 1,2-DCE (%)	K_f (M^{-8})	ΔH° ($kcal \cdot mol^{-1}$)	C_{50}^* (μM)	ΔG° ($kcal \cdot mol^{-1}$)	$T\Delta S^\circ$ ($kcal \cdot mol^{-1}$)
2a₃•(BuCYA)₆	0	$(2.7 \pm 2.1) \times 10^{43}$	-123 ± 11	0.7 ± 0.1	-59.1 ± 0.5	-64 ± 11
	10	$(9.7 \pm 1.1) \times 10^{29}$	-71 ± 2	31 ± 0	-40.9 ± 0.1	-30 ± 2
	20	$(3.4 \pm 2.1) \times 10^{26}$	-50 ± 1	84 ± 1	-36.2 ± 0.1	-14 ± 1
	50	$(5.6 \pm 5.0) \times 10^{23}$	-38 ± 1	186 ± 2	-32.4 ± 0.1	-6 ± 1
2b₃•(BuCYA)₆	0	$(1.4 \pm 0.8) \times 10^{34}$	-96 ± 1	7.1 ± 0.6	-47.9 ± 0.4	-49 ± 1
	10	$(1.4 \pm 1.0) \times 10^{27}$	-60 ± 5	71 ± 6	-36.9 ± 0.4	-23 ± 5
	20	$(4.2 \pm 3.0) \times 10^{24}$	-46 ± 2	150 ± 20	-33.4 ± 0.6	-12 ± 1
	50	$(7.3 \pm 0.6) \times 10^{21}$	-39 ± 2	320 ± 3	-29.8 ± 0.1	-9 ± 2

* See ref. 40 & 41

Compared to neat 1,2-DCE a 1:9 mixture of MeOH/1,2-DCE showed an increase of the C_{50} values from 0.7 μM and 7.1 μM to 31 μM and 71 μM for **2a₃•(BuCYA)₆** and **2b₃•(BuCYA)₆**, respectively (Table 4.2). Further increase of the percentage of MeOH in 1,2-DCE led to a less dramatic increase in C_{50} . The ITC measurements show for both assemblies that upon increasing the percentage of MeOH, a decrease in both enthalpy and entropy is observed. For the formation of **2a₃•(BuCYA)₆** and **2b₃•(BuCYA)₆** in neat 1,2-DCE, ΔH° values of $-123 kcal \cdot mol^{-1}$ and $-96.4 kcal \cdot mol^{-1}$ were obtained, respectively. When 10% of MeOH was present ΔH° values of $-70.5 kcal \cdot mol^{-1}$ and $-59.8 kcal \cdot mol^{-1}$ were obtained, respectively. This loss in enthalpy was partly compensated by a less negative value for $T\Delta S^\circ$ (from $-64.0 kcal \cdot mol^{-1}$ to $-29.6 kcal \cdot mol^{-1}$ and from $-48.6 kcal \cdot mol^{-1}$ to $-22.9 kcal \cdot mol^{-1}$).

An enthalpy-entropy compensation (EEC) plot reflects how an increasingly favorable enthalpy is offset by an increasingly negative entropy change or vice versa. In Figure 4.4 it can be seen that when the entropy and enthalpy of formation for assemblies **2a₃•(BuCYA)₆** and **2b₃•(BuCYA)₆** at different ratios of MeOH in 1,2-DCE are plotted together, a straight line is obtained (black line). Consequently the slope of the obtained EEC plot coincides for both assemblies. This means that the extent to which the decrease

in enthalpy of formation is compensated by lower entropy is identical for both assemblies. The slope of the EEC plot is 1.46. This means that the free energy of formation is sensitive to changes in enthalpy.⁴² A slope above 1 suggests that upon increase of the percentage of MeOH in the solvent mixture, eventually, the decrease in enthalpy change cannot be compensated by entropy changes.⁴³ Nevertheless, for assemblies $2\mathbf{a}_3\cdot(\text{BuCYA})_6$ and $2\mathbf{b}_3\cdot(\text{BuCYA})_6$ this will only happen for strongly endothermic ΔH° values.

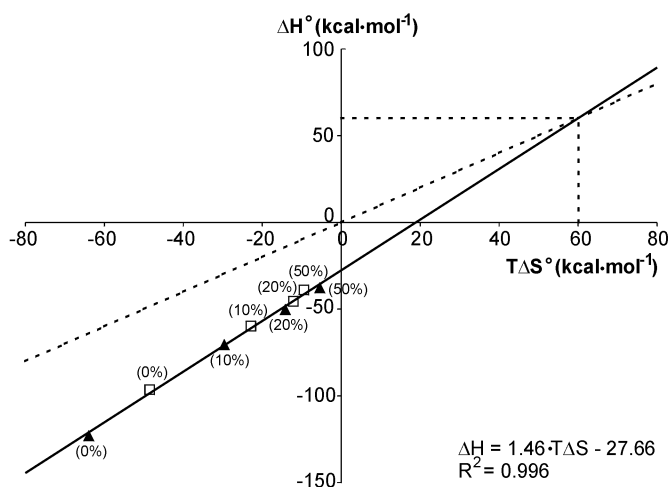


Figure 4.4 Enthalpy-entropy compensation (EEC) plot reflecting how increasing favorable enthalpy is offset by a change in entropy and vice versa (solid line). \blacktriangle : $2\mathbf{a}_3\cdot(\text{BuCYA})_6$, \square : $2\mathbf{b}_3\cdot(\text{BuCYA})_6$. The number between brackets denotes the percentage of MeOH in 1,2-DCE. Dotted line: behavior when the enthalpy changes are completely compensated by entropy changes.

4.2.5 Correlation between solvent polarity and ΔG°

Using methanol as solvent, it was not possible to measure any appreciable heat effect for the formation of double rosettes $2\mathbf{a}_3\cdot(\text{BuCYA})_6$ and $2\mathbf{b}_3\cdot(\text{BuCYA})_6$ in an attempted ITC experiment due to solubility limitations of dimelamines $2\mathbf{a}$ and $2\mathbf{b}$ as well as BuCYA in this solvent. Thus, to estimate the thermodynamic data for the formation of double rosettes in pure methanol (and other polar solvents) a theoretical model was used, in which the solvent polarity is correlated to ΔG° . For this purpose the solvent polarity

parameter E_T^N was determined for solvent mixtures ranging from 0 to 100% MeOH in 1,2-DCE using UV-vis measurements.^{44,45}

Plotting of ΔG° values from Table 4.2 for assemblies $2\mathbf{a}_3\bullet(\text{BuCYA})_6$ and $2\mathbf{b}_3\bullet(\text{BuCYA})_6$ against these E_T^N values resulted in a straight line for both assemblies (Figure 4.5), indicating a linear correlation between ΔG° and the polarity of the solvent (mixture). A steeper curve suggests a more pronounced (negative) effect on rosette stability upon increase of solvent polarity. In pure methanol ($E_T^N = 0.76$) both assemblies have a ΔG° of $-26.8 \text{ kcal}\cdot\text{mol}^{-1}$, implying that assemblies $2\mathbf{a}_3\bullet(\text{BuCYA})_6$ and $2\mathbf{b}_3\bullet(\text{BuCYA})_6$ would exhibit equal stability in pure MeOH ($C_{50} = 0.6 \text{ mM}$).

Correlation of the solvent polarity with ΔG° provides ΔG° values for assemblies $2\mathbf{a}_3\bullet(\text{BuCYA})_6$ and $2\mathbf{b}_3\bullet(\text{BuCYA})_6$ in various solvent. These values, together with the equation describing the EEC plot, allow the calculation of ΔH° and $T\Delta S^\circ$ values for the formation of both assemblies. For both double rosettes in MeOH, these values are $-24.8 \text{ kcal}\cdot\text{mol}^{-1}$ and $2.0 \text{ kcal}\cdot\text{mol}^{-1}$ for ΔH° and $T\Delta S^\circ$, respectively. These data would suggest that, based on solvent-polarity, the self-assembling of $2\mathbf{a}_3\bullet(\text{BuCYA})_6$ and $2\mathbf{b}_3\bullet(\text{BuCYA})_6$ in methanol is possible. Surprisingly, in methanol this process is still mainly enthalpy driven, though reinforced by entropic effects. Thus in MeOH the positive enthalpy of desolvation is not able to override the negative enthalpy for double rosette formation.

For double rosette formation in water ($E_T^N = 1.00$), ΔG° values of $-8.5 \text{ kcal}\cdot\text{mol}^{-1}$ and $-14.7 \text{ kcal}\cdot\text{mol}^{-1}$ for $2\mathbf{a}_3\bullet(\text{BuCYA})_6$ and $2\mathbf{b}_3\bullet(\text{BuCYA})_6$ were calculated, respectively, indicating that in water these two assemblies might also be formed. Calculated C_{50} values of 28.7 mM and 7.8 mM for $2\mathbf{a}_3\bullet(\text{BuCYA})_6$ and $2\mathbf{b}_3\bullet(\text{BuCYA})_6$ indicate that double rosette $2\mathbf{b}_3\bullet(\text{BuCYA})_6$, bearing the lysine moiety exhibit larger stability in water.

Interestingly, ΔH° and $T\Delta S^\circ$ values calculated for $2\mathbf{a}_3\bullet(\text{BuCYA})_6$ ($33.2 \text{ kcal}\cdot\text{mol}^{-1}$ and $41.7 \text{ kcal}\cdot\text{mol}^{-1}$, respectively) and for $2\mathbf{b}_3\bullet(\text{BuCYA})_6$ ($13.5 \text{ kcal}\cdot\text{mol}^{-1}$ and $28.2 \text{ kcal}\cdot\text{mol}^{-1}$, respectively), indicate that in water the formation of both double rosettes would be entropically driven. In water, a positive enthalpy change is expected to arise from a positive enthalpy of desolvation, which overrides the expected negative enthalpy for double rosette formation. These results indicate that solvation abilities of methanol and water are very different, but that assembly formation is, in principle, possible in both solvents.

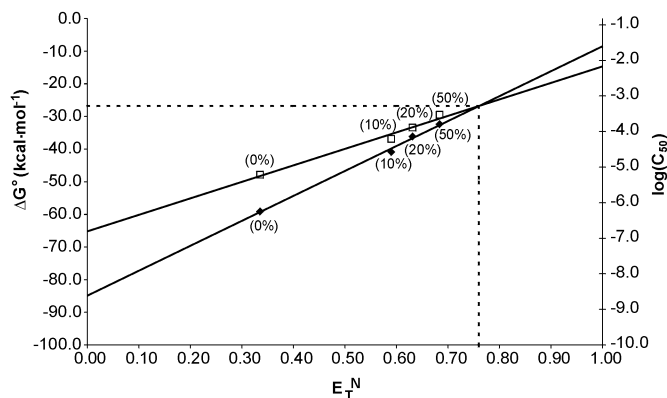


Figure 4.5 Effect of solvent polarity on ΔG^0 for assemblies $2a_3 \cdot \text{BuCYA}_6$ (\blacklozenge) and $2b_3 \cdot \text{BuCYA}_6$ (\square). \blacklozenge : $\Delta G^0 = 76.409 \times E_T^N - 84.897$ ($R^2 = 0.996$), \square : $\Delta G^0 = 50.503 \times E_T^N - 65.86$ ($R^2 = 0.980$). The number between brackets denotes the percentage of MeOH in 1,2-DCE. The cross point of the dashed lines corresponds with formation of double rosettes in pure methanol.

4.2.6 Double rosette formation in MeOH

As it has been mentioned earlier, ITC measurements for the formation of double rosettes in MeOH are not possible. However, the obtained theoretical thermodynamic profile in previous section implies that double rosettes could be formed in this solvent.

^1H NMR and CD spectroscopy was used to prove experimentally the formation of the double rosette $2b_3 \cdot (\text{BuCYA})_6$ in MeOH. These techniques allow the use of more diluted solutions of the building blocks. Moreover, **2b** and BuCYA can be mixed directly in these techniques (ITC requires initially separate solutions of each component), leading to higher solubility of the double rosette compared to the isolated components. Based on the ΔG^0 vs E_T^N plot, 97% formation of $2b_3 \cdot (\text{BuCYA})_6$ in methanol- d_4 was predicted from the free energy.

Mixing of 3 μmol dimelamine **2b** and 30 μmol BuCYA in 1 ml of methanol- d_4 resulted in clear solutions at temperatures above 40 $^\circ\text{C}$. Though precipitation occurred at lower temperature, formation of double rosettes $2b_3 \cdot (\text{BuCYA})_6$ was observed using ^1H NMR spectroscopy (Figure 4.6). Due to rapid exchange, the ^1H NMR spectrum does not show the characteristic hydrogen-bonded protons²⁷ of the assembly in methanol- d_4 . However, the signal at 5.9 ppm belongs to the aromatic proton (H_d) of the calix[4]arene moiety that is only present at this chemical shift when the assembly is formed. The percentage of assembly formed was determined by comparing the integrals of H_d with the

Ar-CH₂-Ar of the calix[4]arene moiety. This resulted in about 63% formation of **2b**₃•(BuCYA)₆ in methanol-*d*₄. The lower observed double rosette formation using ¹H NMR spectroscopy is likely due to precipitation of the assembly (components) at 298 K.

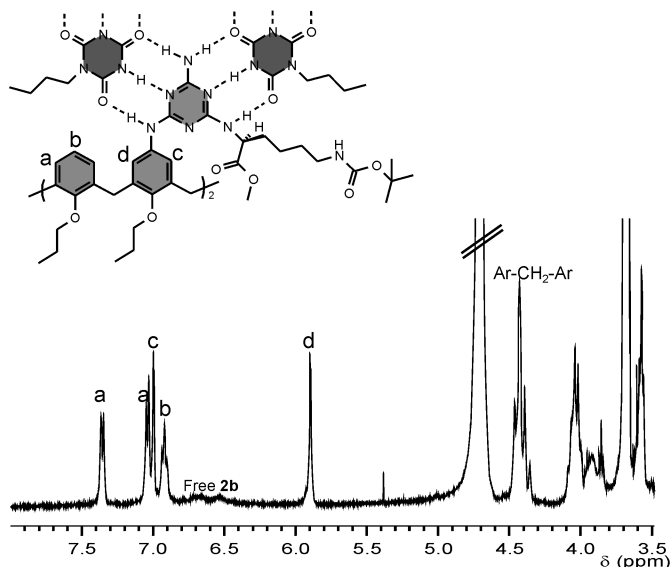


Figure 4.6 Part of the ¹H NMR spectrum of **2b**₃•(BuCYA)₆ in methanol-*d*₄ at 300 MHz and 298 K.

The formation of double rosette **2b**₃•(BuCYA)₆ in MeOH was also shown by circular dichroism (CD) spectroscopy. The dimelamine moieties in **2b** have chiral centers in the lysine residues. Subsequently, due to complete induction of supramolecular chirality, the hydrogen-bonded assembly **2b**₃•(BuCYA)₆ exists exclusively as a single diastereomer.^{27-29,33} As a result, double rosette assemblies exhibit a very strong CD while the individual components are hardly CD active (Figure 4.7). Both the ¹H NMR and CD spectra clearly prove that double rosette **2b**₃•(BuCYA)₆ is formed in pure methanol.

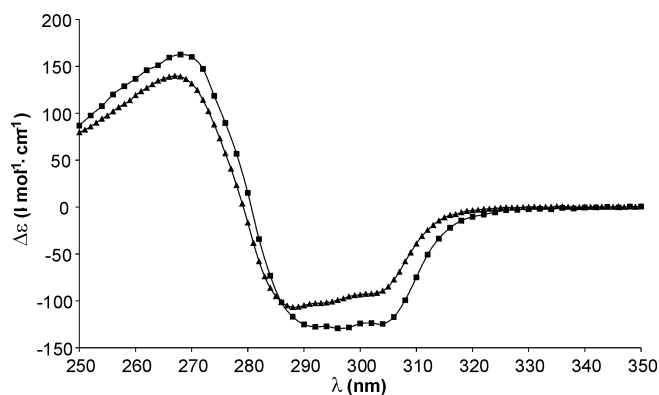


Figure 4.7 CD spectrum of **2b**₃•(BuCYA)₆ in methanol (▲) and chloroform (■) at 298 K.

4.3 Conclusions

The thermodynamic properties for the formation of single and double rosettes were determined by ITC. ITC provides a facile and effective approach to measure changes in binding enthalpy and calculate other thermodynamic parameters for self-assembled systems. Depending on functionalities at the calix[4]arene dimelamine moieties it was found that the thermodynamics for the formation of double rosette assemblies can be either a summation of the self-assembly of two single rosette structures or a summation of two single rosettes reinforced by additional complex stabilizing interactions. As expected, double rosettes bearing cyanuric acid derivatives are more stable than the corresponding rosettes bearing barbiturate derivatives.

Increase of the solvent polarity decreases ΔG° and thereby results in less strong assembly formation. In all 1,2-DCE/MeOH solvent mixtures the negative effect of desolvation on ΔH° did not override the high favorable enthalpy of double rosette formation. Formation of double rosettes remained, therefore, enthalpy driven.

Correlation of ΔG° energies to the solvent polarity indicated that it is possible to obtain double rosette assemblies in methanol and in water. As expected, the simulation shows that formation of double rosettes in water is entropy driven rather than enthalpy driven. However, to our surprise, double rosette formation in MeOH is still enthalpy driven.

Finally, ^1H NMR spectroscopy and CD spectroscopy proved that hydrogen-bonded double rosettes can be formed in neat methanol.

4.4 Experimental

General Methods: THF was distilled from Na/benzophenone. All chemicals were reagent grade and used without further purification. NMR spectra were recorded on a Varian Unity 300 (^1H NMR 300MHz) spectrometer in chloroform- d_1 or methanol- d_4 . Residual solvent protons were used as internal standard, and chemical shifts are given relatively to trimethylsilane (TMS).

FAB spectra were measured on a Finningan MAT 90 spectrometer with *m*-nitrobenzyl alcohol (NBA) matrix. MALDI-TOF mass spectra were recorded on a PerSpective Biosystems Voyager-De-RP spectrometer. A 337 nm UV nitrogen laser

producing 3 ns pulses was used in the linear and reflector modes. Elemental analyses were performed using a Carlo Erba EA1106. Calorimetric measurements were carried out using a Microcal VP-ITC microcalorimeter with a cell volume of 1.4115 ml. For each experiment the heat effect of 60 injections of 5 μ l titrant was measured. Instrument settings were set on injection duration of 30 sec, spacing of 570 sec and low feedback at 16.3 μ cal/sec reference power and a temperature of 25°C. UV-vis measurements were performed on a HP8452A diode array spectrophotometer using solvents of spectroscopic grade.

Synthesis

The synthesis of **1**, **2a** and **2c** have been previously reported.^{28,32} Synthesis of **2b** is described in Chapter 3.

ITC measurements

Hydrogen bonds are weaker in 1,2-dichloroethane (1,2-DCE) than in CHCl_3 ,^{46,47} because the dipole moment and dielectric constants of CHCl_3 ($\mu = 1.1$ D, $\epsilon_r = 4.89$) are lower than the ones for 1,2-DCE ($\mu = 1.8$ D, $\epsilon_r = 10.36$).⁴⁴ Nevertheless, to prevent errors incurred by evaporation, the ITC measurements were performed in 1,2-DCE.

ITC measurements for the formation of $\mathbf{1}_3 \cdot (\text{BuCYA})_3$ in 1,2-DCE were performed in triplicate, using 1 mM solutions of melamine **1** in the cell and 10 mM solution of BuCYA in the burette. In this case, measurement at different concentrations was not possible due to solubility problems at high concentrations of **1** as well as BuCYA. Furthermore, at lower concentrations no assembly formation was observed. ITC measurements with $\mathbf{2}_3 \cdot (\text{DEB/BuCYA})_6$ in 1,2-DCE were performed at three different concentrations. Solutions of DEB or BuCYA were put into the cell and solutions of dimelamine **2a** or **2b** were used as titrant. In addition, the formation of $\mathbf{2a}_3 \cdot (\text{BuCYA})_6$ and $\mathbf{2b}_3 \cdot (\text{BuCYA})_6$ in solvent mixtures containing different percentages of MeOH in 1,2-DCE were studied. ITC measurements were performed in triplicate at 0, 0.1, 0.2 and 0.5 MeOH /1,2-DCE ratio. ITC curves were determined at two different concentrations depending on the amount of MeOH present.

UV/VIS measurements

E_T^N values were determined by measuring the absorbance changes of 2,6-diphenyl-4-(2,4,6-triphenyl-1-pyridinio)phenolate (Reichardt's dye) upon increasing amount of MeOH in 1,2-DCE ranging (0% to 100% methanol). Stock solutions of Reichardt's dye in MeOH and 1,2-DCE (0.12 mg/ml) were prepared and mixed to desired ratios MeOH in 1,2-DCE. UV-vis measurements were performed three times and a blank was recorded for each solvent mixture.

4.5 References

1. The strength of the hydrogen bond depends on the distance between the donor and acceptor atoms, which in turn is dependent on their electronegativities.
2. Takeda, N.; Umemoto, K.; Yamaguchi, K.; Fujita, M. *Nature* **1999**, *398*, 794-799.
3. Zhong, Z.; Ikeda, H.; Ayabe, M.; Shinkai, S.; Sakemoto, S.; Yamaguchi, K. *J. Org. Chem.* **2001**, *66*, 1002-1008.
4. Chand, D. K.; Biradha, K.; Fujita, M. *Chem. Commun.* **2001**, 1652-1653.
5. Umemoto, K.; Tsukui, K. T.; Biradha, K.; Fujita, M. *Angew. Chem. Int. Ed.* **2001**, *40*, 2620-2622.
6. Ikeda, A.; Udzu, H.; Zhong, Z.; Shinkai, S.; Sakemoto, S.; Yamaguchi, K. *J. Am. Chem. Soc.* **2001**, *123*, 3872-3877.
7. Dalcanale, E.; Jacopozzi, P. *Angew. Chem. Int. Ed.* **1997**, *36*, 613-615.
8. Fochi, F.; Wegelius, E.; Rissanen, K.; Cozzini, P.; Marastoni, E.; Fiscaro, E.; Mannini, P.; Fokkens, R.; Dalcanale, R. *J. Am. Chem. Soc.* **2001**, *123*, 7539-7552.
9. Fujita, M.; Nagao, S.; Iida, M.; Ogata, K.; Ogura, K. *J. Am. Chem. Soc.* **1993**, *115*, 1574-1576.
10. Fujita, M.; Umemoto, K.; Yoshizawa, M.; Fujita, N.; Kusukawa, T.; Biradha, K. *Chem. Commun.* **2001**, 509-518.
11. Fox, O.; Dalley, N. K.; Harrison, R. G. *J. Am. Chem. Soc.* **1998**, *120*, 7111-7112.
12. Fox, O. D.; Leung, J. F. Y.; Hunter, J. M.; Dalley, N. K.; Harrison, R. G. *Inorg. Chem.* **2000**, *39*, 783-790.
13. Bok, L. S.; Hong, J.-L. *Tetrahedron Lett.* **1998**, *39*, 4317-4320.
14. Fujita, M.; Oguro, D.; Miyazawa, M.; Oka, I.; Yamagushi, K.; Ogura, K. *Nature*

- 1995**, 378, 469-471.
15. Atwood, J. L.; Barbour, L. J.; Jerga, A. *Chem. Commun.* **2001**, 2376-2377.
 16. Shivanyuk, A.; Rebek, Jr. J. *Chem. Commun.* **2001**, 2374-2375.
 17. Vysotsky, M. O.; Thondorf, I.; Böhmer, V. *Chem. Commun.* **2001**, 1890-1891.
 18. Lee, B. S.; Hong, J.-I. *Tetrahedron Lett.* **1996**, 37, 8501-8504.
 19. Fiammengo, R.; Timmerman, P.; De Jong, F.; Reinhoudt, D. N. *Chem. Commun.* **2000**, 2312-2314.
 20. Grawe, T.; Schrader, T.; Gurrath, M.; Kraft, A.; Osterod, F. *Org. Lett.* **2000**, 2, 29-32.
 21. Hamelin, B.; Jullien, L.; Derouet, C.; Penhoat, C. H. d.; Berthault, P. *J. Am. Chem. Soc.* **1998**, 120, 8438-8447.
 22. Corbellini, F.; Fiammengo, R.; Timmerman, P.; Crego-Calama, M.; Versluis, K.; Heck, A. J. R.; Luyten, I.; Reinhoudt, D. N. *J. Am. Chem. Soc.* **2002**, 124, 6569-6575.
 23. Corbellini, F.; Costanzo, L. D.; Crego-Calama, M.; Geremia, S.; Reinhoudt, D. N. *J. Am. Chem. Soc.* **2003**, 25, 9946-9947.
 24. Mammen, M.; Simanek, E. E.; Whitesides, G. M. *J. Am. Chem. Soc.* **1996**, 118, 12614-12623.
 25. In these studies the average value for a hydrogen-bond measured in chloroform was used to estimate the free energy index, I_G .
 26. Seto, C. T.; Mathias, J. P.; Whitesides, G. M. *J. Am. Chem. Soc.* **1993**, 115, 1321-1329.
 27. Prins, L. J.; Huskens, J.; De Jong, F.; Timmerman, P.; Reinhoudt, D. N. *Nature* **1999**, 398, 498-502.
 28. Timmerman, P.; Vreekamp, R. H.; Hulst, R.; Verboom, W.; Reinhoudt, D. N.; Risannen, K.; Udachin, K. A.; Ripmeester, J. *Chem. Eur. J.* **1997**, 3, 1823-1832.
 29. Vreekamp, R. H.; Van Duynhoven, R. H.; Hubert, M.; Verboom, W.; Reinhoudt, D. N. *Angew. Chem. Int. Ed.* **1996**, 35, 1215-1218.
 30. Jolliffe, K. A.; Crego-Calama, M.; Fokkens, R.; Nibbering, N. M. M.; Timmerman, P.; Reinhoudt, D. N. *Angew. Chem. Int. Ed.* **1998**, 37, 1247-1251.
 31. Prins, L. J.; Jolliffe, K. A.; Hulst, R.; Timmerman, P.; Reinhoudt, D. N. *J. Am. Chem. Soc.* **2000**, 122, 3617-3627.

32. Bielejewska, A. G.; Marjo, C. E.; Prins, L. J.; Timmerman, P.; De Jong, F.; Reinhoudt, D. N. *J. Am. Chem. Soc.* **2001**, *123*, 7518-7533.
33. Prins, L. J.; De Jong, F.; Timmerman, P.; Reinhoudt, D. N. *Nature* **2000**, *408*, 181-184.
34. $\ln(K)$ is plotted against T^{-1} . $\ln(K_2/K_1) = -\Delta H/R(T_1^{-1} - T_2^{-1})$.
35. Some recent examples can be found in: Tobey, S. L.; Anslyn, E. V. *J. Am. Chem. Soc.* **2003**, *125*, 10963-10970.
36. Tobey, S. L.; Anslyn, E. V. *J. Am. Chem. Soc.* **2003**, *125*, 14807-14815.
37. Linton, B. R.; Goodman, M. S.; Fan, E.; Van Arman, S. A.; Hamilton, A. *J. Org. Chem.* **2001**, *66*, 7313-7319.
38. Rekharsky, M. V.; Inoue, Y. *Chem. Rev.* **1998**, *98*, 1875-1917.
39. For a detailed description of the ITC experiments see the experimental part.
40. Single rosettes are built up from 6 components which has the consequence that K_f values are expressed in M^{-5} , while double rosettes are build up from 9 components and therefore K_f values are expressed in M^{-8} .
41. Analogous to the definition of a dissociation constant, K_d , commonly employed for 1:1 complexes, C_{50} is defined as the concentration of assembly present when the components are mixed in the stoichiometry at which they are present in the complex and 50% of the components are incorporated in the complex. Therefore: $K_f = C_{50}/((3 \cdot C_{50})^3 \times (3 \cdot C_{50})^3)$ for single rosette assemblies and $K_f = C_{50}/((3 \cdot C_{50})^3 \times (6 \cdot C_{50})^6)$ for double rosette assemblies.
42. Sun, S.; Fazal, Md. A.; Roy, B. C.; Chandra, B.; Mallik, S. *Inorg. Chem.* **2002**, *41*, 1584-1590.
43. The dotted line in the EEC plot describes the behavior when the enthalpy changes are completely compensated by entropy changes. Beneath this line the $\Delta G^0 < 0$, and above this line $\Delta G^0 > 0$. At the point where the experimental line (solid) crosses the dotted line is ΔH^0 equal to $T\Delta S^0$ and $\Delta G^0 = 0$.
44. Reichardt, C. *Solvents and Solvents Effects in Organic Chemistry*; ed. Wiley-VCH: Weinheim, Germany, 2003.
45. The term solvatochromism is used to describe a pronounced change in position of a UV/VIS absorption band that accompanies a change in the polarity of the solvent. Large solvent-induced shifts of the visible $\pi \rightarrow \pi^*$ absorption band are observed for pyridinium *N*-phenolate betaine. This property has been used to introduce an empirical parameter of solvent polarity, the $E_T(30)$ value. The $E_T(30)$ value is defined as the transition energy of the dissolved betaine dye measured in $\text{kcal}\cdot\text{mol}^{-1}$.

$E_T(30) = h \cdot c \cdot \nu \cdot N_A$, where h is Planck's constant, c the speed of light, ν the wave number and N_A the number of Avogadro. The number 30 is trivial and denotes to the number of the dye when it was first reported. Hence, the normalized E_T^N value is dimensionless and defined as $E_T^N = [E_T(\text{solvent}) - E_T(\text{TMS})] / [E_T(\text{water}) - E_T(\text{TMS})]$. Where, water and tetramethylsilane are used as extreme reference solvents. Hence, the E_T^N scale ranges from 0 for TMS, the least polar solvent, to 1 for water, the most polar solvent.

46. Archer, E. A.; Krische, M. J. *J. Am. Chem. Soc.* **2002**, *124*, 5074-5083.
47. Spencer, J. N.; Sweigart, J. R.; Brown, M. E.; Bensing, R. L.; Hassinger, T. L.; Kelly, W.; Housel, D. L.; Reisinger, G. W. *J. Phys. Chem.* **1976**, *80*, 811-814.

Self-organization of guest molecules in self-assembled molecular containers*

In this chapter the encapsulation of a series of anthraquinone derivatives (2) forming trimeric species inside a hydrogen-bonded double rosette is described. A study of the complexation of the different anthraquinone derivatives by this endo-receptor using ^1H NMR spectroscopy, X-ray crystallography, ITC measurements, and UV spectroscopy indicates different modes of complexation for the different guest molecules. The driving force for the encapsulation is the π - π stacking between the electron deficient center ring of the anthraquinone derivatives and the relatively electron poor melamine units of the receptor. Selectivity of the receptor for the anthraquinone derivatives is due to small differences in steric hindrance between the guest molecules and the receptor cavity. In addition, the complexation is influenced by the formation of a hydrogen-bonded network between the encapsulated guest molecules.

* This work has been submitted for publication: Kerckhoffs; J.M.C.A., Ten Cate, M.G.J.; Mateos-Timoneda, M.A.; Van Leeuwen, F.W.B.; Snellink-Ruël, B.; Spek, A.L.; Kooijman, H.; Crego-Calama, M.; Reinhoudt, D.N., *J. Am. Chem. Soc.* **2004**.

5.1 Introduction

One of the goals of Supramolecular Chemistry is the spontaneous assembly of synthetic building blocks into highly organized structures.¹ Nature provides the perfect example of this approach. For example, highly complex functional natural enclosures, such as cells and viruses are obtained by self-assembly allowing errors to be minimized and/or spontaneously corrected.^{2,3} Unfortunately, the control and organizational complexity found in these biological structures is still far beyond our synthetic abilities.⁴ Nevertheless, many examples of synthetic self-assembled molecular containers have been reported. Some of these synthetic 3-D cavities use multiple hydrogen bonds for their formation,⁵⁻⁷ but also metal coordination^{8,9} and ionic interactions^{10,11} are utilized for the synthesis of such molecular containers. Molecular capsules have many potential applications, ranging from drug delivery and molecular recognition to molecular reaction chambers for catalysis and stabilization of reactive intermediates.¹²⁻¹⁵

Until now, the application of synthetic self-assembled structures for encapsulation of guest molecules has received most attention.¹⁶⁻¹⁸ The noncovalent approach facilitates the encapsulation by the ability of the capsule to (re)assemble around the guest molecules, while covalent capsules^{19,20} should contain a “door” through which the guest molecules can enter the capsule. Entrapment of guest molecules in noncovalent capsules is mostly achieved by the steric constraints in rigid preorganized building blocks.²¹ Only a few examples of self-organization of the guest molecules in a capsule occurs via noncovalent interactions are known.²²⁻²⁵ Recently our group showed the first example where the self-organization of the guest and of the host involves hydrogen bonding.²⁶

This chapter describes the selectivity exhibited by a hydrogen-bonded container (*endo*-receptor) in the encapsulation of anthraquinone derivatives (**2**, Chart 5.1). The dynamic character of our self-assembled capsule allows the rearrangement of the building blocks to obtain the “perfect” fit for each guest molecule. By studying the encapsulation behavior of the different anthraquinone derivatives a binding model was proposed for the entrapment of these guest molecules by the self-assembled host. The driving force for encapsulation of anthraquinone derivatives is π - π stacking between host and guest, while the selective encapsulation of some guests arise from the formation of a hydrogen-bonded

network between the entrapped molecules, and from the steric hindrance between guest molecules and the receptor cavity.

The circular network (rosette)²⁷ of complementary hydrogen bonds formed between melamine and barbituric (BAR) or cyanuric acid (CYA) was used for the noncovalent synthesis of the self-assembled nanometer sized molecular boxes $1_3 \cdot (\text{DEB})_6$ (DEB = 5,5'-diethyl barbituric acid) or $1_3 \cdot (\text{BuCYA})_6$ (BuCYA = *n*-butyl cyanuric acid), respectively.^{28,29} These double rosettes are assembled from calix[4]arene dimelamine **1** with two equivalents DEB or BuCYA (Chart 5.1). Both the top and the bottom of this thermodynamically highly stable molecular container comprise a cyclic hydrogen-bonded rosette motif, with the calix[4]arene units acting as side walls, while the space between the two rosette floors limits the encapsulation area.

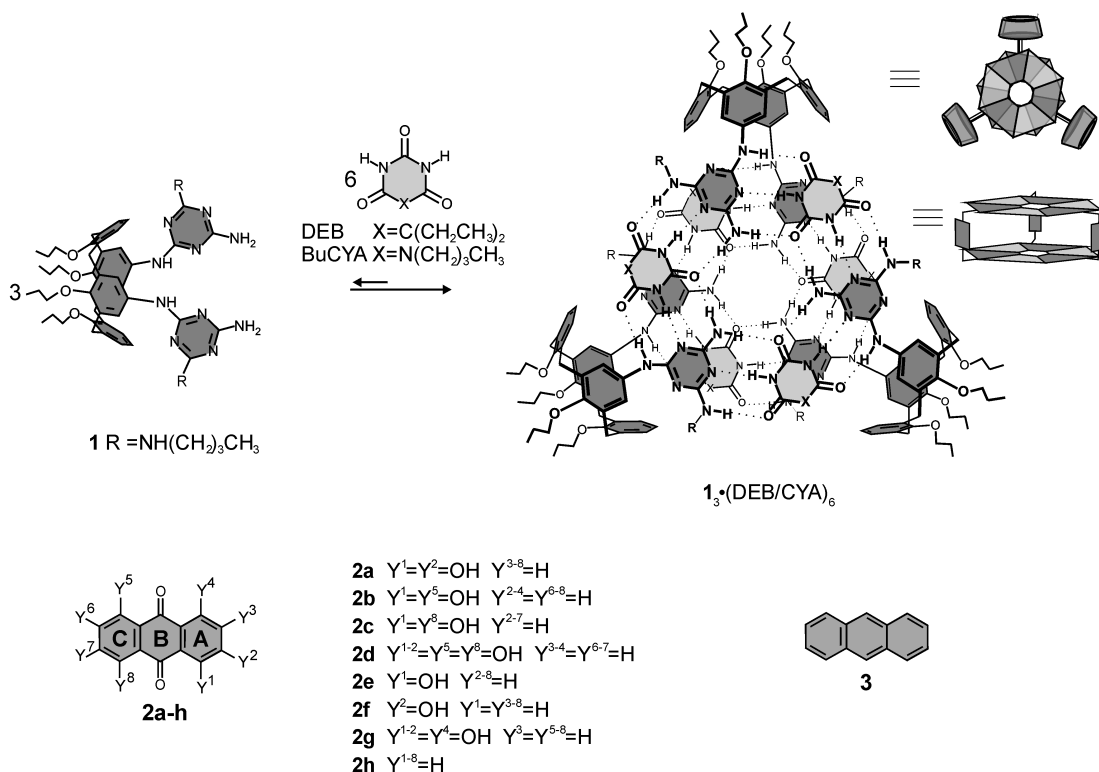


Chart 5.1 Formation of the hydrogen-bonded assemblies $1_3 \cdot (\text{DEB/CYA})_6$ and molecular structures of guest molecules **2** and **3**. The schematic representations of the double rosettes (top and side view) are also shown.

Recently Kerckhoffs *et al.*²⁶ in our group have found that assembly $1_3 \cdot (\text{DEB})_6$ can encapsulate three molecules of alizarin (**2a**) in solution and in the solid state. The crystal

structure (Figure 5.1) revealed that the two melamines of one calix[4]arene are in an *eclipsed* orientation, while in absence of **2a**, these melamines are in a *staggered* orientation. The electron deficient aromatic ring of **2a** (ring B; Chart 5.1) is stacked in between the two relatively electron poor rings of the melamine units with a slight offset of the face-to-face arrangement.

The Hunter-Sanders' model for π - π stacking was used to explain the change from staggered to symmetrical eclipsed conformation of the rosette.³⁰ In the model, the σ -framework and the π -electrons are considered separately. This model shows that the π - σ attraction overcomes the π - π repulsion giving the net favorable π - π interactions. The model reveals that for the interaction between two electron deficient rings, such as, for example, the melamine units of our receptor and the B-ring of **2a**, the π - π repulsion is minimized and therefore stacking of these rings is more favorable. Furthermore, in an offset π -stacked geometry, as can be seen between the melamine units of the receptor and the B-ring of **2a**, the π - σ attraction will dominate and therefore favor the stacking.

The crystal structure also revealed that the three **2a** molecules are interlocked by an array of hydrogen bonds between the carbonyl groups and the 2-hydroxyl groups of **2a**.

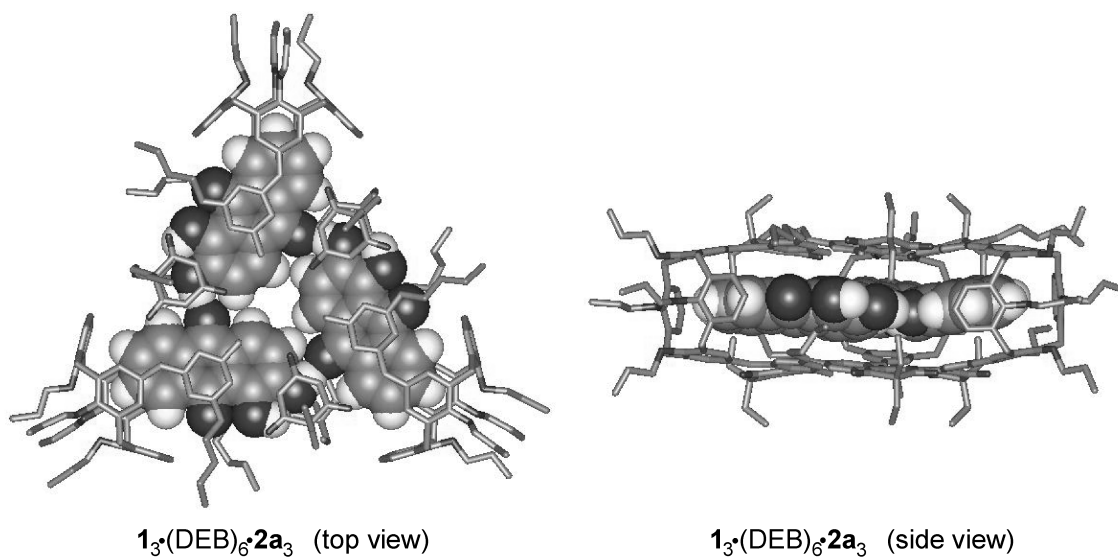


Figure 5.1 Top and side view of the crystal structure of the complex $1_3 \cdot (\text{DEB})_6 \cdot 2\mathbf{a}_3$. A stick model is used for the representation of the molecular cage $1_3 \cdot (\text{DEB})_6$, while a space-filling representation is chosen for the trimer $2\mathbf{a}_3$. Hydrogens of the assembly are not shown and only the main parts for the disordered butyl and propyl groups are depicted. The crystal structure was previously reported in Ref.31

The symmetry of the complex, reflected by the relatively simple ^1H NMR spectrum, indicated that, also in solution, three molecules of **2a** are complexed in between the two rosette layers. The large shifts observed for the alizarin protons (> 3 ppm) clearly indicated the encapsulation of the guest molecules. The aromatic protons of rings C of **2a** (see Chart 5.1) shifted 3.28-3.88 ppm upfield upon complexation, indicating that ring C is partially included in the calix[4]arene cone. The 2-hydroxyl group shifted 3.63 ppm downfield, suggesting that the hydroxyl group is involved in the formation of a hydrogen bond. Furthermore, the NH_{DEB} -protons (H_a and H_b) in the complex $\mathbf{1}_3 \cdot (\text{DEB})_6 \cdot \mathbf{2a}_3$ were shifted upfield in comparison with the free host $\mathbf{1}_3 \cdot (\text{DEB})_6$. In summary, all the shifts confirmed the encapsulation of three molecules of **2a** between the two rosette planes in solution.

5.2 Results and discussion

To study the scope and selectivity of the self-assembled host $\mathbf{1}_3 \cdot (\text{DEB})_6$, a series of anthraquinone derivatives (**2a-h**) with one or more hydroxyl groups at different positions of the anthraquinone skeleton and anthracene (**3**) was chosen.

Cubic red crystals (0.3-1 mm) were obtained from diffusion of hexane into a solution of 1,5-dihydroxyanthraquinone (**2b**) and $\mathbf{1}_3 \cdot (\text{DEB})_6$ in dichloromethane. X-ray analysis revealed the structure of complex $\mathbf{1}_3 \cdot (\text{DEB})_6 \cdot \mathbf{2b}_3$ in the solid state (Figure 5.2). The structure of this complex is similar to the one reported by Kerckhoffs *et al.*²⁶

The two melamines of each calix[4]arene **1** are in an *eclipsed* orientation with respect to each other and with respect to the electron deficient aromatic B-ring of the 1,5-dihydroxyanthraquinone **2b** which is complexed in between the two relatively electron poor aromatic rings of these melamine units. The hydroxyl functionalities of **2b** at the 1-position are pointing outwards, as was the case of the encapsulation of **2a**, allowing the guest molecules to be oriented in such a way that there is no steric interference with the calix[4]arene cone. Since **2b** lacks a hydroxyl group at the 2-position there is no intermolecular hydrogen-bonded network between the three guest molecules of the complex.

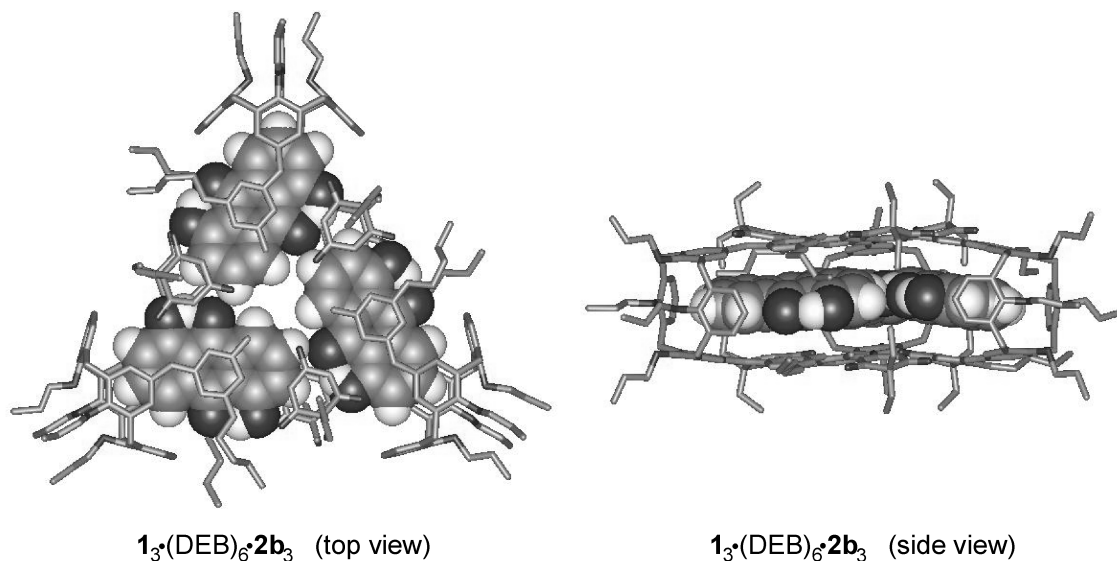


Figure 5.2 Top and side view of the crystal structure of the complex $1_3\bullet(\text{DEB})_6\bullet 2\mathbf{b}_3$. A stick model is used for the representation of the molecular cage $1_3\bullet(\text{DEB})_6$, while a space-filling representation is chosen for the molecules $2\mathbf{b}$. Hydrogens of the assembly are not shown.

The intermolecular separation between the two rosette layers increases upon encapsulation from 3.5 Å at the edges and 3.2 Å in the center for $1_3\bullet(\text{DEB})_6$ ²⁸ to 6.7 Å at the edges and 6.8 Å in the center for $1_3\bullet(\text{DEB})_6\bullet 2\mathbf{b}_3$. These changes were also observed for the complex $1_3\bullet(\text{DEB})_6\bullet 2\mathbf{a}_3$.²⁶ The crystal structures of $1_3\bullet(\text{DEB})_6\bullet 2\mathbf{a}_3$ and $1_3\bullet(\text{DEB})_6\bullet 2\mathbf{b}_3$ are isomorphic regarding the orientation of rosettes in the unit cell.

Complexation of 1,5-dihydroxyanthraquinone ($2\mathbf{b}$) by receptor $1_3\bullet(\text{DEB})_6$ was also observed in solution. ¹H NMR spectroscopy showed that upon addition of $2\mathbf{b}$ to a solution of $1_3\bullet(\text{DEB})_6$ in chloroform a different set of signals for the hydrogen-bonded protons H_{a-e} of the receptor emerged (Figure 5.3), confirming the formation of the complex $1_3\bullet(\text{DEB})_6\bullet 2\mathbf{b}_3$. Upon addition of 10 equiv of $2\mathbf{b}$ to assembly $1_3\bullet(\text{DEB})_6$ (1.0 mM in CDCl₃) only chemical shifts for the complex $1_3\bullet(\text{DEB})_6\bullet 2\mathbf{b}_3$ and free $2\mathbf{b}$ were observed (Figure 5.3). All the signals in the ¹H NMR spectrum of complex $1_3\bullet(\text{DEB})_6\bullet 2\mathbf{b}_3$ were assigned using 2D ¹H NMR experiments. Large shifts for the guest molecules $2\mathbf{b}$ are observed (> 3 ppm), indicating their encapsulation. The aromatic protons H_r , H_s and H_t of $2\mathbf{b}$ have shifted 3.23-2.93 ppm upfield, indicating that ring C (see Figure 5.3) is partially included in the calix[4]arene cone. The intramolecular

hydrogen-bonded protons H_q are shifted 0.26 ppm downfield compared to the position of these protons in the free guest (Figure 5.3a,b). Furthermore, the hydrogen-bonded NH_{DEB} protons H_a and H_b in the complex $1_3 \cdot (DEB)_6 \cdot 2b_3$ are shifted upfield 0.66 ppm and 0.11 ppm, respectively.³² Protons H_e and H_f situated in the internal part of the rosette cavity show a large upfield shift of 0.56 ppm and 0.68 ppm, respectively. In summary, all the shifts confirm the encapsulation of three molecules of **2b** between the two rosette planes.

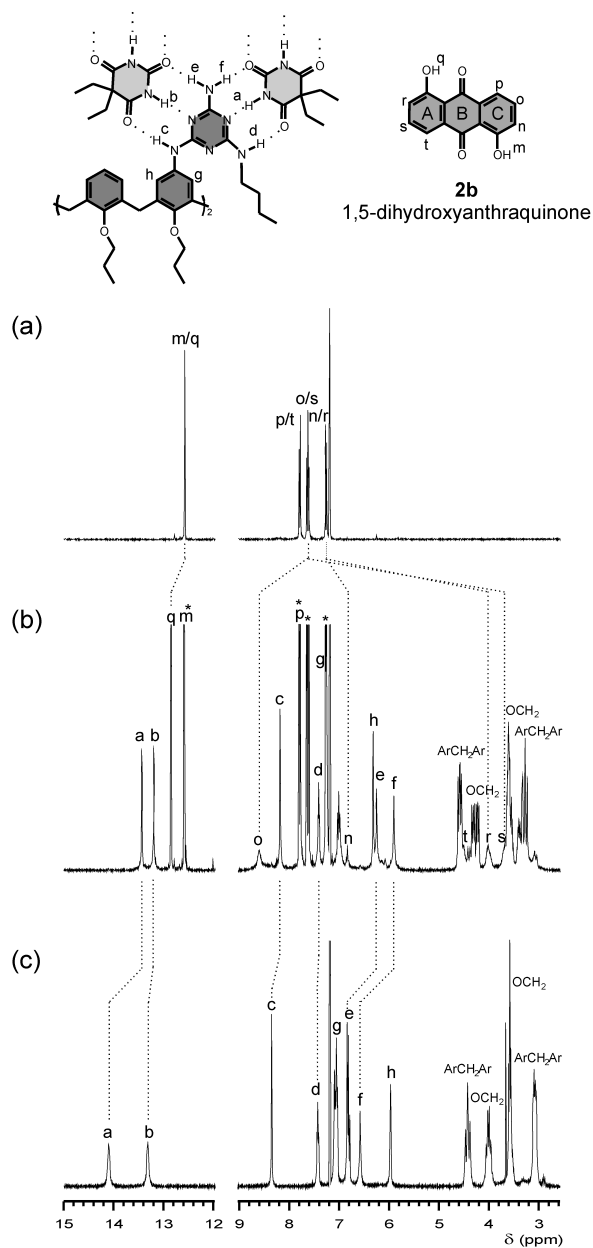
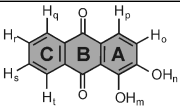
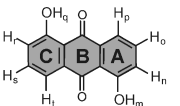
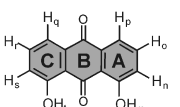
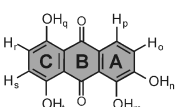
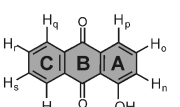
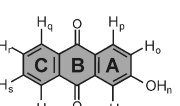
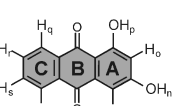


Figure 5.3 Part of the ¹H NMR spectra (400 MHz, CDCl₃) of (a) guest molecule **2b**; (b) complex **1a₃·(DEB)₆·2b₃**; and (c) receptor **1a₃·(DEB)₆**. The signals corresponding to free **2b** are marked with *.

After the successful encapsulation of **2b** by the receptor $\mathbf{1}_3\cdot(\text{DEB})_6$ the influence of the same substituents at different positions in ring C of the anthraquinone skeleton was studied. A different substitution pattern in **2c-d** might decrease the complexation ability as a consequence of the possible steric interference between this ring and the calix[4]arene cone.

Table 5.1 Changes of the chemical shifts ($\Delta\delta$) for the complexation of anthraquinone derivatives **2a-g** by $\mathbf{1}_3\cdot(\text{DEB})_6$ (1.0 mM, CDCl_3 at 293 K). Protons H_a , H_b , H_e and H_f are hydrogen-bonded protons of the receptor $\mathbf{1}_3\cdot(\text{DEB})_6$ (see Figure 5.3).

Structure	$\Delta\delta$ (ppm)									
	H_a	H_b	H_e	H_f	H_m	H_n	H_q	H_r	H_s	H_t
 2a	-0.58	-0.30	-0.71	-0.84	-0.02	3.63	-	-3.88	-3.88	-3.28
 2b	-0.66	-0.11	-0.56	-0.68	0.00	-	0.26	-3.23	-3.93	-3.27
 2c	-0.76	0.04	-0.36	-0.36	-0.40	-	-	-	-3.27	0.25
 2d	0.00	0.00	0.00	0.00	0.00	0.00	0.00	0.00	0.00	0.00
 2e	-0.22	-0.14	-0.93	-0.42	0.00	-	-	-	-	-3.50
 2f	-0.68	-0.16	-1.14	-0.47	-	4.03	-1.22	-3.83	-3.83	-3.30
 2g	-0.50	-0.08	-0.39	-0.27	0.39	3.35	-0.21	-3.73	-3.73	-3.12

Addition of 1,8-dihydroxyanthraquinone (**2c**) (10 equiv) to assembly $\mathbf{1}_3\cdot(\text{DEB})_6$ (1.0 mM in CDCl_3) led also to large shifts for the guest molecule **2c** (Table 5.1), indicating the encapsulation of **2c**. The intramolecular hydrogen-bonded OH_m and OH_t of the guest **2c**

shifted 0.40 ppm upfield and 0.25 ppm downfield, respectively. Furthermore, the hydrogen-bonded NH_{DEB} protons H_a and H_b in the complex $\mathbf{1}_3 \cdot (\text{DEB})_6 \cdot \mathbf{2c}_3$ are shifted 0.76 ppm upfield and 0.04 ppm downfield, respectively.

The orientation of molecule $\mathbf{2c}$ in the complex $\mathbf{1}_3 \cdot (\text{DEB})_6 \cdot \mathbf{2c}_3$ is extrapolated from the X-ray structures of complexes $\mathbf{1}_3 \cdot (\text{DEB})_6 \cdot \mathbf{2a}_3$ and $\mathbf{1}_3 \cdot (\text{DEB})_6 \cdot \mathbf{2b}_3$. Figure 5.4 shows that both, area *i* and *ii* in the receptor cavity of these two crystal structures would be inaccessible if functionalities at the Y^6 and Y^8 positions (see chart 5.1) in the anthraquinone derivatives would be present (this refers to the orientation of the guest molecules where ring C is included in the calix[4]arene cone). Based on this, it is suggested that the guest molecule $\mathbf{2c}$ is complexed with the 1-hydroxyl group (ring A) pointing inwards relative to the rosette plane (Figure 5.5a). In this way, the 8-hydroxyl group of $\mathbf{2c}$ (ring C) occupies the same space in the receptor cavity as it was observed for the 5-hydroxyl group (ring C) of guest $\mathbf{2b}$ in complex $\mathbf{1}_3 \cdot (\text{DEB})_6 \cdot \mathbf{2b}_3$, and thus the C-ring suffers no steric interference with the calix[4]arene cone.

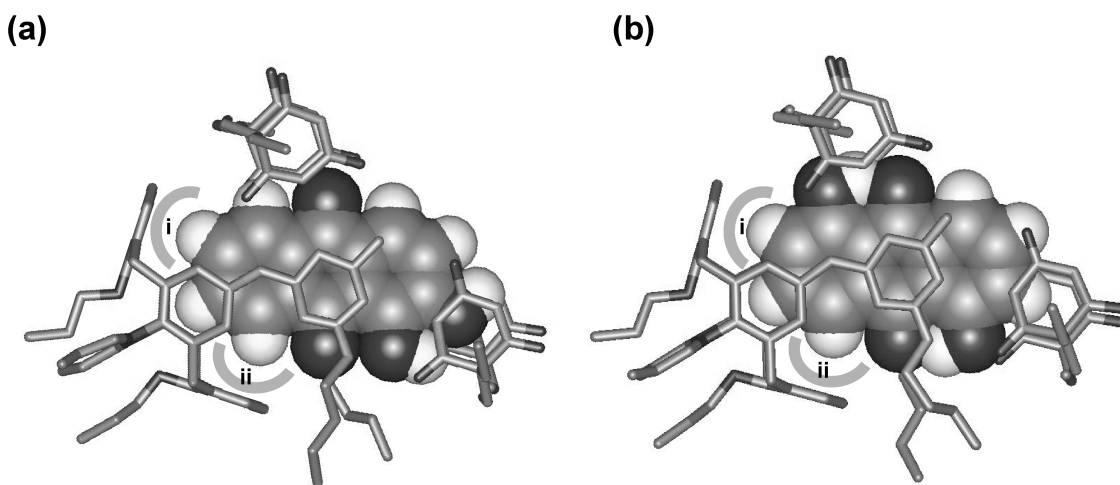


Figure 5.4 Part of the X-ray crystal structures of the complex (a) $\mathbf{1}_3 \cdot (\text{DEB})_6 \cdot \mathbf{2a}_3$ and (b) $\mathbf{1}_3 \cdot (\text{DEB})_6 \cdot \mathbf{2b}_3$. *i* and *ii* denotes the inaccessible areas for functionalities present at the anthraquinone derivatives (positions Y^6 or Y^8 ; see chart 5.1 for assignment of the positions). A stick model is used for the representation of the part of the molecular cage $\mathbf{1}_3 \cdot (\text{DEB})_6$, while a space-filling representation is chosen for the molecules $\mathbf{2a}$ and $\mathbf{2b}$. Hydrogens of $\mathbf{1}_3 \cdot (\text{DEB})_6$ are not shown.

Extrapolated also from the X-ray structures, receptor $1_3\bullet(\text{DEB})_6$ should not complex 1,2,5,8-tetrahydroxyanthraquinone (**2d**), because in all possible orientations of this guest a hydroxyl group will occupy either area *i* or *ii*. Indeed, after addition of **2d** to $1_3\bullet(\text{DEB})_6$, changes in the chemical shifts of either host or guest were not observed, indicating that complexation has not occurred.

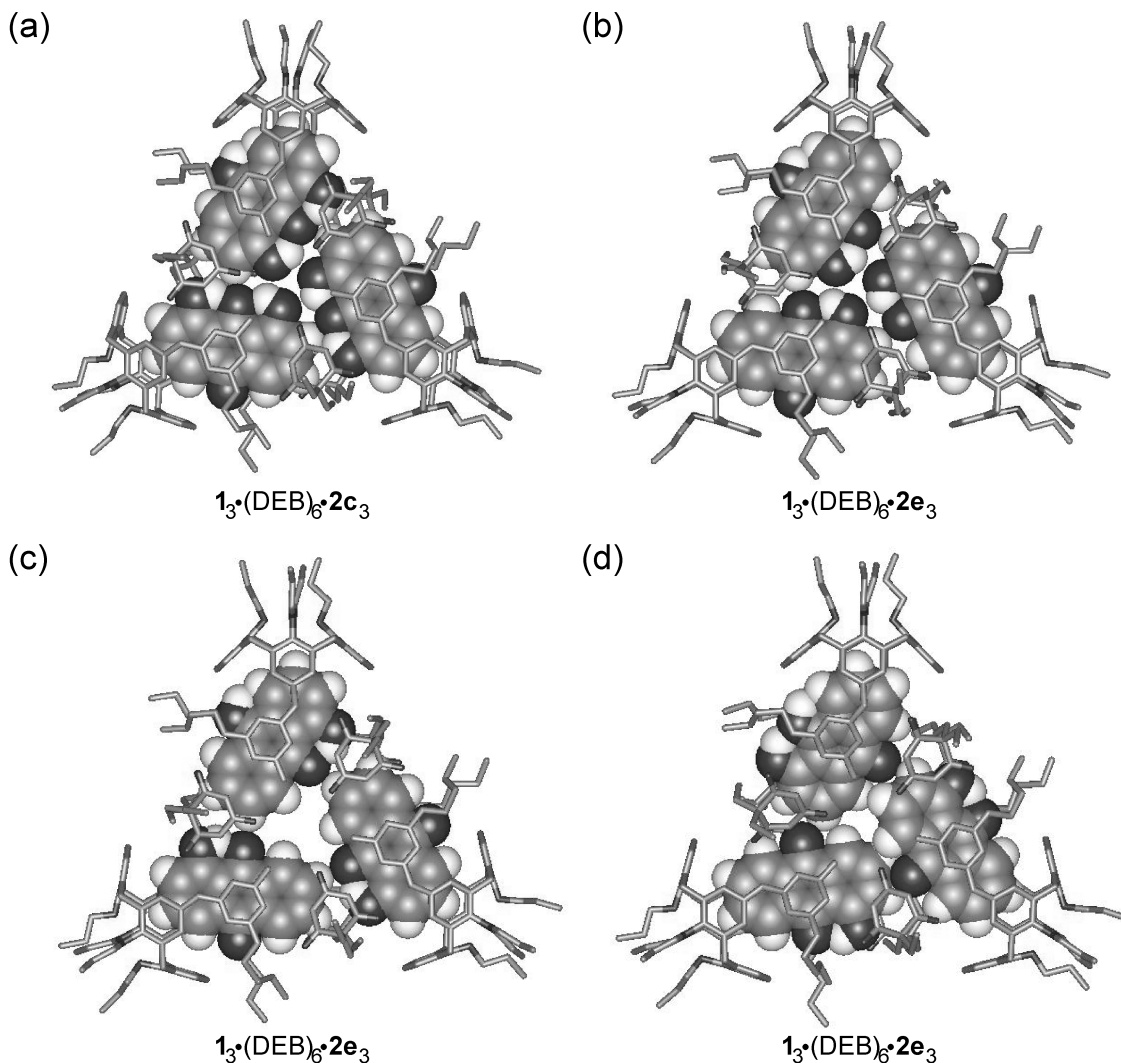


Figure 5.5 Gas-phase minimized structures of $1_3\bullet(\text{DEB})_6\bullet 2c_3$ (a), and $1_3\bullet(\text{DEB})_6\bullet 2e_3$ with the hydroxyl group pointing inwards (b) and (c). In (b) the 1-OH is close to the center of the rosette plane, while in (c) this OH is close to the edge of this plane. The structure of $1_3\bullet(\text{DEB})_6\bullet 2e_3$ where the 1-OH is pointing outwards is shown in (d). A stick model is used for the representation of the molecular cage $1_3\bullet(\text{DEB})_6$, while a space-filling representation is chosen for the guest molecules. No hydrogens of $1_3\bullet(\text{DEB})_6$ are shown.

The substitution pattern at ring A of the anthraquinone skeleton was also studied to examine the importance of the number and position of the hydroxyl groups present at this ring for the complexation. ^1H NMR studies with 1-hydroxyanthraquinone (**2e**, 10 equiv), containing only one hydroxyl group at position-1 (Y^1), and assembly $\mathbf{1}_3\cdot(\text{DEB})_6$ (1.0 mM, CDCl_3) gave upfield shifts of 3.50 ppm for H_t of guest **2e** and upfield shifts of 0.22 ppm and 0.14 ppm for H_a and H_b of the receptor, respectively (Table 5.1), indicating that complex $\mathbf{1}_3\cdot(\text{DEB})_6\cdot\mathbf{2e}_3$ is formed. The guest molecule **2e** can be either complexed with the hydroxyl functionality pointing inwards or outwards (Figure 5.5b-d). As observed for guest **2b**, no shift of the OH_m signal ($\delta = 12.55$ ppm) was observed in the ^1H NMR spectrum of the complex formed with **2e**, indicating the same orientation (outwards) for this proton (Figure 5.5c,d). It is expected that positioning of **2e** with the hydroxyl in the center of the receptor cavity (inwards), as depicted in Figure 5.5b, would result in a shift of OH_m in the ^1H NMR spectrum (as for **2c**), thus the inwards orientation is unlikely. There is no evidence in the ^1H NMR spectrum to rule out one of the two structures with the outward orientation of the hydroxyl groups (Figure 5.5c,d). Nevertheless, from ITC studies (see next Section) the structure presented in Figure 5.5c is ruled out for entropic reasons.

Large shifts of the aromatic protons H_r , H_s and H_t ($\Delta\delta = 3.12\text{-}3.83$ ppm) were also observed when 2-hydroxyanthraquinone (**2f**, 4 equiv), containing only one hydroxyl group at position-2, and purpurin (**2g**, 4 equiv), with three hydroxyl groups in ring A, were added to $\mathbf{1}_3\cdot(\text{DEB})_6$ (1.0 mM, CDCl_3) (Table 5.1). Also in these ^1H NMR spectra a different set of signals for the H_a and H_b protons of $\mathbf{1}_3\cdot(\text{DEB})_6\cdot\mathbf{2f}_3$ and $\mathbf{1}_3\cdot(\text{DEB})_6\cdot\mathbf{2g}_3$ were observed. Furthermore, the large downfield shift of the 2-hydroxyl group (OH_n) of **2f** and **2g** indicates that in both $\mathbf{1}_3\cdot(\text{DEB})_6\cdot\mathbf{2f}_3$ and $\mathbf{1}_3\cdot(\text{DEB})_6\cdot\mathbf{2g}_3$ an intermolecular hydrogen-bonded network is formed between the encapsulated guest molecules, as it was observed for complex $\mathbf{1}_3\cdot(\text{DEB})_6\cdot\mathbf{2a}_3$. Thus, the mode of complexation of guests **2f** and **2g** by $\mathbf{1}_3\cdot(\text{DEB})_6$ is the same as for **2a**, indicating that the complexation is not substantially affected even when three hydroxyl groups are present at ring A.

Also the complexation of anthracene (**3**) and anthraquinone (**2h**) were examined. Addition of anthracene (**3**, 10 equiv), lacking both carbonyl and hydroxyl functionalities, to $\mathbf{1}_3 \cdot (\text{DEB})_6$ (1.0 mM in CDCl_3) did not shift any signal in the ^1H NMR spectrum. The central aromatic ring of **3** is more electron rich compared to, for example **2a**, therefore, the π - π repulsion possibly dominates over the π - σ attraction and thus prevents π - π stacking of the guest in between the two melamine units. Also anthraquinone (**2h**, 10 equiv.), lacking the hydroxyl groups, did not show any shift of the signals in the ^1H NMR spectrum, which means that the presence of at least one hydroxyl group is important for the complexation.

In summary, complexation of anthraquinone derivatives **2** only occurs when there are no hydroxyl groups at the positions Y^6 and Y^8 in the anthraquinone skeleton (referring to the orientation of the guest molecules in the complex where ring C is included in the calix[4]arene cone), otherwise the steric strain between the substituents and the receptor avoids the complexation. When a hydroxyl group is present at the 2-position (ring A) an intermolecular hydrogen-bonded network is formed among the three encapsulated guests. Furthermore, hydroxyl groups at ring A do not substantially affect the complexation. The carbonyl groups in ring B and at least one hydroxyl group in the anthraquinone skeleton are required for complexation.

Isothermal titration microcalorimetry.

Isothermal titration calorimetry (ITC) was used to quantify the thermodynamic parameters ΔG^0 , ΔH^0 , and $T\Delta S^0$ and to determine the association constant for the encapsulation of the guest molecules **2** by the receptor $\mathbf{1}_3 \cdot (\text{DEB})_6$. As an example, Figure 5.6 shows the results of the ITC measurement for the formation of $\mathbf{1}_3 \cdot (\text{DEB})_6 \cdot \mathbf{2a}_3$ using 3.0 mM solutions of **2a** in 1,2-DCE inside the ITC cell and 10 mM of $\mathbf{1}_3 \cdot (\text{DEB})_6$ in 1,2-DCE as titrant.

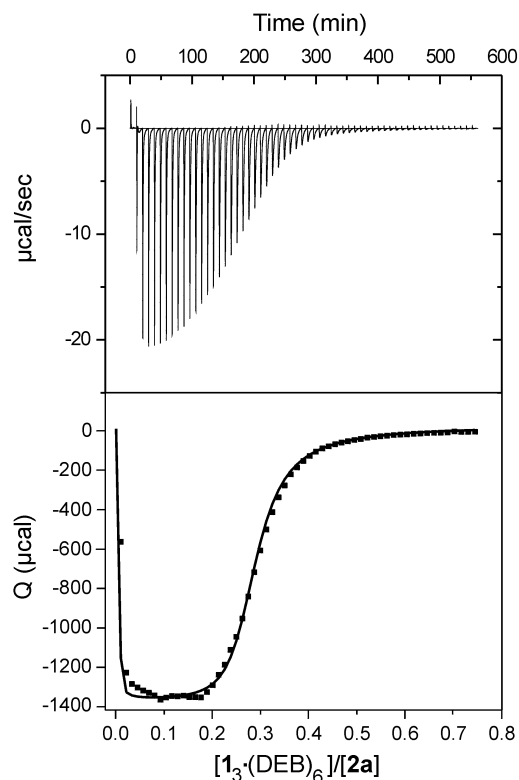


Figure 5.6 ITC measurement for the formation of $1_3 \bullet (DEB)_6 \bullet 2a_3$; cell: 3.0 mM $2a$, burette: 10.0 mM $1_3 \bullet (DEB)_6$. The binding isotherm is fitted to a 1:3 binding algorithm.

Cooperative binding of anthraquinone derivatives **2** by $1_3 \bullet (DEB)_6$ is observed since it was not possible to fit the ITC data to an independent 1:3 binding model. Complex $1_3 \bullet (DEB)_6 \bullet 2_3$ is directly formed from assembly $1_3 \bullet (DEB)_6$ and three molecules **2a**, since only free assembly, free guest and complex are observed in solution with 1H NMR spectroscopy. Therefore, the association constant (K_a) can be written as (K_a is expressed in M^{-3}):

$$K_a = \frac{[1_3 \bullet DEB_6 \bullet 2a_3]}{[2a]^3 [1_3 \bullet DEB_6]} \quad (\text{Eq. 5.1})$$

In the beginning of the titration the concentration of assembly is low and, therefore, a part of the assembly is dissociated. To correct for this, a more precise estimation of the mass balance was calculated based on the formation constant for $1_3 \bullet (DEB)_6$ (see Chapter 4). Equation 5.2, describes the formation of assembly $1_3 \bullet (DEB)_6$ (K_f is the formation

constant of the assembly expressed in M^{-8}). From equations 5.1 and 5.2 the association constant for the encapsulation of **2a** is calculated (Equation 5.3). Heat effects caused by dissociation of the assembly were corrected from data obtained from dilution experiments.

$$K_f = \frac{[\mathbf{1}_3 \cdot DEB_6]}{[\mathbf{1}]^3 [DEB]^6} \quad (\text{Eq. 5.2})$$

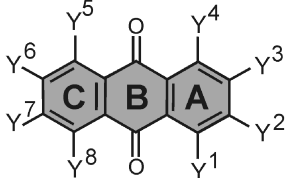
$$K_a = \frac{[\mathbf{1}_3 \cdot DEB_6 \cdot \mathbf{2a}_3]}{K_f \cdot [\mathbf{1}]^3 [DEB]^6 [\mathbf{2a}]^3} \quad (\text{Eq. 5.3})$$

Curve fitting of the binding isotherms for the formation of $\mathbf{1}_3 \cdot (\text{DEB})_6 \cdot \mathbf{2a}_3$ gave a binding constant of $6.0 \times 10^{10} M^{-3}$ (Figure 5.6). Formation of $\mathbf{1}_3 \cdot (\text{DEB})_6 \cdot \mathbf{2a}_3$ is strongly enthalpy driven ($\Delta H^0 = -31.9 \pm 0.6 \text{ kJ} \cdot \text{mol}^{-1}$). The observed negative enthalpy change likely arises from favorable π - π interactions with the rosette layers possibly reinforced by the hydrogen-bonded network formed between the three **2a** molecules. The adverse negative entropy ($T\Delta S^0 = -17.8 \pm 0.8 \text{ kJ} \cdot \text{mol}^{-1}$) arises possibly from the restrictions in translational and rotational freedom of the three guest molecules **2a**.

ITC measurements with **2a** and assembly $\mathbf{1}_3 \cdot (\text{BuCYA})_6$ (with BuCYA instead of DEB) did not show any appreciable heat effect, indicating that complex $\mathbf{1}_3 \cdot (\text{BuCYA})_6 \cdot \mathbf{2a}_3$ is not formed. Probably small geometrical differences between $\mathbf{1}_3 \cdot (\text{DEB})_6$ and $\mathbf{1}_3 \cdot (\text{BuCYA})_6$ account for the inability of $\mathbf{1}_3 \cdot (\text{BuCYA})_6$ to complex **2a**. Molecular modeling (Quanta 97, CHARMm 24.0) indicated that the two rosette floors of $\mathbf{1}_3 \cdot (\text{BuCYA})_6$ are stacked on top of each other with an interatomic separation of 3.2 Å at the edges and 2.8 Å in the center of the rosette, while for $\mathbf{1}_3 \cdot (\text{DEB})_6$ these interatomic separations are 3.5 Å and 3.2 Å. Possibly, additional stabilizing interactions between the rosette layers in $\mathbf{1}_3 \cdot (\text{BuCYA})_6$ might prevent encapsulation of **2a**.

An overview of the ITC results for the encapsulation of the anthraquinone derivatives **2** by $1_3\bullet(\text{DEB})_6$ is presented in Table 5.2. The ITC data show that the presence of a hydroxyl group at the position Y^2 (ring A) and the absence of functionalities in the C-ring of the anthraquinone skeleton (**2a**, **2f**, **2g**) results in strong binding ($K = \sim 10^{10} \text{ M}^{-3}$). Only small differences were observed for the binding enthalpy and entropy of complexes $1_3\bullet(\text{DEB})_6\bullet 2a_3$, $1_3\bullet(\text{DEB})_6\bullet 2f_3$, and $1_3\bullet(\text{DEB})_6\bullet 2g_3$. The main structural difference between guest molecules **2a**, **2f** and **2g** is the number of hydroxyl groups present at the A-ring (Y^1 , Y^2 and Y^4 , Table 5.2). The hydroxyl group at the Y^2 position of these guests is responsible for the formation of the intermolecular hydrogen bonds between the guest trimer. The hydroxyl groups at Y^1 and Y^4 , which form intramolecular hydrogen bonds with the adjacent carbonyl moieties (as was seen by ^1H NMR spectroscopy) do not affect the complexation since only relatively small differences in complexation were observed.

Table 5.2 ITC data for the complexation of the anthraquinone derivatives **2** by the molecular box $1_3\bullet(\text{DEB})_6$ and $1_3\bullet(\text{BuCYA})_6$. $Y^3=Y^7=\text{H}$. (1,2-DCE, 298 K)

Host	Guest							K_a (M^{-3})	ΔH^0 ($\text{kcal}\cdot\text{mol}^{-1}$)	ΔG^0 ($\text{kcal}\cdot\text{mol}^{-1}$)	$T\Delta S^0$ ($\text{kcal}\cdot\text{mol}^{-1}$)
		Y^1	Y^2	Y^4	Y^5	Y^6	Y^8				
$1_3\bullet(\text{DEB})_6$	2a	OH	OH	H	H	H	H	$(2.5\pm 1.5)\times 10^{10}$	-31.9 ± 0.6	-14.1 ± 0.4	-17.8 ± 0.8
$1_3\bullet(\text{BuCYA})_6$	2a	OH	OH	H	H	H	H	-	No heat	-	-
$1_3\bullet(\text{DEB})_6$	2b	OH	H	H	OH	H	H	$(1.1\pm 0.6)\times 10^8$	-31.2 ± 1.1	-10.9 ± 0.3	-20.3 ± 1.0
$1_3\bullet(\text{DEB})_6$	2c	OH	H	H	H	H	OH	$(2.5\pm 0.2)\times 10^7$	-30.2 ± 0.2	-10.1 ± 0.1	-20.1 ± 0.2
$1_3\bullet(\text{DEB})_6$	2d	OH	OH	H	OH	H	OH	-	No heat	-	-
$1_3\bullet(\text{DEB})_6$	2e	OH	H	H	H	H	H	$(3.6\pm 1.9)\times 10^6$	-22.2 ± 0.8	-8.9 ± 0.3	-13.3 ± 0.4
$1_3\bullet(\text{DEB})_6$	2f	H	OH	H	H	H	H	$(4.1\pm 2.0)\times 10^{10}$	-28.7 ± 0.8	-14.4 ± 0.3	-14.2 ± 0.8
$1_3\bullet(\text{DEB})_6$	2g	OH	OH	OH	H	H	H	$(1.5\pm 0.9)\times 10^{11}$	-30.3 ± 1.7	-15.2 ± 0.4	-15.2 ± 2.1
$1_3\bullet(\text{DEB})_6$	2h	H	H	H	H	H	H	-	No heat	-	-

The ITC measurements with **2d**, having four hydroxyl groups, and $1_3\bullet(\text{DEB})_6$ did not show any appreciable heat effects, showing no complexation. As it was also concluded

from ^1H NMR studies, $\mathbf{1}_3\bullet(\text{DEB})_6$ does not complex $\mathbf{2d}$ because upon encapsulation one of the hydroxyl groups would have to occupy one of the forbidden areas in the receptor cavity (area *i* or *ii* in Figure 5.4).

Guest molecules $\mathbf{2b}$, $\mathbf{2c}$ and $\mathbf{2e}$ lacking the hydroxyl group at the position-2, but with a hydroxyl at the position-1 showed appreciable heat effects in the ITC measurements. Binding of these guest molecules to $\mathbf{1}_3\bullet(\text{DEB})_6$ is, however, less efficient ($K_{\text{enc}} \sim 10^6\text{-}10^8 \text{ M}^{-3}$) than binding of $\mathbf{2a}$ and $\mathbf{2f-g}$. It seems that the absence of the intermolecular hydrogen bonds between the guest molecules decreases the binding affinity. Because many factors can contribute to the binding enthalpy and entropy of these complexes, it is difficult to attribute enthalpy and entropy values to specific binding properties, but a few conclusions can be drawn.

The lower binding affinity of $\mathbf{2e}$ for $\mathbf{1}_3\bullet(\text{DEB})_6$ compared to $\mathbf{2a}$, $\mathbf{2f}$ and $\mathbf{2g}$ is mainly due to lower binding enthalpy (Table 5.2) caused by the absence of an intermolecular hydrogen-bonded network between the guest molecules. The entropy change for complex $\mathbf{1}_3\bullet(\text{DEB})_6\bullet\mathbf{2e}_3$ is comparable ($T\Delta S^\circ = -13.3 \pm 0.4 \text{ kcal}\cdot\text{mol}^{-1}$) with that observed for the complexation between $\mathbf{1}_3\bullet(\text{DEB})_6$ and $\mathbf{2a}$, $\mathbf{2f}$ and $\mathbf{2g}$.

On the other hand, when comparing the binding affinities of $\mathbf{2b}$ and $\mathbf{2c}$ with $\mathbf{2a}$, $\mathbf{2f}$ and $\mathbf{2g}$, the differences in the complex formation are mainly due to differences in the binding entropy (Table 5.2), possibly due to the positioning of the hydroxyl group at the C-ring that leads to a decreased freedom of movement of the guests $\mathbf{2b}$ and $\mathbf{2c}$ in the calix[4]arene cone. However, even though no intermolecular hydrogen-bonded network can be formed, the enthalpy values for encapsulation of $\mathbf{2b}$ and $\mathbf{2c}$ are comparable to those obtained for the complexation of $\mathbf{2a}$, $\mathbf{2f}$ and $\mathbf{2g}$. Thus, other enthalpy contributions, different from the enthalpy of formation of the intermolecular hydrogen bonds, have to be responsible for the larger ΔH° values. It is however unclear which enthalpy contributions could explain these larger ΔH° values, but differences in π - π interactions due to different electron densities of the B-ring of $\mathbf{2b}$ and $\mathbf{2c}$ might play a role.

Interestingly, comparison of the entropic values for $\mathbf{2b}$ and $\mathbf{2e}$, indicate that the presence of a hydroxyl group at position Y^5 (ring C) of the anthraquinone skeleton results

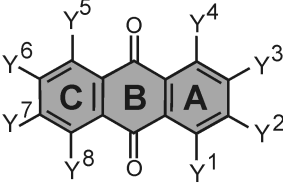
in an entropic penalty, ruling out the structure depicted in Figure 5.5c for complex $\mathbf{1}_3 \bullet (\text{DEB})_6 \bullet \mathbf{2e}_3$.

UV spectroscopy

Anthraquinone derivatives are used as coloring agents, thus UV-vis spectroscopy was also used to determine binding constants of the anthraquinone derivatives **2** to assembly $\mathbf{1}_3 \bullet (\text{DEB})_6$ in a very simple way. Anthraquinone derivatives **2a**, **2d**, **2e** and **2f** were selected for the UV-vis spectroscopy studies in the same solvent for comparison with the ITC studies.

The binding affinity of **2a** for assembly $\mathbf{1}_3 \bullet (\text{DEB})_6$ was determined by titration experiments in 1,2-DCE (Table 5.3) and the changes in the absorbance at 432 nm, 500 nm and 520 nm were monitored while aliquots of **2a** (0 to 5.7 equiv.) were added to $\mathbf{1}_3 \bullet (\text{DEB})_6$ (0.5 mM). At these wavelengths $\mathbf{1}_3 \bullet (\text{DEB})_6$ does not absorb and the absorbance of **2a** is very small ($\epsilon_{\text{complex}} \gg \epsilon_{\mathbf{2a}}$). A correction was made for possible dissociation of assembly as described for the ITC measurements. The resulting binding isotherm was fitted to a 1:3 binding algorithm to yield a binding constant of $1.8 \times 10^9 \text{ M}^{-3}$. Similar titration experiments were used to determine the binding constants of **2e** (0.5 mM assembly and 0-40 equiv of **2e**) and **2f** (0.64 mM assembly and 0-5.7 equiv of **2f**) in 1,2-DCE (Table 5.1).³³ Consistent with the ITC measurements, the association constant for **2e** ($K_a = 6.9 \times 10^5 \text{ M}^{-3}$) is about three decades lower than for **2a** ($K_a = 1.8 \times 10^9 \text{ M}^{-3}$), and the association constant of **2f** ($K_a = 1.0 \times 10^9 \text{ M}^{-3}$) is similar to the one found for **2a**. The UV-vis experiments with **2d** did not show the encapsulation of this guest in $\mathbf{1}_3 \bullet (\text{DEB})_6$, as it was also proven by ITC and ^1H NMR spectroscopy, because of the steric interference of the hydroxyl groups in **2d**.

Table 5.3 Binding constants determined by UV-vis spectroscopy for the encapsulation of guest molecules **2a** and **2d-f** by host $\mathbf{1}_3\bullet(\text{DEB})_6$. $Y^3=Y^7=\text{H}$. (1,2-DCE, 298 K)



guest	Y ¹	Y ²	Y ⁴	Y ⁵	Y ⁶	Y ⁸	K _a (M ⁻³)
2a	OH	OH	H	H	H	H	$(1.8 \pm 0.7) \times 10^9$
2d	OH	OH	H	OH	H	OH	-
2e	OH	H	H	H	H	H	$(6.8 \pm 2.8) \times 10^5$
2f	H	OH	H	H	H	H	$(1.0 \pm 0.1) \times 10^9$

5.3 Conclusions

A series of anthraquinone derivatives (**2**) form a trimeric species by encapsulation between the two rosette layers of the noncovalent hydrogen-bonded assembly $\mathbf{1}_3\bullet(\text{DEB})_6$. This encapsulation process enforces large structural changes in the assembly resulting in complete change of symmetry from *staggered* to *eclipsed*. Using X-ray crystallography, ¹H NMR spectroscopy, ITC, and UV spectroscopy it was possible to identify the different modes for the complexation of the guest molecules. The driving force for the encapsulation is π - π stacking between the electron deficient center ring of the anthraquinone derivatives and the relatively poor melamine units of the receptor $\mathbf{1}_3\bullet(\text{DEB})_6$. The encapsulation of anthraquinone derivatives by the receptor is very selective and sensitive to small structural changes. Positions Y⁶ and/or Y⁸ at the ring C of the anthraquinone skeleton should not be substituted by hydroxyl groups. Functionalities situated adjacent to these positions decrease the binding affinity because of the decreased freedom of the guests in the calix[4]arene cone (entropic penalty). Anthraquinone derivatives with a hydroxyl group at the 2-position and without functionalities in the C-ring have the highest binding affinity due to the formation of a hydrogen-bonded network between the guest molecules and the absence of steric interference between ring C and the calix[4]arene cone. There is no steric hindrance observed when hydroxyl groups are present in ring A of these anthraquinone derivatives.

5.4 Experimental

All chemicals were reagent grade and used without further purification. NMR spectra were recorded on a Varian Unity 300 (^1H NMR 300MHz) spectrometer in chloroform- d_1 or methanol- d_4 . Residual solvent protons were used as internal standard, and chemical shifts are given relatively to trimethylsilane (TMS). Calorimetric measurements were carried out using a Microcal VP-ITC microcalorimeter with a cell volume of 1.4115 ml. For each experiment the heat effect of 60 injections of 5 μl titrant was measured. Instrument settings were set on injection duration of 30 sec, spacing of 570 sec and low feedback at 16.3 $\mu\text{cal/sec}$ reference power and a temperature of 25°C. UV-vis measurements were performed on a HP8452A diode array spectrophotometer using solvents of spectroscopic grade.

ITC measurements

ITC measurements for the encapsulation of anthraquinone derivatives **2** by $\mathbf{1}_3 \cdot (\text{DEB}/\text{BuCYA})_3$ in 1,2-DCE were performed at three different concentrations. Solutions of **2a-d,f-h**, were put into the cell and solutions of assembly were used as titrant. For $\mathbf{1}_3 \cdot (\text{DEB})_3 \cdot \mathbf{2e}_3$, the assembly solutions were put in the cell, while aliquots of **2e** were injected.

UV/VIS measurements

UV-vis measurements were performed in 1,2-DCE, while the changes in absorbance at 432 nm, 500 nm and 520 nm, were monitored when aliquots of **2a** (0-5.7 equiv) or **2b** (0-40 equiv) were added to $\mathbf{1}_3 \cdot (\text{DEB})_3$ (0.5 mM). Due to limitations in solubility of **2c**, in this case, aliquots of $\mathbf{1}_3 \cdot (\text{DEB})_3$ (0-5.7 equiv) were added to **2c** (0.64 mM).

Single crystal X-ray diffraction

Crystal data and structure refinement for $3[\text{C}_{54}\text{H}_{72}\text{N}_{12}\text{O}_4] \cdot 6[\text{C}_8\text{H}_{12}\text{N}_2\text{O}_3] \cdot 3[\text{C}_{14}\text{H}_8\text{O}_4]$
Mr = 4685.58. Red, block-shaped crystals were obtained from diffusion of hexane into a solution of the complex in dichloromethane. A crystal of dimensions 0.3 x 0.3 x 0.3 mm was selected for measurement. The crystal was cubic, space group $Pa\bar{3}$ (no. 205) with $a = 40.970$ (9), $V = 68770$ (26) \AA^3 , $Z = 24$, $D_x = 0.905$ $\text{g}\cdot\text{cm}^3$, $F(000) = 19968$, $\mu(\text{Mo K}\alpha) =$

0.063 mm⁻¹. Where relevant, the contribution of the disordered solvent molecules has not been included in the reported data (*vide infra*). 768947 reflections are measured, 14478 of which were independent, $R_{int} = 0.2737$, $R_{\sigma} = 0.2001$, $1.0^{\circ} < \theta < 22.25^{\circ}$, $T = 150$ K, Mo $K\alpha$ radiation, graphite monochromator, $\lambda = 0.71073$ Å. Data were collected on a Nonius KappaCCD area detector on rotating anode and were not corrected for absorption. The structure was solved by direct methods (SHELXS86) and refined on F^2 using SHELXL-97-2. The unit cell contains a large area with a volume of 25382 Å³ (*i.e.* 41% of the unit cell volume) filled with disordered solvent molecules. No satisfactory model could be constructed. The disordered density was therefore taken into account with the SQUEEZE procedure, as implemented in PLATON. The propyl and butyl moieties of the calix[4]arene molecule displayed large displacement parameters with high anisotropy. A disorder model for these groups gave unrealistic results and was therefore abandoned. Hydrogen atoms were included in the refinement on calculated positions riding on their carrier atoms. All non-hydrogen atoms were refined with anisotropic displacement parameters. The low quality of the available data made it necessary to introduce rigid bond restraints for atom pairs that are bonded to a common third atom or are bonded directly to each other. Similarity restraints were applied to the displacement parameters of atom pairs that are closer than 1.7 Å. Hydrogen atoms were refined with a fixed isotropic displacement parameter linked to the value of the equivalent isotropic displacement parameter of their carrier atoms. Final $wR2 = 0.2420$, $w = 1/[\sigma^2(F^2) + (0.08P)^2 + 15P]$, where $P = (\max(F_o^2, 0) + 2 F_c^2)/3$, $R1 = 0.0869$ (for 5484 $I > 2\sigma(I)$), $S = 1.246$, 1027 refined parameters, $-0.49 < \Delta\rho < 0.53$ e Å⁻³.

5.5 References

1. Lyndsey, L. M.; Philp, D. *Chem. Soc. Rev.* **2001**, *30*, 287-302.
2. Lindsey, J. S. *New J. Chem.* **1991**, *15*, 153-180.
3. Stryer, L. *Biochemistry*; 4th ed. Freeman and Company: New York, 1995.
4. Fiammengo, R.; Crego-Calama, M.; Reinhoudt, D. N. *Curr. Opin. Chem. Biol.* **2001**, *5*, 660-673.
5. Chen, J.; Körner, S.; Craig, S. L.; Rudkevich, D. M.; Rebek, J. Jr. *Nature* **2002**,

- 415, 385-386.
6. Rincon, A. M.; Prados, P.; De Mendoza, J. *J. Am. Chem. Soc.* **2001**, *123*, 3493-3498.
 7. Vysotsky, M. O.; Thondorf, I.; Böhmer, V. *Angew. Chem. Int. Ed.* **2000**, *39*, 1264-1267.
 8. Umemoto, K.; Tsukui, H.; Kusukawa, T.; Biradha, K.; Fujita, M. *Angew. Chem. Int. Ed.* **2001**, *40*, 2620-2622.
 9. Jacopoizzi, P.; Dalcanale, E. *Angew. Chem. Int. Ed.* **1997**, *36*, 613-615.
 10. Corbellini, F.; Fiammengo, R.; Timmerman, P.; Crego-Calama, M.; Reinhoudt, D. N. *J. Am. Chem. Soc.* **2002**, *124*, 6569-6575.
 11. Fiammengo, R.; Wojclichowski, K.; Crego-Calama, M.; Timmerman, P.; Figoli, A.; Wessling, M.; Reinhoudt, D. N. *Org. Lett.* **2003**, *5*, 3367-3370.
 12. Kang, J.; Rebek, J. Jr. *Nature* **1997**, *385*, 50-52.
 13. Kang, J.; Santamaría, J.; Rebek, J. Jr. *J. Am. Chem. Soc.* **1998**, *120*, 7389-7390.
 14. Kang, J.; Hilmersson, G.; Santamaría, J.; Rebek, J. Jr. *J. Am. Chem. Soc.* **1998**, *120*, 3650-3656.
 15. Schalley, C. A. *Adv. Mater.* **1999**, *11*, 1535-1537.
 16. Conn, M. M.; Rebek, J. Jr. *Nature* **1996**, *382*, 239-241.
 17. Hof, F.; Craig, S. L.; Nuckolls, C.; Rebek, J. Jr. *Angew. Chem. Int. Ed.* **2002**, *41*, 1488-1508, and references therein.
 18. Schalley, C. A. *Angew. Chem. Int. Ed.* **2002**, *41*, 1513-1515.
 19. Chopra, N.; Sherman, J. C. *Angew. Chem. Int. Ed.* **1999**, *38*, 1955-1957.
 20. Cram, D. J.; Karbach, S.; Kim, Y. H.; Baczynskyj, L.; Kallemeyn, G. W. *J. Am. Chem. Soc.* **1985**, *107*, 2575-2576.
 21. Ziegler, M.; Brumaghim, J. L.; Raymond, K. N. *Angew. Chem. Int. Ed.* **2000**, *39*, 4119-4121.
 22. Kusukawa, T.; Fujita, M. *J. Am. Chem. Soc.* **1999**, *121*, 1397-1398.
 23. Kang, J.; Rebek, J. Jr. *Nature* **1996**, *382*, 239-241.
 24. Heinz, T.; Rudkevich, D. M.; Rebek, J. Jr. *Nature* **1998**, *394*, 764-766.

25. Kusukawa, T.; Fujita, M. *J. Am. Chem. Soc.* **2002**, *124*, 13576-13582.
26. Kerckhoffs, J. M. C. A.; Van Leeuwen, F. W. B.; Spek, A. L.; Kooijman, H.; Crego-Calama, M.; Reinhoudt, D. N. *Angew. Chem. Int. Ed.* **2003**, *42*, 5717-5722.
27. Seto, C. T.; Whitesides, G. M. *J. Am. Chem. Soc.* **1993**, *115*, 905-916.
28. Timmerman, P.; Vreekamp, R. H.; Hulst, R.; Verboom, W.; Reinhoudt, D. N.; Rissanen, K.; Udachin, K. A.; Ripmeester, J. *Chem. Eur. J.* **1997**, *3*, 1823-1832.
29. Vreekamp, R. H.; van Duynhoven, J. P. M.; Verboom, W.; Reinhoudt, D. N. *Angew. Chem. Int. Ed.* **1996**, *35*, 1215-1218.
30. Hunter, C. A.; Sanders, J. K. M. *J. Am. Chem. Soc.* **1990**, *112*, 5525-5534.
31. Kerckhoffs, J. M. C. A., *Thesis: Synthetic receptors based on hydrogen-bonded assemblies*, University of Twente, Enschede, the Netherlands, ISBN 90-365-1894-6, 2003.
32. Encapsulation of **2b** in the *staggered* conformation would lead to four signals for the NH_{DEB}-protons (two for each rosette; C₃ symmetry). However, only two signals for these protons were observed in the ¹H NMR spectrum implying that upon encapsulation of **2b** a conformational change of the calix[4]arene melamine from *staggered* to *eclipsed* has occurred leading to a complex with a C_{3h} symmetry.
33. Because **2f** exhibit low solubility in 1,2-DCE, in this case, aliquots of assembly were added to a solution of **2f** in 1,2-DCE. The data are corrected for possible dissociation of assembly as described for the ITC measurements.

Chapter 6

Binding of small guest molecules to multivalent receptors

In this chapter, the complexation of phenol derivatives, aromatic carboxylic acids and n-octylgalactopyranoside by hydrogen-bonded exo-receptors is described. The receptors are formed by self-assembly of differently functionalized calix[4]arene dimelamines with 5,5-diethyl barbiturate (DEB) or butyl cyanurate (BuCYA). The multivalent complementary recognition site of the receptors is used very efficiently to complex multiple guests. A 1:6 binding mode was observed for phenol derivatives forming single hydrogen bonds with each ureido functionality, while 1:3 complexation was observed for phenol derivatives which form two hydrogen bonds with two different ureido recognition sites. Aromatic carboxylic acids are complexed in a 1:6 ratio by exo-receptors having amino recognition sites. The complexation of n-octylgalactopyranoside by Gly-L-Ser functionalized exo-receptors is also described, indicating that it is possible to use small peptidic fragments to complex biologically important molecules.

6.1 Introduction

Biochemical processes such as enzymatic action, molecular transport, genetic information and processing, and protein assembly all involve molecular recognition.¹⁻³ The exquisite recognition of an antigen by the antibody is just one example of the remarkable chemical control achieved by biological systems.⁴ Compared to natural systems, most synthetic receptors⁵ use only a limited number of weak interactions. In general, these receptors are able to bind single guest molecules such as cations,⁶⁻⁸ anions,⁹⁻¹⁶ or small neutral molecules.¹⁷⁻²² However, there are essentially no examples of synthetic molecules that bind to a substrate with the strength or selectivity of an antibody.⁴ To enhance binding strength and selectivity of natural receptors, multiple interactions are used by combination of amino acids and nucleotides.²³⁻²⁵ These multiple interactions (multivalency) display unique collective properties compared to the properties of their monovalent binding constituents. Multivalent recognition of substrates with strong and selective binding requires a large contact area and a sufficient number of complementary recognition sites. This mode of molecular recognition is observed at the antibody-antigen interface.²⁶

In Chapter 5 the encapsulation of anthraquinone derivatives by a hydrogen-bonded noncovalent receptor has been described. This receptor possesses an internal cavity where the guest is encapsulated (*endo*-receptor). Binding of guest molecules to *endo*-receptors is restricted to the dimensions of the cavities and they are therefore not very useful for multivalent recognition of guest molecules.

In this chapter, hydrogen-bonded double rosettes with different recognition sites at the exterior part of the assemblies will be described (*exo*-receptors). As described in Chapter 3, these double rosettes are assembled from calix[4]arene dimelamines **1-3** with two equivalents 5,5-diethyl barbituric acid (DEB) or *n*-butyl cyanurates (BuCYA) (Figure 6.1). The melamine units of these assemblies are functionalized with ureido (**1**), amino (**2**) or *L*-serine (**3**) moieties to recognize phenols, aromatic carboxylic acids and carbohydrate derivatives, respectively. As a result, recognition sites are located at the periphery of double rosettes (*exo*-recognition) (Figure 6.1).

These *exo*-receptors were originally designed for the complexation of two large guests²⁷ (*i.e.* one at the bottom and one at the top of the double rosettes), but in this

chapter the focus is on binding multiple guest molecules to these multivalent hydrogen-bonded receptors. Binding of *p*-nitrophenol, diethylstilbestrol (DES) and bisphenol A to $1_3 \cdot (\text{DEB}/\text{BuCYA})_6$, bearing ureido moieties, was studied by ^1H NMR spectroscopy and isothermal titration microcalorimetry (ITC). Furthermore, complexation studies of aromatic carboxylic acids by amino functionalized double rosette $2_3 \cdot (\text{BuCYA})_6$ were performed by ^1H NMR spectroscopy and ITC and complexation of *n*-octylgalactopyranoside by Gly-*L*-Ser functionalized double rosette $3_3 \cdot (\text{BuCYA})_6$ was studied by ^1H NMR spectroscopy. The results show that the complementary recognition sites that are present on the assemblies are efficiently used to complex more than one guest molecule.

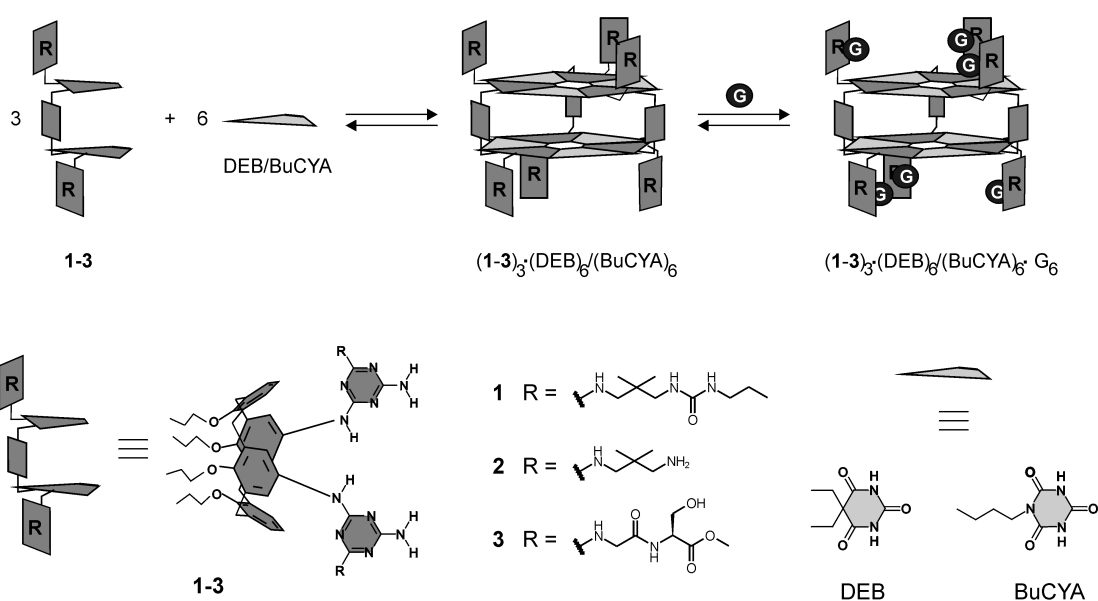


Figure 6.1 Schematic representation of exo-recognition of six guests (*G*) by double rosette assemblies (top) and structures of dimelamines **1-3**, DEB and BuCYA (bottom).

6.2 Results and discussion

Exo-receptors $1-3_3 \cdot (\text{DEB}/\text{BuCYA})_6$ are formed spontaneously by mixing the corresponding dimelamines **1-3** with 2 equivalents of DEB or BuCYA in chloroform-*d*₁ (see Chapter 3 for details). The synthesis of dimelamines **1-3** is described in Chapter 3.

Structural analysis of assemblies $1_3 \cdot (\text{DEB}/\text{BuCYA})_6$ by ^1H NMR spectroscopy using 2D DQF, TOCSY and NOESY gave strong NOE connectivities between H_d and H_j and between H_i and H_m , respectively, (Figure 6.2) indicating a rigid conformation of the 2,2'-

dimethyl propyl side chain.²⁸ Furthermore, the signals for the urea protons of $\mathbf{1}_3 \cdot (\text{DEB}/\text{BuCYA})_6$ resonate at very different chemical shifts in the ^1H NMR spectrum (5.2 and 2.4 ppm) and suggest that one of the urea protons is involved in hydrogen bonding with one of the nitrogen atoms of the triazine ring, causing the ureido moieties to fold back over the calix[4]arene aromatic ring. The result is that the potential ureido recognition sites are (initially) located at the top and the bottom of the double rosette assemblies $\mathbf{1}_3 \cdot (\text{DEB}/\text{BuCYA})_6$.²⁸

For assembly $\mathbf{2}_3 \cdot (\text{BuCYA})_6$ the 2,2'-dimethylpropyl chains should also give a certain preorganization of the complexing amino groups, even though there is no evidence for additional hydrogen bonds. For assembly $\mathbf{3}_3 \cdot (\text{BuCYA})_6$, with Gly-*L*-Ser functionalities but lacking the preorganized chain, there is no evidence that the recognition sites are located at the top and the bottom of the double rosettes.

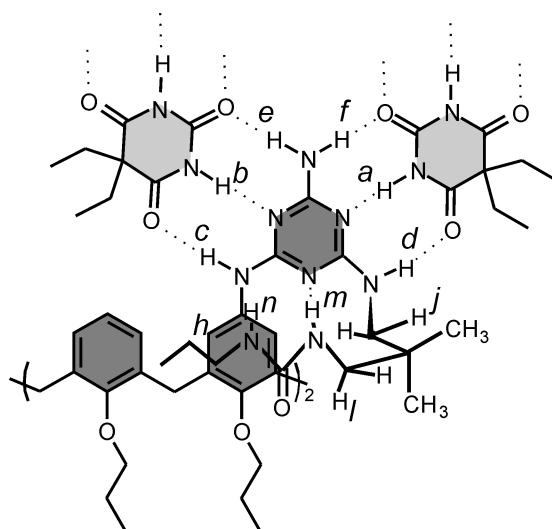


Figure 6.2 Part of the molecular structure of assembly $\mathbf{1}_3 \cdot (\text{DEB}/\text{BuCYA})_6$ where the folding back of the ureido moieties is shown.

6.2.1 Complexation of phenolic guests

6.2.1.1 Complexation of *p*-nitrophenol

The complexation of *p*-nitrophenol (**4a**, see Figure 6.3 for molecular structure) by assembly $\mathbf{1}_3 \cdot (\text{BuCYA})_6$, bearing ureido functionalities, has been studied earlier by Kerckhoffs *et al.*²⁹ in our group using ^1H NMR spectroscopy (CDCl_3 , 298 K) and

MALDI-TOF mass spectrometry. Upon addition of 60 equiv of **4a** to double rosette $\mathbf{1}_3\bullet(\text{BuCYA})_6$ (1.0 mM) they observed a ~ 0.45 ppm and ~ 0.2 ppm downfield shift of urea protons H_m and H_n , respectively. The shifts for other rosette signals were much smaller (< 0.08 ppm). These shifts are probably due to the formation of a hydrogen bond between the hydroxyl group of **4a** and the ureido carbonyl of $\mathbf{1}_3\bullet(\text{BuCYA})_6$. This hypothesis was supported by the observation that no shifts of ureido protons H_m and H_n were observed when *p*-nitroanisole (having a methoxy group) was added to $\mathbf{1}_3\bullet(\text{BuCYA})_6$. Furthermore, with MALDI-TOF mass spectrometry they showed that for 10 mM of double rosette $\mathbf{1}_3\bullet(\text{BuCYA})_6$ and 10 equiv **4a** mainly two complexes, $\mathbf{1}_3\bullet(\text{BuCYA})_6\bullet\mathbf{4a}_5$ and $\mathbf{1}_3\bullet(\text{BuCYA})_6\bullet\mathbf{4a}_6$, were present in solution. These results indicated that a 1:6 complexation seems to be most likely for complexation of **4a** by $\mathbf{1}_3\bullet(\text{BuCYA})_6$.

The work described in this chapter deals with the thermodynamic parameters associated with the binding of **4a** to $\mathbf{1}_3\bullet(\text{BuCYA})_6$ in 1,2-dichloroethane as determined via ITC measurements. The experiments were performed with 0.5 mM and 1.0 mM assembly $\mathbf{1}_3\bullet(\text{BuCYA})_6$ in the ITC cell while aliquots of **4a** (5 μl , 60 mM) were injected. Curve fitting of binding isotherms to a non-cooperative 1:6 binding model gave an intrinsic binding constant (K_i) of $422 \pm 44 \text{ M}^{-1}$ (Figure 6.3). Complexation of **4a** by $\mathbf{1}_3\bullet(\text{BuCYA})_6$ is enthalpy driven ($\Delta H^\circ = -5.6 \pm 0.9 \text{ kcal}\cdot\text{mol}^{-1}$ and $T\Delta S^\circ = -2.0 \pm 1.0 \text{ kcal}\cdot\text{mol}^{-1}$), due to formation of hydrogen bonds between the phenolic hydroxyl groups and the ureido moieties of the receptor.

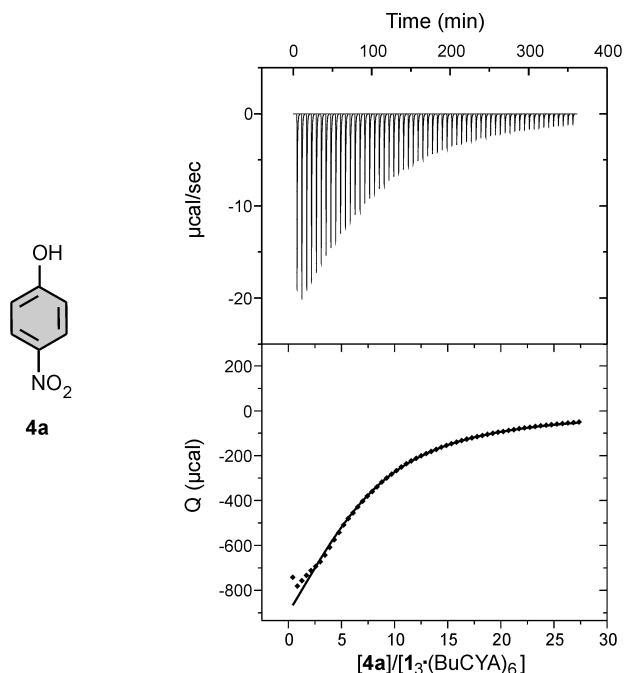


Figure 6.3 ITC measurement of 0.5 mM assembly $1_3\bullet(\text{BuCYA})_6$ (host) with 60 mM **4a** (guest) at 25°C and the molecular structure of **4a**. The plot shows the heat involved per injection of guest solution (5 μl) as function of the ratio $[\mathbf{4a}]/[1_3\bullet(\text{BuCYA})_6]$. The resulting binding isotherm is fitted to a non-cooperative 1:6 binding algorithm.

Complexation of **4a** by $1_3\bullet(\text{BuCYA})_6$ was also studied in increasingly polar mixtures of CD_3OD and CDCl_3 by ^1H NMR spectroscopy (298 K). Complete rosette formation in $\text{CD}_3\text{OD}/\text{CDCl}_3$ mixtures was confirmed by ^1H NMR spectroscopy prior to addition of **4a** to $1_3\bullet(\text{BuCYA})_6$.³⁰ The ^1H NMR spectra of $1_3\bullet(\text{BuCYA})_6$ (1.0 mM) with **4a** (20 equiv) were compared with the ^1H NMR spectra of $1_3\bullet(\text{BuCYA})_6$ at each ratio $\text{CD}_3\text{OD}/\text{CDCl}_3$. The differences in chemical shift of the urea proton H_m (for assignments see Figure 6.2) were plotted against the ratio $\text{CD}_3\text{OD}/\text{CDCl}_3$ (Figure 6.4). The observed chemical shift decreased rapidly when the ratio methanol to chloroform was increased. The interaction between the phenolic hydroxyl and the urea carbonyl is therefore weakened due to the competition for hydrogen bonding by methanol. Unfortunately, this prevents the use of the assembly $1_3\bullet(\text{BuCYA})_6$ for the recognition of more interesting molecules such as paracetamol and adrenaline because these guests are only soluble in polar solvents.

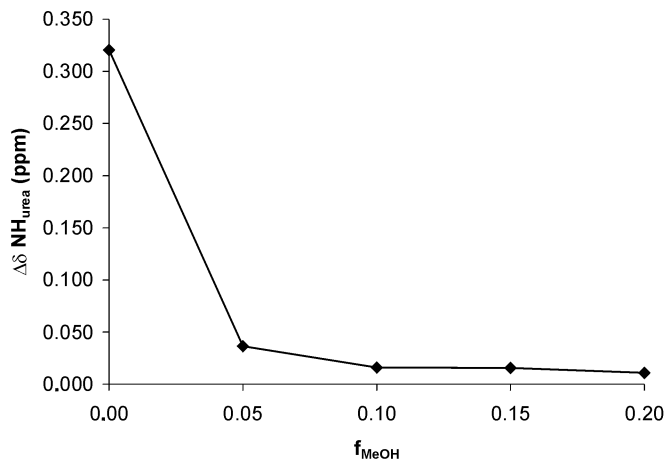


Figure 6.4 Differences in chemical shift for the ureido proton H_m of assembly $\mathbf{1}_3 \cdot (\text{BuCYA})_6$ (1.0 mM) upon addition of $\mathbf{4a}$ (20 equiv) in different solvent ratio $\text{CD}_3\text{OD}/\text{CDCl}_3$ (f_{MeOH}). The differences in the chemical shifts were calculated by comparison of the ^1H NMR spectra of the double rosette assembly $\mathbf{1}_3 \cdot (\text{BuCYA})_6$ with and without $\mathbf{4a}$ at each solvent ratio.

6.2.1.2 Complexation of Diethylstilbestrol (DES)

Diethylstilbestrol (**4b**; Chart 6.1) is a synthetic oestrogen synthesized to mimic the action of the estrogenic hormone estradiol in the body by binding to the estrogen receptor.³¹ Diethylstilbestrol exists as an equilibrium mixture of 75% of the *E*-isomer and 25% of the *Z*-isomer.³² Because **4b** has two phenol moieties it is expected that this guest molecule will be recognized by the ureido moieties of $\mathbf{1}_3 \cdot (\text{BuCYA})_6$.

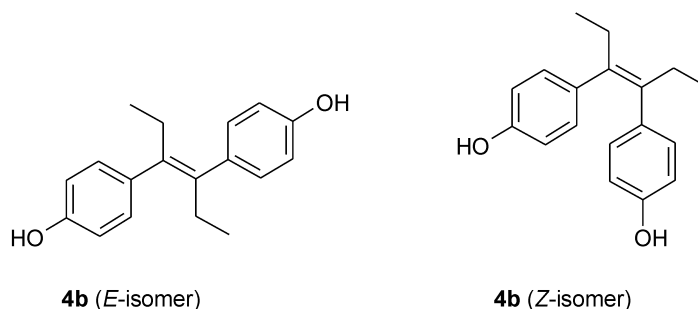


Chart 6.1 Molecular structures of the *E*- and *Z*-isomer of **4b**.

The interaction between **4b** and double rosette $\mathbf{1}_3 \cdot (\text{BuCYA})_6$ (CDCl_3 , 298 K) was studied by ^1H NMR spectroscopy. Addition of 20 equiv **4b** to $\mathbf{1}_3 \cdot (\text{BuCYA})_6$ (1.0 mM) gave a 0.18 and a 0.07 ppm downfield shift of the ureido protons H_m and H_n , respectively

(Figure 6.5a,c). No significant shifts were observed for the other hydrogen-bonded rosette signals (H_{c-f} in figure 6.5).

In $CDCl_3$, the chemical shifts (δ) of the hydroxyl groups OH_E and OH_Z of **4b** are 4.49 and 4.30 ppm, respectively (Figure 6.5d). When 6 equiv of **4b** were added to $\mathbf{1}_3 \cdot (\text{BuCYA})_6$ (1 mM) chemical shifts of 5.29 ($\Delta\delta = 0.80$ ppm) and 4.66 ppm ($\Delta\delta = 0.36$ ppm) were observed for the OH_E and OH_Z protons, respectively (Figure 6.5b). These differences in the chemical shifts are most likely due to the hydrogen bonding between the hydroxyl groups of **4b** and the ureido moieties of $\mathbf{1}_3 \cdot (\text{BuCYA})_6$. Upon addition of 20 equiv **4b** to $\mathbf{1}_3 \cdot (\text{BuCYA})_6$ (1 mM) chemical shifts of 5.03 ($\Delta\delta = 0.54$ ppm) and 4.60 ($\Delta\delta = 0.30$ ppm) were observed for OH_E and OH_Z , respectively (Figure 6.5c). These upfield shifts are the average of free and complexed **4b** in fast exchange.³³ Complexation of **4b** by the double rosette $\mathbf{1}_3 \cdot (\text{DEB})_6$, formed with diethylbarbituric acid, gave very similar results.

Dilution of a 1.0 mM solution of $\mathbf{1}_3 \cdot (\text{BuCYA})_6$ and 20 equiv of **4b** in $CDCl_3$ to a 0.5 mM and a 0.1 mM assembly solution showed shifts of $H_{m,n}$ and $OH_{E,Z}$ in the 1H NMR spectra. This excludes the possibility of proton transfer causing the observed changes in the chemical shifts because proton transfer is independent of the initial concentration of host and guest.

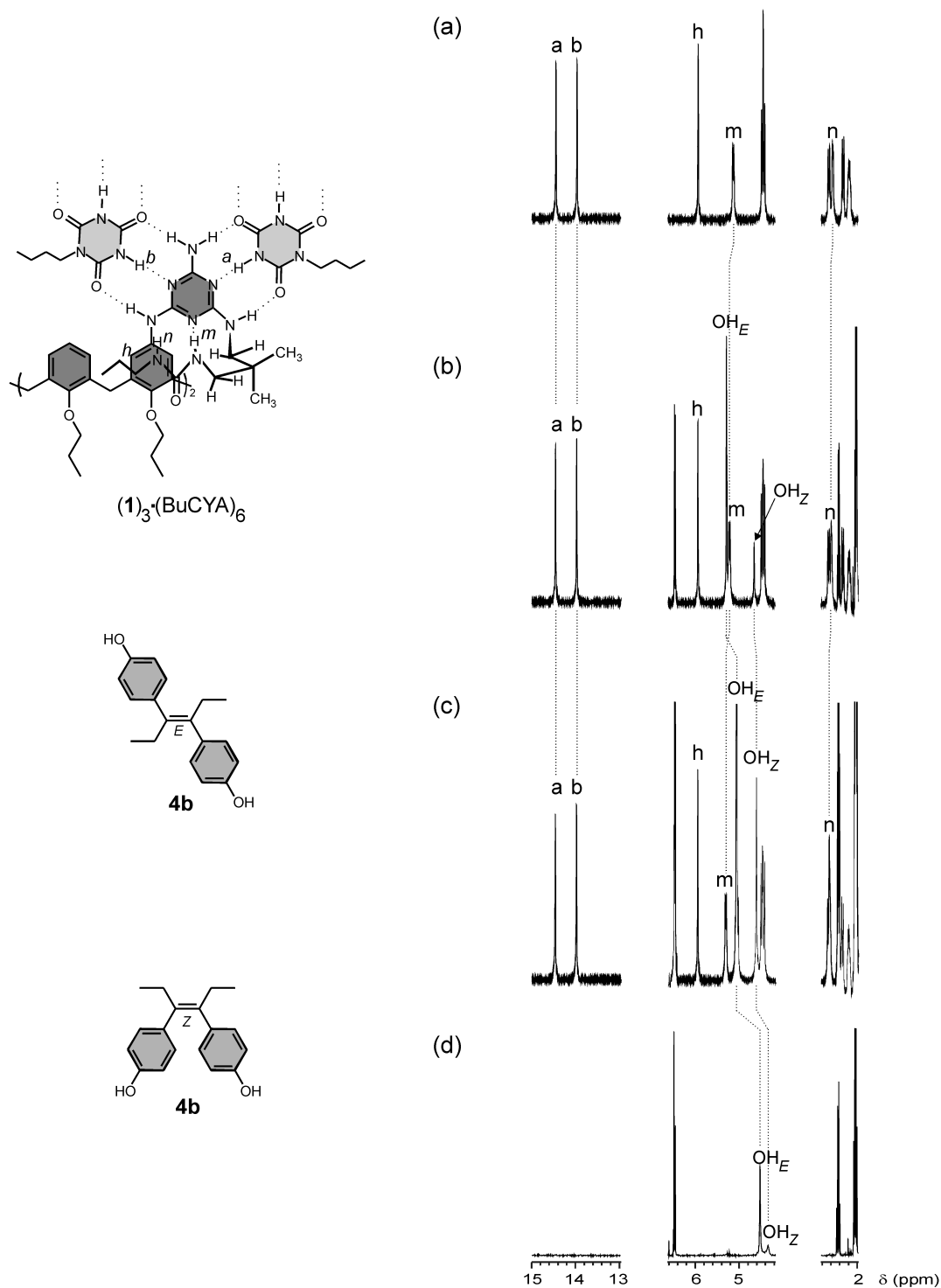


Figure 6.5 Parts of the ^1H NMR spectra of $1_3 \cdot (\text{BuCYA})_6$ (1mM) in CDCl_3 at 298 K after addition of (a) 0, (b) 6, and (c) 20 equivalents of DES, (d) part of ^1H NMR spectrum of $4b$. The structures of $1_3 \cdot (\text{BuCYA})_6$ and the E - and Z -isomers of $4b$ are also shown. $4b$ exists as a tautomeric equilibrium mixture between 75% E -isomer and 25% Z -isomer.

Three different binding modes, *i.e.* 1:2, 1:3 and 1:6, can be envisioned for the complexation of **4b** by $\mathbf{1}_3\bullet(\text{BuCYA})_6$. In the 1:2 binding mode the guest molecules are situated on the top and the bottom of the double rosette platforms. In this binding mode only four ureido functionalities of $\mathbf{1}_3\bullet(\text{BuCYA})_6$ can be used to bind the **4b** molecules (Figure 6.6), but additional π - π interactions of **4b** with the aromatic rosette platforms are possible. Gas-phase molecular modeling calculations (Quanta 97, CHARm 24.0) indicated that the distance between the two hydroxyl groups of **4b** is large enough to allow ditopic binding of one molecule **4b** to two different ureido moieties in each rosette plane (1:2 binding). Nevertheless, a detailed study of the ^1H NMR spectra and the symmetry of the complex exclude this mode of binding. The complexation of two molecules of **4b** to the double rosette $\mathbf{1}_3\bullet(\text{BuCYA})_6$ would break the D_3 -symmetry of the rosette assembly (see Figure 6.6). For the D_3 -isomer two signals for the hydrogen-bonded NH_{DEB} protons H_a and H_b are expected because the three dimelemine in the assembly are identical (Figure 6.5a). If **4b** would bind ditopically to $\mathbf{1}_3\bullet(\text{BuCYA})_6$, the assembly will lose its C_3 -axis (Figure 6.6) and a complex with C_2 -symmetry will be obtained. This result in different chemical shifts for each of the H_a and the H_b protons in the same rosette³⁴ floor and six signals should appear in the ^1H NMR spectrum in the region of 13-15 ppm. On the other hand, if the guest molecules are complexed by $\mathbf{1}_3\bullet(\text{BuCYA})_6$ in fast exchange, the average symmetry of the 1:2 complex would not break the D_3 -symmetry of the rosette assembly and still two signals should be observed, but it is expected that these signals are shifted compared to the NH_{DEB} protons H_a and H_b of the free assembly $\mathbf{1}_3\bullet(\text{BuCYA})_6$ due to interactions with the aromatic rings present in **4b** (see also Section 6.2.2). Only two signals that are not shifted are observed for the hydrogen-bonded rosette protons H_a and H_b in the ^1H NMR spectrum when **4b** is added to $\mathbf{1}_3\bullet(\text{BuCYA})_6$. Thus, it is not likely that **4b** binds to $\mathbf{1}_3\bullet(\text{BuCYA})_6$ in a 1:2 ratio.

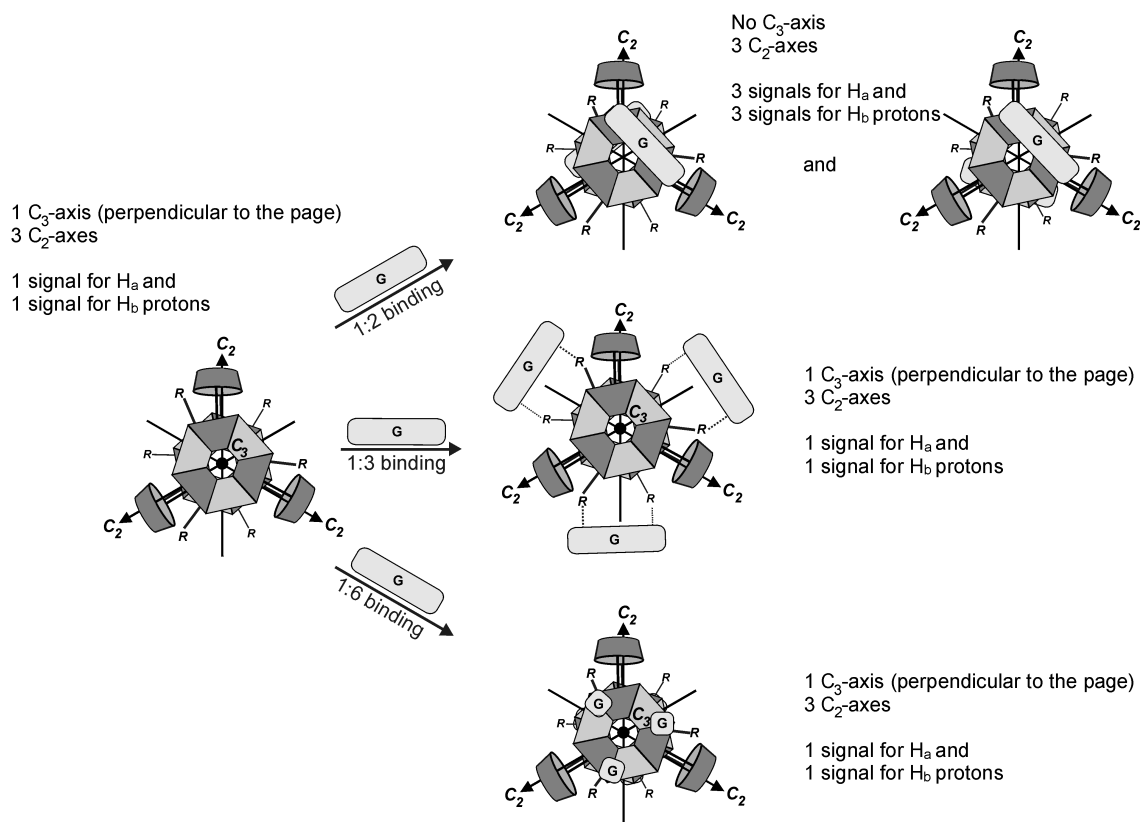


Figure 6.6 Schematic illustration of 1:2, 1:3 and 1:6 binding modes for the complexation of **4b** (**G**) by the assembly $1_3 \cdot (\text{BuCYA})_6$. For 1:6 binding another 3 guest molecules are binding to the second rosette floor.

In the 1:6 binding mode (See Figure 6.6) one molecule **4b** is bound to each ureido moiety via one hydrogen bond. In the 1:3 binding mode each molecule of **4b** forms two hydrogen bonds, one with an ureido moiety at the top floor and one with an ureido at the bottom floor of double rosette assembly $1_3 \cdot (\text{BuCYA})_6$ (Figure 6.6).³⁵ For both, the 1:3 and 1:6 binding mode, all the six ureido functionalities of $1_3 \cdot (\text{BuCYA})_6$ are used to bind **4b**. In these two binding modes complexation of **4b** will not break the D_3 -symmetry of double rosette assembly $1_3 \cdot (\text{BuCYA})_6$, so only two signals for H_a and H_b in the ^1H NMR spectrum are expected. Thus, based on the ^1H NMR results (Figure 6.5; only two signals) both binding modes are possible. The 1:3 binding mode is probably preferred if the driving force for complexation of DES is only hydrogen bonding (most efficient use of binding sites). This mode of binding was previously observed in our group for

complexation of chiral dicarboxylic acids by pyridyl functionalized double rosette assemblies.³⁶

The binding affinity of **4b** to $\mathbf{1}_3\cdot(\text{BuCYA})_6$ was determined by ^1H NMR titration experiments in CDCl_3 (1 mM, 298 K). The chemical shift of H_m was monitored during the titration experiments. Curve fitting of the induced shifts as a function of the **4b**: $\mathbf{1}_3\cdot(\text{BuCYA})_6$ ratio to a 1:3 and 1:6 binding model gave K_i values of 84 M^{-1} and 119 M^{-1} , respectively.

The complexation of **4b** by $\mathbf{1}_3\cdot(\text{BuCYA})_6$ was also studied by ITC. Measurements in 1,2-DCE (298K) with **4b** (6 mM) inside the ITC cell and $\mathbf{1}_3\cdot(\text{BuCYA})_6$ (20 mM) as titrant gave K_i values of 161 M^{-1} or 56 M^{-1} (Table 6.1). Fitting of ITC data to 1:3 and 1:6 binding algorithms indicates that in neat 1,2-DCE, complexation of **4b** by $\mathbf{1}_3\cdot(\text{BuCYA})_6$ is enthalpy driven (Table 6.1). The ΔH° values are -10.5 and $-12.0 \text{ kcal}\cdot\text{mol}^{-1}$ for 1:3 and 1:6 binding, respectively.

Comparison of the ΔH° for the binding of **4a** and **4b** to $\mathbf{1}_3\cdot(\text{BuCYA})_6$ indicates the formation of two hydrogen bonds and thus a 1:3 binding of **4b** to $\mathbf{1}_3\cdot(\text{BuCYA})_6$. For the 1:3 binding one molecule **4b** forms two hydrogen bonds with $\mathbf{1}_3\cdot(\text{BuCYA})_6$. The average enthalpy value for the formation of a single hydrogen bond is then $-5.3 \text{ kcal}\cdot\text{mol}^{-1}$. This value is comparable with ΔH° for the binding of **4a**, that can form only one hydrogen bond, to $\mathbf{1}_3\cdot(\text{BuCYA})_6$ ($-5.6 \text{ kcal}\cdot\text{mol}^{-1}$). The larger gain in ΔH° , due to the formation of two hydrogen bonds is, however, accompanied by a larger unfavorable entropic contribution ($T\Delta S$). As a consequence, ditopic binding of **4b** to $\mathbf{1}_3\cdot(\text{BuCYA})_6$ does not increase the affinity compared to **4a**.

Table 6.1 Thermodynamic parameters determined by ITC (298 K) for the complexation of **4a-c** by assembly $\mathbf{1}_3 \cdot (\text{BuCYA})_6$ in 1,2-DCE.

Guest	Binding mode	K_i (M^{-1})	ΔH° ($\text{kcal} \cdot \text{mol}^{-1}$)	ΔG° ($\text{kcal} \cdot \text{mol}^{-1}$)	$T\Delta S^\circ$ ($\text{kcal} \cdot \text{mol}^{-1}$)
4a (<i>p</i> -Nitrophenol)	1:6	422 ± 44	-5.6 ± 0.9	-3.6 ± 0.1	-2.0 ± 1.0
4b (DES)*	1:3	161	-10.5	-3.0	-7.5
	1:6	56	-12.0	-2.4	-9.6
4c (Bisphenol A)	1:3	113 ± 4	-10.1 ± 0.4	-2.9 ± 0.1	-7.2 ± 0.4
	1:6	no fit			

* ITC measurement was performed at one concentration only.

6.2.1.3 Complexation of Bisphenol A

Bisphenol A (**4c**) is another synthetic ligand for the natural estrogen receptor³⁷ and it has also two phenol moieties like **4b** but these are not conjugated. Binding of **4c** to $\mathbf{1}_3 \cdot (\text{DEB})_6$ and $\mathbf{1}_3 \cdot (\text{BuCYA})_6$ was first studied using ^1H NMR spectroscopy. Addition of 20 equiv of **4c** to $\mathbf{1}_3 \cdot (\text{DEB})_6$ (1.0 mM) gave a 0.14 ppm downfield shift of ureido proton H_m and a 0.09 ppm downfield shift of ureido proton H_n (Figure 6.7). No significant shifts were observed for the hydrogen-bonded rosette signals and only one set of signals was observed for H_a and H_b in the ^1H NMR spectrum. These results indicate that the 1:2 binding mode, as concluded for **4b** (see Section 6.2.1.2) can be excluded. The intrinsic binding constants (K_i) are 155 M^{-1} and 395 M^{-1} for the 1:3 and 1:6 binding modes, respectively.

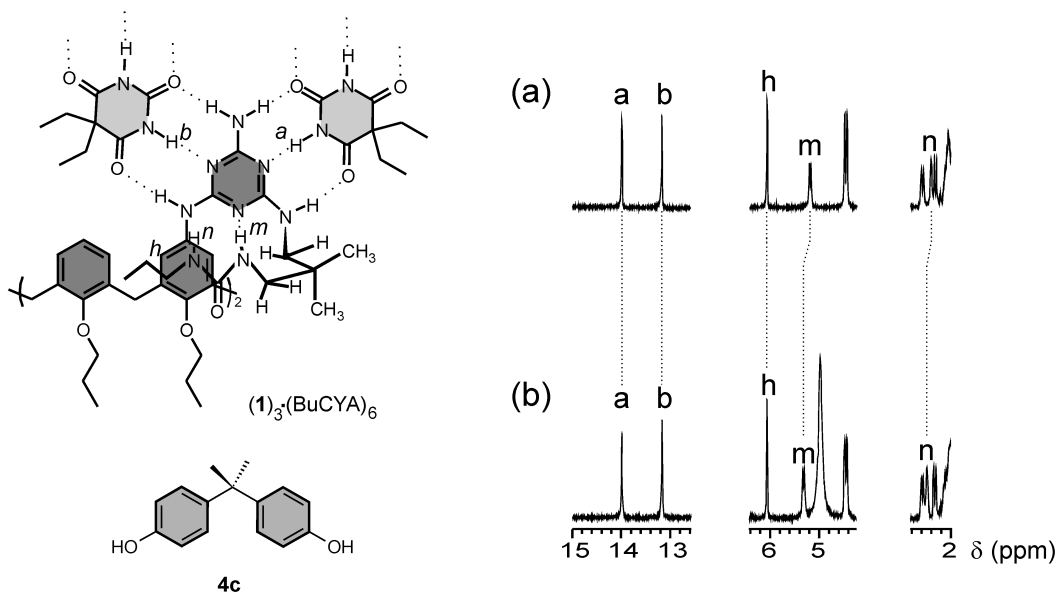


Figure 6.7 Parts of the ^1H NMR spectra of $1_3\bullet(\text{DEB})_6$ (1 mM) in CDCl_3 at 298 K after addition of (a) 0 and (b) 20 equivalents of **4c**.

ITC measurements (1.0 mM assembly in the ITC cell and 60 mM **4c** in the burette, 1,2-DCE, 298K) gave a K_i value of 113 M^{-1} after fitting to 1:3 binding model, while an accurate fit to a 1:6 binding model was not possible (see Table 6.1). Furthermore, ΔH° and $T\Delta S$ values of $-10.1 \text{ kcal}\cdot\text{mol}^{-1}$ and $-7.2 \text{ kcal}\cdot\text{mol}^{-1}$, respectively, were obtained for the 1:3 binding of **4c** to $1_3\bullet(\text{BuCYA})_6$.

6.2.2 Complexation of aromatic carboxylic acids

Binding of 3-(2-furyl)propanoic acid (**5a**), *trans* cinnamic acid (**5b**) and *trans* benzoylbutenoic acid (**5c**) (10 equiv) to *exo*-receptor $2_3\bullet(\text{BuCYA})_6$ (1.0 mM) which has amino moieties, was studied using ^1H NMR spectroscopy (CDCl_3 , 298 K) and ITC (298 K). The amino groups of receptor $2_3\bullet(\text{BuCYA})_6$ are expected to bind with the carboxylic acid groups of guests **5a-c**.

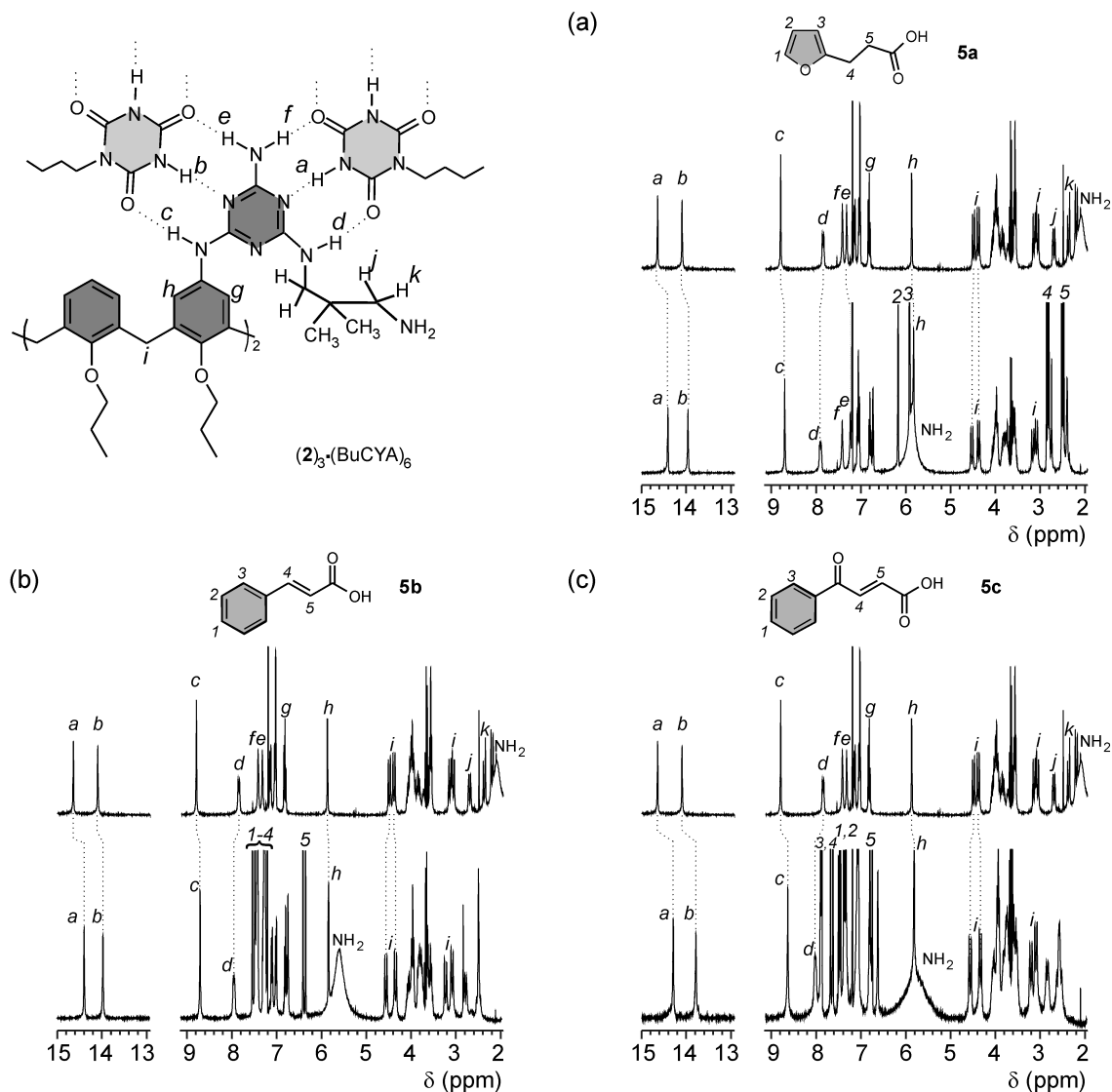


Figure 6.8 Parts of the ^1H NMR spectra of (a) 1.0 mM $2_3\cdot(\text{BuCYA})_6$ (top) and after addition of 10 equiv **5a** (bottom), (b) 1.0 mM $2_3\cdot(\text{BuCYA})_6$ (top) and after addition of 10 equiv **5b** (bottom), (c) 1.0 mM $2_3\cdot(\text{BuCYA})_6$ (top) and after addition of 10 equiv **5c** (bottom). Spectra were recorded in CDCl_3 at 298 K.

The interaction between $2_3\cdot(\text{BuCYA})_6$ with guests **5a-c** becomes apparent from the shifts of several hydrogen-bonded protons in the ^1H NMR spectra (Figure 6.8). These shifts are most pronounced for the hydrogen-bonded rosette protons H_{a-d} . For example, H_a shifted 0.230, 0.259 and 0.352 ppm upfield when 10 equiv of **5a**, **5b** and **5c**, respectively, were added to a 1.0 mM solution of $2_3\cdot(\text{BuCYA})_6$ in CDCl_3 . Also the double doublets of the calix[4]arene bridge protons H_i shifted when **5a**, **5b** or **5c** were added.

Furthermore, the amino protons of assembly $2_3\cdot(\text{BuCYA})_6$ shift from about 2 ppm to 5-6.5 ppm. This broad signal observed around 5-6.5 ppm is probably due to hydrogen bonding between the amino groups of $2_3\cdot(\text{BuCYA})_6$ and the carboxylic acid groups of the guests **5a-c** ($\text{NH}_2\cdots\text{HOOC}$).

Dilution of a 5.0 mM solution of $2_3\cdot(\text{BuCYA})_6$ and 6 equiv **5a** in CDCl_3 to 2.5 mM, 1.0 mM, 0.5 mM and 0.25 mM shows shifts for the $\text{NH}_2\cdots\text{HOOC}$ signal. This excludes that proton transfer causes the observed chemical shifts.

Interaction of guest **5a-c** with $2_3\cdot(\text{BuCYA})_6$ becomes also apparent from the large shifts observed for the guest protons (Table 6.2). The large shifts observed for $\text{H}_{4,5}$ of **5a-c** indicate an interaction between the carboxylic acid moiety of the guest and the amino groups of $2_3\cdot(\text{BuCYA})_6$, while the shifts observed for H_{1-3} are probably due to π - π interactions of the aromatic rings of **5a-c** with the rosette platforms.

Table 6.2 Upfield shift of protons H_{1-5} of **5a-c** after addition of 10 equiv of guest to assembly $2_3\cdot(\text{BuCYA})_6$ (1.0 mM). ^1H NMR spectra were recorded in CDCl_3 at 298 K.

H	$\Delta\delta$ (ppm) 5a	$\Delta\delta$ (ppm) 5b	$\Delta\delta$ (ppm) 5c
1	-	0.062	0.164
2	0.042	0.098	0.170
3	0.060	0.070	0.123
4	0.080	0.205	0.338
5	0.148	0.024	0.122

Summarizing, the ^1H NMR data indicate that binding of **5a-c** to $2_3\cdot(\text{BuCYA})_6$ occurs through hydrogen bonding between the amino functionality of the host and the carboxylic acid moiety of the guests. Furthermore, the shifts of the hydrogen-bonded protons H_{a-d} observed upon complexation of **5a-c** are probably due to interactions between the aromatic moieties of the guests (located on top and bottom) with the rosette platforms.

This hypothesis is supported by the shifts of protons H₁₋₅ of the guest molecules **5a-c** upon complexation with **2₃•(BuCYA)₆**.

ITC measurements using 0.25, 0.5 and 1.0 mM solutions of **2₃•(BuCYA)₆** in the ITC cell and 25, 30, 60 mM of **5a** in 1,2-DCE as titrant, respectively, gave an intrinsic binding constant of 3500 M⁻¹ for the complexation of **5a** by **2₃•(BuCYA)₆** after fitting to an independent 1:6 binding model (Figure 6.9a). Fitting of ITC data to 1:2 and 1:4 models was not possible. Complexation of **5a** by **2₃•(BuCYA)₆** is enthalpy driven ($\Delta H^0 = -6.3 \pm 0.4$ kJ·mol⁻¹, $T\Delta S = -1.5 \pm 0.2$ kJ·mol⁻¹). Similar measurements with **5b** using 0.25, 0.375, 0.5 and 1.0 mM solutions of **2₃•(BuCYA)₆** in the ITC cell and 20, 25, 30 and 50 mM of **5b** in 1,2-DCE as titrant, respectively, gave a K_i value of 1799 M⁻¹ (Figure 6.9b). Complexation of **5b** by **2₃•(BuCYA)₆** is also enthalpy driven ($\Delta H^0 = -5.6 \pm 2.0$ kJ·mol⁻¹, $T\Delta S = -2.5 \pm 1.0$ kJ·mol⁻¹).

Fitting of the measured ITC data for the complexation of **5c** by **2₃•(BuCYA)₆** to an appropriate model was not possible.³⁶ Therefore, ¹H NMR titrations were performed for the complexation of this guest by assembly **2₃•(BuCYA)₆**.

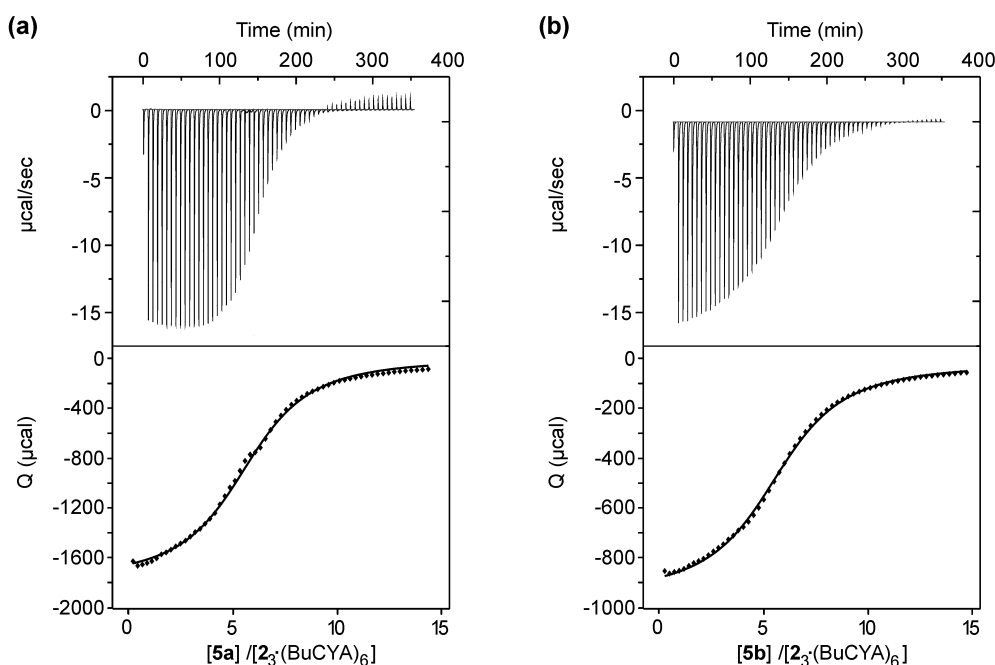


Figure 6.9 ITC measurement of (a) assembly **2₃•(BuCYA)₆** (1.0 mM) with **5a** (60 mM) and (b) assembly **2₃•(BuCYA)₆** (0.375 mM) with **5b** (25 mM) at 25 °C. The plots show the heat involved per injection of titrant (5 µl) as function of [Guest]/[assembly]. The resulting binding isotherms are curve fitted to a non-cooperative 1:6 binding algorithm.

^1H NMR titration of $2_3\cdot(\text{BuCYA})_6$ with **5c** gave a K_i value of 563 M^{-1} when the induced shifts of the NH_2 protons were fitted to an independent 1:6 binding model (Figure 6.10a). However, induced shifts of the hydrogen-bonded H_c protons could only be fitted in a dependent 1:6 binding model (Figure 6.9b), with binding constants of 38, 29, 271, 299, 1057, 3808 M^{-1} for $K_1, K_2, K_3, K_4, K_5,$ and K_6 , respectively. The increase in binding affinity indicates a positive cooperative effect upon binding of **5c**, possibly due to conformational changes of the double rosette $2_3\cdot(\text{BuCYA})_6$.

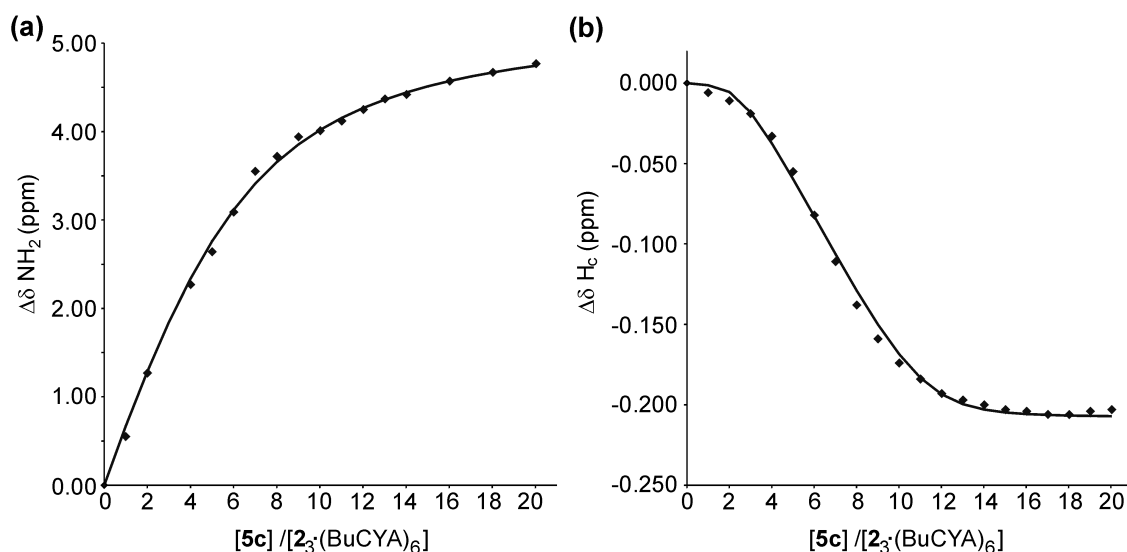


Figure 6.10 Plots of the ^1H NMR induced shifts of the (a) NH_2 protons and (b) H_c protons during the titration of $2_3\cdot(\text{BuCYA})_6$ with **5c** versus $[\text{5c}]/[2_3\cdot(\text{BuCYA})_6]$. The induced shifts are fitted in an (a) independent and (b) dependent 1:6 binding model.

6.2.3 Binding of *n*-octylgalactopyranoside

Carbohydrates act as substrates for specific receptors in a wide range of biological processes.^{23,38} Thus, artificial receptors that can recognize and bind specific saccharides are receiving increased attention.³⁹ Since the affinity of a single carbohydrate unit for its receptor is often low, strong binding is achieved by the simultaneous interaction of several identical glycoside residues with the receptor (often proteins) that has several equivalent binding sites (multivalency).⁴⁰

Binding of *n*-octylgalactopyranoside (**6**; Figure 6.11) to $3_3\cdot(\text{BuCYA})_6$, with Gly-*L*-Ser functionalities, was studied using ^1H NMR spectroscopy (CDCl_3 , 298 K). The

interaction between **6** and $3_3 \bullet (\text{BuCYA})_6$ becomes apparent from the shifts of the OH protons of the serine and the OH protons of **6** (Figure 6.11). Upon addition of 10 equiv of **6** to $3_3 \bullet (\text{BuCYA})_6$ (1.0 mM) the signal of the serine hydroxyl group (H_i) shifts 0.57 ppm downfield, probably as a result of hydrogen bonding. After guest addition all the hydroxyl groups of **6** (H_j) are shifted downfield (Figure 6.11b,c) but only two signals at 3.32 and 2.60 ppm ($\Delta\delta = 0.47$ and 0.88 ppm, respectively) remain clearly visible because the other two H_j protons are under the rosette signals (between $\delta = 3.3$ and 3.9 ppm).

It is unclear how **6** binds to $3_3 \bullet (\text{BuCYA})_6$, but the ^1H NMR results indicate that probably all four hydroxyl groups are involved in hydrogen bonding. Therefore, binding constants were calculated for 1:2, 1:3, 1:4 and 1:6 binding modes.⁴¹

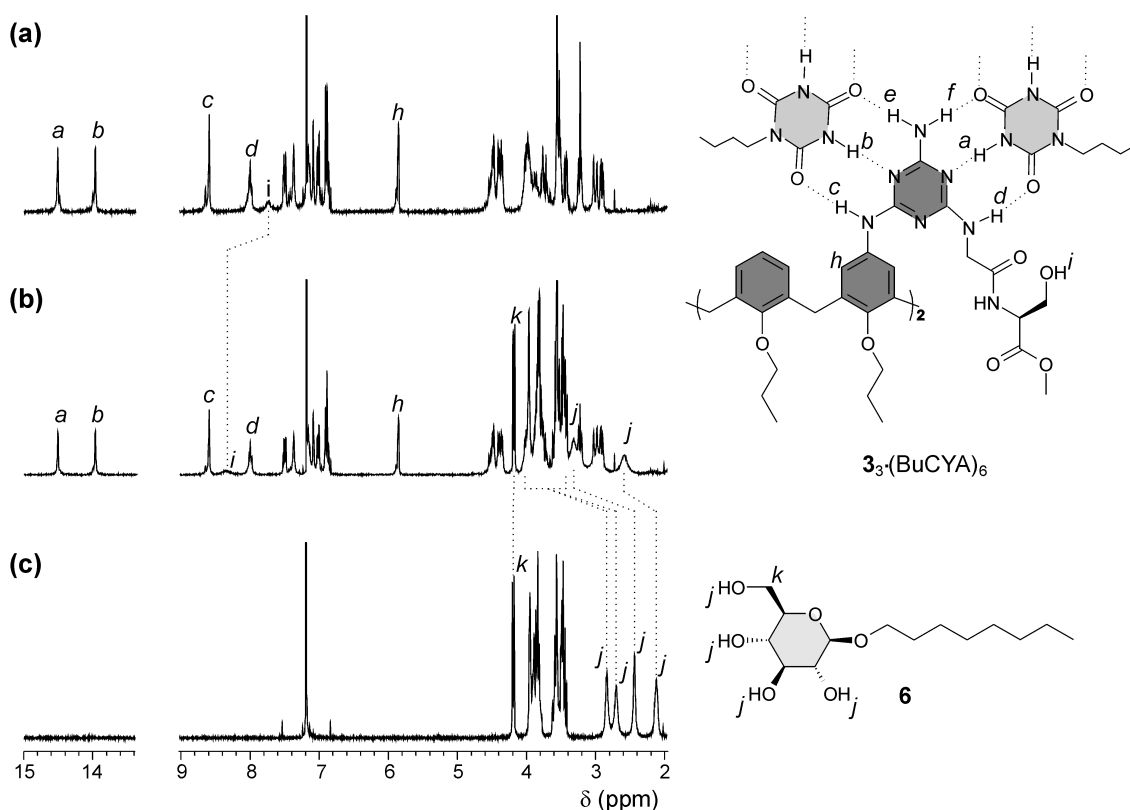


Figure 6.11 Parts of the ^1H NMR spectra of (a) $3_3 \bullet (\text{BuCYA})_6$ (1.0 mM), (b) $3_3 \bullet (\text{BuCYA})_6$ (1.0 mM) and 10 equiv **6**, and (c) **6** (10 mM) and molecular structures of $3_3 \bullet (\text{BuCYA})_6$ and **6**. Spectra were recorded in CDCl_3 at 298 K.

^1H NMR titration experiments gave intrinsic K_i values of 31, 32, 34 and 37 M^{-1} for 1:2, 1:3, 1:4 and 1:6 binding, respectively (Figure 6.12). Unfortunately, ITC

measurements could not be performed due to gelation at high concentrations of **6** in 1,2-DCE. These results indicate that assembly $3_3 \cdot (\text{BuCYA})_6$ binds **6** probably via formation of hydrogen bonds between de serine hydroxyl groups of the receptor and the hydroxyl groups of guest **6** with low affinity.

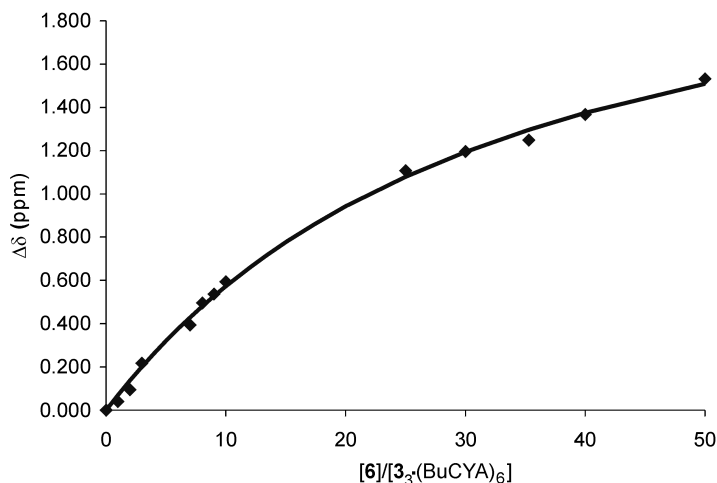


Figure 6.12 Plot of the ^1H NMR induced shifts ($\Delta\delta \text{OH}_{\text{Ser}}$) during titration of $3_3 \cdot (\text{BuCYA})_6$ with **6** versus $[\mathbf{6}] / [3_3 \cdot (\text{BuCYA})_6]$. The induced shifts are fitted in a 1:6 binding model to calculate the intrinsic binding constant K_i .

6.3 Conclusions

Exo-complexation of multiple guests by double rosette assemblies is observed. The results show that recognition sites located at the periphery of double rosette assemblies are used efficiently; *i.e.* minimum number of guest with maximum use of recognition sites.

Only for *exo*-receptor $1_3 \cdot (\text{BuCYA})_6$ and **4a** a 1:6 binding mode was observed by single hydrogen bonding, while a 1:3 binding mode was observed for guests **4b** and **4c** that form two hydrogen bonds with one urea moiety at the first floor and one urea at the second floor of double rosette assembly $1_3 \cdot (\text{BuCYA})_6$. Binding affinities of 422, 161 and 113 M^{-1} were determined for binding of **4a**, **4b** and **4c**, respectively. Thermodynamic data show also that ditopic binding of **4b** and **4c** to $1_3 \cdot (\text{BuCYA})_6$ does not increase the binding affinity compared to **4a**.

Aromatic carboxylic acids **5a-c** bind with *exo*-receptor $2_3 \cdot (\text{BuCYA})_6$ in a 1:6 binding mode. Binding of these guests involved hydrogen bonding between amino groups of the

receptor and carboxylic acid groups of the guests and organization of the guest molecules at the top and the bottom of the receptor. Binding affinities of 3500 M^{-1} and 1799^{-1} were determined for binding of **5a** and **5b**, respectively. The binding affinities obtained for **5c** indicate a positive cooperative effect, possibly due to conformational changes of the double rosette $2_3 \cdot (\text{BuCYA})_6$.

Exo-receptor $3_3 \cdot (\text{BuCYA})_6$ binds **6** ($K_i = 31\text{--}37 \text{ M}^{-1}$), possibly by formation of hydrogen bonds between the serine hydroxyl of the receptor and hydroxyl groups of the carbohydrate guest.

These examples show that structural diversity within the *exo*-receptors, generated by the different functionalities, allows the complexation of different biologically important molecules via different binding motifs, resembling the approach exhibited by natural antibodies.

6.4 Experimental

General Methods: All chemicals were reagent grade and used without further purification. NMR spectra were recorded on a Varian Unity 300 (^1H NMR 300MHz) spectrometer in chloroform- d_1 or methanol- d_4 . Residual solvent protons were used as internal standard, and chemical shifts are given relatively to trimethylsilane (TMS). Calorimetric measurements were carried out using a Microcal VP-ITC microcalorimeter with a cell volume of 1.4115 ml. For each experiment the heat effect of 60 injections of 5 μl titrant was measured. Instrument settings were set on injection duration of 30 sec, spacing of 570 sec and low feedback at 16.3 $\mu\text{cal/sec}$ reference power and a temperature of 25°C.

Synthesis

The synthesis of **1**, **2** and **3** are described in Chapter 3.

6.5 References

1. Page, M. I. *The Chemistry of Enzyme Action*; Elsevier: Amsterdam, the Netherlands, 1984.
2. Hulme, E. C. *Receptor Biochemistry: A Practical Approach*; Oxford University Press: New York, USA, 1990.

3. Roberts, S. M. *Molecular Recognition: Chemical and Biochemical Problems*; Royal Society of Chemistry: Cambridge, England, 1989.
4. Hamilton, A. D. *Nature* **2002**, *418*, 375-376.
5. Review on synthetic receptors: Hartley, J. H.; James, T. D.; Ward, C. J. *Chem. Soc. Perkin Trans. I*, **2000**, 3155-3184.
6. Cram, D. J.; Kaneda, T.; Helgeson, R. C.; Brown, B.; Knobler, C. B.; Meverick, E.; Trueblood, K. N. *J. Am. Chem. Soc.* **1985**, *107*, 3645-3657.
7. Bell, T. W.; Khasanov, A. B.; Drew, M. G. B.; Filikov, A.; James, T. L. *Angew. Chem. Int. Ed.* **1999**, *38*, 2543-2547.
8. Chrisstoffels, L. A. J.; de Jong, F.; Reinhoudt, D. N.; Sivelli, S.; Gazzola, L.; Casnati, A.; Ungaro, R. *J. Am. Chem. Soc.* **1999**, *121*, 10142-10151.
9. Tobey, S. L.; Anslyn, E. V. *J. Am. Chem. Soc.* **2003**, *125*, 10963-10970.
10. Gale, P. A. *Coord. Chem. Rev.* **2001**, *213*, 79-128.
11. Suksai, C.; Tuntulani, T. *Chem. Soc. Rev.* **2003**, *32*, 192-202.
12. Sessler, J. L.; Camiolo, S.; Gale, P. A. *Coord. Chem. Rev.* **2003**, *240*, 17-55.
13. Llinares, J. M.; Powell, D.; Bowman-James, K. *Coord. Chem. Rev.* **2003**, *240*, 57-75.
14. Choi, K. H.; Hamilton, A. D. *Coord. Chem. Rev.* **2003**, *240*, 101-110.
15. Tomapatanaget, B.; Tuntulani, T.; Chailapakul, O. *Org. Lett.* **2003**, *5*, 1539-1542.
16. Sansone, F.; Baldini, L.; Casnati, A.; Lazzarotto, M.; Ugozzoli, F.; Ungaro, R. *Proc. Nat. Acad. Sci. USA* **2002**, *99*, 4842-4847.
17. Middel, O.; Verboom, W.; Reinhoudt, D. N. *Eur. J. Org. Chem.* **2002**, *16*, 2587-2597.
18. Droz, A. S.; Diederich, F. *J. Chem. Soc. Perkin Trans. I*, **2000**, 4224-4226.
19. Tamaru, S.; Shinkai, S.; Khasanov, A. B.; Bell, T. W. *Proc. Nat. Acad. Sci. USA* **2002**, *99*, 4972-4976.
20. Orner, B. P.; Salvatella, X.; Quesada, J. S.; De Mendoza, J.; Giralt, E.; Hamilton, A. D. *Angew. Chem. Int. Ed.* **2002**, *41*, 117-119.
21. Starnes, S. D.; Rudkevich, D. M.; Rebek, J. *J. Am. Chem. Soc.* **2001**, *123*, 4659-4669.

22. Almaraz, M.; Raposo, C.; Martin, M.; Caballero, M. C.; Moran, J. R. *J. Am. Chem. Soc.* **1998**, *120*, 3516-3517.
23. Mammen, M.; Choi, S.-K.; Whitesides, G. M. *Angew. Chem. Int. Ed.* **1998**, *37*, 2754-2794.
24. Lee, Y. C.; Lee, R. T. *Acc. Chem. Res.* **1995**, *28*, 321-327.
25. Lindhorst, T. K. *Top. Curr. Chem.* **2002**, *218*, 201-235.
26. Amit, A. G.; Marinizza, R. A.; Phillips, S. E. V.; Poljak, R. J. *Science* **1986**, *233*, 747-753.
27. Crego-Calama, M.; Timmerman, P.; Reinhoudt, D. N. *Angew. Chem. Int. Ed.* **2000**, *39*, 755-758.
28. Kerckhoffs, J. M. C. A.; Crego-Calama, M.; Luyten, I.; Timmerman, P.; Reinhoudt, D. N. *Org. Lett.* **2000**, *2*, 4121-4124.
29. Kerckhoffs, J. M. C. A.; Ishi-I, T.; Paraschiv, V.; Timmerman, P.; Crego-Calama, M.; Shinkai, S.; Reinhoudt, D. N. *Org. Biomol. Chem.* **2003**, *1*, 2596-2603.
30. Double rosette assemblies with urea functionalized dimelamine **2** are very stable. The stability of double rosette analogue **2₃•((R)-PhEtCYA)₆** in MeOH/CHCl₃ is described in Chapter 3.
31. Meulenberg, E. P. *Eur. J. Lipid. Sci. Technol.* **2002**, *104*, 131-136.
32. Qianhuan, D.; Xin, L. *Chin. Sci. Bul.* **2000**, *45*, 2125-2129.
33. Ratio free/bound guest is higher when 20 equiv are added.
34. H_a and H_b in one rosette are homotopic compared to the corresponding H_a and H_b in the other rosette floor when to molecules **4b** would bind to the assembly **1₃•(BuCYA)₆**.
35. In this case the binding sites have to turn away from the rosette platform.
36. ITC measurements were performed with four different concentrations of assembly **2₃•(BuCYA)₆** (0.25, 0.50, 0.375, 1.0 mM) in the cell and **5c** as titrant (20, 25, 40 and 60 mM, respectively).
37. Steinmetz, R.; Brown, R. G.; Allen, D.; Bigsby, R. M.; BenJonathan, N. *Endocrinology* **1997**, *3*, 97-130.
38. Varki, A. *Glycobiology* **1993**, *3*, 97-130.
39. Fredericks, J. R.; Hamilton, A. D. *Comprehensive Supramolecular Chemistry*; Atwood, J. L.; Davies, J. E. D.; MacNicol, D. D.; Vögte, F., Elsevier: Oxford,

England, 1996; Vol. 9, pp 565-594.

40. Casnati, A.; Sansone, F.; Ungaro, R. *Acc. Chem. Res.* **2003**, *36*, 246-254.
41. 1:1 and 1:5 binding modes are unlikely because they suggest differences in binding affinity between the recognition groups at the top and bottom of assembly $\mathbf{3}_3 \cdot (\text{BuCYA})_6$.

Formation of Hydrogen-Bonded Receptors in Niosomal Membranes: Towards artificial cells*

This chapter describes the self-assembly of hydrogen-bonded receptors in aqueous environment. Hydrogen-bonded receptors were formed after incorporation of the assembly components in bilayer membranes of non-ionic surfactant based vesicles (niosomes). Furthermore, niosomes containing only one of the building blocks are able to extract the second component from the aqueous exterior allowing the formation of the hydrogen-bonded assemblies in the membranes.

* Part of this work has been submitted for publication: Ten Cate, M.G.J.; Crego-Calama, M.; Reinhoudt, D.N., *J. Am. Chem. Soc.* **2004**.

7.1 Introduction

The directionality and specificity provided by hydrogen bonds make this noncovalent interaction an excellent tool for the formation of many self-assembled systems in solution.¹⁻⁷ However, the main disadvantage of the use of hydrogen bonds is their limited strength, due to competition in hydrogen bonding by water.⁸ Most of the well-defined assemblies based exclusively on hydrogen bonding are not stable in water. Nevertheless, when mimicking biological processes, assemblies that are only stable in non-aqueous solutions have a limited scope since water is omnipresent in biological systems. Hence, one of the main goals of Supramolecular Chemistry is the development of dynamic systems that are stable in aqueous solutions. As a possible solution to this important problem, hydrogen bonds are often used in combination with other noncovalent interactions such as cation- π or π - π stacking⁹⁻¹¹ and metal coordination.¹²⁻¹⁵ Another possibility to increase the stability of hydrogen-bonded assemblies in water is to use motifs with large numbers of hydrogen bonds. For example, in chapters 3 and 4 the stability of complex systems assembled through the formation of 36 hydrogen bonds in mixtures of polar solvents is described. Due to the high stability of these hydrogen-bonded systems their assembly in pure methanol was achieved. Nevertheless, the formation of those self-assembled rosettes in water could not be demonstrated.

A closer look to the molecular recognition processes in biological systems reveals that many bio-recognition processes occur at interfaces or at membrane surfaces between two aqueous compartments. For example, membrane proteins embedded in the lipid bilayer allow specific molecules and ions to be recognized and to cross the cell membrane.¹⁶

Thus, a novel and more logical approach to mimic bio-recognition processes would be embedding of the synthetic self-assembled systems in membranes. Therefore, self-assembled artificial cell systems (vesicles) with synthetic pores or receptors are of interest. Until now, only synthetic ion-channels¹⁷⁻²¹ and membrane-anchored receptors that facilitate selective membrane transport or enhanced binding of guest molecules have been reported.²²⁻²⁷ The receptors consist of molecules that are covalently attached to the membrane anchors such as cholesterol.

In order to introduce more structural diversity and to allow selective binding of guest molecules, self-assembled receptors within bilayer membranes are especially attractive.

To incorporate these self-assembled synthetic receptors in artificial membranes is challenging because this requires well-defined nanoscale self-assembled structures that can position the different functionalities in the correct orientation for guest complexation.

This chapter describes the introduction of calix[4]arene dimelamines **1a-b** and barbituric acid (BAR) or cyanuric acid (CYA) derivatives and their assembly into hydrogen-bonded double rosettes **1a-b**₃•(BAR/CYA)₆ in non-ionic surfactant-based vesicles (niosomes) (Figure 7.1).²⁸ In previous chapters it was shown that in organic solvents these double rosettes are *endo*-receptors for anthraquinone derivatives (Chapter 5) and *exo*-receptors for phenol derivatives, aromatic carboxylic acids, or carbohydrates (Chapter 6).²⁹

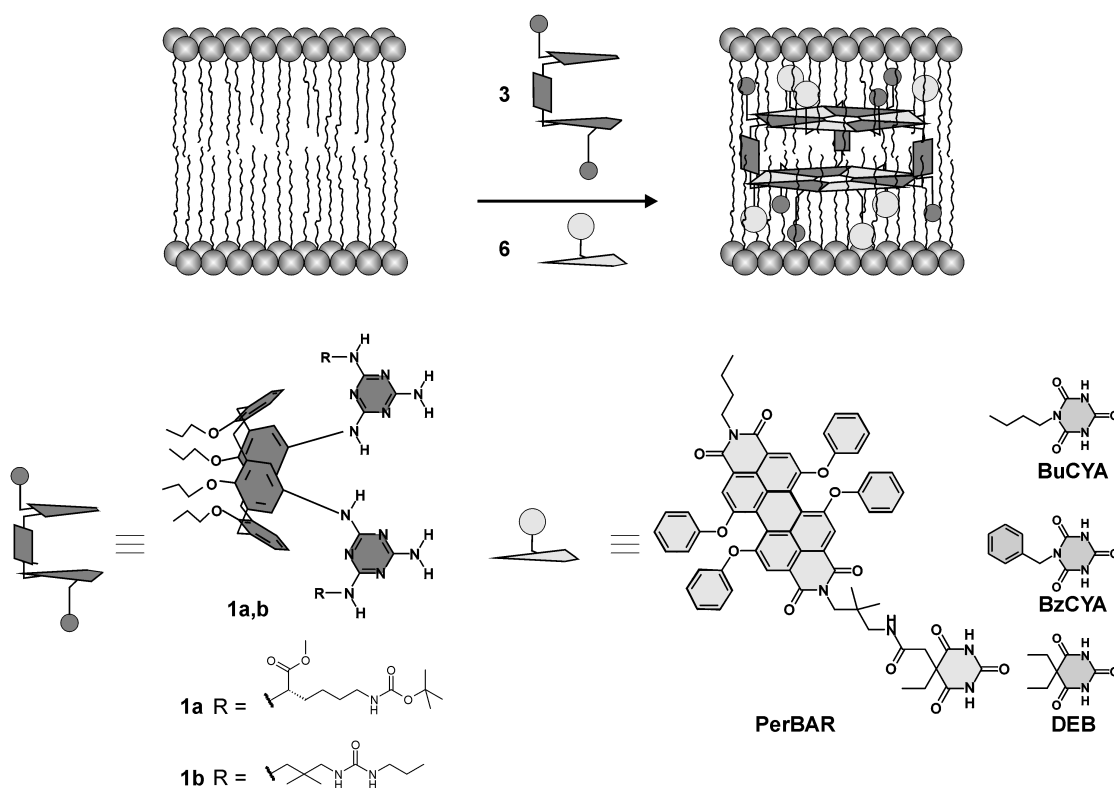


Figure 7.1 Schematic representation of the incorporation of **1a-b** and barbituric or cyanuric acid derivatives in bilayer membranes and their self-assembly into double rosettes **1a-b**₃•(BAR/CYA)₆. The molecular structures of dimelamines **1a-b** and barbituric acid and cyanuric acid derivatives are also shown.

Surfactants and membrane lipids can readily self-assemble into various ordered lamellar structures, like micelles and liposomes, because of their amphiphilic character.³⁰⁻

³⁵ Compared to liposomes, surfactant based vesicles have the advantage of superior stability and toughness.³⁶

7.2 Results and discussion

The double rosette assemblies **1a-b**₃•(BAR/CYA)₆ are spontaneously formed when one equivalent of calix[4]arene dimelamine **1a-b** is mixed with two equivalents of BAR or CYA in chloroform or toluene due to the formation of 36 hydrogen bonds.^{37,38}

7.2.1 Synthesis

The synthesis of dimelamines **1a-b** is described in Chapter 3. Barbituric acid derivative **2** was synthesized by condensation of diethyl ethyl malonate with urea in a sodium ethoxide solution in absolute ethanol at reflux temperature (43%). Reaction of **2** with triethanolamine and bromoacetic acid in water at room temperature afforded **3** (47%), which was hydrolyzed with NaOH at room temperature giving **4** (89%).

Refluxing of perylene tetracarboxylic dianhydride with propylamine in DMF gave **5** (95%). Heating of compound **5** at 70°C in thionylchloride with iodine afforded **6**, which was reacted with potassium *tert*-butylphenol in the presence of K₂CO₃ in NMP to give **7** (85%). Refluxing of **7** with KOH in H₂O/*t*BuOH (1:20) gave **8** (83%). This compound was reacted successively with Boc-3-amino-2,2'-dimethylpropylamine and an excess of butylamine in toluene at reflux, to afford **9** (50%). Deprotection of **9** with TFA/CH₂Cl₂ (1:10) at room temperature resulted in compound **10** (87%). Coupling of **4** and **10** using standard peptide coupling conditions (HBTU, DIPEA, CH₂Cl₂/DMF 4:1) afforded PerBAR (69%).

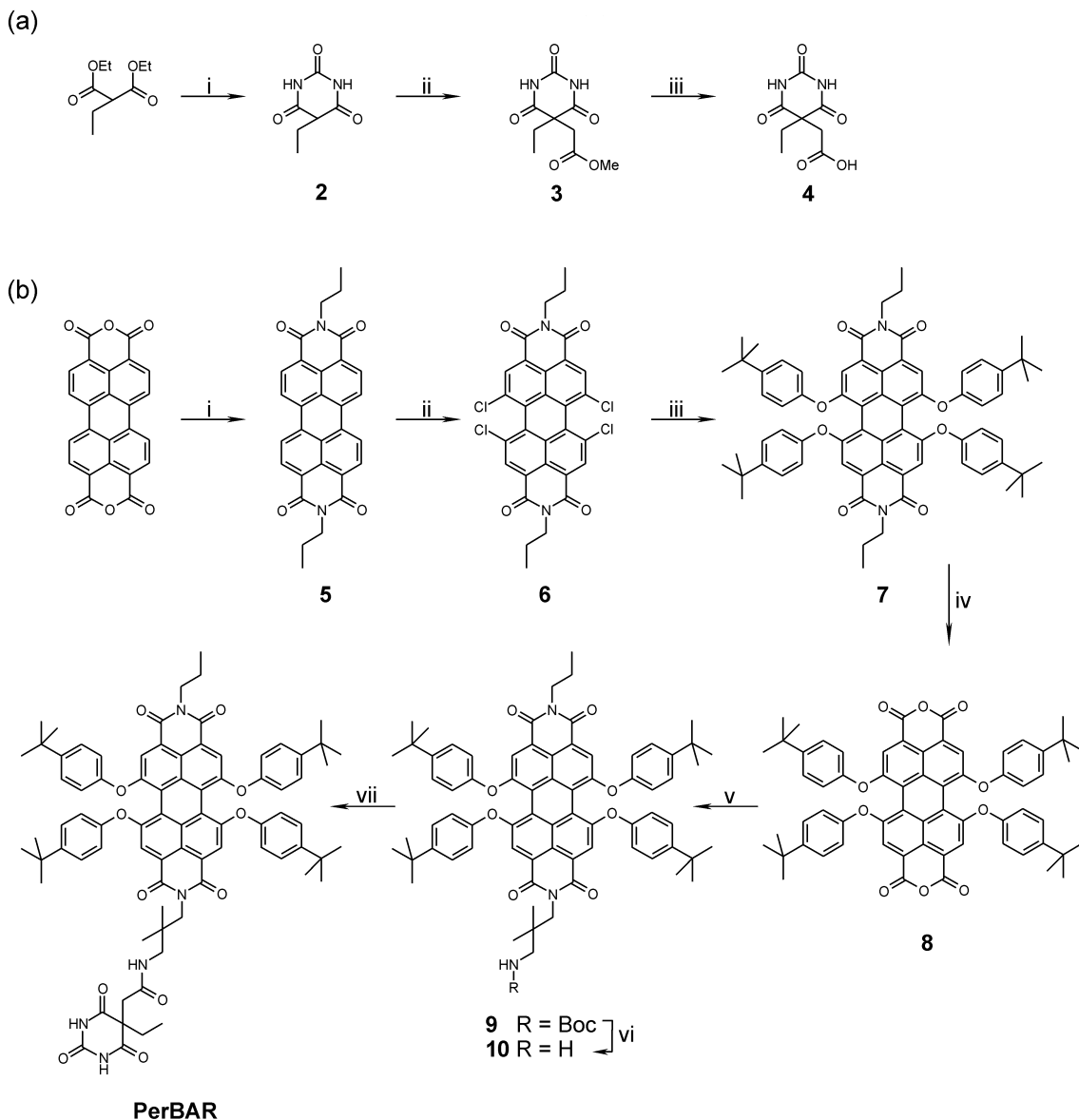


Chart 7.1 (a) i. Urea, NaOEt, Δ ; ii. Bromoacetic acid, $N(\text{EtOH})_3$, H_2O ; iii. NaOH, H_2O . (b) i. Propylamine, DMF; ii. I_2 , SOCl_2 , Δ ; iii. *K-tButylphenol*, K_2CO_3 , NMP; iv. KOH, H_2O , *tBuOH*; v. *Boc-3-amino-2,2'-dimethyl propylamine*, butylamine, toluene, Δ ; vi. TFA/ CH_2Cl_2 ; vii. **4**, HBTU, DIPEA, CH_2Cl_2 /DMF.

7.2.2 Niosome formation

A mixture of polyoxyethylene alkyl ether surfactants C_{12}EO_3 and C_{14}EO_3 (Serdox NES3; Figure 7.2) was used to prepare the niosomes.³⁹ Niosomal solutions containing 2.2

$\mu\text{l/ml}$ Serdox NES3 and 0.06 mM **1a-b** and/or 0.12 mM BAR/CYA were prepared by sonication.

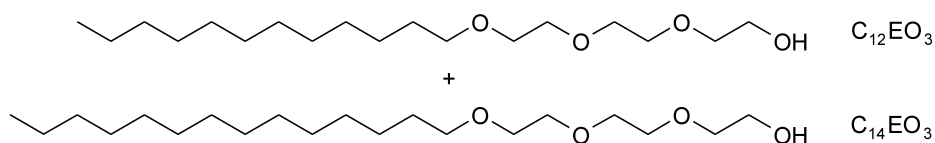


Figure 7.2 Molecular structures of polyoxyethylene alkyl ether surfactants C_{12}EO_3 and C_{14}EO_3 of Serdox NES3.

Formation of niosomes in water containing 1% (v/v) glycerol was confirmed by transmission electron microscopy (TEM).⁴⁰ The TEM graph (Figure 7.3a), indicates niosomes in coexistence with rodlike and spherical micelles. Observed niosome sizes ranged from 100 to 600 nm. For all niosome solutions dynamic light scattering gave z-average diameters between 430 nm and 480 nm. The incorporation of PerBAR into the membrane was confirmed by confocal microscopy. The observed fluorescent dots (Figure 7.3b), in strong contrast with the background in confocal micrographs, show that PerBAR is not present in the external aqueous solution. The aqueous interior phase of the niosomes is identical to the external aqueous phase, which renders the presence of PerBAR inside the vesicles unlikely.

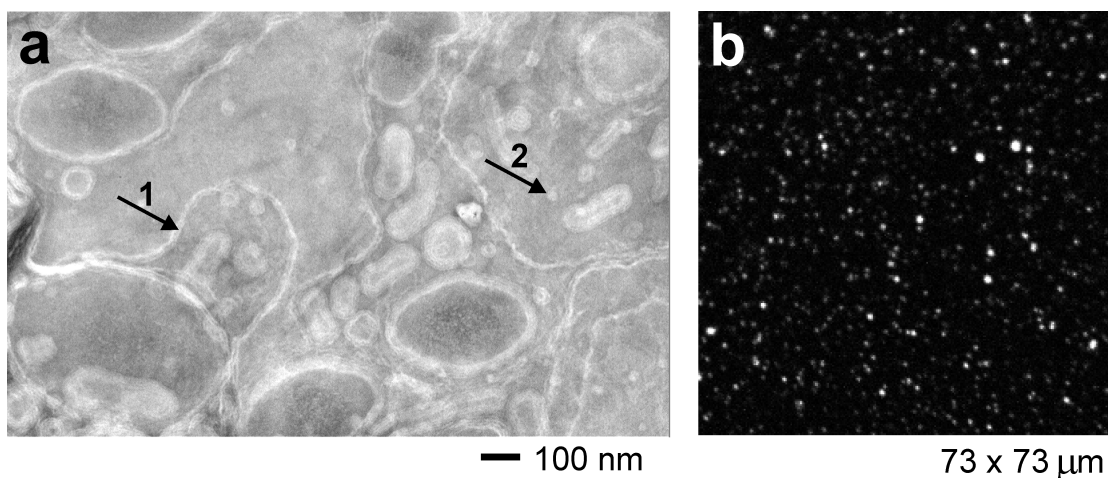


Figure 7.3 (a) Transmission electron micrograph (TEM) of niosomes containing $\mathbf{1a}_3\bullet(\text{PerBAR})$. Niosomes are in dominant coexistence with rodlike (1) and spherical (2) micelles, (b) Confocal micrograph of niosomes with $\mathbf{1a}_3\bullet(\text{PerBAR})$ (white dots). Niosome solutions are prepared in water containing 1% (v/v) glycerol. $[\text{surfactant}] = 2.2 \text{ mg/ml}$, $[\text{PerBAR}] = 0.12 \text{ mM}$, $[\mathbf{1a}] = 0.06 \text{ mM}$.

7.2.3 Formation of the double rosettes in niosomes

Due to the presence of chiral centers in dimelamine **1a** (*L*-Lys) only one diastereomer ((*P*)-**1a**₃•(PerBAR)₆) is formed in chloroform or toluene, which means "total" induction of supramolecular chirality^{41,42}. This makes it possible to study double rosette formation using circular dichroism (CD) spectroscopy.⁴³ Double rosette assemblies exhibit a very strong induced CD signal, while the individual components are hardly CD active (see Chapter 3).

The strong CD intensity at $|\Delta\epsilon_{\max}|$ ($96 \text{ l}\cdot\text{mol}^{-1}\cdot\text{cm}^{-1}$) of the CD signal for niosomes containing both, dimelamine **1a** and PerBAR, provides strong evidence that hydrogen-bonded double rosettes **1a**₃•(PerBAR)₆ are formed within the vesicular membranes (Figure 7.4). The (small) differences observed between induced supramolecular chirality of **1a**₃•(PerBAR)₆ in niosomal membranes and in toluene are probably due to the differences in solvent-solute interactions.⁴⁴⁻⁴⁶

Dimelamine **1a** alone in vesicular membranes gave only a weak CD signal ($|\Delta\epsilon_{\max}| \sim 3 \text{ l}\cdot\text{mol}^{-1}\cdot\text{cm}^{-1}$), while niosomes with PerBAR or without assembly components are CD silent. The CD intensity observed for niosomes with dimelamine **1a** indicates that this building block is incorporated in the bilayer.⁴⁷

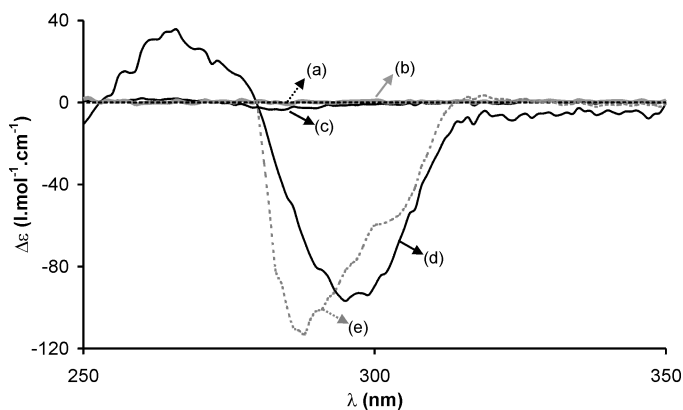


Figure 7.4 CD spectra of niosomes containing: (a) no assembly components, (b) 0.120 mM PerBAR, (c) 0.06 mM **1a** and (d) 0.02 mM **1a**₃•(PerBAR)₆. (e) CD spectrum of 0.5 mM **1a**₃•(PerBAR) in toluene. Because the wavelength limit for toluene is 280 nm, the CD spectrum in toluene was measured from 280-350 nm. Niosome solutions were prepared with 2.2 $\mu\text{l}/\text{ml}$ surfactant in water containing 1% (v/v) glycerol.

Solubilization of the assembly components into the niosomal membranes gives a high effective concentration of **1a** and PerBAR allowing the formation of the hydrogen-bonded assembly $\mathbf{1a}_3 \cdot (\text{PerBAR})_6$ in contact with aqueous environment.⁴⁸ The lower local polarity within the membranes, compared to water, contributes also to the assembly of $\mathbf{1a}_3 \cdot (\text{PerBAR})_6$. Furthermore, Serdox NES3 niosomes with a calculated membrane thickness about 3 nm, allow the double rosette assemblies with dimensions of 3 nm x 1.2 nm³⁷ to fit well in the bilayer membranes horizontally or vertically to the membrane surface.

To determine the stability of the assembly $\mathbf{1a}_3 \cdot (\text{PerBAR})_6$ in the niosomal membrane, CD spectra were recorded after storage for 3 days or 1 week at room temperature (Figure 7.5). Small decreases in the CD intensity (10% and 17% of the $|\Delta\epsilon_{\text{max}}|$ ⁴⁹ after 3 and 7 days, respectively) indicated that the assembly $\mathbf{1a}_3 \cdot (\text{PerBAR})_6$ in the membrane is relatively stable under these conditions.

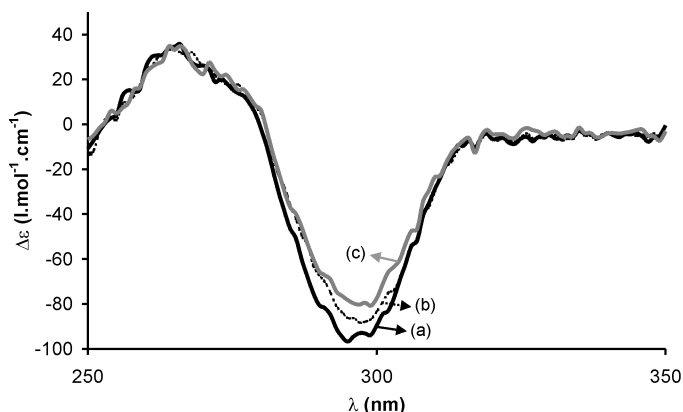


Figure 7.5 Stability of niosomes with $\mathbf{1a}_3 \cdot (\text{PerBAR})_6$ measured by CD spectroscopy. CD spectra were recorded at the day of preparation (a), after 3 days (b) and 7 days (c). The niosome solution was stored at room temperature.

When the same experiments were performed with the chiral *L*-(α)-phosphatidylcholine lipids instead of Serdox NES3 surfactants, incorporation of **1a** and PerBAR was observed. However, assembly formation could not be detected.

Experiments with dimelamine **1b**, bearing ureido moieties, and (*R*)-PhEtCYA gave evidence that the hydrogen-bonded double rosettes $\mathbf{1b}_3 \cdot ((R)\text{-PhEtCYA})_6$ are also formed

within the non-ionic niosomal membranes (Figure 7.6). When both **1b** and (*R*)-PhEtCYA are solubilized in the membranes the expected CD spectrum was observed. Niosomes with only dimelamine **1b** or (*R*)-PhEtCYA were CD silent. The differences in $\Delta\epsilon$ between the CD spectra of **1b**₃•((*R*)-PhEtCYA)₆ in the niosomes ($|\Delta\epsilon_{300}| \sim 68 \text{ l}\cdot\text{mol}^{-1}\cdot\text{cm}^{-1}$) and in chloroform ($|\Delta\epsilon_{300}| \sim -115 \text{ l}\cdot\text{mol}^{-1}\cdot\text{cm}^{-1}$) might be due to the incomplete formation of the double rosette **1b**₃•((*R*)-PhEtCYA)₆⁵⁰ or solvent polarity.^{44-46,51} Extraction experiments (see next section) show, however, the quantitative formation of similar double rosettes also bearing CYA in the niosomal membranes. The values of $|\Delta\epsilon_{300}|$ for these rosettes compare very well with the value obtained for **1b**₃•((*R*)-PhEtCYA)₆, indicating that this assembly is also formed quantitative.

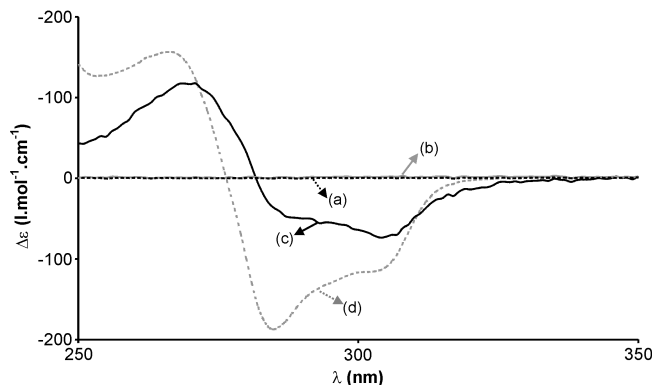


Figure 7.6 CD spectra of niosomes containing: (a) 0.12 mM (*R*)-PhEtCYA, (b) 0.06 mM **1b**, and (c) 0.02 mM **1b**₃•(*R*)-PhEtCYA)₆. (d) CD spectrum of 1.0 mM **1b**₃•(*R*)-PhEtCYA)₆ in CHCl₃. Niosome solutions were prepared with 2.2 μl/ml surfactant in water containing 1% (v/v) glycerol.

Extraction experiments

Different experimental procedures were performed to assess the ability of niosomes with dimelamine **1a** incorporated into the membrane, to extract barbiturate or cyanurate derivatives from the aqueous exterior and to form the double rosettes within the niosomal membrane. The strong CD signal observed when 3 μmol of DEB was added to a niosome solution containing **1a** (250 μl, 0.06 mM) indicated that assembly **1a**₃•(DEB)₆ was formed in the niosomal membranes (Figure 7.7a). Further addition of 3 μmol of DEB to this solution gave a small increase of the CD intensity of the assembly **1a**₃•(DEB)₆,

indicating that this assembly was not formed quantitatively after the first addition of DEB. Addition of 3 μmol of BuCYA or BzCYA to a niosome solution containing **1a** (250 μl , 0.06 mM) gave also strong CD signals, indicating the formation of **1a** $_3$ •(BuCYA) $_6$ and **1a** $_3$ •(BzCYA) $_6$ in the niosomal membranes (Figure 7.7b,c). Further addition of 3 μmol of BuCYA or BzCYA to these solutions did not result in an increase of the CD intensity, indicating that assemblies **1a** $_3$ •(BuCYA) $_6$ and **1a** $_3$ •(BzCYA) $_6$ were formed quantitatively after the first addition of BuCYA and BzCYA, respectively.

The (stepwise) extraction of the barbiturate or cyanurate derivatives by the niosomes containing **1a** offers the possibility to prove quantitative double rosette formation. This would make it possible to quantify the binding of guest molecules to the double rosettes using techniques such as isothermal titration microcalorimetry because the exact concentration of the host can be calculated.

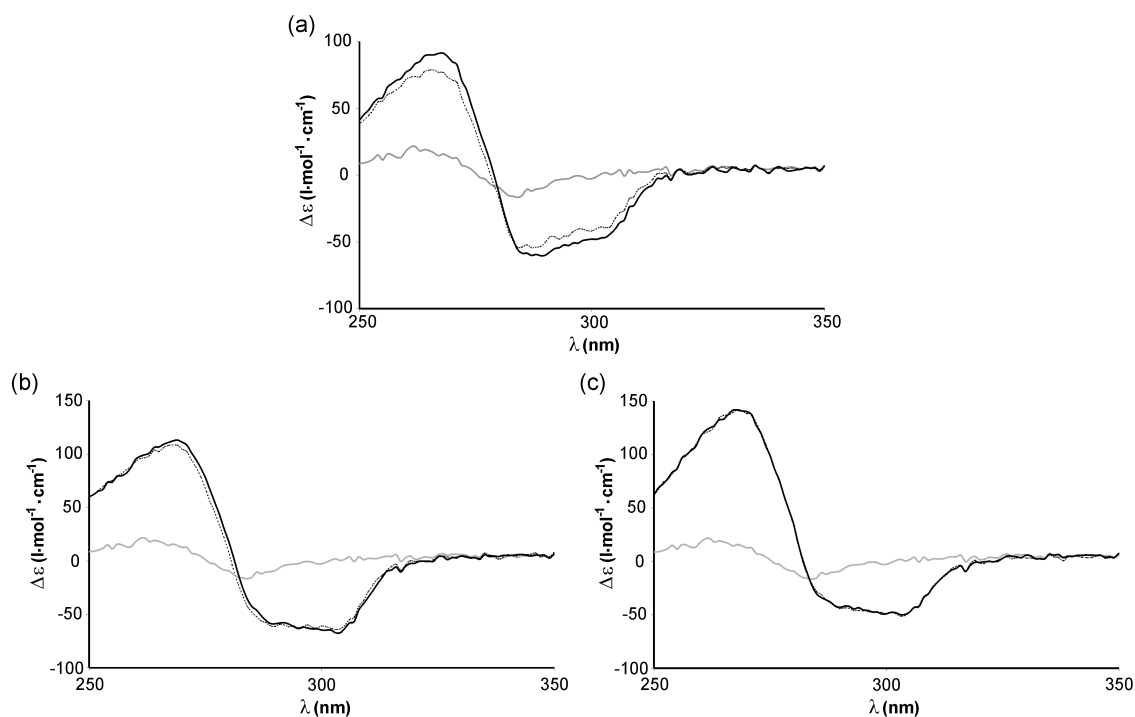


Figure 7.7 CD spectra of niosomes with **1a** (0.06 mM) before (solid grey) and after addition of 3 μmol (dotted black) and 6 μmol (solid black) of (a) DEB, (b) BuCYA and (c) BzCYA to the niosome solution (250 μl). $\Delta\epsilon$ is calculated from the measured CD signal in mdeg using the maximum possible concentration of assembly that could be formed from **1a**.

7.2.4 Exchange of DEB molecules in double rosettes by BuCYA in niosomes

Upon addition of DEB (200 equiv) to the niosomes containing **1a** (0.06 mM), CD spectroscopy showed that the assembly $\mathbf{1a}_3 \bullet (\text{DEB})_6$ is formed in the *P*-conformation (Figure 7.8, left). Successive addition of BuCYA (200 eq) to the niosomes with $\mathbf{1a}_3 \bullet (\text{DEB})_6$ resulted in the formation of double rosette *P*- $\mathbf{1a}_3 \bullet (\text{BuCYA})_6$ (Figure 7.8, left). The shape of the observed CD signal is the same as the one observed after direct addition of BuCYA (6 μmol) to the niosomes containing **1a** (0.06 mM) in the membrane, indicating that the DEB molecules are exchanged by BuCYA in the niosomal membranes (Figure 7.8, right) in the same way as in chloroform.⁵²

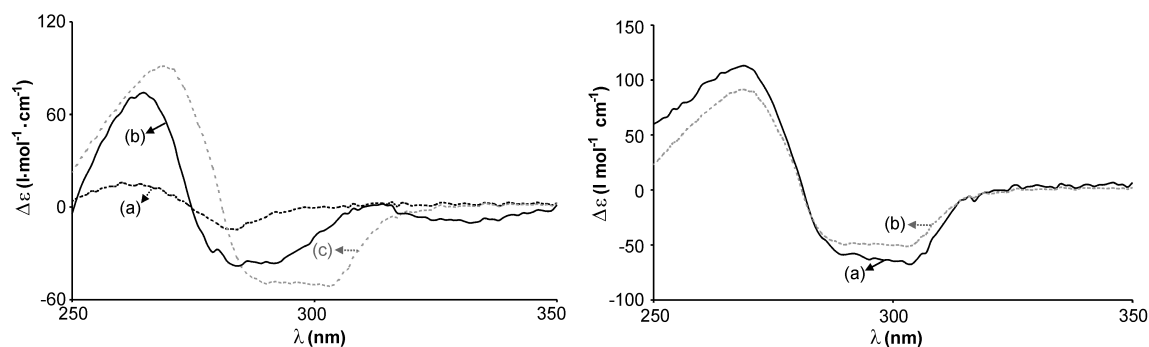


Figure 7.8 Left: CD spectra of niosomes with **1a** (0.06 mM) before (a) and after successive addition of 200 equiv of DEB (b), and 200 equiv of BuCYA (c). Right: CD spectra of niosomes with **1a** (0.06 mM) after addition of BuCYA (6 μmol) (a) and after successive addition of DEB and BuCYA (b). $\Delta\epsilon$ is calculated from the measured CD signal in mdeg using the maximum possible concentration of assembly that could be formed from **1a**.

7.3 Conclusions

The niosomes prepared from non-ionic surfactants C_{12}EO_3 and C_{14}EO_3 are a new tool that allows the self-assembly based on hydrogen-bonding to occur in contact with aqueous environments. Incorporation of dimelamine **1a** and PerBAR or **1b** and (*R*)-PhEtCYA within niosomal membranes led to the formation of well-defined hydrogen-bonded assemblies $\mathbf{1a}_3 \bullet (\text{PerBAR})_6$ and $\mathbf{1b}_3 \bullet ((R)\text{-PhEtCYA})_6$, respectively, within these membranes.

Niosomes with only dimelamine **1a** in their membrane extract BAR and CYA derivatives from the external aqueous media and form double rosette assemblies in the

bilayer membranes. Furthermore, exchange of DEB molecules for BuCYA is also possible in the membrane.

The niosomes presented in this chapter provide a way to form hydrogen-bonded receptors in aqueous environments and a useful template to introduce synthetic receptors into artificial cell systems. When the dimelamine components would be functionalized with, for example, peptides or carbohydrates that are able to complex guest molecules such as carbohydrates (see chapter 6), these self-assembled receptors could, after their incorporation into the niosomes, respond to different external triggering processes.⁵³ In our laboratory work is ongoing in this direction as a first step towards artificial cells systems.

7.4 Experimental

¹H NMR spectra were recorded on a Varian Unity 300 (¹H NMR 300MHz) spectrometer in chloroform-*d*₁, methanol-*d*₄ or dimethylsulphoxide-*d*₆. Residual solvent protons were used as internal reference, and chemical shifts are given relatively to trimethylsilane (TMS). FAB spectra were measured on a Finningan MAT 90 spectrometer with *m*-nitrobenzyl alcohol (NBA) matrix. CD spectra were measured on a JASCO J-715 spectropolarimeter using a cell width of 0.01 or 0.1 cm. THF was distilled from Na/benzophenone ketyl and CH₂Cl₂ from K₂CO₃. All commercially available reagents were reagent grade and used without further purification. Flash chromatography was performed on silica gel (SiO₂, E. Merck 0.040 – 0.063 mm, 230 – 240 mesh). Serdox NES3 was donated by Servo Sasol (Delden, the Netherlands).

Niosome preparation

Serdox NES3 (5.5 μl), and double rosette (50 μl, 1.0 mM), dimelamine (50 μl, 3.0 mM) or BAR/CYA (50 μl, 6.0 mM), were dissolved in CHCl₃ (3 ml). The solvent was removed slowly by vacuum (rotary evaporator; no heating!) in such way that a small film of Serdox NES3 was obtained, and the film was dried further under vacuum for three hours. The film is hydrated slowly with 2.5 ml of milliQ water containing 1% glycerol (v/v) at room temperature and the niosomes were sonicated for 20-30 minutes at 10-15°C.

Synthesis

The synthesis of **1a** and **1b** is described in chapter 3.

5-ethylbarbituric acid (2). Urea (3.6 g, 60 mmol) was dissolved in a freshly prepared solution of Na (s) (2.0 g, 87 mmol) in absolute ethanol (45 ml). Diethyl ethyl malonate (11.2 g, 60 mmol) was added and the reaction mixture was refluxed for 24 hours. The solvent was removed under reduced pressure and water (20 ml) was added. The solution was stirred for 1 hour until it became clear. Then concentrated HCl (conc.) was added until pH = 4. The precipitate was filtered off and washed with cold MeOH, to obtain pure **2** in 43% yield as a white solid (3.97 g, 25.5 mmol).

$^1\text{H-NMR}$ (DMSO- d_6): δ = 11.20 (s, 2H, NH), 3.50 (t, 1H, $^3J_{\text{HH}}=5.1$ Hz, CH), 1.92 (m, 2H, CH₂), 0.84 (t, 3H, $^3J_{\text{HH}}=7.5$ Hz, CH₃) ppm.

5-ethyl, 5'-(2-ethanoic acid methyl ester)barbituric acid (3). A mixture of **2** (1.0 g, 6.4 mmol) and triethanolamine (0.85 ml, 6.4 mmol) was stirred in water (50 ml) at room temperature until **2** was completely dissolved. Bromoacetic acid methyl ester (1.0 g, 6.5 mmol) was added over 10 minutes and the reaction mixture was stirred for 3 days at room temperature. The precipitated product was filtered off and washed with cold methanol to obtain pure **3** in 47% yield as a white solid (0.69 g, 3.0 mmol).

$^1\text{H-NMR}$ (DMSO- d_6): δ = 11.49 (s, 2H, NH), 3.56 (s, 3H, OCH₃), 3.00 (s, 2H, CH₂), 1.76 (q, 2H, $^2J_{\text{HH}}=7.8$ Hz, CH₂), 0.81 (t, 3H, $^3J_{\text{HH}}=7.5$ Hz, CH₃) ppm.

5-ethyl, 5'-(2-ethanoic acid)barbituric acid (4). Barbituric acid **3** (0.54 g, 2.36 mmol) was dissolved in NaOH (2 M) in water (10 ml) and stirred at room temperature for 3 hours. HCl (conc.) was added dropwise until pH = 7. The water was removed by lyophilization and the white solid was washed with THF and dried *in vacuo*. Compound **4** was obtained as a white solid in 89% yield (0.45 g, 2.09 mmol).

$^1\text{H-NMR}$ (DMSO- d_6): δ = 10.34 (s, 2H, NH), 3.01 (s, 2H, CH₂), 1.82 (q, 2H, $^2J_{\text{HH}}=7.2$ Hz, CH₂), 0.91 (t, 3H, $^3J_{\text{HH}}=7.5$ Hz, CH₃) ppm.

N,N'-Bis(propyl)perylene-3,4,9,10-tetracarboxylic diimide (5). A mixture of perylene-3,4,9,10-tetracarboxylic dianhydride (3.0 g, 7.65 mmol) and propylamine (5.0 ml, 61

mmol) in DMF was refluxed for 3 hours. The precipitate was filtered off, added to hot 1% NaOH (aq.) and stirred for 15 minutes. The precipitate was filtered off, added to water and acidified with HCl (dilut.) and filtered off again. The product was washed with water and dried *in vacuo*. Compound **5** was obtained as a purple solid in 95% yield (3.45 g, 7.28 mmol) and was used without further purification.

1,6,7,12-tetrachloro-N,N'-Bis(propyl)perylene-3,4,9,10-tetracarboxylic diimide (6).

Compound **5** (1.0 g, 2.1 mmol) and iodine (0.19 g, 0.75 mmol) were dissolved in SOCl₂ (15 ml) and heated for 12 hours at 70°C. The solvent was removed under reduced pressure and the residual SOCl₂ was removed azeotropically under reduced pressure with toluene. Compound **6** was obtained as purple solid in quantitative yield and used without further purification.

MS (FAB): $m/z = 611.2$ ([M+H⁺], calcd 611.0).

1,6,7,12-tetra(*p*-*tert*butylphenoxy)-N,N'-Bis(propyl)perylene-3,4,9,10-tetracarboxylic diimide (7).

Compound **6** (1.03 g, 1.68 mmol) was added to a solution of potassium-*p*-*tert*butylphenol (2.54 g, 16.9 mmol) and K₂CO₃ (2.8 g, 20 mmol) in NMP and the solution was stirred at 120°C for 8 hours. After cooling down to room temperature, the reaction mixture was filtered and the precipitate was stirred in water (200 ml). The reaction product was filtered off and purified by column chromatography (CH₂Cl₂/Hexane = 3:2) giving compound **7** as a purple solid in 85% yield (1.53 g, 1.43 mmol).

¹H-NMR (CDCl₃): δ = 8.25 (s, 4H, CH_{Per}), 7.26 (d, ²J_{HH}=8.7 Hz, 8H, CH_{ortho}), 6.86 (d, ²J_{HH}=9.0 Hz, 8H, CH_{meta}), 4.11 (t, ³J_{HH}=7.4 Hz, 4H, CH₂), 1.73 (m, 4H, CH₂), 1.32 (s, 36H, *t*Bu), 0.99 (t, ³J_{HH}=7.5 Hz, 6H, CH₃) ppm. ¹³C-NMR (CDCl₃): δ = 162.9, 155.4, 152.3, 146.7, 132.4, 126.1, 121.9, 120.0, 119.4, 118.9, 41.6, 33.8, 30.9, 29.2, 28.8, 20.9, 11.0 ppm. MS (FAB): $m/z = 1067.7$ ([M+H⁺], calcd 1067.5).

1,6,7,12-tetra(*p*-*tert*butylphenoxy)-perylene-3,4,9,10-tetracarboxylic dianhydride (8).

A solution of KOH (6.0 g, 0.1 mol) in H₂O (3 ml) was added to *t*BuOH (60 ml). Then **7** (0.72 g, 0.67 mmol) was added to the two-phase solution and the mixture was stirred

vigorously and refluxed for 24 hours. The organic layer was separated and HCl (2M, 60 ml) was added. The mixture was stirred for 8 hours at room temperature and the precipitate was filtered off, washed with water to neutral pH and dried *in vacuo* at 100°C. The dianhydride was redissolved in 5% NaOH in ethanol and precipitated with 2N HCl. The product was dried *in vacuo* at 120°C, resulting in compound **8** as purple solid in 83% yield (0.55 g, 0.56 mmol), that was used without further purification.

1,6,7,12-tetra(*p*-*tert*butylphenoxy)-N-propyl-N'-(N-Boc-3-amino-2,2'-dimethyl propyl)-perylene-3,4,9,10-tetracarboxylic diimide (9). Compound **8** (0.50 g, 0.51 mmol) and N-Boc-3-amino-2,2'-dimethyl-propylamine (82 mg, 0.41 mmol) were refluxed in toluene (15 ml) for 20 hours. Butylamine (5 ml, 50 mmol) was added and the mixture was refluxed for 5 hours. The solvents were removed under reduced pressure. CH₂Cl₂ was added and the organic layer was washed with water. The organic layer was dried over Na₂SO₄, the solvent removed under reduced pressure and the reaction product dried *in vacuo*. The product was purified by column chromatography (CH₂Cl₂) to give pure **9** as purple solid in 50% yield (0.3 g, 0.25 mmol).

¹H-NMR (CDCl₃): δ = 8.28 (s, 2H, CH_{Per}), 8.23 (s, 2H, CH_{Per}), 7.26 (m, 8H, CH_{ortho}), 6.88 (m, 8H, CH_{meta}), 5.84 (t, 1H, NH), 4.14 (t, ³J_{HH}=7.5 Hz, 2H, CH₂), 4.04 (s, 2H, CH₂), 2.86 (d, ²J_{HH}=6.3 Hz, 2H, CH₂), 1.68 (m, 2H, CH₂), 1.46 (s, 9H, Boc), 1.40-1.36 (m, 2H, CH₂), 1.32 (s, 36H, *t*Bu), 0.97 (m, 9H, CH₃).

1,6,7,12-tetra(*p*-*tert*butylphenoxy)-N-propyl-N'-(3-amino-2,2'-dimethylpropyl) perylene-3,4,9,10-tetracarboxylic diimide (10). Compound **9** (0.28g, 0.23 mmol) was dissolved in TFA/CH₂Cl₂ (1:10; 22 ml) and the reaction mixture was stirred overnight at room temperature. Then water was added and the aqueous layer was neutralized (pH = 7) with solid sodium bicarbonate. The organic layer was separated and the aqueous layer was extracted with CH₂Cl₂. The combined organic layers were washed with NaOH (1 N), water and dried over Na₂SO₄. The solvents were evaporated and the product was purified by column chromatography (MeOH/CH₂Cl₂ = 1:20) to give pure **10** in 87% yield (0.23 g, 0.20 mmol).

1,6,7,12-tetra(*p*-*tert*butylphenoxy)-N-propyl-N'-((5-ethyl,5'-(2-amidoethyl)barbituric acid)-3-amino-2,2'-dimethylpropyl) perylene -3,4,9,10-tetracarboxylic diimide (PerBAR). To a solution of aminoperylene **10** (0.16 g, 0.17 mmol) and barbituric acid **4** (40 mg, 0.19 mmol) in CH₂Cl₂/DMF (4:1; 5 ml), DIPEA (50 μl, 0.36 mmol) and HBTU (74 mg, 0.20 mmol) were added. The reaction mixture was stirred overnight at room temperature. CH₂Cl₂ was added and the organic layer was washed with water, dried over Na₂SO₄ and concentrated *in vacuo*. The product was purified by column chromatography (MeOH:CH₂Cl₂ = 1:80) to give pure PerBAR as a purple solid in 69% yield (0.16 mg, 0.11 mmol).

¹H-NMR (CDCl₃): δ = 8.28 (s, 2H, CH_{Per}), 8.26 (s, 2H, NH), 8.23 (s, 2H, CH_{Per}), 7.26 (t, ³J_{HH}=7.8 Hz, 8H, CH_{ortho}), 7.18 (t, 1H, NH), 6.85 (dd, 8H, CH_{meta}), 4.13 (t, ³J_{HH}=7.5 Hz, 2H, CH₂), 4.01 (s, 2H, CH₂), 3.22 (s, 2H, CH₂), 2.90 (d, ²J_{HH}=6.3 Hz, 2H, CH₂), 1.94 (q, 2H, CH₂), 1.68 (m, 2H, CH₂), 1.5-1.4 (m, 2H, CH₂), 1.325 & 1.317 (s, 2 x 9H, *t*Bu), 1.05-0.85 (m, 12H, CH₃) ppm.

7.5 References

1. Zimmerman, S. C.; Corbin, P. S. *Struct. Bonding* **2000**, *96*, 63-94.
2. Schalley, C. A.; Rebek, J. Jr. *Stimulating Concepts in Chemistry*; Vögte, F.; Stoddart, J. F.; Shibaski, M., Wiley-VCH: Weinheim, Germany, 2000; pp 199-210.
3. Rebek, J. Jr. *Acc. Chem. Res.* **1999**, *32*, 278-286.
4. Conn, M. M.; Rebek, J. Jr. *Chem. Rev.* **1997**, *97*, 1647-1668.
5. Whitesides, G. M.; Simanek, E. E.; Mathias, J. P.; Seto, C. T.; Chin, D. N.; Mammen, M.; Gordon, D. M. *Acc. Chem. Res.* **1995**, *28*, 37-44.
6. MacDonald, C.; Whitesides, G. M. *Chem. Rev.* **1994**, *94*, 2383-2420.
7. Glusker, J. P. *Top. Curr. Chem.* **1998**, *198*, 1-56.
8. Jeffrey, G. A. *An Introduction to Hydrogen-Bonding*; Oxford University Press: New York, 1997.
9. Atwood, J. L.; Barbour, L. J.; Jerga, A. *Chem. Commun.* **2001**, 2376-2377.
10. Shivanyuk, A.; Rebek, J. Jr. *Chem. Commun.* **2001**, 2374-2375.
11. Vysotsky, M. O.; Thondorf, I.; Böhmer, V. *Chem. Commun.* **2001**, 1890-1891.

12. Fujita, M. *Chem. Soc. Rev.* **1998**, *27*, 417-426.
13. Stang, P. J. *Chem. Eur. J.* **1998**, *4*, 19-27.
14. Linton, B.; Hamilton, A. D. *Chem. Rev.* **1997**, *97*, 1669-1681.
15. Stang, P. J.; Olenyuk, B. *Acc. Chem. Res.* **1997**, *30*, 502-518.
16. Singer, S. J.; Nicolson, G. L. *Science* **1972**, *175*, 720-731.
17. Sakai, N.; Houdebert, D.; Matile, S. *Chem. Eur. J.* **2003**, *9*, 223-232.
18. Sidorov, V.; Kotch, F. W.; Abdrakhmanova, G.; Mizani, R.; Fettingner, J. C.; Davis, J. T. *J. Am. Chem. Soc.* **2002**, *124*, 2267-2278.
19. Sakai, N.; Matile, S. *J. Am. Chem. Soc.* **2002**, *124*, 1184-1185.
20. Kim, H. S.; Hartgerink, D.; Ghadiri, M. R. *J. Am. Chem. Soc.* **1998**, *120*, 4417-4424.
21. Sanchez-Quesada, J.; Kim, H. S.; Ghadiri, M. R. *Angew. Chem. Int. Ed.* **2001**, *40*, 2503-2506.
22. Doyle, E. L.; Hunter, C. A.; Phillips, H. C.; Webb, S. J.; Williams, N. H. *J. Am. Chem. Soc.* **2003**, *125*, 4593-4599.
23. Janout, V.; Lanier, M.; Regen, S. L. *J. Am. Chem. Soc.* **1996**, *118*, 1573-1574.
24. Janout, V.; Di Giorgio, C.; Regen, S. L. *J. Am. Chem. Soc.* **2000**, *122*, 2671-2672.
25. Janout, V.; Staina, I. V.; Bandyopadhyay, P.; Regen, S. L. *J. Am. Chem. Soc.* **2001**, *123*, 9926-9927.
26. Janout, V.; Jing, B.; Staina, I. V.; Regen, S. L. *J. Am. Chem. Soc.* **2003**, *125*, 4436-4437.
27. Martin, S. E.; Peterson, B. R. *Bioconjugate Chem.* **2003**, *14*, 67-74.
28. For a detailed description about double rosette assemblies see references 37-38, 42-43.
29. Other examples of guest complexation by double rosettes are reported in: (a) Crego-Calama, M.; Timmerman, P.; Reinhoudt, D. N. *Angew. Chem. Int. Ed.* **2000**, *39*, 755-758; (b) Ishi-I, T.; Crego-Calama, M.; Timmerman, P.; Reinhoudt, D. N.; Shinkai, S. *Angew. Chem. Int. Ed.* **2002**, *41*, 1924-1929; (c) Ishi-I, T.; Mateos-Timoneda, M. A.; Timmerman, P.; Crego-Calama, M.; Reinhoudt, D. N.; Shinkai, S. *Angew. Chem. Int. Ed.* **2003**, *42*, 2300-2305; (d) Kerckhoffs, J. M. C. A.; Ishi-I, T.; Paraschiv, V.; Timmerman, P.; Crego-Calama, M.; Shinkai, S.; Reinhoudt, D. N. *Org. Biomol. Chem.* **2003**, *1*, 2596-2603.

30. Liu, T.; Diemann, E.; Li, H. L.; Dress, A. W. M.; Muller, A. *Nature* **2003**, *426*, 59-62.
31. Discher, B. M.; Won, Y. Y.; Ege, D. S.; Lee, J. C. M.; Bates, F. S.; Discher, D. E.; Hammer, D. A. *Science* **1999**, *284*, 1143-1146.
32. Hajduk, D. A.; Kossuth, M. B.; Hillmyer, M. A.; Bates, F. S. *J. Phys. Chem. B* **1998**, *102*, 4269-4276.
33. Warriner, H. E.; Idziak, S. H. J.; Slack, N. L.; Davidson, P.; Safinya, C. R. *Science* **1996**, *271*, 969-973.
34. Won, Y. Y.; Davis, H. T.; Bates, F. S. *Science* **1999**, *283*, 960-963.
35. Yu, K.; Eisenberg, A. *Macromolecules* **1998**, *31*, 3509-3518.
36. Antonietti, M.; Forster, S. *Adv. Mater.* **2003**, *15*, 1323-1333.
37. Timmerman, P.; Vreekamp, R. H.; Hulst, R.; Verboom, W.; Reinhoudt, D. N.; Rissanen, K.; Udachin, K. A.; Ripmeester, J. *Chem. Eur. J.* **1997**, *3*, 1823-1832.
38. Vreekamp, R. H.; van Duynhoven, J. P. M.; Hubert, M.; Verboom, W.; Reinhoudt, D. N. *Angew. Chem. Int. Ed.* **1996**, *35*, 1215-1218.
39. Niosomes of surfactants with HLB (hydrophilic lipophilic balance) values between 7.5 and 10.5 are formed spontaneously when the gel-liquid transition temperature (T_c) is below the experimental temperature. $C_{12}EO_3$ and $C_{14}EO_3$ have HLB values of 8.6 and 9.4, respectively, while T_c for $C_{12}EO_3$ is below 15°C and for $C_{14}EO_3$ between 15-20. Van Hal, *et al.*, *J. Colloid Interface Sci.* **1996**, *178*, 263-273.
40. Samples were negatively stained with 2% uranyl acetate solution.
41. Racemic mixtures of *P*- and *M*-enantiomers are formed in the absence of a chiral center.
42. Prins, L. J.; Huskens, J.; De Jong, F.; Timmerman, P.; Reinhoudt, D. N. *Nature* **1999**, *398*, 498-502.
43. Prins, L. J.; Thalacker, C.; Wurthner, F.; Timmerman, P.; Reinhoudt, D. N. *P. Natl. Acad. Sci. USA* **2001**, *98*, 10042-10045.
44. Borovkov, V. V.; Hembury, G. A.; Inoue, Y. *Angew. Chem. Int. Ed.* **2003**, *42*, 5310-5314.
45. Hill, D. J.; Moore, J. S. *Proc. Natl. Acad. Sci.* **2002**, *99*, 5053-5057.
46. Brunsveld, L.; Meijer, E. W.; Prince, R. B.; Moore, J. S. *J. Am. Chem. Soc.* **2001**, *123*, 7978-7984.

47. After filtering of samples where water (containing 1% (v/v) glycerol) was added to **1a**, no CD activity was observed due to insolubility of **1a** in aqueous solution.
48. Solubilization of **1a** and PerBAR in bilayer membranes gives roughly an estimated effective concentration of ~ 9 mM **1a**₃•(PerBAR)₆ (based on added amount of assembly components and used volume of Serdox NES3). In chloroform or toluene double rosettes are already observed at concentrations down to 0.1 mM.
49. The average of the CD intensities between 290 and 300 nm was used to calculate the decrease in CD intensity.
50. The possible incomplete formation of **1b**₃•((R)-PhEtCYA)₆ in the bilayers is not expected to be the result of lower stability compared to **1a**₃•(PerBAR)₆. In chapters 3 and 4 is shown unambiguously that cyanurates (CYA) give more stable rosettes than barbiturates (BAR). Moreover, it has also been shown that especially **1b**₃•((R)-PhEtCYA)₆ exhibit high stability in MeOH/CHCl₃ solvent mixtures. On the other hand, it is known that hydrophobic compounds solubilize better in the lipophilic membranes than hydrophilic compounds. Therefore, it could be that due to the hydrophobic perylene moieties, the solubility of PerBAR in the membranes is better than the solubility of (R)-PhEtCYA. As a consequence, a lower concentration of (R)-PhEtCYA would be present in the membranes and thus, a smaller percentage of the assembly **1b**₃•((R)-PhEtCYA)₆ would be formed. Large differences in membrane solubility between dimelamines **1a** and **1b** are not expected because both compounds have similar molecular structure.
51. Cheuk, K. K. L.; Lam, J. W. Y.; Lai, L. M.; Dong, Y.; Tang, B. Z. *Macromolecules* **2003**, *36*, 9752-9762.
52. Bielejewska, A. G.; Marjo, C. E.; Prins, L. J.; Timmerman, P.; De Jong, F.; Reinhoudt, D. N. *J. Am. Chem. Soc.* **2001**, *123*, 7518-7533.
53. Barton, P.; Hunter, C. A.; Potter, T. J.; Web, S. J.; Williams, N. H. *Angew. Chem. Int. Ed.* **2002**, *41*, 3878-3881.

Summary

Self-assembly is nature's favorite, most economic and reliable way to generate large and complex biological systems. Due to the high efficiency of nature using noncovalent interactions to assemble complex aggregates, self-assembly is nowadays considered as one of the most promising ways for building synthetic functional structures. This thesis describes the assembly of large hydrogen-bonded systems (double rosettes) and their ability to act as receptors. Due to the formation of 36 hydrogen bonds that bring together three calix[4]arene dimelamines and six barbiturates or cyanurates, these double rosettes exhibit a high thermodynamic stability.

Chapter 2 reviews briefly the assembly of hydrogen-bonded aggregates that have been described in the literature in the past decade. The chapter describes the most representative examples of this type of noncovalent assemblies with emphases on the hydrogen-bonded motifs forming the assemblies and the ability of the assemblies to complex guest molecules.

Chapter 3 shows that a large range of functional groups can be introduced in the rosette platform, allowing the generation of large molecular diversity in a very simple way. Calix[4]arene dimelamines functionalized with alkyl, aminoalkyl, ureido, pyridyl, carbohydrate, amino acid and peptide functionalities self-assemble with a variety of barbiturates or cyanurates to form double rosettes. These functionalities influence strongly the stability of the double rosettes in MeOH/CHCl₃ solvent mixtures. Steric hindrance close to the rosette platform exerted by the building blocks decreases the stability. In general, carbohydrate moieties in the calix[4]arene dimelamines decrease the thermodynamic stability of the assemblies dramatically, while with amino acid functionalities stable assemblies are obtained. For peptide functionalized assemblies, the amino acids at the first position do not seem to affect the stability, while certain amino acids at the second position seem to decrease the stability of the assemblies. Furthermore, the stability of double rosettes with different amino acids in MeOH/CHCl₃ mixtures strongly depends on the structure of the barbiturate or the cyanurate building blocks. In

all cases, assemblies with barbiturate derivatives are less stable than double rosettes with cyanurates. Furthermore, bulkier branched cyanurates also decrease the thermodynamic stability of the double rosettes.

Chapter 4 describes a detailed thermodynamic study of the self-assembly of single- and double rosettes by isothermal titration microcalorimetry. ΔG° , ΔH° and $T\Delta S^\circ$ values indicate that the thermodynamics exhibited by the double rosettes reflect in some cases the independent assembly of two individual rosette structures while in other cases the assembly process is the result of the assembly of two individual rosettes reinforced by additional stabilizing interactions. Correlating the ΔG° with the solvent polarity, the formation of double rosettes in pure methanol or water is predicted. The formation of the hydrogen-bonded double rosette assemblies in pure methanol is proven by ^1H NMR and CD spectroscopy.

Chapter 5 describes the encapsulation of different anthraquinone derivatives inside of a double rosette (*endo*-receptor). The dynamic character of the double rosettes allows the internal rearrangement of the building blocks to obtain the “perfect” fit for three guest molecules. The encapsulation of the anthraquinone derivatives is very selective and sensitive to small structural changes. The selectivity exhibited by the receptor is due to small differences in steric hindrance between the guest molecules and the receptor cavity. The highest binding affinity was observed for anthraquinone derivatives that can form an intermolecular hydrogen-bonded network between the three encapsulated guest molecules.

Double rosettes can also function as *exo*-receptors. Chapter 6 describes the binding of phenol derivatives, aromatic carboxylic acids and *n*-octylgalactopyranoside to the exterior of double rosettes functionalized with ureido, amino and Gly-*L*-Ser moieties, respectively. The multivalent complementary recognition site of the receptors is used efficiently to complex multiple guests. A 1:3 binding mode was found for the complexation of the phenol derivatives DES and bisphenol-A. These guests bind ditopically to their receptor via the formation of two hydrogen bonds. Binding of the aromatic carboxylic acids in a 1:6 binding fashion, involves hydrogen bonding between the amino groups of the receptor and the carboxylic acid groups of the guests. *n*-Octylgalactopyranoside binds to a Gly-*L*-Ser functionalized double rosette probably by

formation of hydrogen bonds between the serine hydroxyl of the receptor and the hydroxyl groups of the guest. In this case, the number of guest molecules bound to the receptor is not determined unambiguously.

Most of the well-defined assemblies based exclusively on hydrogen bonding are not stable in water. But a close look to the molecular recognition processes in biological systems reveals that many bio-recognition processes occur at interfaces or at membrane surfaces between two aqueous compartments. Chapter 7 describes a novel approach to mimic bio-recognition processes by embedding of the hydrogen-bonded double rosettes in the membranes of non-ionic surfactant based vesicles (niosomes). CD spectroscopy indicates the formation of double rosettes after incorporation of the assembly components in bilayer membranes. Furthermore, niosomes containing only calix[4]arene dimelamine are able to extract barbiturates or cyanurates from the aqueous exterior allowing the formation of the hydrogen-bonded assemblies in the membranes.

Samenvatting

Zelf-assemblage is de favoriete, meest economische en betrouwbare manier om grote en complexe biologische systemen te genereren. Vanwege de hoge mate van efficiëntie waarmee de natuur niet-covalente interacties gebruikt om complexe aggregaten samen te stellen, wordt zelf-assemblage vandaag de dag beschouwd als één van de meest veelbelovende manieren om langs synthetische weg functionele structuren te maken. Dit proefschrift beschrijft de assemblage van grote waterstofbrug-gebonden systemen (dubbele rozetten) en de mogelijkheid om deze te laten functioneren als receptoren. Door de vorming van 36 waterstofbruggen, die drie calix[4]areen dimelamines en zes barbituraten samenbrengen, vertonen deze dubbele rozetten een hoge thermodynamische stabiliteit.

Hoofdstuk 2 geeft een overzicht van de vorming van waterstofbrug-gebonden aggregaten die in het laatste decennium in de literatuur zijn beschreven. Het hoofdstuk beschrijft de meest representatieve voorbeelden van dit soort niet-covalente assemblages, waarbij de nadruk wordt gelegd op de waterstofbrug-gebonden motieven die de assemblages vormen en de mogelijkheid van de assemblages om gastmoleculen te binden.

Hoofdstuk 3 laat zien dat een groot aantal functionele groepen geïntroduceerd kunnen worden in het rozet platform, waardoor het mogelijk is om op een eenvoudige manier een grote moleculaire diversiteit te genereren. Calix[4]areen dimelamines, voorzien van alkyl-, aminoalkyl-, ureido-, pyridyl-, koolhydraat-, aminozuur- en peptide-functionaliteiten, vormen met een reeks barbituraten en cyanuraten dubbele rozetten. Deze functionele groepen hebben een sterke invloed op de stabiliteit van de dubbele rozetten in MeOH/CHCl₃ mengsels. Sterische hindering dichtbij het rozet platform, die veroorzaakt wordt door de bouwstenen, verlaagt de stabiliteit van de dubbele rozetten. In het algemeen verlagen koolhydraatgroepen in de calix[4]areen dimelamines de thermodynamische stabiliteit van de assemblages drastisch, terwijl met aminozuren stabiele assemblages worden verkregen. Voor assemblages met peptiden geldt dat de

aminozuren op de eerste positie de stabiliteit niet beïnvloeden, terwijl een aantal aminozuren op de tweede positie de stabiliteit verlagen.

De stabiliteit van de aminozuurgefunctionaliseerde dubbele rozetten in MeOH/CHCl₃ mengsels hangt sterk af van de structuur van de barbituraat of de cyanuraat bouwstenen. In alle gevallen zijn de assemblages met barbituraatderivaten minder stabiel dan de dubbele rozetten met cyanuraten. Verder verminderen volumineus vertakte cyanuraten ook de thermodynamische stabiliteit van de dubbele rozetten.

Hoofdstuk 4 beschrijft een gedetailleerde thermodynamische studie naar de zelf-assemblage van enkele en dubbele rozetten waarbij gebruik gemaakt is van isothermische titratie microcalorimetrie. Waarden van ΔG° , ΔH° en $T\Delta S^\circ$ geven aan dat de thermodynamica voor de formatie van de dubbele rozetten in sommige gevallen beschouwd kan worden als de onafhankelijke assemblage van twee individuele rozetstructuren, terwijl in andere gevallen het assemblageproces het resultaat is van de assemblage van twee individuele rozetten, versterkt met bijkomende stabiliserende interacties. Door de ΔG° -waarden te correleren met de oplosmiddelpolariteit is de formatie van waterstofbrug-gebonden dubbele rozetten in zuiver methanol voorspeld. De formatie van een waterstofbrug-gebonden dubbele rozet in zuiver methanol is vervolgens aangetoond door middel van ¹H NMR en CD spectroscopie.

Hoofdstuk 5 beschrijft het insluiten van verscheidene anthrachinonverbindingen binnen een dubbele rozet (*endo*-receptor). Het dynamische karakter van de dubbele rozetten staat een interne herschikking van de bouwstenen toe om zo de "perfecte" pasvorm voor drie gastmoleculen te verkrijgen. De insluiting van anthrachinonverbindingen is zeer selectief en gevoelig voor kleine structurele veranderingen in de anthrachinonderivaten. De sterke selectiviteit van deze *endo*-receptor is het gevolg van kleine verschillen in sterische hindering tussen de gastmoleculen en de receptorholte. De hoogste bindingsaffiniteit werd waargenomen voor anthrachinonverbindingen die een intermoleculair waterstofbrug-gebonden netwerk kunnen vormen tussen de drie ingesloten gastmoleculen.

Dubbele rozetten kunnen ook functioneren als *exo*-receptoren. Hoofdstuk 6 beschrijft de binding van fenolderivaten, aromatische carbonzuren en *n*-octylgalactopyranose aan de oppervlakte van dubbele rozetten die gefunctionaliseerd zijn met respectievelijk

ureido-, amino- en Gly-*L*-Ser-groepen. De multivalente complementaire herkenningsplaats van de receptoren wordt efficiënt gebruikt om meerdere gastmoleculen te binden. Een 1:3 bindingsmodus werd gevonden voor de binding van de fenolderivaten DES en bisfenol-A. Deze gasten binden aan hun receptor door het vormen van twee waterstofbruggen. De binding van de aromatische carbonzuren in een 1:6 bindingswijze gaan gepaard met het vormen van waterstofbruggen tussen de aminogroepen van de receptor en de carbonzuurgroepen van de gastmoleculen. *n*-Octylgalactopyranose bindt met de Gly-*L*-Ser-gefunctionaliseerde dubbele rozet door de vorming van waterstofbruggen tussen de serine-hydroxylgroep van de receptor en de hydroxylgroepen van de gast. In dit geval is het aantal gastmoleculen dat bindt met de receptor niet eenduidig vastgesteld.

De meeste goed-gedefinieerde assemblages die uitsluitend gebaseerd zijn op het vormen van waterstofbruggen zijn niet stabiel in water. Echter, een nadere beschouwing van de moleculaire herkenningsprocessen in biologische systemen laat zien dat veel biologische herkenningsprocessen zich afspelen op grensvlakken of aan membraanoppervlakken tussen twee watercompartimenten. Hoofdstuk 7 beschrijft een nieuwe benadering om biologische herkenningsprocessen na te bootsen door het verankeren van waterstofbrug-gebonden dubbele rozetten in de membranen van niet-ionische surfactantgebaseerde vesicles (niosomen). CD spectroscopie toont de vorming van dubbele rozetten aan nadat de assemblage componenten zijn geïncorporeerd in de membranen. Verder zijn niosomen die enkel calix[4]areen dimelamines bevatten in staat om barbituraten of cyanuraten te extraheren uit de buitenliggende wateromgeving, waarna de waterstofbrug-gebonden assemblages in de membranen kunnen worden gevormd.

Dankwoord

Nu we zijn aangekomen bij het dankwoord, bedenk ik me dat mijn promotieonderzoek toch echt tot een einde is gekomen. Een einde aan ruim vier jaar zelfstandig onderzoek binnen de internationaal georiënteerde vakgroep Supramoleculaire Chemische Technologie van Prof. David Reinhoudt. Het proefschrift dat U in handen heeft vormt de kroon op mijn werk. Maar hoewel je als promovendus je onderzoek in hoge mate van zelfstandigheid dient te realiseren, hebben een aantal mensen bijgedragen aan de totstandkoming van dit proefschrift.

Ik heb dit proefschrift opgedragen aan mijn moeder die zich altijd goed kon verplaatsen in het enthousiasme dat ik kon opbrengen voor het onderzoek binnen de chemie. Ik ben mijn ouders dankbaar dat zij altijd in staat waren om zich in mij in te leven, adviezen te geven en vervolgens mij te stimuleren in de keuzen die ik maakte. Zelf kunnen nadenken, oordelen en beslissen vonden zij altijd belangrijk. Hiermee hebben zij een goede basis gegeven om de ‘wetenschappelijke wereld’ te kunnen betreden.

Na het afronden van mijn studie heb ik de eerste stappen kunnen zetten in deze wereld. Hiervoor wil ik mijn promotor David Reinhoudt graag bedanken. David jij bent degene geweest die mijn intree in de ‘wetenschappelijke wereld’ heeft mogelijk gemaakt. De hoge mate van vrijheid, de faciliteiten, het internationale karakter en de ambitieuze sfeer in de vakgroep hebben er toe bijgedragen dat onder jou leiding kwalitatief hoogstaand onderzoek is verricht.

I would like to thank my copromotor Mercedes Crego Calama, with who I experienced the successes and troubles within my research. I especially appreciate the effort you put in the realization of my thesis. Thank you for structuring my chapters during the implementation of my thesis.

Peter Timmerman, onder wiens begeleiding ik met dit onderwerp ben begonnen wil ik graag bedanken voor het enthousiasme waarvan voor mij een grote stimulans is uitgegaan.

Jurriaan Huskens wil ik graag bedanken voor zijn hulp in het verwezenlijken van de gecompliceerde bindingsmodellen. De manier waarop je dit hebt gedaan heeft me erg gestimuleerd en ervoor gezorgd dat ik met veel plezier zat te stoeien met de modellen. Het heeft er voor gezorgd dat hoofdstuk 4 ‘een mooi stukje werk’ is geworden.

Bart Jan Ravoo wil ik bedanken voor de enthousiaste discussies over ‘vesicles’, al dan niet onder het genot van een fris biertje. Je tip om na een aantal tegenslagen met de liposomen eens in de niet-ionische ‘vesicles’ te duiken heeft zijn vruchten afgeworpen!

Merdan Omerović bedank ik voor de synthese van de tripeptidegefunctionaliseerde calix[4]areen dimelamines, beschreven in Hoofdstuk 3. I would like to thank Prof. Stefan Matile and dr. Naomi Sakai for teaching me to prepare small unilamellar vesicles and to measure transport activities in bilayer membranes. Unfortunately, the double rosettes did not form in the liposomes.

Rico Keim en Henk-Jan van Maanen wil ik bedanken voor het maken van, respectievelijk, de TEM en de confocale microscopie plaatjes. Fijs van Leeuwen dank ik voor het kristalliseren van de dubbele rozetten en Huub Kooijman voor het ophelderen van deze structuren. Tieme Stevens, Roel Fokkens, Bianca Snellink, Hannie Visser en Annemarie Montanaro ben ik dankbaar voor de analyses van nieuwe verbindingen. Richard Egberink bedank ik voor de technische- en computerondersteuning en Marcel de Bruine voor de snelle toevoer van chemicalien en kantoorbenodigdheden. Maar bovenal wil ik jullie beide bedanken voor de gezellige en leerzame tijd die we hebben doorgebracht bij de BHV. Carla Weber - van der Ploeg en Izabel Katalanc dank ik voor de secretariële ondersteuning.

Besides these people, many other friends and colleagues supported me during my Ph.D. Therefore, I would like to thank all the members of SMCT group that I’ve met in the past years. I would like to mention some special people that I have met during my stay at the University of Twente. Miguelito, you have shown to be a real friend on which I could always count. We certainly have to make the culinary trip through Spain! Jessica, mijn labpartner, wanneer jij in de buurt bent, is het altijd gezellig. Dat jij één van mijn paranimfen bent is niet verwonderlijk gezien de leuke tijden die ik met jou heb doorgebracht zowel op het lab, in de kroeg als op de skates. Olgita, also my paranimf, the first after your arrival you earned already a special place in my heart. Your concern for

other people makes you a great girl. Monica you was always the happy and correct girl. However the Dutch influence and the arrival of Barbara possibly changed you to be just a happy girl. With both of you around it will certainly never be boring. Emiel thank you for your amusing efforts to convince people what is right. Alart, sugar boy, it always impressed me how easy you can generate so much pleasant nonsense. It was nice to pass these years with you on the lab. Vasile it was an honor to meet “Count Dracula”! For sure he sticks its teeth in chemical problems. Also I would like to thank the following people for the nice and pleasant stays we had at the University and in town: Jasper, Oskar, Wiljan, Steffen, Juanjo, Fransesca, Alessio (keep on going!), Fernando, Lourdes, Roberto, Becky (your cat is always welcome!), Amela, Paolo, Marta, Ana, and Javier.

Monse you deserve of course a special part. You are the one who made my time here as a Ph.D. student really special! Being the sun in my live you were always ready to support me, motivate me and spent good times with me. I know that you will say: “That is obvious; you are doing the same for me.” But then again, I will refer to the verse in the beginning of this thesis and make you realize that you are really special!

Mattijs ten Cate